

DEVELOPMENT AND PERFORMANCE EVALUATION OF AN INNOVATIVE ANTI-  
BIOFOULING REVERSE OSMOSIS MEMBRANE FOR WATER PURIFICATION  
APPLICATIONS

Ariel Jasmine Atkinson

A dissertation submitted to the faculty at the University of North Carolina at Chapel Hill in partial fulfillment of the requirements for the degree of Doctor of Philosophy in the Department of Environmental Sciences and Engineering in the Gillings School of Global Public Health.

Chapel Hill  
2016

Approved by:

Orlando Coronell

Maria José Farré

Avram Gold

Jill Stewart

Howard Weinberg

Zhenfa Zhang

© 2017  
Ariel Jasmine Atkinson  
ALL RIGHTS RESERVED

## **ABSTRACT**

Ariel Jasmine Atkinson: DEVELOPMENT AND PERFORMANCE EVALUATION OF AN INNOVATIVE ANTI-BIOFOULING REVERSE OSMOSIS MEMBRANE FOR WATER PURIFICATION APPLICATIONS  
(Under the direction of Orlando Coronell)

Biofouling is a main operational problem plaguing membrane use in the water purification industry. Biofouling limits water productivity, water quality, membrane life, and increases operational costs. Therefore, developing an effective, widely applicable technology to control biofouling would facilitate membrane implementation and enable efficient use of membrane technology.

Accordingly, the overall goal of this dissertation was to develop and evaluate the performance of a novel anti-biofouling reverse osmosis (RO) membrane(s) with 2-aminoimidazoles (2-AIs) incorporated as the active compound. 2-AIs are non-biocidal, bioactive compounds that actively disrupt biofilm formation mechanisms. 2-AIs are unique because they are one of the only compound classes that actively disrupts biofilm formation across different bacteria phyla, classes, and orders.

To achieve the overall goal, the following specific objectives were met:

- (1) to develop an anti-biofouling water purification membrane(s) through 2-AI incorporation into active layers of commercially available RO membranes,
- (2) to develop an anti-biofouling water purification membrane(s) through 2-AI incorporation into active layers of RO membranes during active layer casting,

- (3) to characterize 2-AI membrane(s) performance in terms of biofouling inhibition, water productivity, and contaminant removal.

Experimental results led to the following conclusions:

- (i) 2-AI membranes significantly inhibited *Pseudomonas aeruginosa* biofilms by 39-96% ( $p=0.002-0.12$ ) due to the presence of 2-AI and not changes in membrane physico-chemical properties.
- (ii) Compared to (2-AI lacking) control membranes, 2-AI incorporation decreased initial membrane water permeability by 0-44% and salt rejection by -0.4-4.3 percentage points, without efforts to optimize these parameters.
- (iii) Incorporating 2-AI into active layers of commercial RO membranes by activating carboxylic acid groups with 1-ethyl-3-(3-dimethylaminopropyl)carbodiimide produced a more effective membrane than incorporating 2-AI during active layer casting.
- (iv) Under operationally realistic conditions (e.g., using cross-flow and real waters), biofilm formation was significantly inhibited (98%,  $p<0.001$ ) by 2-AI membranes; and when biofilm formation was a fouling mechanism, 2-AI membranes had higher water permeability (10-11%) and organics rejection (11-12 percentage points) than (2-AI-lacking) control membranes.

Overall, this work constitutes the proof-of-concept for 2-AI membranes and 2-AI incorporation represents a promising, novel enhancement for biofouling prevention and control. Based on these results, further 2-AI membrane optimization and performance testing is warranted.

## ACKNOWLEDGEMENTS

I have so many people to thank for their help and providing encouragement throughout my PhD and dissertation research. Though this is the culmination of my graduate career, I am excited to see how my professional relationships will evolve and carry forward. I look forward to seeing all these friendly faces many more times and the continued fellowship and comradery. There are many more to thank than I can list here, but I am thinking of all of you as I write.

I would like to start by expressing appreciation of my committee. I am very grateful to my advisor, Dr. Orlando Coronell, for his wonderful guidance, commitment, and support. I know that my future work will be greatly colored by his exceptional teaching and advising style. I am so thankful to have started my graduate career under the advisement of Dr. Howard S. Weinberg. I have learned so much from him and value his continued advice, enthusiasm, and kindness. I would like to thank Dr. Zhenfa Zhang and Dr. Avram Gold for their invaluable expertise and countless hours of help with organic chemistry and synthesis. Dr. Jill Stewart, thank you so much for your research advice and always providing a smile. I am deeply grateful to Dr. Maria José Farré for her commitment, caring, and endless support. Thank you, MJ, for opening up your lab to me and providing me such a valuable experience in Oz. I have so enjoyed learning, exploring, and growing amongst and with my committee: many thanks.

I am appreciative of the opportunity that I had to visit and work at the University of Queensland. Thank you to the EAPSI folks, many friends, and researchers that made my Australian adventure so valuable and fun. Thank you particularly to Katrin Doederer and Bonnie Lyon for providing endless fun and invaluable support and help. Thank you to the many researchers and facilities that have contributed their time, expertise, and instrumentation. Special thanks to Dr. Carrie Donley and Dr. Amar Kumbhar of Chapel Hill Analytical and Nanofabrication Laboratory (CHANL), Dr. Thomas Clegg and Triangle Universities Nuclear Laboratory (TUNL) for their help with RBS analyses, Leonard Collins and the UNC Biomarker Mass Spectrometry Center for running LC-MS samples, UNC Energy Frontier Research Center (EFRC), and the Miller research group for use of contact angle equipment. Thank you also to Hydranautics for donation of membranes used in my work. Thank you to those in the department that have always been a tremendous support and provided many smiles including, Rebecca Gunn, Robin Whitley, Jack Whaley, and Wake Harper.

A tremendous thank you to those at Agile Sciences, Inc. for allowing me to use their 2-aminoimidazole technology and apply it to water treatment membranes. I would like to thank them for discussing my ideas and assisting me in any way they could. I would also like to express appreciation to Agile for allowing me to work in their lab for several months, where I learned the fundamentals and performed a good amount of organic synthesis from Dr. David Jung and biological methods from Dr. Angie Pollard and Dr. Daina Zeng. I also appreciate Gabby Brautman, Raul Doyle, and Brian Kang for aiding me with whatever I asked.

I would like to acknowledge the sources of my research, travel, and personal funding throughout my PhD including the UNC Biology Department, WRRI, NSF-EAPSI, UNC GPSF, American Chemical Society's (ACS) Emerging Leaders Award, ACS-ENVR conference travel

grant, National Science Foundation (NSF) Grant Opportunities for Academic Liaison with Industry (GOALI) and Chemical, Bioengineering, Environmental, and Transport Systems (CBET) program under Award#1264690, the National Water Research Institute (NWRI) and American Membrane Technology Association (AMTA) Fellowship for Membrane Technology, and The UNC Graduate School Dissertation Completion Fellowship.

All past and present members of Coronell and Weinberg labs particularly Mikayla Armstrong, Bonnie Lyon, Jingbo Wang, Kasia Grzebyk, Panitan Jutaporn, Yi Liu, John Eskew, Breanne Holmes, Kirsten Studer, Alma Berciragic, Kathleen McDermott, Alex Gorzalski, and Ryan Kingsbury for invaluable assistance, endless laughs, and teaching me the meaning of teamwork. I appreciate your friendship and support both in and out of the lab. The time we have spent together is irreplaceable and I look forward to seeing how we each evolve in our lives and careers.

Last, but definitely not least, to my family and friends: Thank you for your support and love. There is no way I could accomplish what I have without you! A special thank you to Mikayla and Matt Armstrong for being there to both whip me into shape and provide distractions in these last few months. Thank you so much for the positivity. I have had so much fun and will miss being so close in distance to you! Thank you to those who have always inspired and fostered my scientific interests including my mom and dad, and my undergraduate advisor Dr. Carol Babyak. Gratitude goes out to all my family and friends for giving me confidence and encouraging me to pursue my dreams and future aspirations, no matter how crazy they may seem at times. Though some say that I'm a dreamer (see introduction of my departmental seminar), thank you to the Cubbies+fans, for showing me that I'm not the only one. And showing me that there was light in 2016 and with hard work and perseverance you can overcome (even a 108-year

losing streak). Thank you to Louie for the long walks, cuddles, and kisses. Most of all there is one who has really been through the thick and the thin of my graduate career and my life thus far. There are absolutely no words to describe how much love and support that I have received from my husband, Brandon Fiedor. You make me feel so special, so loved, as if I can accomplish whatever I set my heart and mind to, that I can actually do good in this world. I can only hope to give back in some way for all that I have received. Much love!



## TABLE OF CONTENTS

LIST OF TABLES .....	xiv
LIST OF FIGURES .....	xv
LIST OF ABBREVIATIONS .....	xviii
LIST OF SYMBOLS .....	xx
CHAPTER 1: INTRODUCTION .....	1
1.1. Background and Motivations .....	1
1.1.1. Broader motivations .....	1
1.1.2. General membrane background .....	3
1.1.3. Fouling .....	7
1.1.4. Biofouling.....	7
1.1.5. Biofouling control .....	8
1.1.6. Anti-biofouling membranes .....	9
1.1.7. Biofilm disruption .....	10
1.1.8. Summary of motivation.....	10
1.2. Objectives .....	11
1.2.1. Overall Goal .....	11
1.2.2. Specific Objectives.....	11
1.3. Dissertation Organization.....	12
REFERENCES .....	14

CHAPTER 2: DEVELOPMENT OF ANTI-BIOFILM MEMBRANES THROUGH THE INCORPORATION OF 2-AMINOIMIDAZOLE INTO COMMERCIAL RO/NF MEMBRANES .....	20
2.1.Introduction .....	20
2.2. Materials and Methods .....	23
2.2.1. Reagents and membranes .....	23
2.2.2. Synthesis of 2-aminoimidazole (2-AI) compounds .....	23
2.2.3. Model reaction for incorporation of 2-AIs into membrane active layers .....	24
2.2.4. 2-AI benzoyl conjugates.....	25
2.2.5. Crystal violet biofilm inhibition assay .....	25
2.2.6. Incorporation of 2-AI-para into commercial membranes .....	25
2.2.7. 4-bromoaniline incorporation.....	27
2.2.8. Filtration of water with bromoaniline-modified membranes .....	27
2.2.9. Membrane cleaning .....	27
2.2.10. Attenuated total reflectance- Fourier transform infrared spectroscopy (ATR-FTIR) .....	28
2.2.11. Silver ion probing of membrane samples.....	28
2.2.12. RBS .....	28
2.2.13. Contact Angle.....	29
2.2.14. Zeta potential via streaming current.....	29
2.2.15. AFM .....	30
2.2.16. Membrane performance tests .....	30
2.2.17. Statistical significance testing .....	32
2.3. Results and Discussion.....	32

2.3.1. Model reaction for incorporation of a 2-AI into a commercial polyamide membrane .....	32
2.3.2. Verification of 2-AI incorporation in the polyamide active layers of RO/NF membranes .....	38
2.3.3. Evaluation of the concentration and stability of 4-bromoaniline incorporated in membranes as a surrogate for 2-AIs .....	40
2.3.4. Performance of 2-AI-modified membranes .....	46
2.3.5. Changes in membrane charge, hydrophobicity, and roughness as a result of 2-AI incorporation and their potential contribution to biofilm inhibition.....	49
2.4. Conclusions.....	53
2.5. Acknowledgements.....	55
REFERENCES .....	56
 CHAPTER 3: DEVELOPMENT OF ANTI-BIOFOULING RO/NF MEMBRANES THROUGH INCORPORATION OF 2-AMINOIMIDAZOLE INTO THE ACTIVE LAYER DURING POLYAMIDE CASTING .....	
3.1. Introduction.....	61
3.2. Materials and Methods .....	65
3.2.1. Reagents and membranes .....	65
3.2.2. Incorporation of 2-AI-para into active layers during polyamide casting .....	66
3.2.3. Incorporation of 2-AI surrogate compound (4-iodoaniline) into active layers during polyamide casting.....	67
3.2.4. Cleaning procedures and use of iodoaniline membranes for water purification .....	68
3.2.5. Chemical characterization of membrane samples .....	68

3.2.6. Physical characterization of membrane samples .....	70
3.2.7. Membrane performance tests .....	71
3.2.8. Statistical significance testing .....	73
3.3. Results and Discussion .....	73
3.3.1. Verification of polyamide active layer formation in 2-AI membranes .....	73
3.3.2. Verification of 2-AI incorporation into polyamide active layer of 2-AI membranes .....	74
3.3.3. Evaluation of concentration and stability of 4-iodoaniline incorporated in membranes as a surrogate for 2-AIs .....	76
3.3.4. Performance of 2-AI membranes .....	80
3.3.5. Membrane charge, hydrophobicity, and roughness in 2-AI membranes and their potential contribution to biofilm inhibition .....	85
3.4. Conclusions.....	88
3.5. Acknowledgements.....	89
REFERENCES .....	91
<b>CHAPTER 4: CHARACTERIZATION OF PERFORMANCE OF NOVEL 2-AMINOIMIDAZOLE ANTI-BIOFOULING MEMBRANES UNDER OPERATIONALLY REALISTIC CONDITIONS.....</b>	<b>96</b>
4.1. Introduction.....	96
4.2. Materials and Methods .....	99
4.2.1. Reagents, control membranes, and 2-AI membranes .....	99
4.2.2. Cross-flow Apparatus.....	100
4.2.3. Feed solutions.....	101
4.2.4. Fouling experiments and cleaning of membrane system .....	104

4.2.5 Scanning electron microscopy (SEM).....	105
4.2.6. Attenuated total reflectance-Fourier transform infrared (ATR-FTIR) .....	105
4.2.7. Dissolved (non-purgeable) organic carbon (DOC) .....	106
4.2.8. EPS extraction and characterization of polysaccharide and protein content .....	106
4.2.9. PA14 enumeration in feed solutions and membrane samples .....	107
4.2.10. Water permeability and solute rejection.....	108
4.2.11. Statistical significance testing .....	108
4.3. Results and Discussion .....	109
4.3.1. Characterization of membrane foulant layers in control and 2-AI membranes .....	109
4.3.2. Membrane performance under fouling conditions. ....	118
4.3.3. Connections between fouling mechanisms and performance .....	124
4.4. Conclusions .....	124
4.5. Acknowledgements .....	125
REFERENCES .....	127
CHAPTER 5: CONCLUSIONS.....	131
CHAPTER 6: FUTURE WORK .....	135
APPENDIX 1: SUPPORTING INFORMATION FOR CHAPTER 2 .....	138
APPENDIX 2: SUPPORTING INFORMATION FOR CHAPTER 3 .....	172
APPENDIX 3: SUPPORTING INFORMATION FOR CHAPTER 4 .....	181

## LIST OF TABLES

Table 2.1. The three 2-AI compounds and surrogate compound (4-bromoaniline) considered for incorporation into commercial membranes .....	24
Table 2.2. Benzoic acid conjugates of 2-AI-para, $m/z$ $[M+H]^+$ , by ESI-MS and relative yield calculated from peak areas of LC/ESI-MS trace. ....	33
Table 2.3. Characteristics of unmodified commercial control and 2-AI-modified membranes .....	44
Table 2.4. Bromoaniline (BA) concentrations and associated percent loss in NF270 membranes after chemical cleaning and/or use for filtering ultrapure water for 6 hours .....	46
Table 3.1. The 2-AI compound and the 2-AI surrogate compound (iodoaniline) incorporated into polyamide thin-film composite membranes .....	66
Table 3.2. Contents of monomers in solutions used to fabricate control and 2-AI polyamide active layers .....	67
Table 3.3. Contents of iodoaniline (IA) in solutions used to fabricate IA membranes.....	77
Table 3.4. Characteristics of control and 2-AI membranes.....	82
Table 4.1. Description of feed solutions used in cross-flow fouling experiments. ....	103
Table 4.2. Distinctive FTIR peaks of fouled membranes (Column 1).....	113

## LIST OF FIGURES

Figure 1.1. Structure of a thin-film composite (TFC) water purification membrane shown operated under a cross-flow regime .....	4
Figure 1.2. Representative schematic of the formation reaction of the polyamide active layer.....	6
Figure 1.3. Stages of biofilm formation on a membrane surface .....	8
Figure 2.1. Mechanism of 2-AI incorporation into polyamide membrane matrix.....	26
Figure 2.2. PA14 biofilm inhibition by 2-AI-benzoyl conjugates (at 7.8 $\mu$ M- 0.5 mM) and corresponding IC50 values .....	35
Figure 2.3. Chemical structures of unconjugated 2-AI-para (top), 5-(4-nitrophenyl) 2-AI (2 <sup>nd</sup> row), 5-(4-nitrophenyl)-1-benzoyl 2-AI conjugate (3 <sup>rd</sup> row), and di-benzoyl-2-AI conjugate (bottom).....	37
Figure 2.4. FTIR spectra of ESPA 3 membrane (blue line) and ESPA 3 modified by 2-AI-para (red line) .....	39
Figure 2.5. Volume-averaged concentration of Ag <sup>+</sup> in polyamide active layers of commercial unmodified control (blue bars) and 2-AI-modified membranes (red bars) after exposure to Ag <sup>+</sup> probing solution at pH=10.5. ....	40
Figure 2.6. Concentration of bromoaniline incorporated into (a) polyamide active layer and (b) polysulfone support layer of an XLE membrane .....	42
Figure 2.7. Volume-averaged concentrations of bromoaniline (BA) incorporated into the polyamide active layers of four modified commercial membranes. ....	43
Figure 2.8. Concentration of bromoaniline in the active layer of the bromoaniline-modified XLE membrane after filtration of ultrapure water .....	45
Figure 2.9. Biomass areal density of PA14 biofilm on the surface of unmodified control (blue bars) and corresponding 2-AI-modified membranes (red bars).....	48

Figure 2.10. Zeta potential, measured by streaming current, of unmodified control (blue square) and 2-AI-modified membranes (red diamond) as a function of pH. ....	50
Figure 2.11. Contact angle of unmodified control (blue bars) and corresponding 2-AI-modified membranes (red bars) as measured by the captive bubble contact angle method. ....	51
Figure 2.12. Root-mean-squared (RMS) roughness of unmodified control membranes (blue bars) and corresponding 2-AI-modified membranes (red bars).....	53
Figure 3.1. Average concentration of silver ion ( $\text{Ag}^+$ ) measured by RBS in the polyamide active layers of control and 2-AI membranes after being exposed to $\text{Ag}^+$ probing solution at pH=10.5 .....	75
Figure 3.2. Concentration of iodoaniline (IA) incorporated into the polyamide active layer of membranes, as measured by RBS, using IA incorporation solutions with varying concentrations as defined in Table 3.3 .....	78
Figure 3.3. Concentration of iodoaniline (IA) incorporated into the polyamide active layer of four commercial membranes .....	79
Figure 3.4. Concentration of iodoaniline (IA) in IA-membranes after membrane storage, membrane cleaning, and water filtration tests .....	80
Figure 3.5. Areal Biomass of PA14 biofilm (as biomass per membrane area) on the surface of the control and 2-AI membranes .....	83
Figure 3.6. Comparison of regressed zeta potential in the pH range of 3-10 for the control and 2-AI membranes.....	86
Figure 3.7. Contact angle for the control and 2-AI membranes as measured by the captive bubble method .....	87
Figure 3.8. Root-mean-squared (RMS) roughness of control membranes and 2-AI membranes.....	88
Figure 4.1. The 2-AI molecule (5-(4-aminophenyl)-1H-imidazol-2-amine, or 2-AI-para for short) incorporated into commercial membranes to produce 2-AI membranes .....	100



Figure 4.2. A custom-built laboratory-scale cross-flow system, equipped with four flat-sheet membrane cells (7.65 cm x 4.65 cm effective membrane area each) in series, electronic pressure transducers, a flow indicator, sampling ports, a recirculating chiller for temperature control, pH electrode and meter, and metering valves to control flow and pressure .....	101
Figure 4.3. Representative surface SEM images of fouled control and fouled 2-AI membranes at 1000x (rows 1 and 3) and 10000x (rows 2 and 4) magnifications .....	110
Figure 4.4. ATR-FTIR spectra of unfouled control membranes (blue solid line), fouled control membranes (green dotted line), and fouled 2-AI membranes (red dashed line) fouled by using organic-only, biofouling-only, cell-deposition-only, and organic&biofouling feed solutions.....	112
Figure 4.5. Areal mass density of polysaccharide (PS, dark blue bars) and protein (PN, purple striped bars) on the surface of fouled control and fouled 2-AI membranes that were fouled using biofouling-only feed solution .....	116
Figure 4.6. Areal density of organic content on the surface of fouled control and fouled 2-AI membranes .....	117
Figure 4.7. Areal mass of biofilm (log-scale) on fouled control and fouled 2-AI membranes.....	118
Figure 4.8. Normalized water permeabilities ( $A_t/A_0$ ) over 75 hours of filtration under each fouling condition for control membranes (green squares) and 2-AI membranes (red diamonds) .....	120
Figure 4.9. Water permeabilities over 75 hours of filtration under each fouling condition for control membranes (green squares) and 2-AI membranes (red diamonds).....	122
Figure 4.10. Rejection of dissolved organic carbon in feed solutions by control membranes (solid green) and 2-AI membranes (red striped) after 75 hours of filtration.....	123

## LIST OF ABBREVIATIONS

<sup>1</sup> HNMR	Proton nuclear magnetic resonance
2-AI	2-aminoimidazole
2-AI-butyl	5-(4-aminobutyl)-1 <i>H</i> -imidazol-2-amine
2-AI-meta	5-(3-aminophenyl)-1 <i>H</i> -imidazol-2-amine
2-AI-nitro	5-(4-nitrophenyl)-1 <i>H</i> -imidazol-2-amine
2-AI-nitro-benzoyl	(2-amino-5-(4-nitrophenyl)-1 <i>H</i> -imidazol-1-yl)(phenyl)methanone
2-AI-para	5-(4-aminophenyl)-1 <i>H</i> -imidazol-2-amine
AFM	Atomic force microscopy
ATR-FTIR	Attenuated reflectance-fourier transform infrared spectroscopy
BA	4-bromoaniline
CFU	colony forming units
dibenzoyl-2-AI-para	<i>N</i> -(40(2-amino-1-benzoyl-1 <i>H</i> -imidazol-5-yl)phenyl)benzamide
DO	dissolved oxygen
DOC	dissolved organic carbon
EDC	ethyl-3-(3-dimethylaminopropyl)carbodiimide
EPS	Extracellular polymeric substances
HSL	Homoserine Lactones
IA	4-iodoaniline
IC <sub>50</sub>	Half maximal inhibitory concentration
LC-MS	Liquid chromatography-mass spectrometry
MPD	m-phenylenediamine
NF	Nanofiltration

PA	polyamide
PA14	<i>Pseudomonas aeruginosa</i> strain 14
RBS	Rutherford backscattering spectrometry
RMS	root-mean-square
RO	reverse osmosis
SEM	scanning electron microscopy
TFC	thin-film composites
TMC	trimesoyl chloride
XPS	X-ray photoelectron spectroscopy

## LIST OF SYMBOLS

$\%Inh$	biofilm inhibition
$\%R$	contaminant rejection
$A$	water permeability coefficient
$A_t/A_0$	normalized water permeability
$C_f$	conductivity of feed
$C_p$	conductivity of permeate
$H_0$	null hypothesis
$H_1$	alternative hypothesis
$J_w$	water flux
$pKa$	acid disassociation constant
$\bar{x}_{2AI}$	sample mean of 2-AI membrane sample
$\bar{x}_{CTL}$	sample mean of control membrane sample

## **CHAPTER 1: INTRODUCTION**

### **1.1. Background and Motivation**

#### **1.1.1. Broader motivations**

The complexity of addressing water scarcity and providing safe drinking water to the global population is exacerbated by global climate change, increasing water demand, and increasing contamination of traditional source waters. These challenges establish a vital need to evaluate alternatives to traditional drinking water sources and treatment. Though fresh water supply can be further stretched through increased efficiency in use, this option is not enough to meet current and future needs. Desalination and water reuse are becoming a crucial part of the water equation and represent some of the most prominent options that exist to manage the fresh water scarcity problems around the world.<sup>1-6</sup>

Frequently, drinking water treatment plants use feed waters that are compromised by upstream wastewater effluent inputs, industrial effluent, agricultural runoff, and/or non-point sources of pollution that already make unplanned wastewater reuse an important component of drinking water production.<sup>5,6</sup> Although planned potable reuse is seldom used in the U.S., other countries and areas of the world with already extensive water scarcity issues such as the Middle East and Australia, have for many years widely utilized advanced water treatment plants to produce high quality recycled water for supplementing drinking water supplies without impacting human health.<sup>5,7,8</sup> Desalination of sea and brackish waters have been used for decades and continue to expand rapidly in many countries such as the U.S., Spain, Israel, and Japan.<sup>8-11</sup>

Accordingly, planned potable reuse of highly treated wastewaters and desalination of brackish and/or seawaters has great potential to meet future water needs.<sup>5,12</sup>

In most modern water reuse and desalination plants, reverse-osmosis (RO) and/or nanofiltration (NF) membrane treatment is the most critical step for removing contaminants (including salts) from source waters in one step and without the use of chemicals. Though less costly than other desalination technologies, membrane treatment can be expensive, due mainly to energy consumption and fouling control expenses. Energy use can account for up to 50% of total water production costs in desalination plants.<sup>13,14</sup> The high-energy consumption is due to the hydraulic pressure required to operate RO/NF membranes, which can be greatly exacerbated by fouling. To decrease energy costs, plants generally try to keep fouling at a minimum, which may result in decreased energy expenses but fouling control measures are themselves an added cost. For example, Water Factory 21 (former water reuse plant using RO in California) spent an estimated 30% of the total operating costs to control biofouling alone.<sup>15</sup> Decreasing the fouling potential of membranes could lead to significant savings from decreased energy costs, decreased cleaning/control costs, and extended membrane lifespans. Given that fouling can also lead to increased passage of contaminants into the permeate, decreasing fouling would not only lower costs but also potentially improve the quality of the product water.<sup>16-23</sup>

RO/NF membrane treatment can be a powerful tool for improving water security worldwide, but the costs associated with fouling are a major hindrance for efficient use and more widespread implementation of water reuse and desalination. These facts serve as the broader motivations for this dissertation. The remainder of the background section explains the more field specific motivations and additional information to give context to the dissertation topic.

### 1.1.2. General membrane background

RO/NF membranes, typically used for water purification, are thin-film composites (TFCs), consisting of 3 polymeric layers as depicted in **Figure 1.1**. Contaminants in the feed water are rejected by the top polyamide layer of the membrane, also known as the “active layer”. The mechanisms of contaminant rejection are a combination of size exclusion, electrostatic repulsion, and the relatively low diffusivity/partitioning of contaminants through the membrane compared to water.<sup>24</sup>

As depicted in **Figure 1.1.**, the cross-flow regime is used in full-scale applications, where two streams are generated from the single feed stream. One stream is the purified product water referred to as the “permeate”, and the second stream known as the “concentrate” (or brine) is the feed water that did not permeate the membrane. Since the membranes reject contaminants, the concentrate (brine) stream contains a higher concentration of contaminants than the feed stream. The permeate typically goes on to further treatment before distribution to end users, whether that be a rare additional pass through membrane treatment to further remove contaminants or the final step(s) in the treatment train to polish water quality (e.g., remineralization, disinfection, advanced oxidation). The concentrate can pass through another stage(s) of membrane treatment, to get a higher water recovery from the feed waters, and/or is used in an energy recovery device. Eventually the concentrate becomes the waste stream.

**Figure 1.1.** Structure of a thin-film composite (TFC) water purification membrane shown operated under a cross-flow regime. A TFC consists of three layers: (1) a top active layer made of polyamide, (2) an intermediate polysulfone support, and (3) a bottom layer made of polyester fabric. The general structure for each polymer is also shown below its label. For cross-flow configuration the feed enters a membrane module and flows parallel to the surface of the membrane, a portion of the water diffuses through the membrane and is called “permeate”, the water that does not permeate the membrane and exits the module is called “concentrate”.



The active layer is usually a polyamide based polymer. A representative polyamide formation reaction is shown in **Figure 1.2**. The polyamide is formed through interfacial polymerization where two monomer solutions, e.g., trimesoyl chloride (TMC) and m-phenylenediamine (MPD), cross-link through the formation of amide bonds. Typically, the active layer fabrication is done by first soaking a polysulfone support in an aqueous MPD solution, and then exposing the support+MPD to a TMC-organic solvent solution to form polyamide at the interface between the two solutions. After polymerization, the polyamide is exposed to water, hydrolyzing the acid chlorides to form carboxylic acids. As seen in **Figure 1.2**, the active layer contains terminal functional groups, mostly carboxylic acids ( $\approx 0.2$ - $0.7$  M) and some primary amines ( $\approx 0.01$ - $0.08$  M).<sup>25</sup> These functional groups ionize at particular pH conditions, with amine groups protonating at acidic conditions ( $\text{pK}_a \approx 4$ ), and carboxylic acid groups deprotonating at alkaline conditions (typically having two  $\text{pK}_a$ 's at around 5 and 9).<sup>25</sup>

The active layer fabrication process and surface chemistry are important factors to take into account when attempting to control/prevent fouling as well as when modifying the active layer to provide the membrane surface with anti-fouling properties.<sup>26-30</sup>



### 1.1.3. Fouling

As mentioned in *Section 1.1*, membrane fouling is a major problem in both water reuse and desalination of sea and brackish waters, as it leads to lower final water quality as well as increased costs in the form of energy, cleaning, and premature membrane degradation.<sup>16–23</sup> There are four types of fouling that occur in membrane systems: organic, inorganic, colloidal, and biofouling. Only biofouling cannot be resolved by the pre-treatment of feed waters; even if 99.99% of microbes are removed, significant biofouling can still occur.<sup>15,31</sup> Biofouling is present in most, if not all, membrane treatment plants and it is frequently irreversible, meaning that cleaning will not fully recover the membranes to their original efficiency.<sup>32–36</sup> Out of the four major types of fouling, biofouling is the most complex and challenging to manage.

### 1.1.4. Biofouling

Biofouling is the accumulation of a biofilm on a membrane surface. The biofilms on membrane surfaces consist of a matrix of bacteria and associated substances known as extracellular polymeric substances (EPS).<sup>18,22,37,38</sup> Biofilm formation is thought to consist of 2–4 stages, as shown in **Figure 1.3.**, where the first stage is usually described as the initial adhesion of microorganisms, though this may be preceded by the conditioning of the surface (e.g., accumulation of organic substances that increase attachment of microbes).<sup>15,33,39–41</sup> This initial attachment is critical because if adhesion of bacteria can be avoided, biofouling may be prevented altogether. If adhesion of bacteria can be significantly reduced, but not fully eliminated, biofouling may still occur, though likely lessened and/or slowed. After the adhesion of bacteria, cells grow, multiply and produce EPS, and more bacteria and even particulates adhere to the surface.<sup>15,33,39–41</sup> The last phase of biofilm development is when the growth and detachment of bacteria and/or matrix reach equilibrium, and is commonly called the plateau phase.<sup>15,33,39–41</sup>



**Figure 1.3.** Stages of biofilm formation on a membrane surface. Blue arrows represent the direction of water flow. (a) Initial attachment: bacteria sense/adjust to their environment, communicate via chemical signaling, and attach to membrane surface. (b) Biofilm formation: bacteria excrete extracellular polymeric substances (EPS), grow, reproduce and form a complex matrix known as a biofilm. (c) Plateau phase: growth and detachment of bacteria and/or matrix reach equilibrium, with detachment occurring due to shear forces.

RO/NF membrane surfaces present a suitable environment for bacterial attachment and biofilm growth because feed waters are generally non-sterile, bacteria are actively transported towards the membrane (with the water), and nutrients are constantly supplied with continuous flow of fresh feed water.<sup>18,31,42</sup> There are several physico-chemical properties that can vary between membranes and have been identified as impacting biofouling. Increased hydrophobicity, increased roughness, and decreased surface charge have been linked to increased fouling potential;<sup>26–28,32,43,44</sup> however, the surface may be conditioned by other types of fouling changing the physical properties of the membrane surface.<sup>35</sup> Hydrodynamics (e.g., shear forces) and the bacteria characteristics (e.g., flagellar motility) can also influence fouling.<sup>42,45,46</sup>

### 1.1.5. Biofouling control

The most widely employed biofouling control methods in membrane treatment are the application of biocides and regular membrane cleaning. For example, feed waters are typically pre-disinfected with chloramines or free chlorine to inactivate or kill the microorganisms that could foul the membrane.<sup>15,31,36,38,39</sup> If free chlorine is used, sodium bisulfite is used to quench the

residual disinfectant before the membrane step because TFC membranes are sensitive to chlorine and can be significantly degraded even at low free chlorine concentrations (i.e.,  $<0.1 \text{ mg.L}^{-1}$ ).<sup>12,47–</sup>

<sup>51</sup> Biocides are generally unsuccessful because even with very high log reductions/inactivation of bacteria, only a few bacterial cells are needed to start a biofilm and biofilm formation may also be a protective response of bacteria.<sup>15,31,38</sup> Along with its limited efficacy, there are additional downsides to pre-disinfection including membrane degradation, the formation of potentially harmful by-products (i.e., disinfection by-products), and that membrane cleaning is still needed to keep biofouling under control.<sup>15,31,36,38,39,52</sup> Usually the biofouling control approach is specific to the treatment plant, with most plants using a combination of control methods. Along with disinfection, other strategies used may include nutrient limitation, physical removal of microbes, and frequent membrane cleaning. Currently, there is no widely applied control strategy/combination of strategies that is efficacious and cost-effective.<sup>15,31,36,38,39,52,53</sup>

#### **1.1.6. Anti-biofouling membranes**

There has been an effort to alter the membrane surfaces to combat biofouling. Most studies in the literature attempt to either incorporate biocides into the membrane or alter the physical properties of the membrane surface to make it less amenable to attachment.<sup>44,53–57</sup> The biocide incorporation approach is meant to inactivate or kill bacteria but not to necessarily prevent attachment. This approach has been relatively unsuccessful and in some cases the anti-microbials in membranes have promoted biofouling.<sup>53,58</sup> The physical approaches have aimed at increasing the hydrophilicity of or constructing nano-patterns on the membrane surface.<sup>44,53,55</sup> These alterations are meant to minimize bacterial attachment, but unfortunately these physical approaches have also been unsuccessful because once bacteria is on the surface, the physical alterations do not actively prevent excretion of EPS or biofilm formation itself. A solution that

prevents both attachment and EPS excretion/biofilm formation would be ideal, but as far as the author is aware no such approach has been used successfully in membrane treatment as of yet.

#### **1.1.7. Biofilm disruption**

In the biofilm literature, there has been a new approach to disrupt biofilm formation on non-membrane materials through the use of bioactive, but non-biocidal molecules. One of the most promising classes of molecules discussed is 2-aminoimidazoles (2-AIs), which are proposed to interfere with two-component regulatory systems through binding to response regulator proteins.<sup>59-61</sup> The two component-regulatory systems are responsible for bacteria sensing and responding to environmental changes; and disruptions of these systems could inhibit bacteria from sensing/reacting to chemical signals from other bacteria, changing from planktonic to sessile state, producing pilli, and excreting EPS.<sup>59-64</sup>

2-AIs have not been previously incorporated into water treatment membranes, but have been used successfully in other applications and present a promising alternative for application to membrane biofouling prevention. 2-AIs have some advantages, making them an ideal candidate for use in water treatment membranes. The proposed system disrupted by 2-AIs is conserved in many different types of bacteria and so 2-AIs are widely effective at inhibiting biofilm formation.<sup>62,63,65-67</sup> 2-AIs are one of the only molecule classes that maintain anti-biofilm activity across different classes, orders, and phyla of bacteria.<sup>60</sup> The anti-biofilm activity of 2-AIs has also been preserved when incorporated into polymers and is stable under pH and temperature ranges that are relevant to membrane treatment.<sup>61</sup>

#### **1.1.8. Summary of motivation**

Biofouling is one of the main operational problems in the use of water purification membranes. This issue limits water productivity, treated water quality, and

membrane life, and increases energy and other operational (e.g., membrane cleaning) costs. Accordingly, there is a need for an effective, widely applicable technology for controlling biofouling on water purification membranes.

## **1.2. Objectives**

### **1.2.1. Overall goal**

The overall goal of this dissertation is to develop and evaluate the performance of a novel anti-biofouling reverse osmosis (RO) membrane(s) with 2-AI(s) incorporated as the active compound.

### **1.2.2. Specific objectives**

To achieve this overall research goal, the dissertation meets the following specific objectives:

- (1) to synthesize and evaluate 2-AI molecules in terms of their capacity to be incorporated into polyamide active layers and their capability to inhibit biofilm
- (2) to develop an anti-biofouling water purification membrane(s) through 2-AI incorporation into active layers of commercially available RO membranes,
- (3) to develop an anti-biofouling water purification membrane(s) through 2-AI incorporation into active layers of RO membranes during polyamide casting,
- (4) to characterize 2-AI membrane(s) performance in terms of biofouling inhibition, water productivity, and contaminant removal.

### 1.3. Dissertation Organization

This dissertation is organized into six chapters and three appendices. Chapter 1 introduces background concepts and explains the motivations for the dissertation, setting the framework for the subsequent chapters. Chapters 2-4 describe the research performed to address the overall and specific objectives of the dissertation. Chapters 2-4 are independently comprehensive with introductions, materials and methods, results and discussions, conclusions, acknowledgements, and reference sections. The subjects of Chapters 2-4 are described briefly:

- Chapter 2: This chapter addresses specific objective 1 and 2, and partly addresses specific objective 4. Novel anti-biofouling water purification membranes are developed through the incorporation of 2-AI molecules into the active layer of commercial RO/NF membranes. The process of choosing which 2-AI to incorporate into the membrane active layers, as well as the extent and the stability of 2-AI incorporation are reported. The impact of 2-AI incorporation on the physico-chemical properties, water permeability, and salt rejection of the membranes are discussed. The extent of biofilm inhibition by 2-AI membranes in comparison to (2-AI lacking) control membranes is quantified.
- Chapter 3: This chapter addresses specific objective 3 and partly addresses specific objective 4. Novel anti-biofouling water purification membranes are developed through the incorporation of 2-AI molecules during membrane active layer casting. The extent and stability of 2-AI incorporation are reported. The impact of 2-AI incorporation on the physico-chemical properties, water permeability, and salt rejection of the membranes are discussed. The extent of



biofilm inhibition by 2-AI membranes in comparison to (2-AI lacking) control membranes is quantified.

- Chapter 4: This chapter addresses specific objective 4. The application of novel 2-AI membranes under operationally realistic conditions is described. 2-AI membranes and (2-AI lacking) control membranes are fouled by combinations of organic matter accumulation, bacterial cell deposition, and biofilm formation, while operated in cross-flow mode over 75 hours. The characteristics of foulant layers on the 2-AI and control membranes are analyzed and the performance of the membranes reported. The differences in water permeability and contaminant rejection between 2-AI and control membranes were related to differences in fouling observed.

Chapter 5 integrates the results from Chapters 2-4 and provides the overall conclusions of the dissertation work. Chapter 6 describes how the work in this dissertation can be carried forward and what questions remain to be answered. The appendices following Chapter 6 include supporting materials that are referenced in the text of Chapters 2-4.

## REFERENCES

- (1) Leverenz, H. L.; Tchobanoglous, G.; Asano, T. Direct Potable Reuse: A Future Imperative. *J. Water Reuse Desalin.* **2011**, *1* (1), 2.
- (2) Khawaji, A. D.; Kutubkhanah, I. K.; Wie, J. M. Advances in Seawater Desalination Technologies. *Desalination* **2008**, *221*, 47–69.
- (3) Shannon, M. A.; Bohn, P. W.; Elimelech, M.; Georgiadis, J. G.; Mariñas, B. J.; Mayes, A. M. Science and Technology for Water Purification in the Coming Decades. *Nature* **2008**, *452* (March), 301–310.
- (4) Tchobanoglous, G.; Leverenz, H.; Nellor, M.; Crook, J. *Direct Potable Reuse: A Path Forward*; 2011.
- (5) U.S. Environmental Protection Agency. *2012 Guidelines for Water Reuse*; EPA/600/R-12/618; Washington D.C., 2012.
- (6) Rodriguez, C.; Van Buynder, P.; Lugg, R.; Blair, P.; Devine, B.; Cook, A.; Weinstein, P. Indirect Potable Reuse: A Sustainable Water Supply Alternative. *Int. J. Environ. Res. Public Health* **2009**, *6* (3), 1174–1209.
- (7) Schroeder, E.; Tchobanoglous, G.; Leverenz, H.; Asano, T. *Direct Potable Reuse: Benefits for Public Water Supplies, Agriculture , the Environment , and Energy Conservation*; NWRI-2012-01; 2012.
- (8) Tal, A. Evolving Israel’s Sustainability: Water Management Strategy. *Science* (80-. ). **2006**, *313*, 1081–1084.
- (9) Schiermeier, Q. Water: Purification with a Pinch of Salt. *Nature* **2008**, *452* (March 2008), 260–261.
- (10) Magara, Y.; Kawasaki, M.; Sekino, M.; Yamamura, H. Development of Reverse Osmosis Membrane Seawater Desalination in Japan. *Water Sci. Technol.* **2000**, *41* (10–11), 1–8.
- (11) Reverter, J. A.; Talo, S.; Alday, J. Las Palmas III - The Success Story of Brine Staging. *Desalination* **2001**, *138*, 207–217.
- (12) Greenlee, L. F.; Lawler, D. F.; Freeman, B. D.; Marrot, B.; Moulin, P. Reverse Osmosis Desalination: Water Sources, Technology, and Today’s Challenges. *Water Res.* **2009**, *43* (9), 2317–2348.
- (13) Semiat, R. Energy Issues in Desalination Processes. *Environ. Sci. Technol.* **2008**, *42* (22), 8193–8201.
- (14) Wilf, M.; Bartels, C. Optimization of Seawater RO Systems Design. *Desalination* **2005**, *173*, 1–12.

- (15) Flemming, H.-C. Reverse Osmosis Membrane Biofouling. *Exp. Therm. Fluid Sci.* **1997**, *14* (4), 382–391.
- (16) Hoek, E. M. V.; Elimelech, M. Cake-Enhanced Concentration Polarization: A New Fouling Mechanism for Salt-Rejecting Membranes. *Environ. Sci. Technol.* **2003**, *37* (24), 5581–5588.
- (17) Agenson, K. O.; Urase, T. Change in Membrane Performance due to Organic Fouling in Nanofiltration (NF)/reverse Osmosis (RO) Applications. *Sep. Purif. Technol.* **2007**, *55* (2), 147–156.
- (18) Herzberg, M.; Elimelech, M. Biofouling of Reverse Osmosis Membranes: Role of Biofilm-Enhanced Osmotic Pressure. *J. Memb. Sci.* **2007**, *295* (1–2), 11–20.
- (19) Huertas, E.; Herzberg, M.; Oron, G.; Elimelech, M. Influence of Biofouling on Boron Removal by Nanofiltration and Reverse Osmosis Membranes. *J. Memb. Sci.* **2008**, *318* (1–2), 264–270.
- (20) Xu, P.; Drewes, J. E.; Kim, T.-U.; Bellona, C.; Amy, G. Effect of Membrane Fouling on Transport of Organic Contaminants in NF/RO Membrane Applications. *J. Memb. Sci.* **2006**, *279* (1–2), 165–175.
- (21) Bellona, C.; Marts, M.; Drewes, J. E. The Effect of Organic Membrane Fouling on the Properties and Rejection Characteristics of Nanofiltration Membranes. *Sep. Purif. Technol.* **2010**, *74* (1), 44–54.
- (22) Herzberg, M.; Kang, S.; Elimelech, M. Role of Extracellular Polymeric Substances (EPS) in Biofouling of Reverse Osmosis Membranes. *Environ. Sci. Technol.* **2009**, *43* (12), 4393–4398.
- (23) Vogel, D.; Simon, A.; Alturki, A. A.; Bilitewski, B.; Price, W. E.; Nghiem, L. D. Effects of Fouling and Scaling on the Retention of Trace Organic Contaminants by a Nanofiltration Membrane: The Role of Cake-Enhanced Concentration Polarisation. *Sep. Purif. Technol.* **2010**, *73* (2), 256–263.
- (24) Bellona, C.; Drewes, J. E.; Xu, P.; Amy, G. Factors Affecting the Rejection of Organic Solutes during NF/RO Treatment--a Literature Review. *Water Res.* **2004**, *38* (12), 2795–2809.
- (25) Coronell, O.; González, M. I.; Mariñas, B. J.; Cahill, D. G. Ionization Behavior, Stoichiometry of Association, and Accessibility of Functional Groups in the Active Layers of Reverse Osmosis and Nanofiltration Membranes. *Environ. Sci. Technol.* **2010**, *44* (17), 6808–6814.
- (26) Habimana, O.; Semião, a. J. C.; Casey, E. The Role of Cell-Surface Interactions in Bacterial Initial Adhesion and Consequent Biofilm Formation on Nanofiltration/reverse Osmosis Membranes. *J. Memb. Sci.* **2014**, *454*, 82–96.

- (27) Khan, M. M. T.; Stewart, P. S.; Moll, D. J.; Mickols, W. E.; Burr, M. D.; Nelson, S. E.; Camper, A. K. Assessing Biofouling on Polyamide Reverse Osmosis (RO) Membrane Surfaces in a Laboratory System. *J. Memb. Sci.* **2010**, *349* (1–2), 429–437.
- (28) Elimelech, M.; Zhu, X.; Childress, A. E.; Hong, S. Role of Membrane Surface Morphology in Colloidal Fouling of Cellulose Acetate and Composite Aromatic Polyamide Reverse Osmosis Membranes. *J. Memb. Sci.* **1997**, *127*, 101–109.
- (29) Karkhanechi, H.; Takagi, R.; Matsuyama, H. Biofouling Resistance of Reverse Osmosis Membrane Modified with Polydopamine. *Desalination* **2014**, *336*, 87–96.
- (30) Low, D.; Hamood, A.; Reid, T.; Mosley, T.; Tran, P.; Song, L.; Morse, A. Attachment of Selenium to a Reverse Osmosis Membrane to Inhibit Biofilm Formation of *S. Aureus*. *J. Memb. Sci.* **2011**, *378* (1–2), 171–178.
- (31) Flemming, H.-C.; Schaule, G.; Griebe, T.; Schmitt, J.; Tamachkierowa, a. Biofouling—the Achilles Heel of Membrane Processes. *Desalination* **1997**, *113* (2–3), 215–225.
- (32) Sweity, A.; Oren, Y.; Ronen, Z.; Herzberg, M. The Influence of Antiscalants on Biofouling of RO Membranes in Seawater Desalination. *Water Res.* **2013**, *47* (10), 3389–3398.
- (33) Matin, A.; Khan, Z.; Zaidi, S. M. J.; Boyce, M. C. Biofouling in Reverse Osmosis Membranes for Seawater Desalination: Phenomena and Prevention. *Desalination* **2011**, *281*, 1–16.
- (34) Yu, C.; Wu, J.; Contreras, A. E.; Li, Q. Control of Nanofiltration Membrane Biofouling by *Pseudomonas Aeruginosa* Using D-Tyrosine. *J. Memb. Sci.* **2012**, *423–424*, 487–494.
- (35) Ying, W.; Siebdrath, N.; Uhl, W.; Gitis, V.; Herzeberg, M. New Insights on Early Stages of RO Membranes Fouling during Tertiary Wastewater Desalination. *J. Memb. Sci.* **2014**, *466*, 26–35.
- (36) Nguyen, T.; Roddick, F.; Fan, L. Biofouling of Water Treatment Membranes: A Review of the Underlying Causes, Monitoring Techniques and Control Measures. *Membranes (Basel)*. **2012**, *2* (4), 804–840.
- (37) Al Ashhab, A.; Herzberg, M.; Gillor, O. Biofouling of Reverse-Osmosis Membranes under Different Shear Rates during Tertiary Wastewater Desalination: Microbial Community Composition. *Water Res.* **2014**, *67*, 86–95.
- (38) Baker, J. S.; Dudley, L. Y. Biofouling in Membrane Systems — A Review. *Desalination* **1998**, *118* (1–3), 81–89.
- (39) Al-Ahmad, M.; Aleem, F. A.; Mutiri, A.; Ubaisy, A. Biofuoling in RO Membrane Systems. Part 1: Fundamentals and Control. *Desalination* **2000**, *132* (October), 173–179.

- (40) Malaeb, L.; Le-Clech, P.; Vrouwenvelder, J. S.; Ayoub, G. M.; Saikaly, P. E. Do Biological-Based Strategies Hold Promise to Biofouling Control in MBRs? *Water Res.* **2013**, *47* (15), 5447–5463.
- (41) Lee, W.; Ahn, C. H.; Hong, S.; Kim, S.; Lee, S.; Baek, Y.; Yoon, J. Evaluation of Surface Properties of Reverse Osmosis Membranes on the Initial Biofouling Stages under No Filtration Condition. *J. Memb. Sci.* **2010**, *351* (1–2), 112–122.
- (42) Ying, W.; Gitis, V.; Lee, J.; Herzberg, M. Effects of Shear Rate on Biofouling of Reverse Osmosis Membrane during Tertiary Wastewater Desalination. *J. Memb. Sci.* **2013**, *427*, 390–398.
- (43) Subramani, A.; Hoek, E. M. V. Direct Observation of Initial Microbial Deposition onto Reverse Osmosis and Nanofiltration Membranes. *J. Memb. Sci.* **2008**, *319*, 111–125.
- (44) Varin, K. J.; Lin, N. H.; Cohen, Y. Biofouling and Cleaning Effectiveness of Surface Nanostructured Reverse Osmosis Membranes. *J. Memb. Sci.* **2013**, *446*, 472–481.
- (45) O'Toole, G. a; Kolter, R. Flagellar and Twitching Motility Are Necessary for *Pseudomonas Aeruginosa* Biofilm Development. *Mol Microbiol* **1998**, *30*, 295–304.
- (46) Heffernan, R.; Habimana, O.; Semião, a. J. C.; Cao, H.; Safari, a.; Casey, E. A Physical Impact of Organic Fouling Layers on Bacterial Adhesion during Nanofiltration. *Water Res.* **2014**, *67*, 118–128.
- (47) DOW FILMTEC. *Filmtec NF90-400 Nanofiltration Element Product Information*; 609-00345–0406.
- (48) DOW FILMTEC. *FILMTEC SW30-2540 Membranes Product Information*; 609-00377–0406.
- (49) The Dow Chemical Company. *FILMTEC XLE-4040 Membranes Product Information*; 609-00245–1011.
- (50) Nitto Denko. *Foulants and Cleaning Procedures for Composite Polyamide RO Membrane Elements*; TSB107.21; 2011.
- (51) American Membrane Technology. *Pretreatment for Membrane Processes*; FS-12; 2007.
- (52) Al-Juboori, R. A.; Yusaf, T. Biofouling in RO System: Mechanisms, Monitoring and Controlling. *Desalination* **2012**, *302*, 1–23.
- (53) Altman, S. J.; Cappelle, M.; Clem, P. G.; Cook, A. W.; Christopher, H.; Hart, W. E.; Hibbs, M. R.; Ho, C. K.; Jones, H. D. T.; Khalsa, S.; Noek, R.; Sun, A. C.; Webb, S. W.; Mcgrath, L. K.; James, D. L.; Adout, A.; Elimelech, M.; Kang, S. *Analysis of Micromixers and Biocidal Coatings on Water Treatment Membranes to Minimize Biofouling*; SAND2009-8316; Albuquerque, NM, 2009.

- (54) Xu, J.; Wang, Z.; Yu, L.; Wang, J.; Wang, S. A Novel Reverse Osmosis Membrane with Regenerable Anti-Biofouling and Chlorine Resistant Properties. *J. Memb. Sci.* **2013**, *435*, 80–91.
- (55) Malaisamy, R.; Berry, D.; Holder, D.; Raskin, L.; Lepak, L.; Jones, K. L. Development of Reactive Thin Film Polymer Brush Membranes to Prevent Biofouling. *J. Memb. Sci.* **2010**, *350*, 361–370.
- (56) Vercellino, T.; Morse, A.; Tran, P.; Song, L.; Hamood, A.; Reid, T.; Moseley, T. Attachment of Organo-Selenium to Polyamide Composite Reverse Osmosis Membranes to Inhibit Biofilm Formation of *S. Aureus* and *E. Coli*. *Desalination* **2013**, *309*, 291–295.
- (57) Zhu, X.; Bai, R.; Wee, K. H.; Liu, C.; Tang, S. L. Membrane Surfaces Immobilized with Ionic or Reduced Silver and Their Anti-Biofouling Performances. *J. Memb. Sci.* **2010**, *363* (1–2), 278–286.
- (58) Hoffman, L. R.; D'Argenio, D. a; MacCoss, M. J.; Zhang, Z.; Jones, R. a; Miller, S. I. Aminoglycoside Antibiotics Induce Bacterial Biofilm Formation. *Nature* **2005**, *436*, 1171–1175.
- (59) Worthington, R.; Richards, J.; Melander, C. Small Molecule Control of Bacterial Biofilms. *Org. Biomol. Chem.* **2012**, *10* (37), 7457–7474.
- (60) Rogers, S.; Melander, C. Construction and Screening of a 2-Aminoimidazole Library Identifies a Small Molecule Capable of Inhibiting and Dispersing Bacterial Biofilms across Order, Class, and Phylum. *Angew. Chemie Int. Ed* **2008**, *47* (28), 5229–5231.
- (61) Peng, L.; DeSousa, J.; Su, Z.; Novak, B. M.; Nevzorov, A. a; Garland, E. R.; Melander, C. Inhibition of *Acinetobacter Baumannii* Biofilm Formation on a Methacrylate Polymer Containing a 2-Aminoimidazole Subunit. *Chem. Commun.* **2011**, *47* (17), 4896–4898.
- (62) Bourret, R. B.; Silversmith, R. E. Two-Component Signal Transduction. *Curr. Opin. Microbiol.* **2010**, *13*, 113–115.
- (63) Gotoh, Y.; Eguchi, Y.; Watanabe, T.; Okamoto, S.; Doi, A.; Utsumi, R. Two-Component Signal Transduction as Potential Drug Targets in Pathogenic Bacteria. *Curr. Opin. Microbiol.* **2010**, *13* (2), 232–239.
- (64) Beier, D.; Gross, R. Regulation of Bacterial Virulence by Two-Component Systems. *Curr. Opin. Microbiol.* **2006**, *9*, 143–152.
- (65) Thompson, R. J.; Bobay, B. G.; Stowe, S. D.; Olson, A. L.; Peng, L.; Su, Z.; Actis, L. a; Melander, C.; Cavanagh, J. Identification of BfmR , a Response Regulator Involved in Biofilm Development, as a Target for a 2-Aminoimidazole-Based Antibiofilm Agent. *Biochemistry* **2012**, No. 51, 9776–9778.

- (66) Hentzer, M.; Riedel, K.; Rasmussen, T. B.; Heydorn, A.; Andersen, J. B.; Parsek, M. R.; Rice, S. a.; Eberl, L.; Molin, S.; Høiby, N.; Kjelleberg, S.; Givskov, M. Inhibition of Quorum Sensing in *Pseudomonas Aeruginosa* Biofilm Bacteria by a Halogenated Furanone Compound. *Microbiology* **2002**, *148*, 87–102.
- (67) Hentzer, M.; Wu, H.; Andersen, J. B.; Riedel, K.; Rasmussen, T. B.; Bagge, N.; Kumar, N.; Schembri, M. a.; Song, Z.; Kristoffersen, P.; Manefield, M.; Costerton, J. W.; Molin, S.; Eberl, L.; Steinberg, P.; Kjelleberg, S.; Høiby, N.; Givskov, M. Attenuation of *Pseudomonas Aeruginosa* Virulence by Quorum Sensing Inhibitors. *EMBO J.* **2003**, *22* (15), 3803–3815.

## **CHAPTER 2: DEVELOPMENT OF ANTI-BIOFILM MEMBRANES THROUGH THE INCORPORATION OF 2-AMINOIMIDAZOLE INTO COMMERCIAL RO/NF MEMBRANES**

### **2. 1. Introduction**

Reverse osmosis (RO) and nanofiltration (NF) membrane treatment can be a powerful tool for improving water security worldwide, but the costs associated with membrane fouling are a major hindrance for efficient use and more widespread implementation of water reuse and desalination. Membrane fouling consists of the accumulation of particles, dissolved substances, and/or bacteria on the surface of the membrane, which results in membrane performance deterioration, including decreased water permeability and contaminant removal. Decreasing the fouling potential of membranes could lead to significant savings from decreased energy costs, fouling control and membrane cleaning, and extended membrane lifespan.<sup>1-5</sup> Given that fouling can lead to decreased contaminant removal, lessening fouling would not only lower costs but also potentially improve the quality of the product water.<sup>6-8</sup>

Four types of fouling occur in membrane systems: organic, inorganic, colloidal, and biofouling. All but biofouling can be dealt with by pretreatment of the feed waters; however, even after 4-log removal of microbes, significant biofouling can occur.<sup>3,9-11</sup> Biofouling is ubiquitous in membrane treatment plants and is frequently irreversible and consequently, cleaning will not fully restore membrane efficiency. Biofouling consists of the formation of a biofilm on the membrane surface, and is thought to progress in several stages. The first stage is usually described as the initial adhesion of microorganisms, though this may be preceded by the



conditioning of the surface (e.g. adhesion of organic substances that increase attachment of microbes).<sup>3,10-14</sup> The initial attachment is critical because if adhesion can be avoided then biofouling may be prevented altogether. After adhesion, microbes grow, multiply, and excrete extracellular polymeric substances (EPS), forming what is defined as a biofilm, comprised of cells and EPS. The bacteria within the biofilm can communicate with and attract other bacteria (quorum sensing) from the external environment. The biofilm will continue to grow through continued accumulation of EPS, adherence/recruitment of additional microbes and particulates from the feed water, and reproduction within the biofilm.<sup>3,11-13</sup> The majority of biofilm consists of EPS, up to 90% by volume; therefore, preventing EPS excretion could be a highly effective strategy to control biofouling.<sup>3,11,15</sup>

While application of biocides and membrane cleaning are commonly used to remove and prevent biofilm, there is no current widely applied control strategy or combination of strategies that is efficacious and cost-effective for preventing or controlling biofouling on RO/NF membranes. To this end, there has been an effort by researchers to alter the membrane active layer to combat biofouling,<sup>4,16-25</sup> since contact is initially established on the polyamide active layer and properties of the active layer have a significant impact on fouling.<sup>26-29</sup> Most membrane modification studies either incorporate biocides into the membrane active layer or alter the surface physical properties to make the membrane less amenable to attachment. Incorporation of biocides is intended to inactivate or kill bacteria rather than prevent attachment. This approach has had limited efficacy in inhibiting biofouling and in some cases has promoted biofouling.<sup>4,30</sup> Approaches to altering surface physical properties include nanopatterning and decreasing surface hydrophobicity because roughness, hydrophobicity, and decreased surface

charge have been linked to increased biofouling potential.<sup>4,16,17,27-29</sup> The efficacy of modifying physical properties of membranes has been limited, most likely because once bacteria attach to a surface, the physical modifications do not actively prevent excretion of EPS or biofilm formation. Thus, a more promising approach to biofouling control would be to prevent both bacterial attachment and EPS excretion/biofilm formation without activating a protective response by the bacteria.

Another approach to control biofilm is disruption of biofilm formation by bioactive but non-biocidal chemicals. One of the most effective compound classes examined in the literature has been 2-aminoimidazoles (2-AIs),<sup>31-33</sup> which inhibit bacterial attachment to surfaces and biofilm formation. 2-AIs have been reported to act both as film dispersants and inhibitors, which are thought to broadly target response regulator proteins in two-component bacterial regulatory systems that control biofilm development, cell attachment, pilli production, and cell morphology.<sup>31-37</sup> The disrupted signaling networks and response regulator proteins that are the proposed targets are present in all bacteria, and 2-AIs have been one of the only non-biocidal class of molecule thus far to be shown as effective at preventing biofilm formation and dispersing existing biofilms across different classes, orders, and phyla of bacteria.<sup>32,34</sup> Additionally, 2-AIs anti-biofilm activity is preserved upon incorporation into polymers.<sup>33</sup> Non-biocidal 2-AIs have been successfully used in medical<sup>38,39</sup> and agricultural<sup>40</sup> applications, and are promising candidates for membrane biofouling prevention and control.

Accordingly, we sought to evaluate incorporation of 2-AIs into commercially available RO/NF membranes as anti-biofouling agents. Our specific objectives were: (1) to demonstrate

that 2-AIs are amenable to incorporation by covalent bonding to the membrane active layer and, once bonded, maintain anti-biofouling properties; (2) to prioritize a specific 2-AI based on ability to inhibit biofilms and to incorporate this 2-AI into four commercial membranes using carbodiimide induced grafting; (3) to characterize the extent and stability of 2-AI incorporated into the membranes; (4) to characterize the changes in the physico-chemical properties of the membranes due to incorporation of 2-AI; and (5) to evaluate the performance of 2-AI-modified membranes compared to unmodified commercial membranes in terms of biofilm inhibition, water productivity, and salt rejection.

## **2.2. Materials and Methods**

### **2.2.1. Reagents and membranes**

All reagents were ACS reagent grade or better, purchased from commercial sources, and used without further purification unless otherwise noted. House-prepared ultrapure water ( $\geq 17.9$  M $\Omega$ .cm) was used for all aqueous solutions unless otherwise noted. Commercial membranes were obtained from Hydranautics, Oceanside, CA (ESPA3 and SWC4+) and The Dow Chemical Company, Midland, MI (XLE and NF270) as flat sheets. The ESPA3, SWC4+, and XLE membranes have MPD-based polyamide active layers.<sup>41</sup> The NF270 membrane has a piperazine-based polyamide active layer.<sup>41</sup>

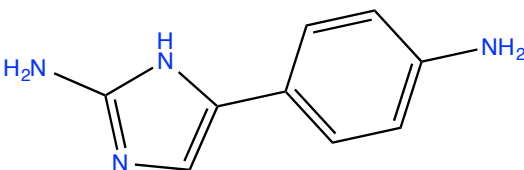
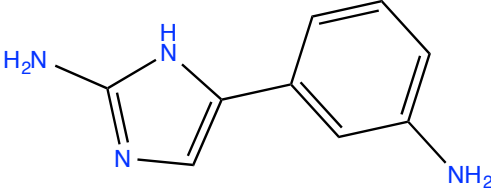
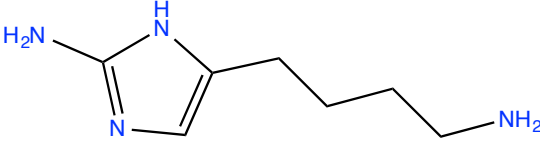
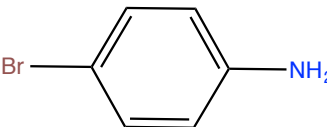
### **2.2.2. Synthesis of 2-aminoimidazole (2-AI) compounds**

The 2-AI derivatives and benzoyl conjugates were synthesized in-house. Structures and purities were confirmed by proton nuclear magnetic resonance (<sup>1</sup>H NMR). Synthetic procedures and <sup>1</sup>H NMR data are presented in detail in the *Supporting Information*.

### 2.2.3. Model reaction for incorporation of 2-AIs into membrane active layers

Benzoic acid was used as a polyamide surrogate and 2-AI-para (**Table 1**) as a representative 2-AI to be appended to the membrane matrix. Benzoic acid and 2-AI were mixed in water (pH>8) in a 1:1 ratio. N-methylmorpholine (2 eq) was added as an organic base, followed by 1-ethyl-3-(3-dimethylaminopropyl)carbodiimide (2 eq, EDC) and hydroxybenzotriazole (1 eq) as catalyst. The solution was stirred overnight (~18 hours). Products were extracted with chloroform, dried, and solvent was evaporated under vacuum. The reaction mixture was analyzed by LC/ESI-MS.

**Table 2.1.** The three 2-AI compounds and surrogate (4-bromoaniline) considered for incorporation into commercial membranes.

IUPAC Name	Molecule Abbreviation	Structure
5-(4-aminophenyl)-1 <i>H</i> -imidazol-2-amine	2-AI-para	
5-(3-aminophenyl)-1 <i>H</i> -imidazol-2-amine	2-AI-meta	
5-(4-aminobutyl)-1 <i>H</i> -imidazol-2-amine	2-AI-butyl	
4-bromoaniline	bromoaniline	

#### 2.2.4. 2-AI benzoyl conjugates

The benzoyl conjugates of the 2-AIs in **Table 1** were synthesized in house for biofilm inhibition assays (procedure given in *Supporting Information*).

#### 2.2.5. Crystal violet biofilm inhibition assay

A PA14 crystal violet biofilm inhibition assay described elsewhere<sup>42</sup> was used to quantify the ability of 2-AI-benzoyl compounds to inhibit PA14 biofilm formation. In brief, for each 2-AI compound, the assay was repeated 2 or 3 times on separate days with a range of concentrations and 8 replicates per concentration. A PA14 optical density at 600 nm (OD<sub>600</sub>) of 0.05 was used and incubation was 6 hours at 37° C.

#### 2.2.6. Incorporation of 2-AI-para into commercial membranes

To incorporate 2-AI-para into the commercial membranes a procedure (see **Figure 2.1.**) was used where carboxylic acid groups of the polyamide matrix were activated so that the 2-AI could attach at that site. A solution of 2-AI-para (1.6 mmol), EDC (1.0 mmol), *N*-methylmorpholine (1.5 mmol), and hydroxybenzotriazole (1.0 mmol) in ultrapure water that was then adjusted to pH>8 with sodium hydroxide and stirred vigorously for 20 minutes, and the commercial membrane (425 cm<sup>2</sup>) was then immersed. The solution was stirred gently overnight (~18 hours), avoiding contact of the stir bar with the membrane. The membrane was removed from the solution, rinsed thoroughly with ultrapure water and then stored in ultrapure water until used.

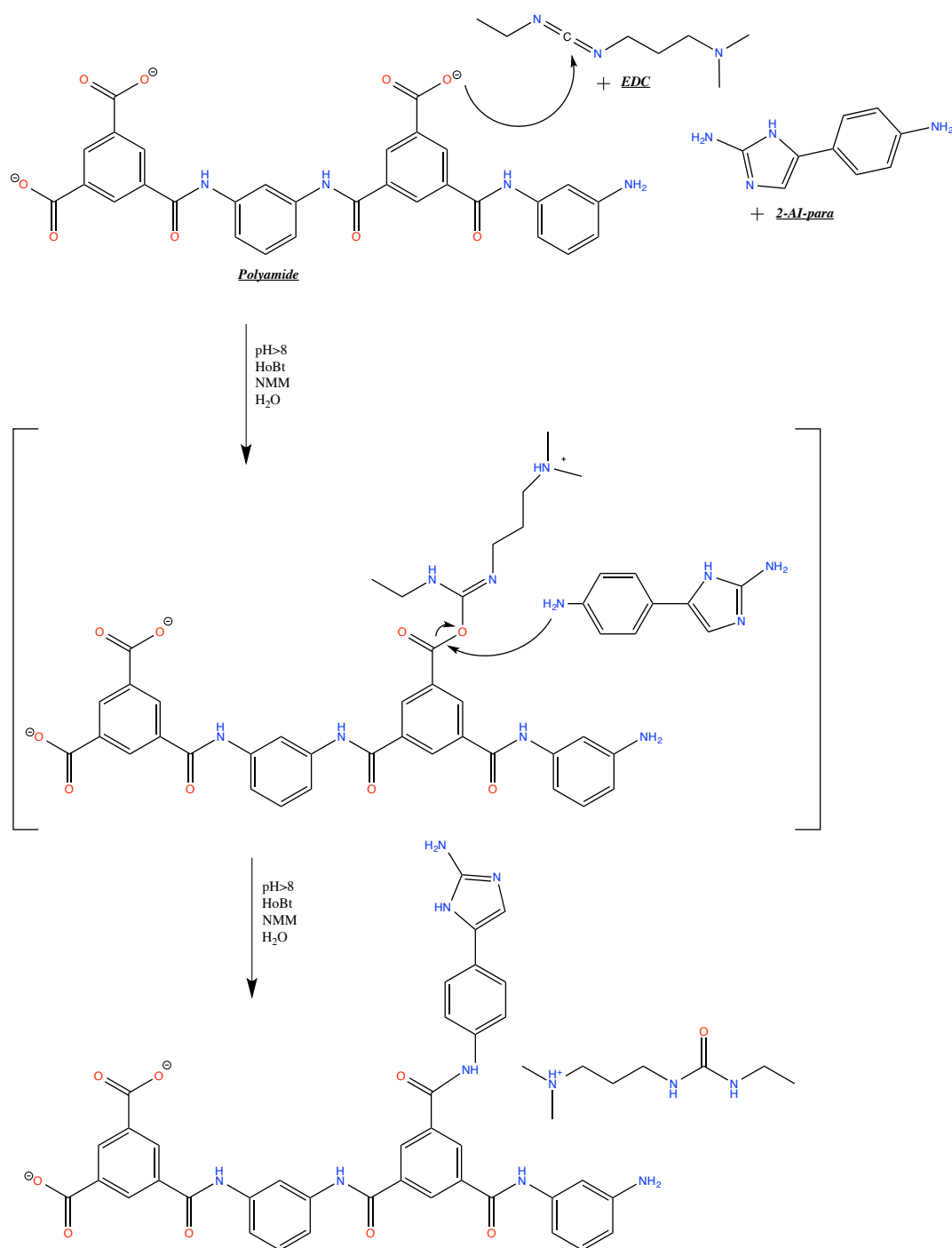


**Figure 2.1.** Mechanism of 2-AI incorporation into polyamide membrane matrix. The deprotonated carboxylic acid groups (pH > 8) of the MPD-based polyamide (or polypiperazinamide for NF270) membrane are activated by coupling with EDC (Top) to form a urethane intermediate (Middle); which is displaced by the 2-AI to generate an amide linkage (Bottom). The linkage can be formed at a primary amino group (as shown) or an imidazole nitrogen. HoBt=hydroxybenzotriazole, NMM=n-methylmorpholine, EDC=1-ethyl-3-(3-dimethylaminopropyl)carbodiimide, 2-AI-para=5-(4-aminophenyl)-1H-imidazol-2-amine.

#### **2.2.7. 4-bromoaniline incorporation**

4-Bromoaniline was incorporated into the commercial membranes by the procedure described above (*Section 2.2.6*).

#### **2.2.8. Filtration of water with bromoaniline-modified membranes**

Bromoaniline-modified XLE and NF270 membrane samples were placed in a dead-end stirred cell (HP4750, Sterlitech, Kent, WA) filled with ultrapure water. The cell was stirred at 350 rpm and placed under 200 psi of pressure for up to 100 hours. When necessary, pressure was released and the cell refilled with solution. The bromoaniline-modified membranes before and after filtration were analyzed by RBS and bromine concentration quantified and compared to assess stability of incorporation.

#### **2.2.9. Membrane cleaning**

Bromoaniline-modified NF270 membranes were subjected to cleaning procedures using either citric acid solution (2%, pH=2.2) or ethylenediaminetetraacetic acid/sodium tripolyphosphate solution (0.8%/2%, pH=10.2). Samples were immersed in cleaning solution and shaken for 1 hour, then washed with ultrapure water three times. Membranes that were evaluated in both cleaning and filtration tests, were first subjected to the filtration tests. The bromoaniline-modified membranes before and after cleaning were analyzed by RBS and bromine concentration quantified and compared to assess stability of incorporation.

#### **2.2.10. Attenuated total reflectance-Fourier transform infrared spectroscopy (ATR-FTIR)**

ATR-FTIR analyses were performed at a resolution of  $2\text{ cm}^{-1}$  over a  $400\text{--}3997\text{ cm}^{-1}$  range with a Bruker Alpha spectrometer (Bruker Optics, Billerica, MA) using an IR source at a  $45^\circ$  incident angle and an Alpha-P ATR accessory that analyzed a sample area of  $3.1\text{ mm}^2$ . Samples were air-dried for  $> 48$  hours prior to analysis. A minimum of three replicate samples were analyzed for each sample type and 24 scans were performed per replicate sample. The spectra are reported as an average of replicates.

#### **2.2.11. Silver ion probing of membrane samples**

The process of active layer probing with  $\text{Ag}^+$  is described in detail elsewhere.<sup>43–45</sup> In brief, membrane samples were immersed in dilute silver nitrate solution at  $\text{pH}=10.5^{45}$  and the volume-averaged content of silver in active layer was quantified using RBS<sup>43,46</sup>. Duplicate or triplicate samples were prepared for each type of membrane.

#### **2.2.12. RBS**

RBS analyses were performed with a tandem Van de Graaff accelerator and a semi-automatic target system, as described elsewhere.<sup>46</sup> A  $2\text{-MeV He}^{2+}$  beam was used with incident, exit, and scattering angles of  $22.5^\circ$ ,  $42.5^\circ$ , and  $160^\circ$ , respectively, the fluence of  $\text{He}^{2+}$  beam maintained below  $10^{14}\text{ He}^{2+}/\text{cm}^2$  to prevent membrane damage.<sup>47,48</sup> The analysis area of each sample was approximately  $12.5\text{ cm}^2$ . SIMNRA 6.06v<sup>49</sup> was used to simulate RBS spectra from experimental data to determine elemental composition. Results are reported as an average and standard error of duplicate or triplicate samples.



### 2.2.13. Contact angle

The captive bubble method was applied as described in the literature.<sup>50</sup> Briefly, the membrane samples were attached to a non-treated crystal grade polystyrene support and immersed surface side down in ultrapure water as shown in *Supporting Information*. A 10  $\mu\text{L}$  air bubble was placed on the surface and an image is recorded within 15 seconds of bubble attachment with a high-resolution camera. For each membrane type, 4-8 replicate images in different areas of the membrane surface were collected and analyzed. The contact angle was calculated by multiple methods (manual angle, ellipse, and circle best fits) with ImageJ 1.47v software (NIH provided public domain Java image processing software)<sup>51</sup> with Contact Angle Plugin.<sup>52</sup> Manual angle on left, manual angle on right, and ellipse best fits yielded contact angles within  $0.3^\circ$ ; the circle method yielded contact angles  $5^\circ$  larger. We report the contact angles obtained with the ellipse best fit as this method appeared in the images to give the closest fit. Results are reported as an average and standard error of 4-8 replicate samples.

### 2.2.14. Zeta potential via streaming current

The membrane charge of control and 2-AI-modified membranes were analyzed with the streaming current method described elsewhere<sup>53</sup> using a SurPASS Electrokinetic Analyzer with an adjustable gap cell. The analyzer uses two membrane samples, each with an area of  $2.0\text{ cm}^2$ , for analysis. The channel height of the gap cell was adjusted to  $\sim 100\text{ }\mu\text{m}$  and a solution of 1.0 mM potassium chloride was used as the electrolyte solution. Streaming current was measured four times at each pH, initially from pH=6 to pH=11, and then with fresh solution from pH=8 to pH=4, adjusting pH with potassium hydroxide and hydrochloric acid. Measurements were repeated on separate days with different membrane samples. The zeta potentials were calculated

using the Helmholtz-Smoluchowski equation. Results reported correspond to the average zeta potential calculated from four measurements at each pH.

### **2.2.15. AFM**

Control and 2-AI-modified membrane samples were air dried for >48 hours prior to analysis. An Asylum Research MFP-3D AFM (Santa Barbara, CA) loaded with BudgetSensors Tap300AI tips (Sofia, Bulgaria) was operated in tapping mode to scan an area of  $10 \times 10 \mu\text{m}^2$  on each membrane sample. Root-mean-square (RMS) roughness was calculated for each sample from the surface topography profile collected.<sup>54</sup> Results are reported as the average and standard error of triplicate samples.

### **2.2.16. Membrane performance tests**

#### *2.2.16.1. Biofilm formation inhibition*

Membrane samples were dried for >24 hours prior to analysis. Each sample was then mounted in a frame between two aluminum plates (mirrored finish inside) positioned so that the active layer was in a window ( $1.0 \times 1.5 \text{ cm}^2$ ) in the top plate. The membrane surfaces were exposed to 300  $\mu\text{L}$  of PA14 solution ( $\text{OD}_{600}=0.05$ ) and incubated at room temperature for 24 hours. Following incubation, the membrane samples were removed from the frames, and rinsed thoroughly with ultrapure water to remove unattached bacteria and solution to quantify bacteria in biofilm. The membrane samples were each placed into 2.0 mL of LB broth, vortexed for 30 seconds, and then sonicated for 30 seconds. Vortexing and sonicating were repeated twice more. Samples were vortexed a final time immediately before collecting 150  $\mu\text{L}$  of the solution, for a total of three sonication and four vortexing cycles. The collected solution was diluted 10-fold

serially and  $9 \times 5 \mu\text{L}$  of each dilution was spotted onto LB-agar plates, which were incubated at  $37^\circ\text{C}$  overnight. For each dilution, colonies were counted and the areal density of colony forming units (CFUs), reported as  $\text{CFU} \cdot \text{cm}^{-2}$ . The areal densities of CFUs of 2-AI-modified membranes and corresponding control membranes were compared to calculate the percent inhibition ( $\%_{inh}$ ) by the formula

$$\%_{inh} = \left[ 1 - \left( \frac{\bar{x}_{2AI}}{\bar{x}_{CTL}} \right) \right] \times 100\%, \quad (1)$$

where  $\bar{x}_{2AI}$  and  $\bar{x}_{CTL}$  correspond to the mean of the areal density of CFUs for the 2-AI-modified membrane samples and commercial control samples, respectively. This analysis was repeated twice for each set of membranes on separate days, and each day 4-12 replicate samples for each type of membrane studied were tested. We report the average areal density of CFUs as an average  $\pm$  standard error, percent inhibition, and p-value for each day separately.

#### 2.2.16.2. *Water productivity and salt rejection*

Tests solutions consisted of  $500 \text{ mg} \cdot \text{L}^{-1}$  sodium chloride in ultrapure water with pH adjusted to and maintained at 8.0 with sodium hydroxide for all the membranes except NF270. For the latter, the test solution was  $500 \text{ mg} \cdot \text{L}^{-1}$  magnesium sulfate in ultrapure water at pH=8.0. Tests were performed using a bench scale cross-flow system with four flat-sheet cells in series. The system was operated at  $22.0^\circ \text{C}$ , with  $15 \text{ cm}^3 \cdot \text{s}^{-1}$  cross-flow velocity, and an applied trans-membrane pressure of 13.8 bar for 70-91 hours until water flux and salt rejection were stable. The water permeability coefficients ( $A$ ,  $\text{m} \cdot \text{s}^{-1} \cdot \text{bar}^{-1}$ ) were calculated according to the formula

$$A = \frac{J_w}{13.8 \text{ bar} \times 0.00146 \text{ m}^2} \quad (2)$$

where  $J_w$  ( $\text{m}^3 \cdot \text{s}^{-1}$ ) is the water flux. The percent salt rejection ( $\%R$ ) values were calculated as

$$\%R = \left[ 1 - \left( \frac{C_p}{C_f} \right) \right] \times 100\% \quad (3)$$

where  $C_p$  ( $\mu\text{S} \cdot \text{cm}^{-2}$ ) and  $C_f$  ( $\mu\text{S} \cdot \text{cm}^{-2}$ ) correspond to the conductivity of the permeate and the feed, respectively.

### 2.2.17. Statistical significance testing

Statistical significance testing was performed when appropriate to compare the performance and physico-chemical properties of control membranes and 2-AI-modified membranes. In general, a two-tail unpaired two-sample t-test assuming unequal variances was used. The null hypothesis ( $H_0$ ) was that the mean of the control membrane was equal to the mean of the 2-AI-modified membrane ( $\mu_{\text{ctl}} = \mu_{2\text{-AI}}$ ); the alternative hypothesis ( $H_1$ ) was that the means were not equal ( $\mu_{\text{ctl}} \neq \mu_{2\text{-AI}}$ ). A one-tailed test was used when comparing the biofilm results of the commercial control and 2-AI-modified membranes to evaluate whether the biofilm areal density of CFUs was significantly higher for control membranes than 2-AI-modified membranes ( $H_0: \mu_{\text{ctl}} = \mu_{2\text{-AI}}$  and  $H_1: \mu_{\text{ctl}} > \mu_{2\text{-AI}}$ ). Differences were considered to be significant for  $p < 0.15$ .

## 2.3. Results and Discussion

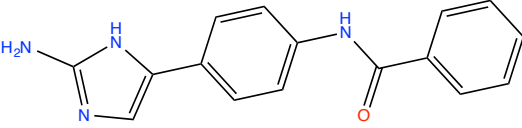
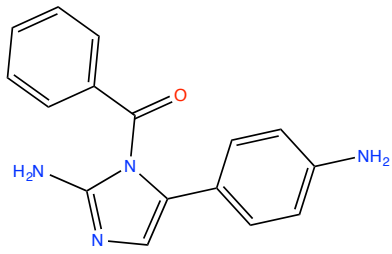
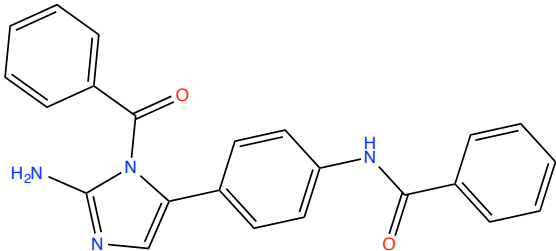
### 2.3.1. Model reaction for incorporation of a 2-ai into a commercial polyamide membrane

#### 2.3.1.1. Regiochemistry of attachment in a model reaction

Because structural integrity of the 2-AI moiety is critical to antifouling activity<sup>31,32</sup> the regiochemistry of EDC-mediated coupling was investigated by a model reaction under

conditions applicable to the target membranes. 2-AI attached to a 4-aminophenyl linker (2-AI-para; **Table 2.1.**) was selected as the 2-AI component and benzoic acid as a surrogate for the polyamide membrane matrix. Three major products were isolated and characterized by LC-ESI/MS and  $^1\text{H}$  NMR (**Table 2.2.**). Two products with parent ions at  $m/z$  279 ( $\text{M}+\text{H}^+$ ) were assigned as coupling at the linker amino group and the endocyclic nitrogen of the imidazole ring. Coupling at the endocyclic imidazole nitrogen rather than the 2-amino substituent of imidazole is based on observations that the imidazole endocyclic nitrogen is the preferred site for acylation of 2-AIs.<sup>55,56</sup> The predominant product (**Table 2.2.**) had a parent ion at  $m/z$  383 ( $\text{M}+\text{H}^+$ ), corresponding to a di-benzoylated product substituted at the amino group of the phenyl and an endocyclic imidazole nitrogen.

**Table 2.2.** Benzoic acid conjugates of 2-AI-para,  $m/z$   $[\text{M}+\text{H}]^+$ , by ESI-MS and relative yield calculated from peak areas of LC/ESI-MS trace.

Bonding site on 2-AI	Product Structure	$m/z$ $[\text{M}+\text{H}]^+$	Relative Yield of Products
Amino group of phenyl		279	12%
Imidazole Nitrogen		279	
Both amino of phenyl and imidazole nitrogen		383	88%

The model coupling reaction in bulk solution supported EDC-mediated coupling as the method for modification of the polyamide matrix, which has a high concentration of carboxylate groups<sup>43,45</sup>. Identification of the monobenzoylated product coupled through the 4-aminophenyl linker also indicates that the unmodified 2-AI head will be present in the modified membrane. Steric constraints posed by the membrane matrix makes bis-coupling, which was the predominant reaction in the model experiment, unlikely.

#### *2.3.1.2. Inhibition of biofilm formation by 2-AI-benzoyl conjugates*

The structures of the three 2-AIs that were evaluated for incorporation into commercial membranes are given in **Table 2.1.** To prioritize 2-AIs for incorporation into membranes, the purified 2-AI-mono benzoyl conjugates of the 2-AIs in **Table 2.1.**, where the 2-AIs are coupled to benzoyl at the amino group of the phenyl, were tested for inhibition of biofilm formation by *Pseudomonas aeruginosa* (PA14) and the results were evaluated using the calculated half-maximal inhibitory concentrations (IC<sub>50</sub>). The 2-AIs were assayed as mono benzoyl conjugates, with benzoyl coupled at the amino group of phenyl, to simulate attachment to the polyamide membrane matrix and to determine whether the matrix might influence activity. The 2-AI-para-mono benzoyl conjugate was most effective at inhibiting biofilm formation (IC<sub>50</sub>=162 µM), followed by the 2-AI-meta-mono benzoyl conjugate (IC<sub>50</sub>=256 µM), and 2-AI-butyl-mono benzoyl conjugate (IC<sub>50</sub>=420 µM) (**Figure 2.2.**) and on this basis 2-AI-para was selected for incorporation into the commercial membranes. It should be noted that all 2-AI benzoyl conjugates inhibited biofilm at micro-molar concentrations and any of the 2-AIs in **Table 2.1.** could be effective if incorporated into the membranes.

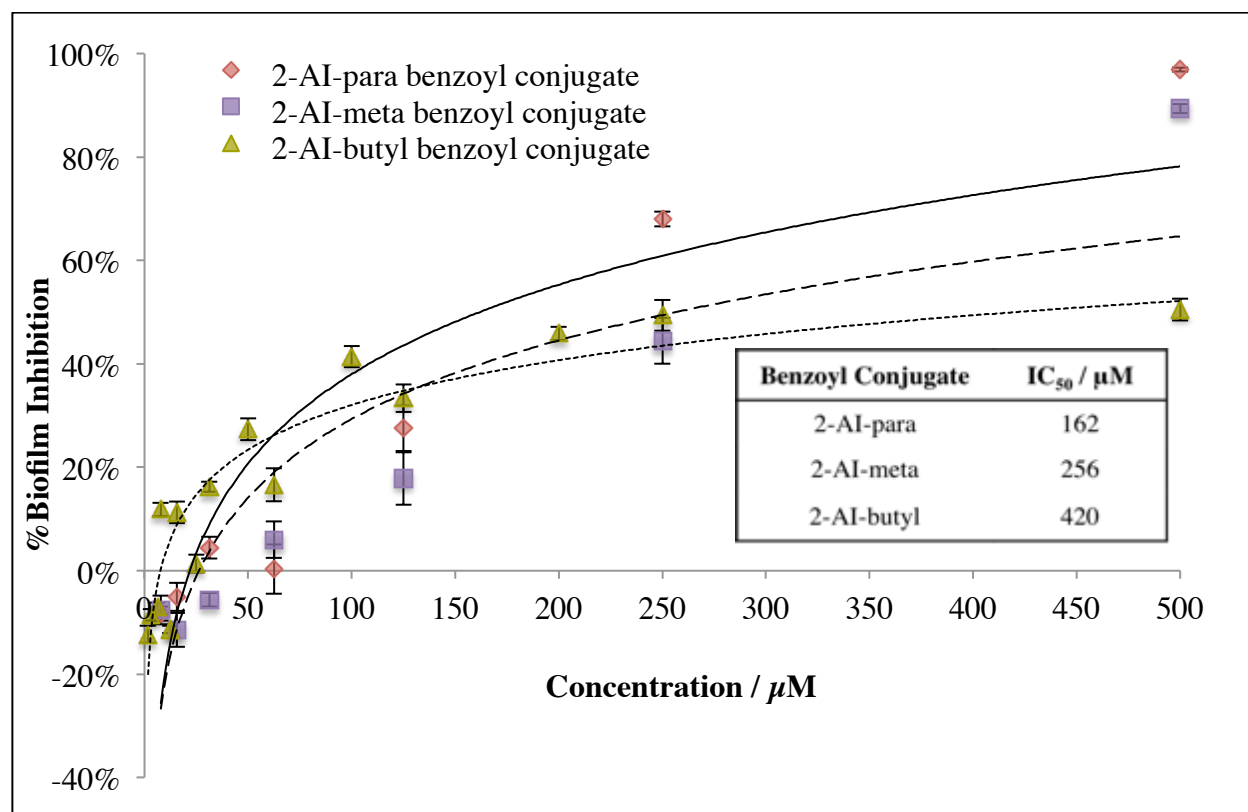


**Figure 2.2.** PA14 biofilm inhibition by 2-AI-mono benzoyl conjugates (at 7.8  $\mu\text{M}$ - 0.5 mM) and corresponding IC<sub>50</sub> values. Each point corresponds to 3 bioassays performed on separate days, with 8 replicates at each concentration on each day. Error bars indicate standard error. The corresponding best-fit logarithmic correlations are shown for each conjugate. IC<sub>50</sub> values were calculated using the best-fit logarithmic correlations.

To verify the influence of the regiochemistry of conjugation on biofilm inhibition, we evaluated the unconjugated 2-AI-para and the 2-AI-benzoyl conjugates at the target linker amino group, the endocyclic imidazole nitrogen, and bis-conjugate at these positions. Conjugation of 2-AI-para through the amino group of the phenyl linker enhanced biofilm inhibition, decreasing the IC<sub>50</sub> from 215  $\mu\text{M}$  to 162  $\mu\text{M}$ . 2-AI-para conjugated at an endocyclic imidazole nitrogen could not be synthesized in pure form. The corresponding 5-(4-nitrophenyl) 2-AI, and 5-(4-nitrophenyl)-1-benzoyl 2-AI (**Figure 2.3.**), were compared instead to assess the effect of endocyclic substitution of the imidazole ring. However, it should be noted that the highly electron withdrawing nitro substituent has a strong negative impact on biofilm inhibition, the unconjugated nitro analog (5-

(4-nitrophenyl)) having an  $IC_{50}$  of 1.2 mM compared to 215  $\mu$ M for the unconjugated 2-AI-para. The effect of conjugation at an endocyclic imidazole nitrogen can nevertheless be assessed through comparison of the activity of the two nitro compounds towards biofilm inhibition. While the unconjugated 5-(4-nitrophenyl) 2-AI inhibited PA14 biofilm formation with an  $IC_{50}$  of 1.2 mM, the 5-(4-nitrophenyl)-1-benzoyl 2AI, with coupling at the endocyclic imidazole nitrogen, showed no activity over a 16  $\mu$ M-2 mM range. This result is consistent with reports that any modification of the 2-AI ring eliminates anti-biofouling activity.<sup>31,32</sup> In accord with this result, di-benzoyl-2-AI conjugate (**Figure 2.3.**) was also inactive over the 16  $\mu$ M-2 mM range. The results of the model coupling reaction and biofilm inhibition tests indicate that anti-biofouling activity requires coupling of 2-AI to the polyamide membrane through the amino group of the phenyl linker, and this coupling pathway is expected to be present in the 2-AI-modified membrane.



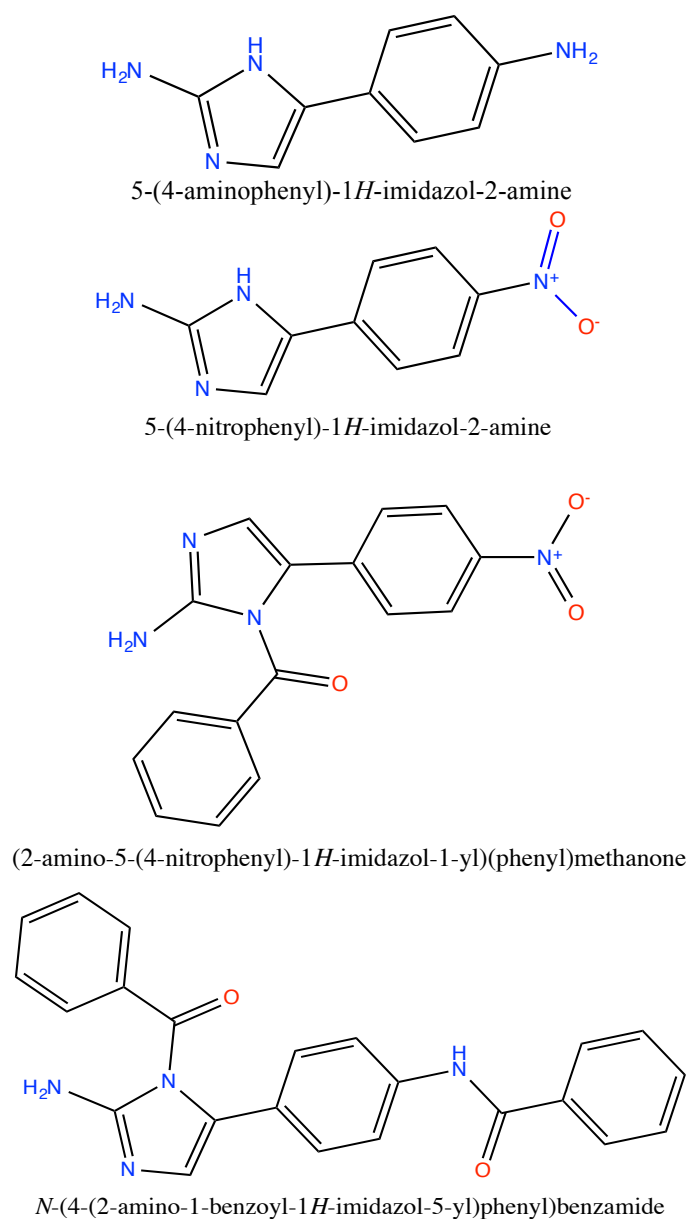


**Figure 2.3.** Chemical structures of unconjugated 2-AI-para (top), 5-(4-nitrophenyl) 2-AI (2<sup>nd</sup> row), 5-(4-nitrophenyl)-1-benzoyl 2-AI conjugate (3<sup>rd</sup> row), and di-benzoyl-2-AI conjugate (bottom).

While coupling of 2-AI-para to RO/NF membranes exclusively through the amino group of the phenyl linker could be achieved by protection of the endocyclic site, the requirement for deprotection following incorporation did not appear to be justified by the preliminary nature of this investigation, since the bioactive coupling product was likely to be present at a concentration

higher than the  $IC_{50}$  (162  $\mu$ M) necessary for significant biofilm inhibition. The target concentration requires 0.5% or less of the carboxylate groups in the polyamide active layer to be modified by conjugation at the amino group of the 2-AI-para linker. Hence, membrane incorporation experiments were pursued using unconjugated 2-AI-para.

### **2.3.2. Verification of 2-AI incorporation in the polyamide active layers of RO/NF membranes**

Differences in chemical bonding between 2-AI-modified membranes and corresponding control membranes were characterized by comparison of FTIR signatures for evidence of coupled product (**Figure 2.4**). The FTIR spectra of the unmodified membranes were consistent with previously published literature.<sup>41</sup> FTIR spectra of 2-AI-modified membranes showed increases in absorbance at the N—H frequencies 1650  $cm^{-1}$  and 3400  $cm^{-1}$  relative to the spectra of the corresponding control membranes, consistent with the increased concentration of N—H bonds expected in the 2-AI-modified structure.<sup>7,57</sup> Statistically significant increases ( $p < 0.05$ ) at 1650  $cm^{-1}$  were observed for the 2-AI-ESPA3 (82%), 2-AI-SWC4+ (9%) and 2-AI-NF270 (15%) membranes, while a substantial though not statistically significant increase ( $p = 0.11$ ) was observed for the 2-AI-XLE (9%) membrane. At 3400  $cm^{-1}$  a statistically significant increase ( $p < 0.05$ ) in absorbance was observed for the 2-AI-ESPA3 membrane (165%), while the remaining 2-AI-modified membranes showed substantial though not statistically significant increases (21%, 13% and 22% for 2-AI-SWC4+, 2-AI-NF270 and 2-AI-XLE membranes, respectively). Overall, we conclude that the FTIR comparison supports 2-AI incorporation into polyamide active layers.

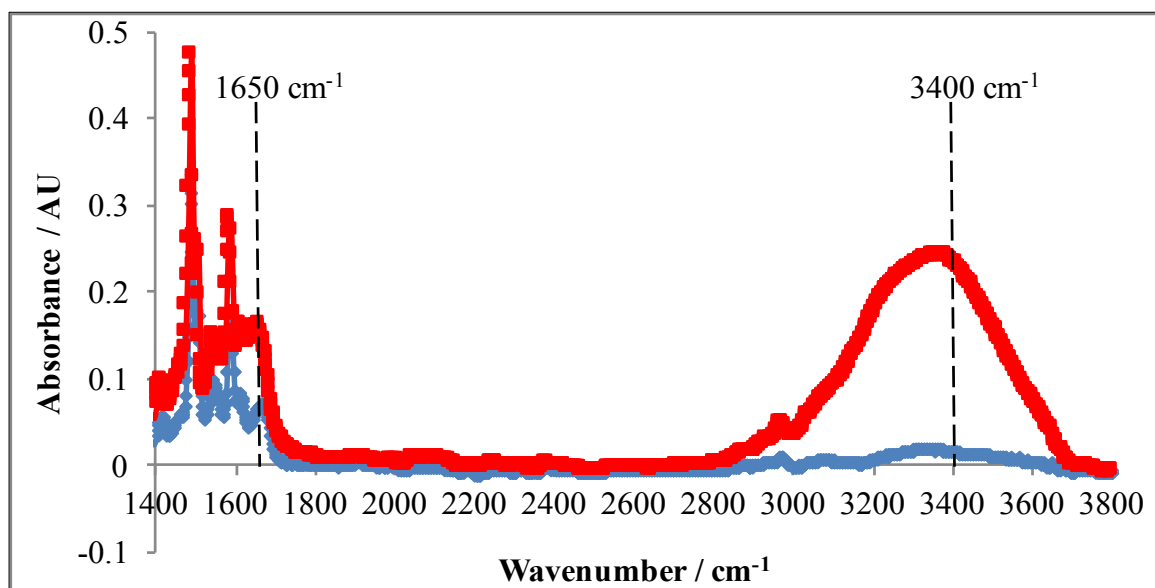


**Figure 2.4.** FTIR spectra of unmodified ESPA3 membrane (blue line) and ESPA3 modified by 2-AI-para (red line). Increase/presence of peaks at  $1650\text{ cm}^{-1}$  and  $3400\text{ cm}^{-1}$  are ascribed to C=N bond stretching and N-H bond stretching in the 2-AI structure respectively. Each spectrum reported corresponds to the average of triplicate sample measurements.

Additional support for 2-AI incorporation was obtained by probing the active layers of 2-AI-modified and unmodified control membranes for absorbance of  $\text{Ag}^+$  at pH=10.5 using Rutherford backscattering spectrometry (RBS) to analyze for differences in  $\text{Ag}^+$  concentration. The  $\text{Ag}^+$  cation pairs with the anionic carboxylate groups in the polyamide active layers. Additionally  $\text{Ag}^+$  may complex with amines, but in unmodified membranes this contributes negligibly to  $\text{Ag}^+$  concentration ( $\sim 0.015\text{ M}$  maximum); however, upon the incorporation of 2-AI, the amine concentration increases substantially and is expected to contribute to the  $\text{Ag}^+$  concentration.<sup>58,59</sup> **Figure 2.5.** shows that in all cases the volume-averaged concentration of  $\text{Ag}^+$ , was higher in 2-AI-modified membranes than control membranes. Since 2-AI incorporation occurs by coupling at the carboxylate groups, the concentration of anionic groups for ion pairing with  $\text{Ag}^+$  decreases in the active layer. Therefore, the observed increase in  $\text{Ag}^+$  concentration in

2-AI-modified membranes can be attributed to an increase in amine content and provides further evidence of the presence of 2-AI in the active layer.

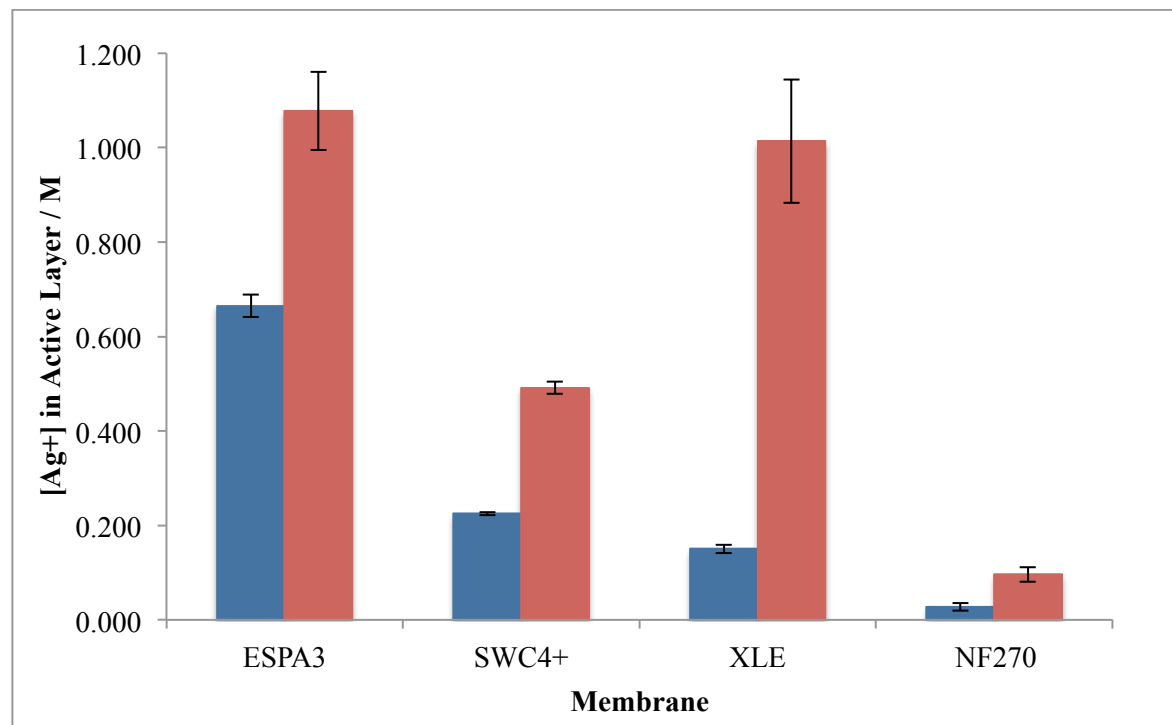


**Figure 2.5.** Volume-averaged concentration of  $\text{Ag}^+$  in polyamide active layers of commercial unmodified control (blue bars) and 2-AI-modified membranes (red bars) after exposure to  $\text{Ag}^+$  probing solution at pH=10.5. Results for the control membranes represent the concentration of carboxylic acid groups ( $\text{R-COO}^-$ ). Each bar represents the average of two samples and error bars indicate the range.

### 2.3.3. Evaluation of the concentration and stability of 4-bromoaniline incorporated in membranes as a surrogate for 2-AIs

4-Bromoaniline (bromoaniline; **Table 2.1.**) was incorporated into membranes as a surrogate for 2-AIs to estimate 2-AI concentration and stability in active layers by RBS.

### *2.3.3.1. Impact of procedural variables on concentration of bromoaniline incorporated into membranes*

An XLE membrane was exposed by total immersion or at the surface only, to the bromoaniline incorporation solution and the volume-averaged concentration of bromoaniline incorporated into the membrane active layer measured by RBS. The method of contact did not have a substantial impact on the concentration of bromoaniline incorporated into the polyamide active layer and therefore total immersion of membranes was adopted as the most convenient procedure for incorporation of bromoaniline into commercial membranes.

An XLE membrane was treated to varying concentrations (normalized by membrane area) of bromoaniline. At the lowest tested membrane-area normalized bromoaniline concentration ( $1.01 \times 10^{-3} \text{ Mm}^{-2}$ ) incorporation was more than three orders of magnitude higher (0.28 M) than the  $\text{IC}_{50}$  of 2-AI-para (162  $\mu\text{M}$ ) (**Figure 2.6a.**). Incorporation plateaued at approximately 0.76 M with a bromoaniline concentration of  $4.3 \times 10^{-2} \text{ Mm}^{-2}$ . Further bromoaniline incorporation tests were performed with a membrane-area normalized concentration of  $4.3 \times 10^{-2} \text{ Mm}^{-2}$ , which yielded the highest level of bromoaniline incorporation. At this concentration, the bromoaniline content of the polysulfone support layer of the XLE membrane was 0.08 M (**Figure 2.6b.**) Preparation of modified membranes using the same procedure and membrane-area normalized concentrations of 2-AI/bromoaniline allows direct comparison of membrane properties.

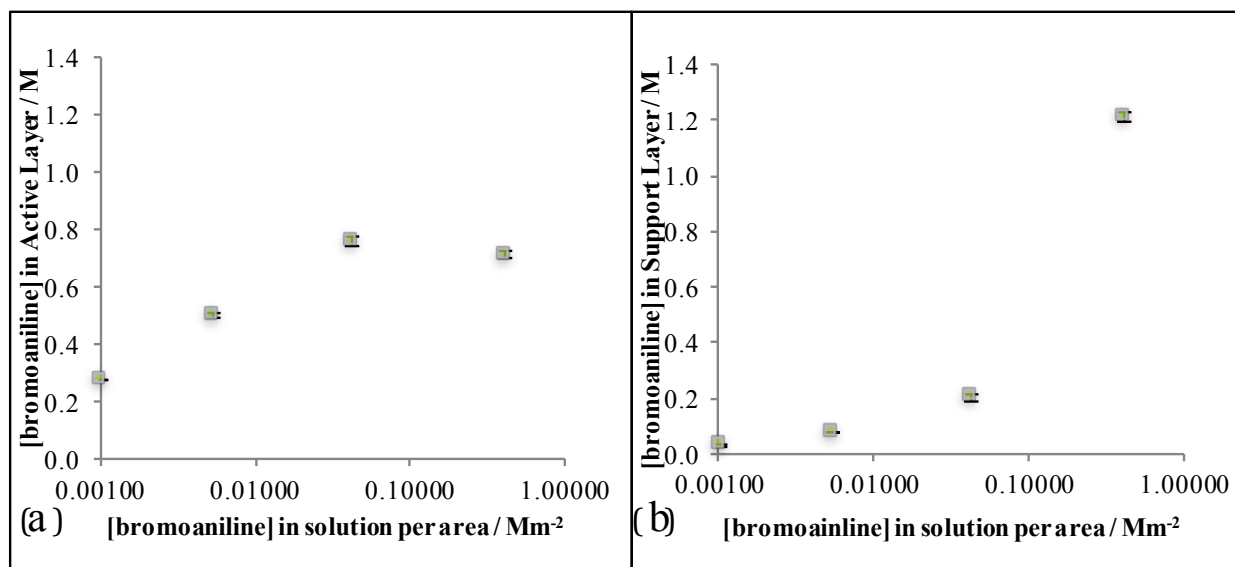


**Figure 2.6.** Concentration of bromoaniline incorporated into (a) polyamide active layer and (b) polysulfone support layer of an XLE membrane. The bromoaniline concentration in solution has been normalized by membrane area (425 cm<sup>2</sup>) ( $x$ -axes). Each point corresponds to 4 replicate measurements with error bars representing the standard error.

### 2.3.3.2. Bromoaniline concentration incorporated into different polyamide RO/NF membranes

Bromoaniline was incorporated into four different commercial membranes resulting in the active layer volume-averaged bromoaniline concentrations shown in **Figure 2.7.** Estimates of 2-AI incorporation based on these results are given in **Table 2.3.** The volume-averaged concentrations of carboxylate groups in unmodified membranes, estimated by Ag<sup>+</sup> probing (**Table 2.3.**, **Figure 2.5.**), tracked with the volume-averaged concentrations of bromoaniline incorporated, supporting the assumption that carboxylate groups have been modified by the coupling with bromoaniline. The apparent bromoaniline content in excess of the estimated carboxylate groups (**Table 2.3.**) is likely explained by bromoaniline that is trapped or adsorbed in the matrix as suggested by the stability experiments described below.

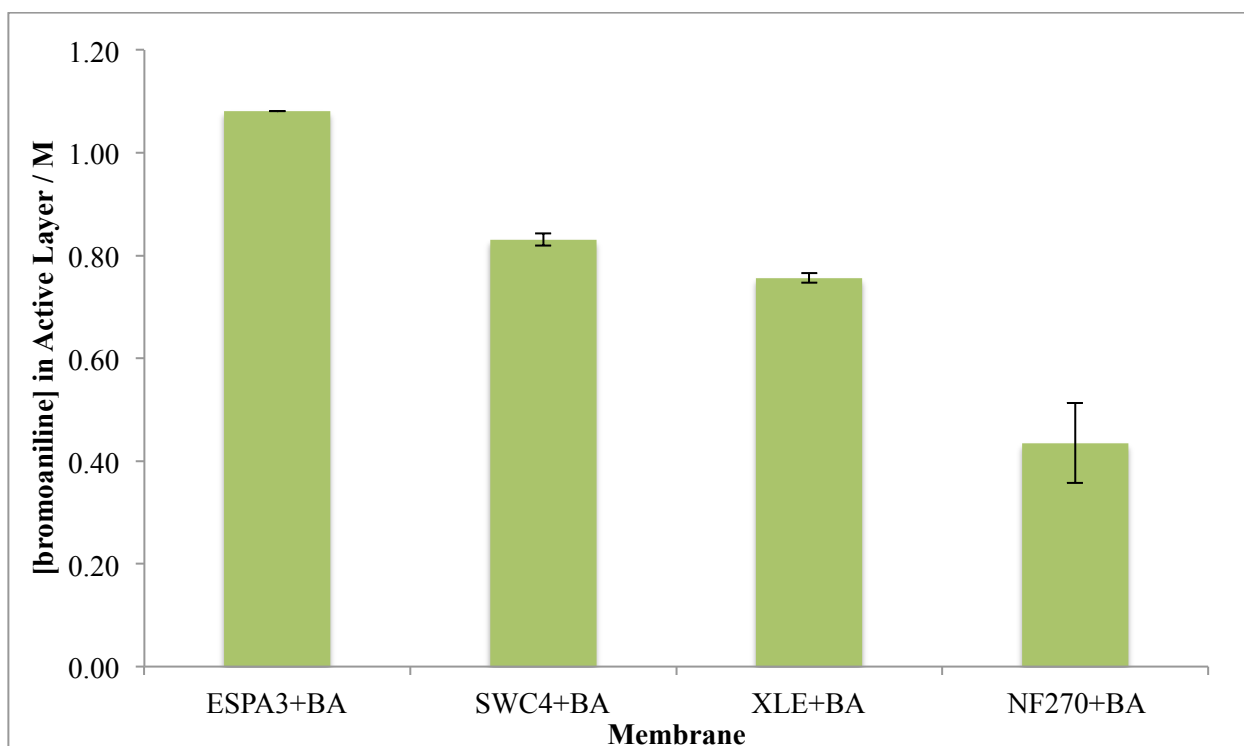


**Figure 2.7.** Volume-averaged concentrations of bromoaniline (BA) incorporated into the polyamide active layers of four modified commercial membranes. Each bar represents 2-4 replicate measurements and error bars indicate standard error.

**Table 2.3.** Characteristics of unmodified commercial control and 2-AI-modified membranes. Uncertainties indicate standard error. The significance of the difference in means between 2-AI and control membranes are indicated in the key.

Membrane	PA14 Biofilm inhibition <sup>d)</sup>	Estimated [2-AI] <sup>e)</sup> /M	[R-COO] <sup>f)</sup> /M	Contact Angle /degrees	RMS roughness /nm	Water permeability <sup>g)</sup> /x10 <sup>-6</sup> ms <sup>-1</sup> bar <sup>-1</sup>	Salt rejection <sup>g)</sup>
<b>ESPA 3</b>			0.66±0.02	26±2	77±2	1.69±0.01	98.7±0.1%
<b>ESPA3</b>	92% <sup>a)</sup> ;	1.08±0.01		23±2 <sup>c)</sup>	97±5 <sup>a)</sup>	1.27±0.01 <sup>a)</sup>	98.8% 0.1% <sup>c)</sup>
<b>+2-AI-para</b>	71% <sup>b)</sup>						
<b>SWC4+</b>			0.22±0.003	25±1	94±14	0.72±0.008	98.4±0.2%
<b>SWC4+</b>	96% <sup>b)</sup> ;	0.83±0.08		26±1 <sup>c)</sup>	114±16 <sup>c)</sup>	0.62±0.01 <sup>a)</sup>	97.8±0.1% <sup>a)</sup>
<b>+2-AI-para</b>	83% <sup>b)</sup>						
<b>XLE</b>			0.15±0.01	23±5	91±4	2.72±0.02	97.5±0.1%
<b>XLE</b>	86% <sup>b)</sup> ;	0.76±0.01		20±1 <sup>c)</sup>	79±7 <sup>c)</sup>	2.74±0.02 <sup>c)</sup>	97.2±0.1% <sup>c)</sup>
<b>+2-AI-para</b>	70% <sup>b)</sup>						
<b>NF270</b>			0.03±0.01	17±1	18±7	4.81±0.1	91.2±0.8%
<b>NF270</b>	76% <sup>b)</sup> ;	0.44±0.01		19±2 <sup>c)</sup>	26±13 <sup>c)</sup>	4.81±0.07 <sup>c)</sup>	91.3±1.1% <sup>c)</sup>
<b>+2-AI-para</b>	61% <sup>a)</sup>						

<sup>a)</sup> p-value<0.05. <sup>b)</sup> p-value<0.15. <sup>c)</sup> p-value≥0.15. <sup>d)</sup> each value corresponds to biofilm inhibition measured on one day. <sup>e)</sup> measured [bromoaniline] by RBS in bromoaniline-modified membranes. <sup>f)</sup> Measured as [Ag<sup>+</sup>] with RBS of Ag<sup>+</sup>-probed control membranes. <sup>g)</sup> Values obtained using 500 ppm sodium chloride solution for all membranes except for the NF270 and NF270+2-AI-para membranes for which 500 ppm magnesium sulfate was used instead.



### 2.3.3.3. Stability of incorporated bromoaniline

To approximate operational losses of 2-AI, bromoaniline-modified XLE membranes were used to filter ultrapure water in a dead-end cell for up to 100 hours. **Figure 2.8.** shows the volume-averaged bromoaniline concentration in the active layer, measured after filtration for different periods of time. After a significant loss within the first ~48 hours of filtration, the bromoaniline content plateaus at approximately 0.15 M, which is the concentration of carboxylate groups, estimated by  $\text{Ag}^+$  probing of the unmodified XLE membrane (**Table 2.3.**). As discussed above, the curve in **Figure 2.8.** can be explained by leaching of unreacted bromoaniline absorbed or trapped in the membrane matrix. Though this represents an ~80% loss, the concentration of bromoaniline is still three orders of magnitude higher than the  $\text{IC}_{50}$  of the 2-AI-para-mono benzoyl conjugate (162  $\mu\text{M}$ ; **Figure 2.2.**).

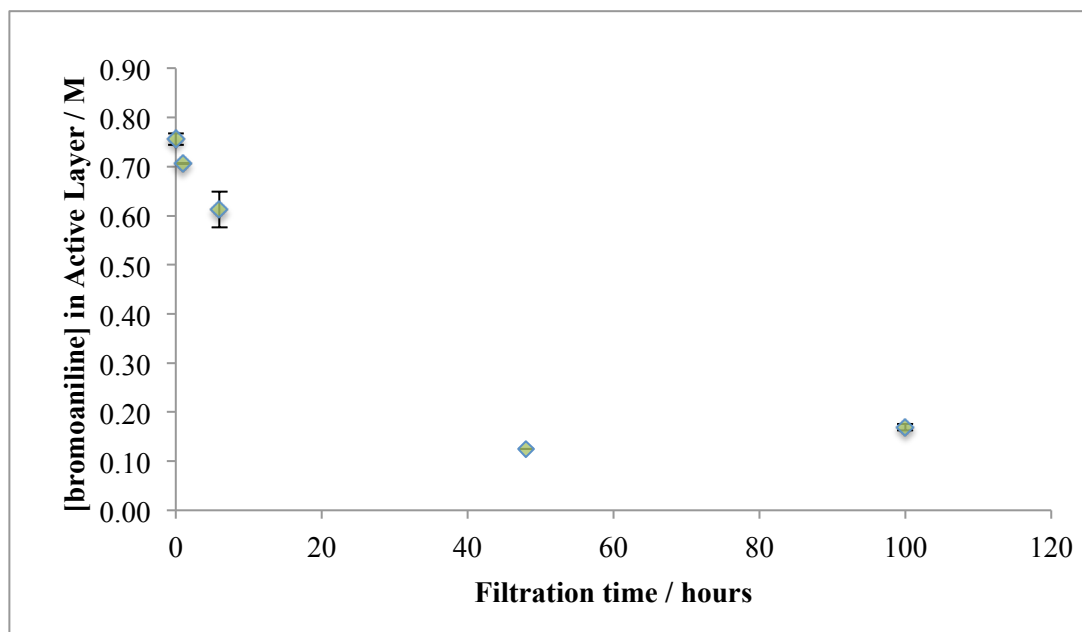


**Figure 2.8.** Concentration of bromoaniline in the active layer of the bromoaniline-modified XLE membrane after filtration of ultrapure water. Each point corresponds to the average of duplicate measurements with error bars representing the two measured values.

Bromoaniline-modified NF270 membranes were subjected to a combination of common chemical cleaning practices and used for filtration of ultrapure water over 6 hours to approximate the loss of 2-AI. Loss of bromoaniline was low after cleaning with basic (EDTA/STPP) and/or acidic (citric acid) solutions (**Table 2.4.**). The greatest loss of bromoaniline (71%) was observed during filtration of ultrapure water, and was similar to loss of bromoaniline from XLE-modified membranes (~80%) after filtration of ultrapure water. Chemical cleaning after filtration did not lead to further losses. As in the case of the bromoaniline-modified XLE membranes, the concentration of residual bromoaniline following use for filtration (0.11 M) remained orders of magnitude higher in the bromoaniline-modified NF270 than the  $IC_{50}$  of the 2-AI-para-mono benzoyl conjugate.

**Table 2.4.** Bromoaniline (BA) concentrations and associated percent loss in bromoaniline-modified NF270 membranes after chemical cleaning and/or use for filtering ultrapure water for 6 hours.

	Average [BA] in Active Layer/M	%BA Lost
No treatment	0.43	-
Citric Acid	0.31	30%
EDTA	0.39	11%
6 hours use for water filtration	0.12	71%
6 hours use for water filtration + Citric Acid	0.12	71%
6 hours use for water filtration + EDTA	0.11	74%

#### 2.3.4. Performance of 2-AI-modified membranes

##### 2.3.4.1. Biofilm inhibition by 2-AI-modified membranes

To evaluate inhibition of biofouling by 2-AI-modified membranes, the surfaces of the control and 2-AI-modified membranes were exposed to *Pseudomonas aeruginosa* (PA14) in

nutrient broth solutions under static conditions, and the biofilm mass that formed on the membranes was measured. Under full-scale operation, hydrodynamic forces and turbulence from water flowing across the surface of the membrane limit the growth of biofilms.<sup>29,60</sup> By contrast, in this test growth occurred in the presence of excess nutrient supply and was uninhibited by hydrodynamic forces, conditions highly favorable for biofilm development. For each type of membrane, the tests were performed at least twice on separate days.

Growth of PA14 biofilm was inhibited 61-96% ( $p=0.01-0.12$ ) on 2-AI-modified membranes compared to the corresponding unmodified controls, in order of effectiveness, SWC4+ > ESPA3 > XLE > NF270 (**Table 2.3.**, **Figure 2.9.**). The results suggest large reductions in the frequency of membrane cleaning and higher performance over an extended period may be possible under real-world operating conditions. Previous investigations of anti-biofouling membranes have not reported the statistical significance of biofilm inhibition, and most measure effectiveness in terms of inactivated or non-viable bacteria on membrane surfaces or in solution, reduction of polysaccharides, or increase in water flux;<sup>16-19,21,22,24</sup> which are indirect measurements of biofilm formation. In contrast, the results reported here directly demonstrate that 2-AI-modified membranes significantly disrupt biofilm formation and growth.

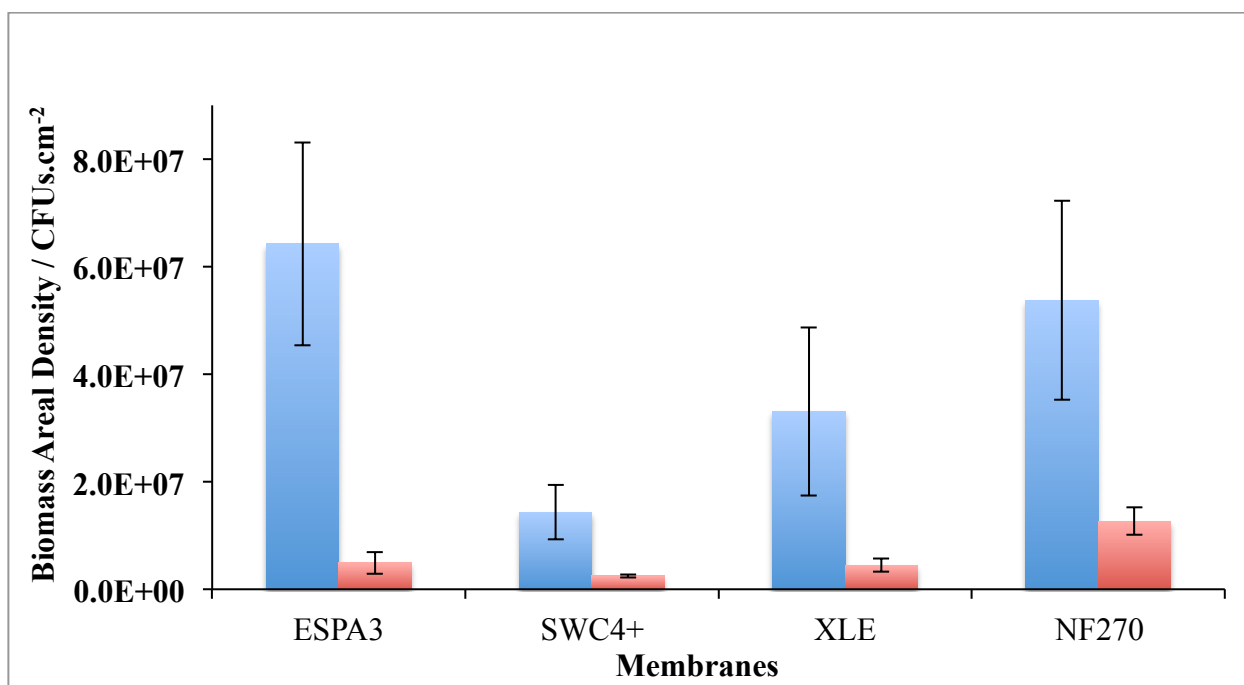


**Figure 2.9.** Biomass areal density of PA14 biofilm on the surface of unmodified control (blue bars) and corresponding 2-AI-modified membranes (red bars). Bars represent the average areal density of 4-10 replicates. Error bars indicate standard error. The data shown correspond to data from one day with 92%, 83%, 86%, and 76% biofilm inhibition by ESPA3+2-AI-para ( $p=0.01$ ), SWC4+2-AI-para ( $p=0.07$ ), XLE+2-AI-para ( $p=0.07$ ), and NF270+2-AI-para ( $p=0.06$ ) membranes, respectively.

#### 2.3.4.2. Changes in salt rejection and water productivity due to 2-AI incorporation

**Table 2.3.** summarizes results for the water productivity and salt rejection by control and corresponding 2-AI-modified membranes. XLE, NF270, and ESPA3 modified membranes show no statistical difference ( $p>0.05$ ) in salt rejection. A significant decrease ( $p<0.05$ ) of the salt rejection by only 0.6% for SWC4+ modified by 2-AI would in most cases be operationally inconsequential. Thus, we conclude that incorporation of 2-AI in the membranes inhibited biofilm formation without substantially affecting salt rejection.

**Table 2.3.** shows no statistical difference in water permeability between control and 2-AI-modified XLE and NF270 membranes. However, statistically significant decreases ( $p<0.05$ )

in water permeability were observed for 2-AI-modified ESPA3 (13%) and SWC4+ (25%). ESPA3 and SWC4+ membranes had the highest levels of 2-AI incorporation (**Table 2.3.**) which may account for the reduction in water permeability. It should be noted that in this preliminary study we made no systematic effort to maximize water permeability or salt rejection in 2-AI-modified membranes, although long-term benefits in water permeability from reduced biofouling could compensate for lower initial water permeabilities.

### **2.3.5. Changes in membrane charge, hydrophobicity, and roughness as a result of 2-AI incorporation and their potential contribution to biofilm inhibition**

#### *2.3.5.1. Charge*

Increased negative charge on the membrane surface has been established as an important factor in controlling biofouling potential.<sup>27,29</sup> We evaluated membrane surface charge by streaming current analysis. Although physical changes to the membrane active layer may have resulted from 2-AI coupling to carboxylate groups of the polyamide, the streaming current results in **Figure 2.10.** show no substantial change in zeta potential between the control and 2-AI-modified membranes over the pH range (6-9) typical of full-scale operations. Therefore, we conclude that changes in membrane charge did not play a role in the observed reduction in biofouling potential.

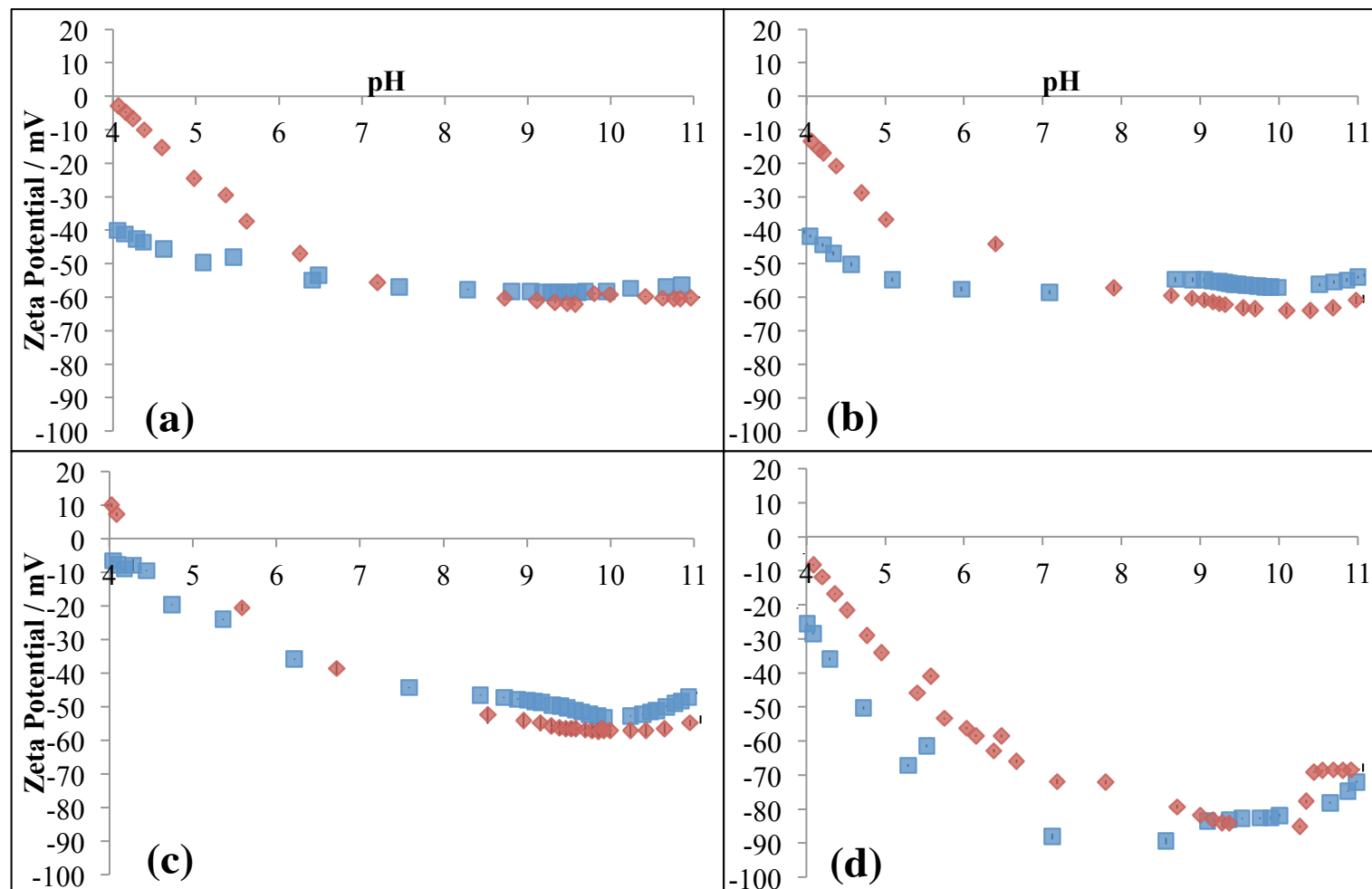


**Figure 2.10.** Zeta potential, measured by streaming current, of unmodified control (blue square) and 2-AI-modified membranes (red diamond) as a function of pH. (a) ESPA3, (b) SWC4+, (c) XLE, (d) NF270. Each point corresponds to quadruplicate measurements and each curve consists of data from two separate measurements on different days with different sets of membrane samples.

### 2.3.5.2. Hydrophobicity

Surfaces with increased hydrophobicity generally have higher biofouling potential,<sup>27,29</sup> and to determine whether changes in hydrophobicity may have influenced the activity of 2-AI-modified membranes, the hydrophobicity of modified and control membranes was assessed by contact angle measurements using a captive bubble method. The results for control and 2-AI-modified membranes are summarized in **Figure 2.11**. Hydrophobicities measured for unmodified controls were consistent with published results,<sup>50,57</sup> with statistically similar hydrophobicities (20-26°) for MPD-based polyamide membranes (XLE, ESPA3, SWC4+) and somewhat greater hydrophilicity (17-19°) for the piperazine-based polyamide membrane (NF270). **Figure 2.11** shows that modification of the membranes caused no significant changes in hydrophobicity ( $p > 0.15$ ) and consequently the biofilm inhibition properties observed in 2-AI-modified membranes are not attributable to changes in hydrophobicity.

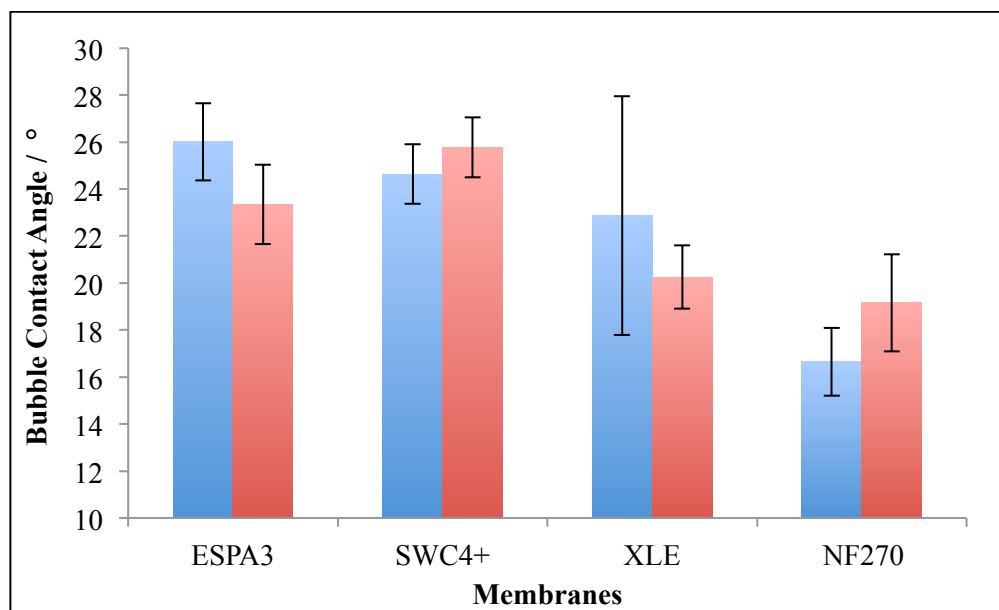


**Figure 2.11.** Contact angle of unmodified control (blue bars) and corresponding 2-AI-modified membranes (red bars) as measured by the captive bubble contact angle method. Each bar represents 4 replicate measurements. Error bars indicate standard error.

#### 2.3.5.3. Surface roughness

Increased potential for biofouling has been correlated with increased surface roughness of membrane surfaces.<sup>27–29</sup> Possible influence of changes in membrane surface roughness resulting from 2-AI modification was analyzed by Atomic Force Microscopy (AFM). Results for the controls (**Table 2.3., Figure 2.12.**) are in accord with published values,<sup>57</sup> with similar measurements obtained for the MPD-based polyamide membranes (ESPA3, SWC4+, XLE) (77–114 nm;  $p>0.15$ ), and a smoother surface measured for the piperazine-based polyamide membrane (NF270) (18–26 nm;  $p<0.05$ ). Modification by 2-AI incorporation resulted in no statistically significant changes in surface roughness for SWC4+, XLE, and NF270 membranes, ruling out any effects on biofilm inhibition. A statistically significant increase in roughness was observed for the 2-AI-modified ESPA3 membrane ( $p=0.05$ ); however, since the 2-AI modification of ESPA3 had a net effect of strong reduction in biofilm formation (up to 92%, **Table 2.3.**) the anti-biofouling properties of 2-AI clearly compensate for the change in surface roughness.



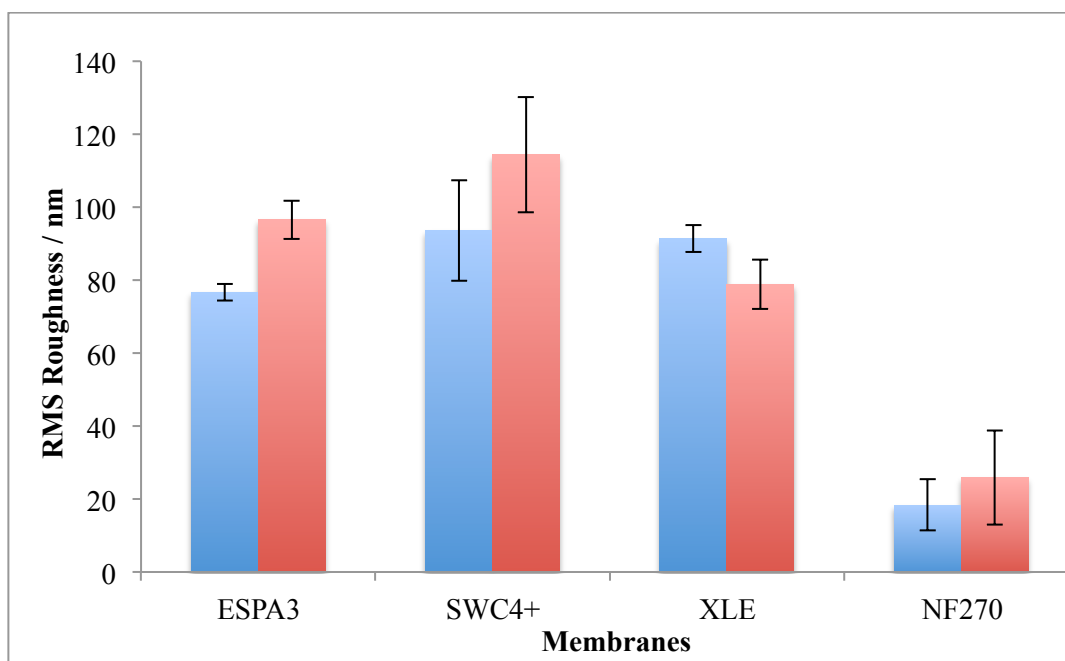


**Figure 2.12.** Root-mean-squared (RMS) roughness of unmodified control membranes (blue bars) and corresponding 2-AI-modified membranes (red bars). Each bar corresponds to the average of triplicate samples. Error bars indicate standard error. The roughness of ESPA3 and ESPA3+2-AI are significantly different.

Measurements of membrane charge, hydrophobicity and roughness rule out the possibilities that modification by 2-AI caused changes in physico-chemical properties known to affect biofouling potential. The observed reduction in biofouling by 2-AI-modified membranes can therefore be attributed to the established anti-biofouling properties 2-AI-para in the polyamide active layer.

## 2.4. Conclusions

We developed new anti-biofouling membranes through the incorporation of a 2-AI into commercial RO and NF membranes with polyamide active layers. The method of 2-AI incorporation, the stability of 2-AI incorporation, the performance of 2-AI-modified membranes,

and the physico-chemical changes due to 2-AI incorporation were evaluated. Our experimental results support the following main conclusions:

- PA14 biofilm was significantly inhibited (61-96%) by 2-AI-modified membranes.
- Partial loss of a 2-AI surrogate compound was observed after extended use for water filtration but is likely a result of leaching of non-covalently bonded compound. Nevertheless, residual concentrations are orders of magnitude higher than required for effective biofilm inhibition.
- The observed biofilm inhibition properties of 2-AI-modified membranes were attributable to the presence of 2-AI molecules in the active layer, not to changes in membrane physico-chemical properties (charge, hydrophobicity, and roughness).
- In general, salt rejection of 2-AI-modified membranes was equivalent to that of controls.
- While two (XLE, NF270) of the four membranes had no substantial change in water permeability after 2-AI incorporation, the other two (ESPA3, SWC4+) showed a moderate decrease in water permeability (13% and 25%, respectively); however, the fabrication procedure of 2-AI-modified membranes was not optimized to maximize water productivity, and long-term benefits in water permeability due to reduced biofouling could potentially compensate for lower initial water permeabilities.

Overall, these findings demonstrate that anti-biofouling membranes, with water permeability and salt rejection properties comparable to those of state-of-the-art RO/NF membranes, and biofilm inhibition properties superior to others reported in the literature, can be fabricated by 2-AI incorporation into the polyamide active layers of commercial RO/NF membranes.

## **2.5. Acknowledgements**

This work was supported by the National Science Foundation (NSF) Grant Opportunities for Academic Liaison with Industry (GOALI) and Chemical, Bioengineering, Environmental, and Transport Systems (CBET) program under Award#1264690, NSF Environmental Engineering program under Award#1336532, a Sigma Xi Grant-in-Aid of Research (GIAR) award, the National Water Research Institute (NWRI) and American Membrane Technology Association (AMTA) Fellowship for Membrane Technology, and The UNC Graduate School Dissertation Completion Fellowship. The authors would like to thank Dr. Thomas Clegg for his help with RBS analyses, Dr. Carrie Donley for assistance with XPS and AFM analyses, Leonard Collins for running samples on the LC-MS, and the Miller research group for use of contact angle equipment. The authors also thank Hydranautics for donation of membranes. LC-MS analyses were performed at The Biomarker Mass Spectrometry Core Facility at UNC, Chapel Hill, NC. RBS analyses were performed at the Triangle Universities Nuclear Laboratories (TUNL), Durham, NC, which is partially supported by the US Department of Energy Office of Nuclear Physics (Grant Numbers 97ER41041 and 97ER41033). XPS and AFM were performed at the Chapel Hill Analytical and Nanofabrication Laboratory (CHANL) at UNC, a member of the North Carolina Research Triangle Nanotechnology Network (RTNN), which is supported by the National Science Foundation (Grant ECCS-1542015) as part of the National Nanotechnology Coordinated Infrastructure (NNCI).

## REFERENCES

- (1) Herzberg, M.; Elimelech, M. Biofouling of Reverse Osmosis Membranes: Role of Biofilm-Enhanced Osmotic Pressure. *J. Memb. Sci.* **2007**, 295 (1–2), 11–20.
- (2) Nguyen, T.; Roddick, F.; Fan, L. Biofouling of Water Treatment Membranes: A Review of the Underlying Causes, Monitoring Techniques and Control Measures. *Membranes (Basel)*. **2012**, 2 (4), 804–840.
- (3) Flemming, H.-C. Reverse Osmosis Membrane Biofouling. *Exp. Therm. Fluid Sci.* **1997**, 14 (4), 382–391.
- (4) Altman, S. J.; Cappelle, M.; Clem, P. G.; Cook, A. W.; Christopher, H.; Hart, W. E.; Hibbs, M. R.; Ho, C. K.; Jones, H. D. T.; Khalsa, S.; Noek, R.; Sun, A. C.; Webb, S. W.; Mcgrath, L. K.; James, D. L.; Adout, A.; Elimelech, M.; Kang, S. *Analysis of Micromixers and Biocidal Coatings on Water Treatment Membranes to Minimize Biofouling*; SAND2009-8316; Albuquerque, NM, 2009.
- (5) Belfer, S.; Gilron, J.; Daltrophe, N.; Oren, Y. Comparative Study of Biofouling of NF Modified Membrane at SHAFDAN. *Desalination* **2005**, 184 (1–3), 13–21.
- (6) Huertas, E.; Herzberg, M.; Oron, G.; Elimelech, M. Influence of Biofouling on Boron Removal by Nanofiltration and Reverse Osmosis Membranes. *J. Memb. Sci.* **2008**, 318 (1–2), 264–270.
- (7) Xu, P.; Drewes, J. E.; Kim, T.-U.; Bellona, C.; Amy, G. Effect of Membrane Fouling on Transport of Organic Contaminants in NF/RO Membrane Applications. *J. Memb. Sci.* **2006**, 279 (1–2), 165–175.
- (8) Vogel, D.; Simon, A.; Alturki, A. A.; Bilitewski, B.; Price, W. E.; Nghiem, L. D. Effects of Fouling and Scaling on the Retention of Trace Organic Contaminants by a Nanofiltration Membrane: The Role of Cake-Enhanced Concentration Polarisation. *Sep. Purif. Technol.* **2010**, 73 (2), 256–263.
- (9) Flemming, H.-C.; Schaule, G.; Griebe, T.; Schmitt, J.; Tamachkiarowa, a. Biofouling—the Achilles Heel of Membrane Processes. *Desalination* **1997**, 113 (2–3), 215–225.
- (10) Flemming, H. C. Biofouling in Water Systems - Cases, Causes and Countermeasures. *Appl. Microbiol. Biotechnol.* **2002**, 59 (6), 629–640.
- (11) Matin, A.; Khan, Z.; Zaidi, S. M. J.; Boyce, M. C. Biofouling in Reverse Osmosis Membranes for Seawater Desalination: Phenomena and Prevention. *Desalination* **2011**, 281, 1–16.
- (12) Al-Ahmad, M.; Aleem, F. A.; Mutiri, A.; Ubaisy, A. Biofuoling in RO Membrane Systems. Part 1: Fundamentals and Control. *Desalination* **2000**, 132 (October), 173–179.

- (13) Herzberg, M.; Elimelech, M. Physiology and Genetic Traits of Reverse Osmosis Membrane Biofilms: A Case Study with *Pseudomonas Aeruginosa*. *ISME J.* **2008**, 2 (2), 180–194.
- (14) Al-Juboori, R. A.; Yusaf, T. Biofouling in RO System: Mechanisms, Monitoring and Controlling. *Desalination* **2012**, 302, 1–23.
- (15) Lee, W.; Ahn, C. H.; Hong, S.; Kim, S.; Lee, S.; Baek, Y.; Yoon, J. Evaluation of Surface Properties of Reverse Osmosis Membranes on the Initial Biofouling Stages under No Filtration Condition. *J. Memb. Sci.* **2010**, 351 (1–2), 112–122.
- (16) Varin, K. J.; Lin, N. H.; Cohen, Y. Biofouling and Cleaning Effectiveness of Surface Nanostructured Reverse Osmosis Membranes. *J. Memb. Sci.* **2013**, 446, 472–481.
- (17) Malaisamy, R.; Berry, D.; Holder, D.; Raskin, L.; Lepak, L.; Jones, K. L. Development of Reactive Thin Film Polymer Brush Membranes to Prevent Biofouling. *J. Memb. Sci.* **2010**, 350, 361–370.
- (18) Xu, J.; Wang, Z.; Yu, L.; Wang, J.; Wang, S. A Novel Reverse Osmosis Membrane with Regenerable Anti-Biofouling and Chlorine Resistant Properties. *J. Memb. Sci.* **2013**, 435, 80–91.
- (19) Nikkola, J.; Liu, X.; Li, Y.; Raulio, M.; Alakomi, H. L.; Wei, J.; Tang, C. Y. Surface Modification of Thin Film Composite RO Membrane for Enhanced Anti-Biofouling Performance. *J. Memb. Sci.* **2013**, 444, 192–200.
- (20) Bera, A.; Gol, R. M.; Chatterjee, S.; Jewrajka, S. K. PEGylation and Incorporation of Triazine Ring into Thin Film Composite Reverse Osmosis Membranes for Enhancement of Anti-Organic and Anti-Biofouling Properties. *Desalination* **2015**, 360, 108–117.
- (21) Zhu, X.; Bai, R.; Wee, K. H.; Liu, C.; Tang, S. L. Membrane Surfaces Immobilized with Ionic or Reduced Silver and Their Anti-Biofouling Performances. *J. Memb. Sci.* **2010**, 363 (1–2), 278–286.
- (22) Karkhanechi, H.; Takagi, R.; Matsuyama, H. Biofouling Resistance of Reverse Osmosis Membrane Modified with Polydopamine. *Desalination* **2014**, 336, 87–96.
- (23) Blok, A. J.; Chhasatia, R.; Dilag, J.; Ellis, A. V. Surface Initiated Polydopamine Grafted Poly ([2-( Methacryoyloxy) Ethyl] Trimethylammonium Chloride ) Coatings to Produce Reverse Osmosis Desalination Membranes with Anti-Biofouling Properties. *J. Memb. Sci.* **2014**, 468, 216–223.
- (24) Wei, X.; Wang, Z.; Zhang, Z.; Wang, J.; Wang, S. Surface Modification of Commercial Aromatic Polyamide Reverse Osmosis Membranes by Graft Polymerization of 3-Allyl-5,5-Dimethylhydantoin. *J. Memb. Sci.* **2010**, 351 (1–2), 222–233.

- (25) Vercellino, T.; Morse, A.; Tran, P.; Song, L.; Hamood, A.; Reid, T.; Moseley, T. Attachment of Organo-Selenium to Polyamide Composite Reverse Osmosis Membranes to Inhibit Biofilm Formation of *S. Aureus* and *E. Coli*. *Desalination* **2013**, *309*, 291–295.
- (26) Habimana, O.; Semião, a. J. C.; Casey, E. The Role of Cell-Surface Interactions in Bacterial Initial Adhesion and Consequent Biofilm Formation on Nanofiltration/reverse Osmosis Membranes. *J. Memb. Sci.* **2014**, *454*, 82–96.
- (27) Kang, S.; Hoek, E. M. V.; Choi, H.; Shin, H. Effect of Membrane Surface Properties During the Fast Evaluation of Cell Attachment. *Sep. Sci. Technol.* **2006**, *41* (7), 1475–1487.
- (28) Li, Q.; Xu, Z.; Pinnau, I. Fouling of Reverse Osmosis Membranes by Biopolymers in Wastewater Secondary Effluent: Role of Membrane Surface Properties and Initial Permeate Flux. *J. Memb. Sci.* **2007**, *290* (1–2), 173–181.
- (29) Subramani, A.; Hoek, E. M. V. Direct Observation of Initial Microbial Deposition onto Reverse Osmosis and Nanofiltration Membranes. *J. Memb. Sci.* **2008**, *319*, 111–125.
- (30) Hoffman, L. R.; D’Argenio, D. a; MacCoss, M. J.; Zhang, Z.; Jones, R. a; Miller, S. I. Aminoglycoside Antibiotics Induce Bacterial Biofilm Formation. *Nature* **2005**, *436*, 1171–1175.
- (31) Worthington, R.; Richards, J.; Melander, C. Small Molecule Control of Bacterial Biofilms. *Org. Biomol. Chem.* **2012**, *10* (37), 7457–7474.
- (32) Rogers, S.; Melander, C. Construction and Screening of a 2-Aminoimidazole Library Identifies a Small Molecule Capable of Inhibiting and Dispersing Bacterial Biofilms across Order, Class, and Phylum. *Angew. Chemie Int. Ed* **2008**, *47* (28), 5229–5231.
- (33) Peng, L.; DeSousa, J.; Su, Z.; Novak, B. M.; Nevzorov, A. a; Garland, E. R.; Melander, C. Inhibition of *Acinetobacter Baumannii* Biofilm Formation on a Methacrylate Polymer Containing a 2-Aminoimidazole Subunit. *Chem. Commun.* **2011**, *47* (17), 4896–4898.
- (34) Thompson, R. J.; Bobay, B. G.; Stowe, S. D.; Olson, A. L.; Peng, L.; Su, Z.; Actis, L. a; Melander, C.; Cavanagh, J. Identification of BfmR , a Response Regulator Involved in Biofilm Development, as a Target for a 2-Aminoimidazole-Based Antibiofilm Agent. *Biochemistry* **2012**, No. 51, 9776–9778.
- (35) Gotoh, Y.; Eguchi, Y.; Watanabe, T.; Okamoto, S.; Doi, A.; Utsumi, R. Two-Component Signal Transduction as Potential Drug Targets in Pathogenic Bacteria. *Curr. Opin. Microbiol.* **2010**, *13* (2), 232–239.
- (36) Beier, D.; Gross, R. Regulation of Bacterial Virulence by Two-Component Systems. *Curr. Opin. Microbiol.* **2006**, *9*, 143–152.
- (37) Melander, C.; Rogers, S. A.; Huigens, R. W.; Reed, C. S. Inhibition and Dispersion of Bacterial Biofilms with Imidazole-Triazole Derivatives. US Patent 7,897,631, 2011.

- (38) Rogers, S. A.; Huigens, R. W.; Cavanagh, J.; Melander, C. Synergistic Effects between Conventional Antibiotics and 2-Aminoimidazole-Derived Antibiofilm Agents. *Antimicrob. Agents Chemother.* **2010**, *54* (5), 2112–2118.
- (39) Worthington, R. J.; Bunders, C. A.; Reed, C. S.; Melander, C. Small Molecule Suppression of Carbapenem Resistance in NDM-1 Producing *Klebsiella Pneumonia*. *ACS Med. Chem. Lett.* **2012**, *3*, 357–361.
- (40) Melander, C.; Cavanagh, J.; Ritchie, D.; Huigens III, R.; Ballard, T. E.; Richards, J. J.; Lindsey, T. W.; Lindsey, J. S. Inhibition of Biofilms in Plants with Imidazole Derivatives. US 8,278,340 B2, 2012.
- (41) Tang, C. Y.; Kwon, Y.-N.; Leckie, J. O. Effect of Membrane Chemistry and Coating Layer on Physiochemical Properties of Thin Film Composite Polyamide RO and NF Membranes. *Desalination* **2009**, *242* (1–3), 149–167.
- (42) Richards, J. J.; Ballard, T. E.; Huigens, R. W.; Melander, C. Synthesis and Screening of an Oroidin Library against *Pseudomonas Aeruginosa* Biofilms. *ChemBioChem* **2008**, *9* (8), 1267–1279.
- (43) Coronell, O.; Mariñas, B. J.; Zhang, X.; Cahill, D. G. Quantification of Functional Groups and Modeling of Their Ionization Behavior in the Active Layer of FT30 Reverse Osmosis Membrane. *Environ. Sci. Technol.* **2008**, *42* (14), 5260–5266.
- (44) Coronell, O.; Marinas, B. J.; Cahill, D. G. Depth Heterogeneity of Fully Aromatic Polyamide Active Layers in Reverse Osmosis and Nanofiltration Membranes. *Environ. Sci. Technol.* **2011**, *45* (10), 4513–4520.
- (45) Coronell, O.; González, M. I.; Mariñas, B. J.; Cahill, D. G. Ionization Behavior, Stoichiometry of Association, and Accessibility of Functional Groups in the Active Layers of Reverse Osmosis and Nanofiltration Membranes. *Environ. Sci. Technol.* **2010**, *44* (17), 6808–6814.
- (46) Attayek, P. J.; Meyer, E. S.; Lin, L.; Rich, G. C.; Clegg, T. B.; Coronell, O. A Remotely Controlled, Semi-Automatic Target System for Rutherford Backscattering Spectrometry and Elastic Recoil Detection Analyses of Polymeric Membrane Samples. *Nucl. Instruments Methods Phys. Res. Sect. A Accel. Spectrometers, Detect. Assoc. Equip.* **2012**, *676*, 21–25.
- (47) Meyer, E. S. Degradation Behavior of Nanofiltration and Reverse Osmosis Membrane Supports from Ion Beam Irradiation, The University of North Carolina at Chapel Hill, 2012.
- (48) Mi, B.; Cahill, D. G.; Mariñas, B. J. Physico-Chemical Integrity of Nanofiltration/reverse Osmosis Membranes during Characterization by Rutherford Backscattering Spectrometry. *J. Memb. Sci.* **2007**, *291* (1), 77–85.
- (49) Mayer, M. *SIMNRA User's Guide*; Garching, Germany, 2002.

- (50) Baek, Y.; Kang, J.; Theato, P.; Yoon, J. Measuring Hydrophilicity of RO Membranes by Contact Angles via Sessile Drop and Captive Bubble Method: A Comparative Study. *Desalination* **2012**, *303*, 23–28.
- (51) Rasband, W. ImageJ. National Institutes of Health, USA 2013, p 2013.
- (52) Brugnara, M. Contact Angle Plugin. National Institutes of Health, USA 2006.
- (53) Buksek, H.; Luxbacher, T.; Petrinic, I. Zeta Potential Determination of Polymeric Materials Using Two Differently Designed Measuring Cells of an Electrokinetic Analyzer. *Acta Chim Slov* **2010**, *57*, 700–706.
- (54) Kwak, S. Y.; Jung, S. G.; Yoon, Y. S.; Ihm, D. W. Details of Surface Features in Aromatic Polyamide Reverse Osmosis Membranes Characterized by Scanning Electron and Atomic Force Microscopy. *J. Polym. Sci. Part B Polym. Phys.* **1999**, *37* (13), 1429–1440.
- (55) Zidar, N.; Jakopin, Z.; Madge, D. J.; Chan, F.; Tytgat, J.; Peigneur, S.; Dolenc, M. S.; Tomasic, T.; Ilas, J.; Masic, L. P.; Kikelj, D. Substituted 2-Phenyl-2-aminoimidazoles and 4-Phenyl-4,5-Dihydro-2-Aminoimidazoles as Voltage-Gated Sodium Channel Modulators. *Eur. J. Med. Chem.* **2014**, *74*, 23–30.
- (56) Wan, Z. K.; Woo, G. H. C.; Snyder, J. K. Dienophilicity of Imidazole in Inverse Electron Demand Diels-Alder Reactions: Cycloadditions with 1,2,4,5-Tetrazines and the Structure of Zarzissine. *Tetrahedron* **2001**, *57*, 5497–5507.
- (57) Tang, C. Y.; Kwon, Y. N.; Leckie, J. O. Effect of Membrane Chemistry and Coating Layer on Physiochemical Properties of Thin Film Composite Polyamide RO and NF Membranes. II. Membrane Physiochemical Properties and Their Dependence on Polyamide and Coating Layers. *Desalination* **2009**, *242* (1–3), 168–182.
- (58) Coronell, O.; Mariñas, B. J.; Cahill, D. G. Accessibility and Ion Exchange Stoichiometry of Ionized Carboxylic Groups in the Active Layer of FT30 Reverse Osmosis Membrane. *Environ. Sci. Technol.* **2009**, *43* (13), 5042–5048.
- (59) IUPAC. Stability Constants Database. Academic Software: Yorks, UK 2001.
- (60) van Loosdrecht, M.; Eikelboom, D.; Gjaltema, A.; Mulder, A.; Tijhuis, L.; Heijnen, J. Biofilm Structures. *Water Res.* **1995**, *32* (8), 35–43.



## **CHAPTER 3: DEVELOPMENT OF ANTI-BIOFOULING RO/NF MEMBRANES THROUGH INCORPORATION OF 2-AMINOIMIDAZOLE INTO THE ACTIVE LAYER DURING POLYAMIDE CASTING**

### **3.1. Introduction**

Nanofiltration (NF) and reverse osmosis (RO) membranes are increasingly common desalination technologies used in the production of drinking water and ultrapure water for manufacturing (e.g. semiconductors, pharmaceuticals, food and beverage). However, the fouling of membrane surfaces is a widespread problem leading to decreased productivity, higher energy use, higher costs (e.g. cleaning time and supplies, decreased membrane life), and lower quality water or products.<sup>1,2 3-5</sup> Given these negative impacts, developing effective and efficient methods to decreasing fouling of membranes is critical.

There are a few different types of fouling that occur during RO/NF use, but biofouling is one of the most frequently occurring and difficult to control.<sup>2,6-9</sup> Significant biofouling occurs even if high levels of microbes are removed from the feed water (e.g. 4-log removal) and the productivity of the membranes is generally not recoverable due to irreversibility of biofouling. Biofouling during membrane treatment starts with planktonic microbes, from the feed solution, attaching to the surface.<sup>1,7,10,11</sup> If bacteria were kept in planktonic state and attachment were effectively prevented, then biofouling could be limited significantly or eliminated altogether. After the bacteria are fixed on the membrane, a biofilm is formed through bacterial growth, reproduction, and particularly excretion of extracellular polymeric substances (EPS). Biofouling

consists mostly of EPS (up to 90% by volume), and thus EPS is a critical concern when considering and developing biofouling control strategies.<sup>1,7,12</sup>

Biofouling control strategies that are currently in use or in development aim to either decrease attachment or inactivate/kill bacteria upon attachment. These strategies include physical removal of bacteria and/or nutrients (e.g. green sand filtration, low-pressure membranes), biocidal methods (e.g. disinfection, biocidal membranes), and membrane property alteration (e.g. nanopatterned membrane surfaces, hydrophilic membranes).<sup>13 14–25</sup> While disinfection of feed waters prior to the membranes in combination with chemical cleaning is the most commonly used strategy, there is no widely applicable, cost-effective, and efficacious biofouling control method at this time. In some cases biofouling control strategies have actually promoted biofouling.<sup>14,26</sup>

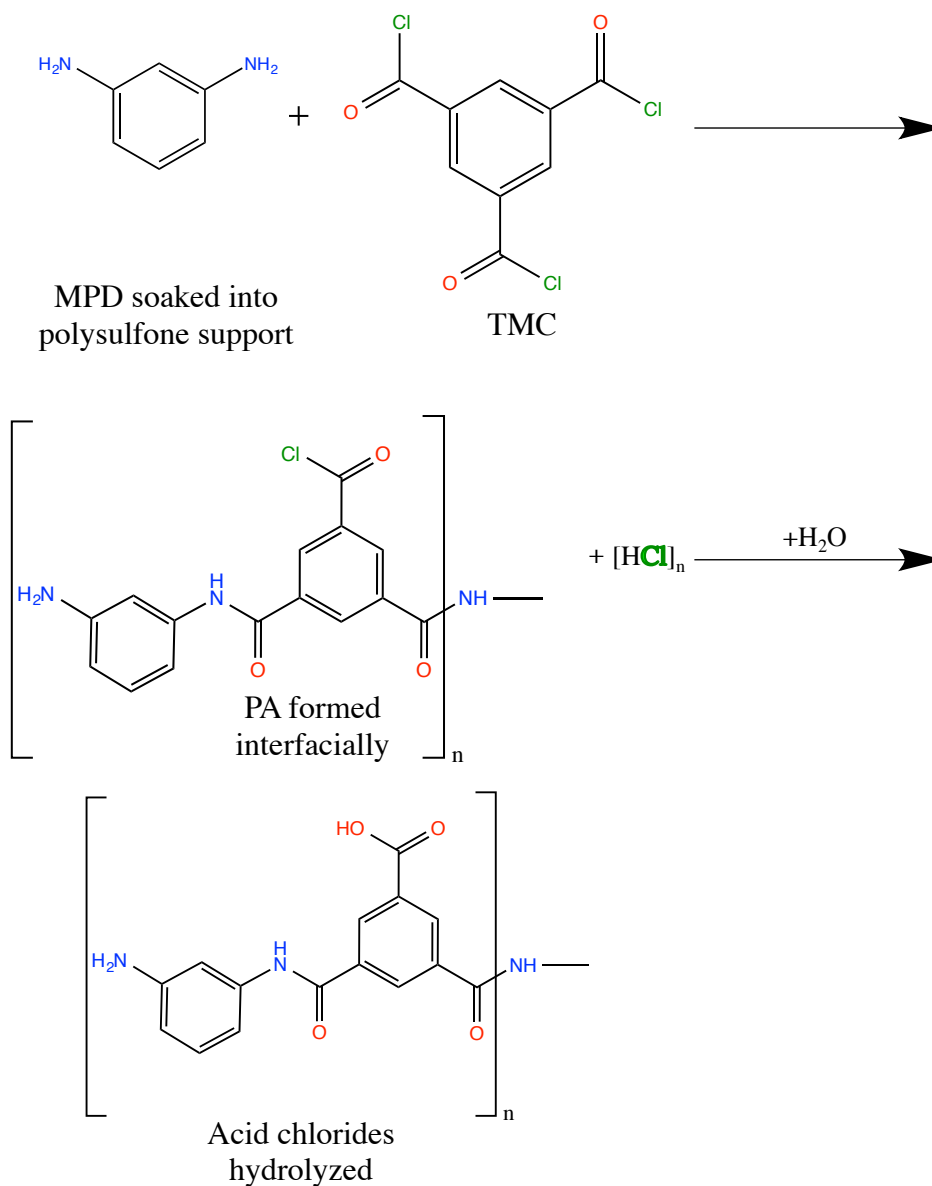
An ideal approach to control biofouling would actively prevent or eliminate attachment of bacteria, excretion of EPS, and not trigger a protective response. To this end some researchers have been working on incorporating bioactive, non-biocidal molecules that actively disrupt biofilm formation into different materials. One of the most discussed anti-biofilm compound classes in the general biofilm literature is 2-aminoimidazoles (2-AIs).<sup>27–29</sup> The chemical structure of the 2-AI used in this chapter, 5-(4-aminophenyl)-1H-imidazol-2-amine, is shown in **Table 3.1**. It is proposed that 2-AIs interfere with bacteria's two-component regulatory systems through bonding to response regulator proteins. These systems are used by bacteria for sensing and responding to their environment, including control over bacteria remaining in planktonic state or changing to a sessile state, producing pilli, excreting EPS, and formation and maintenance of biofilms. 2-AIs are the only non-biocidal compound class that is effective at preventing biofilm formation and growth, and dispersing existing biofilms formed by bacteria across classes, orders,

and phyla.<sup>28,30–34</sup> 2-AIs have successfully been used in medicine<sup>35,36</sup> and agriculture<sup>37</sup> and are stable under pH and temperatures that are relevant to membrane processes.

In *Chapter 2*, the incorporation of a 2-AI into the active layer of commercially available RO/NF membranes using a carbodiimide-induced grafting technique was reported on. These modified membranes significantly (61-96%) inhibited *Pseudomonas aeruginosa* biofilms. Although this method produced membranes that were effective, there may be more effective and efficient ways to incorporate 2-AIs without having to add additional chemicals (aside from the 2-AI) and that takes advantage of current manufacturing processes.

The chemical process of RO/NF membrane manufacturing is described in **Scheme 3.1**. The active layer of RO and NF membranes, usually polyamide based, is typically cast on a flat sheet polysulfone ultrafiltration membrane as a support. The polyamide (PA) is formed through interfacial polymerization, where two monomer solutions, e.g. m-phenylenediamine (MPD) in water and trimesoyl chloride (TMC) in an organic solvent, cross-link through the formation of amide bonds. A portion of the terminal functional groups of the monomers remain unreacted, e.g. amine groups from MPD (0.01-0.1 M) and acid-chloride groups from TMC (0.2-0.7 M).<sup>38</sup> The acid-chloride groups remain reactive until exposed to water, when they hydrolyze into carboxylic acids. There are three potential approaches to incorporate 2-AIs into the polyamide during this manufacturing process, without having to add more chemicals aside from 2-AI. The first two consist of adding the 2-AI to either (a) the MPD monomer solution or (b) the TMC monomer solution. It is expected that with approach (a) the 2-AI would act similarly to the MPD and bond to TMC via amide bonds during the interfacial polymerization. With approach (b) the 2-AI could potentially react with a portion of the TMC molecules in solution prior to polymerization with MPD. The third approach would be to (c) expose the membrane surface to an organic solution of

2-AI, after polyamide formation but prior to hydrolysis of the acid-chloride groups. In approach (c) the 2-AI would react with the free acid-chloride groups and bond to the membrane matrix also through amide bonds.



**Scheme 3.1.** Chemical processes that take place during the manufacturing of RO/NF water purification membranes. The active layer typically consists of fully aromatic polyamide (shown here), and is formed by interfacial polymerization on a polysulfone support. Post-polymerization, the active layer is contacted with water and the acid-chlorides are hydrolyzed to carboxylic acids. MPD=m-phenylene diamine, TMC=trimesoyl chloride, PA=polyamide.

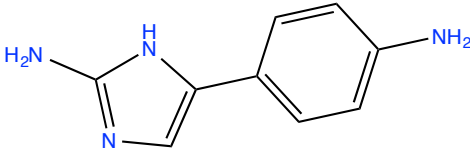
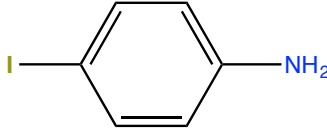
Accordingly, the overall goal of this chapter was to prepare and evaluate anti-biofouling 2-AI membranes where 2-AI is incorporated during the polyamide active layer casting without addition of other chemicals. In order to achieve this overall research goal we sought to achieve four objectives: (1) incorporate 2-AI during polyamide active layer casting using approaches (a)-(c) described above, (2) quantify the extent and stability of incorporation of 2-AI into the membranes, (3) characterize the changes in membrane physico-chemical properties due to the incorporation of 2-AI, and (4) evaluate the performance of 2-AI membranes in terms of biofilm inhibition, water productivity, and salt rejection as compared to a control membrane that has not had 2-AI incorporated.

## **3.2. Materials and Methods**

### **3.2.1. Reagents and membranes**

All reagents were of ACS reagent grade or better and were used without further purification unless otherwise stated. The 2-AI that was used throughout experiments is 5-(4-aminophenyl)-1H-imidazol-2-amine (2-AI-para) (see **Table 3.1.**), and was synthesized in-house following our procedure in *Appendix 1* and discussed in *Chapter 1*. 2-AI-para was chosen as the representative 2-AI because of its low half maximal inhibitory concentration ( $IC_{50}$ ) of 162  $\mu$ M and its demonstrated ability to inhibit biofilm on membranes, as shown in *Chapter 1*.

**Table 3.1.** The 2-AI compound and the 2-AI surrogate compound (iodoaniline) incorporated into polyamide thin-film composite membranes.

IUPAC Name	Molecule Abbreviation	Structure
5-(4-aminophenyl)-1H-imidazol-2-amine	2-AI-para	
4-iodoaniline	IA	

### 3.2.2. Incorporation of 2-AI-para into active layers during polyamide casting

To incorporate 2-AI-para during polyamide active layer casting, 2-AI-para was either added to one of the monomer solutions or the membrane was exposed to a 2-AI-para solution prior to exposing the polyamide to water (hydrolyzing the acid chlorides).. Five monomer solutions were prepared and used for the casting of polyamide active layers on a polysulfone support to produce four different polyamide membranes, according to **Table 3.2**. Polysulfone supports (PS20 ultrafiltration membrane, Nanostone Water, Inc., Oceanside, CA) were cut into 309 cm<sup>2</sup> coupons, and then sprayed with ethanol until the surface was fully covered in ethanol. The supports were rinsed and soaked in ultrapure water for a minimum of 24 hours before being used to produce membranes. The soaked support was taped to a glass plate. After being out of solution for 12 minutes, the support was placed support side down in MPD-only or 2-AI-MPD for 2 minutes. Then the support was squeegeed, top to bottom and side to side, and placed into a vertical container holding either TMC-only or 2-AI-TMC for 1 minute. The membrane was then either placed active layer side up in 2-AI-soak for 5 minutes or rinsed with 100 mL of hexane.

The membrane was then left out of solution for 1 minute in a position with the active layer perpendicular to the bench. The tape was then removed, and the membrane was taken off the glass plate to be rinsed and stored in ultrapure water at 4°C.

**Table 3.2.** Contents of monomers in solutions used to fabricate control and 2-AI polyamide active layers.

Monomer Solution	MPD added (mM)	TMC added (mM)	2-AI-para added (mM)	Solvent	Membrane produced
MPD-only	0.39			Water	Control, 2-AI-TMC-PA, 2-AI-soak-PA
2-AI-MPD	0.39		7.5	Water	2-AI-MPD-PA
TMC-only		4.4		Isopar G	Control, 2-AI-MPD-PA, 2-AI-soak-PA
2-AI-TMC		4.4	0.85	Isopar G	2-AI-TMC-PA
2-AI-soak			1.6	Hexane	2-AI-soak-PA

### 3.2.3 Incorporation of 2-AI surrogate compound (4-iodoaniline) into active layers during polyamide casting

2-AI-para is not easily distinguished from the polyamide matrices when using currently available chemical surface analyses. Therefore, to estimate the quantity of 2-AI-para that is incorporated, the location of incorporation, and the stability of incorporation, a surrogate compound was used. The surrogate compound, 4-iodoaniline (IA), is of similar size and structure to 2-AI-para, but has an iodine atom that is absent in membranes and is easily detected with X-ray photoelectron spectroscopy (XPS) and Rutherford backscattering spectrometry (RBS). IA was used in place of 2-AI in the incorporation process (see *Section 3.2.2*) to produce IA-MPD-

PA, IA-TMC-PA, and IA-soak-PA membranes (instead of 2-AI-MPD-PA, 2-AI-TMC-PA and 2-AI-soak-PA membranes, respectively).

### **3.2.4 Cleaning procedures and use of iodoaniline membranes for water purification**

In order to evaluate the stability of incorporation, IA content in membranes was measured after IA membranes were used to filter ultrapure water, exposed to common cleaning procedures, and/or stored in ultrapure water. The IA membranes were stored in ultrapure water for 24 hours, then they were subjected to cleaning or were used to filter water. Cleaning tests were performed by immersing samples either in citric acid (2%, pH=2.2) solution and/or ethylenediaminetetracetic acid/sodium tripolyphosphate (0.8%/2%, pH=10.2) solution for 1 hour while being shaken. The samples were then rinsed with ultrapure water three times. Water filtration tests were performed in a dead-end cell (HP4750, Sterlitech, Kent, WA) that was filled with ultrapure water, and stirred at 350 RPM under 200 psi of applied pressure for 6 hours. IA membranes that were stored for 2 months were stored at room temperature in ultrapure water. The membrane samples were air-dried for >48 hours after being cleaned, used to filter water, or stored prior to further analysis.

### **3.2.5. Chemical characterization of membrane samples**

#### ***3.2.5.1. ATR-FTIR***

ATR-FTIR analyses were used to characterize the chemical signatures of control and 2-AI-membranes. Analyses were performed with a Bruker Alpha spectrometer (Bruker Optics, Billerica, MA) using an IR source with a 45° incident angle and an Alpha-P ATR accessory. The spectra were collected with a resolution of 2 cm<sup>-1</sup> over the 400-3997 cm<sup>-1</sup> wavenumber range with



a sample analysis area of 3.1 mm<sup>2</sup> analyzed. Prior to analysis, samples were air-dried for > 48 hours. Three or four replicates were analyzed for each sample type and 24 scans were taken per replicate sample. Spectra reported correspond to the average spectra of the 3-4 replicates.

### 3.2.5.2. Silver ion probing

Control and 2-AI membrane samples were probed with silver ions (Ag<sup>+</sup>) to evaluate whether there was an increase in amine groups and/or changes in free carboxylic acid groups in their active layers. The volume-averaged and near-surface ( $\approx$  top 7 nm) concentrations of silver in the active layers were measured using Rutherford backscattering spectrometry (RBS) and X-ray photoelectron spectroscopy (XPS) analyses, respectively.<sup>39</sup> The Ag<sup>+</sup> ion procedure was previously described in the literature and *Chapter 2*.<sup>40,41</sup> Results reported correspond to the average and concentration range of triplicate samples.

### 3.2.5.3. RBS

The volume-averaged elemental composition of polyamide active layers and polysulfone layers were obtained using RBS. A tandem Van de Graaff accelerator was used to produce a 2-MeV He<sup>2+</sup> analysis beam which irradiated samples with incident, exit, and scattering angles of 22.5°, 42.5°, and 160° respectively, and a He fluence lower than 10<sup>14</sup> He<sup>2+</sup>/cm<sup>2</sup> to prevent sample damage.<sup>41,42</sup>ref Samples with analysis area of approximately 12.5 cm<sup>2</sup> were mounted onto a semi-automatic target system<sup>41</sup> under vacuum in the scattering chamber. Experimental data was used to simulate RBS spectra and determine elemental composition using SIMNRA 6.06v<sup>43</sup>. For each type of membrane sample tested, triplicate or quadruplicate samples were analyzed and results discussed correspond to the average concentrations and standard errors.

#### 3.2.5.4. XPS

The elemental composition in the near-surface region ( $\approx$  top 7 nm) of IA-membrane samples were obtained using XPS. A Kratos Axis Ultra DLD system was used with a monochromatic Al K $\alpha$  X-ray source (1486.6 eV) operated at 150 W, 90° take-off angle, and a beam analysis area of 300 x 700  $\mu\text{m}^2$ . High-resolution scans (0.1 eV) for IA-membranes were collected for carbon (C 1s), oxygen (O 1s), nitrogen (N 1s), and iodine (I 3d). Results discussed correspond to the average and concentration range of duplicate samples.

### 3.2.6. Physical characterization of membrane samples

#### 3.2.6.1. Contact Angle

The hydrophobicity of control and 2-AI membranes was quantified using captive bubble contact angle analysis, which is described in detail elsewhere<sup>44</sup> and in *Chapter 2*. The contact angle was calculated from digital images using several best fits methods with ImageJ 1.47v software (NIH provided public domain Java image processing software)<sup>45</sup> with the Contact Angle Plugin.<sup>46</sup> For each membrane, 19 unique replicate images in different areas of the surface were collected and analyzed. The results reported correspond to the averages and standard errors.

#### 3.2.6.2. Zeta potential via streaming current

The surface charge of control and 2-AI membranes was evaluated using a SurPASS Electrokinetic Analyzer using the streaming current method described in the literature.<sup>47</sup> Two membrane samples of 2.0  $\text{cm}^2$  each were placed in the adjustable gap cell with  $\approx$ 100  $\mu\text{m}$  gap height for analysis. A solution of 1.0 mM potassium chloride was used as the electrolyte

solution. Streaming current was measured twice per sample type at pH=6 to pH=10, then with fresh solution from pH=8 to pH=3, with the pH adjusted using potassium hydroxide and hydrochloric acid, respectively. The Helmholtz-Smoluchowski equation was used to calculate zeta potential values.

### 3.2.6.3. AFM

The surface roughness of control and 2-AI membranes was measured using an Asylum Research MFP-3D AFM (Santa Barbara, CA), equipped with BudgetSensors Tap300AI tips (Sofia, Bulgaria) and operated in tapping mode. Prior to analysis membrane samples were air-dried for >48 hours. For each membrane type, three unique 10×10  $\mu\text{m}^2$  regions were scanned. Each surface topography profile collected was used to calculate root-mean-square (RMS) roughness. Results reported correspond to the average and standard error of triplicate sample measurements.

## 3.2.7. Membrane performance tests

### 3.2.7.1 Biofilm inhibition

A static colony counting method was used to measure biofilm formation on membrane samples, as described in detail in *Chapter 2*. The biomass, measured as colony forming units (CFUs), of biofilms on membrane samples were measured and normalized by the membrane area to give the areal density of CFUs on the membranes, reported as  $\text{CFU}\cdot\text{cm}^{-2}$ . The areal densities of CFUs on control and 2-AI membranes were used to determine biofilm inhibition on 2-AI membrane samples. *P. aeruginosa* was chosen as the model bacteria to perform biofilm inhibition tests because they are ubiquitous in the environment, have been found in foulant at

membrane treatment plants, and are known to aggressively form biofilms.<sup>11,48</sup> The sample mean of the areal density of colony forming units (CFU) for control ( $\bar{x}_{CTL}$ , CFU.cm<sup>-2</sup>) samples and 2-AI ( $\bar{x}_{2AI}$  CFU.cm<sup>-2</sup>) membrane samples were used to calculate biofilm inhibition (%Inh) as

$$\%Inh = \left[ 1 - \left( \frac{\bar{x}_{2AI}}{\bar{x}_{CTL}} \right) \right] \times 100\% . \quad (1)$$

For each membrane type, biofilm inhibition tests were performed on a minimum of two separate days, with a minimum of six to twelve replicate samples analyzed each day. Results for average areal CFU density, biofilm inhibition, and p-values are reported separately for each day.

### 3.2.7.2. Water permeability and salt rejection

The water permeability and salt rejection of each membrane was evaluated using a bench scale cross-flow system operated at an applied pressure of 13.8 bar, 22.0° C, and 13.5 cm.s<sup>-1</sup> cross flow velocity. The membranes were first compacted with ultrapure water at pH=8.0 for 24 hours. Then the feed was switched to 500 mg.L<sup>-1</sup> sodium chloride dissolved in ultrapure water at pH=8.0. The feed was recirculated for 75 hours, with water permeability and salt rejection samples were taken at 15, 30, 40, 55, 65, and 75 hours. The water permeability coefficient ( $A$ , m.s<sup>-1</sup>.bar<sup>-1</sup>) was calculated as

$$A = \frac{J_w}{13.8 \text{ bar} \times 0.00146 \text{ m}^2} , \quad (2)$$

where  $J_w$  (m<sup>3</sup>.s<sup>-1</sup>) represents the water flux. The salt rejection (% $R$ ) of each membrane sample was calculated as

$$\%R = \left[ 1 - \left( \frac{c_p}{c_f} \right) \right] \times 100\% , \quad (3)$$

where  $C_p$  and  $C_f$  correspond to the conductivity of the permeate and feed waters, respectively. Each membrane type was run in two separate cross-flow tests (i.e. duplicate tests). The water permeability and salt rejection were reported as the average at each time point in the two separate tests.

### **3.2.8. Statistical significance testing**

The performance and physico-chemical properties of control and 2-AI membranes were compared using statistical significance testing. Unless otherwise specified, two-tailed, unpaired, two-sample t-tests assuming unequal variance were performed. The null hypothesis ( $H_0$ ) for these tests was that the mean of the control and 2-AI membrane were equal ( $\mu_{ctl} = \mu_{2-AI}$ ) and the alternative hypothesis ( $H_1$ ) was that the means were unequal ( $\mu_{ctl} \neq \mu_{2-AI}$ ). Throughout the results and discussion section  $p < 0.05$  (i.e. 95% confidence) is considered to indicate a statistically significant difference.

## **3.3. Results and Discussion**

### **3.3.1. Verification of formation of polyamide active layer in 2-AI membranes**

To verify the formation of the polyamide active layer in 2-AI membranes, FTIR and RBS were used to compare chemical bonds and elemental compositions, respectively, between the 2-AI and control membranes. The FTIR spectra of 2-AI and control membranes were consistent with those reported for other fully aromatic polyamide RO/NF membranes in the literature<sup>49</sup> (see *Appendix 2*). No significant differences in FTIR signature were observed when comparing the 2-AI membranes to control membranes. The RBS spectra of 2-AI and control membranes were also similar to those of other fully aromatic polyamide membranes in the literature<sup>39,40</sup> and no

significant changes due to 2-AI incorporation were observed. Therefore, FTIR and RBS results confirmed the successful casting of polyamide active layers in 2-AI membranes.

### **3.3.2. Verification of 2-AI incorporation into polyamide active layers in 2-AI membranes**

As indicated in Section 3.1, it was not possible to distinguish untreated samples of 2-AI and control membranes using FTIR or RBS analyses. This is because 2-AI-para does not contain chemical bonds or elements absent in polyamide. Therefore, we followed two different approaches to verify 2-AI incorporation into the polyamide active layers. First, we probed active layers with silver ion ( $\text{Ag}^+$ ) and evaluated via RBS measurement whether silver concentration in active layers differed between 2-AI and control membranes. Second, we used an iodine-containing surrogate molecule (4-iodoaniline) instead of 2-AI-para and evaluated via RBS detection of iodine whether 4-iodoaniline was incorporated into the active layers. In the remainder of this section we describe the first approach. The second approach is described in *Section 3.3.3.1*.

Silver ions associate with negatively charged functionalities (i.e. free carboxylic acid groups), and can also potentially complex with functional groups (i.e. amines).<sup>50,51</sup> **Figure 3.1.** shows that the  $\text{Ag}^+$  concentrations in the polyamide of 2-AI membranes were significantly different from those in the polyamide of the control membrane. The  $\text{Ag}^+$  concentration was highest in the 2-AI-Soak-PA membrane followed by 2-AI-MPD-PA, 2-AI-TMC-PA and control membranes. These results suggest increased concentration of free carboxylic acid groups or amines in the 2-AI membranes compared to in the control membranes.

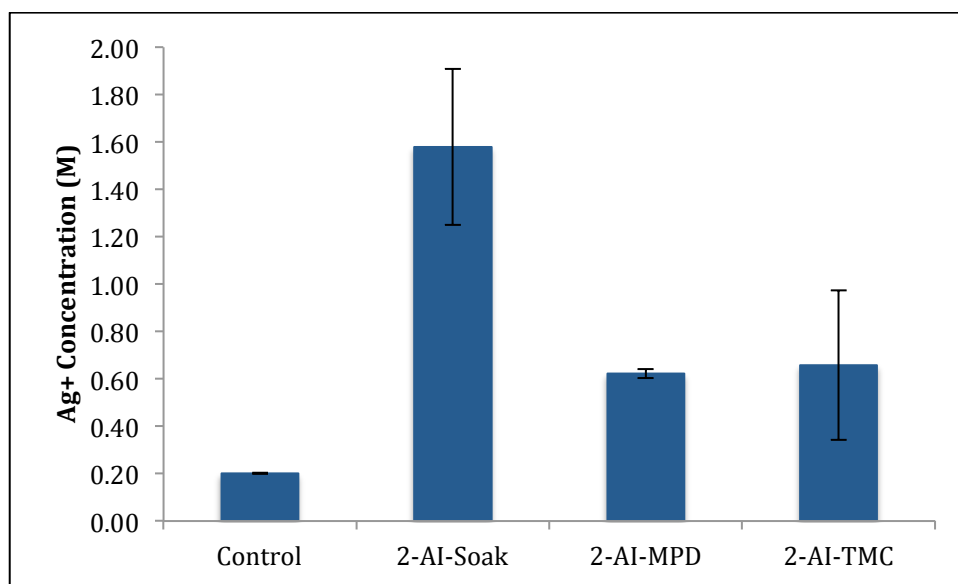


**Figure 3.1.** Average concentration of silver ion ( $\text{Ag}^+$ ) measured by RBS in the polyamide active layers of control and 2-AI membranes after being exposed to  $\text{Ag}^+$  probing solution at  $\text{pH}=10.5$ . Each bar corresponds to the average of triplicate samples, and error bars represent standard error.

There are two potential explanations for the higher silver content in 2-AI membranes. First, 2-AI-para is characterized by amine groups at both ends of the molecule (see **Table 3.1.**), and therefore it is reasonable to expect that incorporation of 2-AI-para into the 2-AI membranes would result in increased  $\text{Ag}^+$  concentration due to complexation. Second, increased silver concentration in  $\text{Ag}^+$ -probed 2-AI membranes could be the result of a higher concentration of free carboxylic acid groups in their active layers. A higher concentration of carboxylic groups, however, could result in changes in performance (e.g. increased water permeability and decreased salt rejection) and increased negative charge as measured by alternate methods.<sup>52</sup> Given that performance and surface charge results (see *Sections 3.3.4.* and *3.3.5.1.*) show that performance and charge did not substantially differ between 2-AI and control membranes, we conclude that the observed higher  $\text{Ag}^+$  concentration in 2-AI membranes, compared to in control membranes, is due to complexation of silver with amine moieties in the 2-AI-para, thus providing indirect evidence of 2-AI incorporation into the 2-AI membranes.

### **3.3.3. Evaluation of concentration and stability of 4-iodoaniline incorporated in membranes as a surrogate for 2-AIs**

#### *3.3.3.1. Verification of 4-iodoaniline incorporation into polyamide active layers*

We chose 4-iodoaniline (IA) as a surrogate for 2-AI because of their similar structure and size (see **Table 3.1.**). IA was incorporated into membranes in the same manner as 2-AI-para, adding it in the MPD, TMC or soak solutions instead, as described for 2-AI-para in *Section 3.2.2* and *3.3.2*. IA contains an iodine, which is not normally present in the polyamide active layer, and thus IA was quantified via measurement of iodine by RBS. The concentration of IA was used to approximate 2-AI concentration and stability. Results show an iodine signal in the RBS spectra of IA membranes (see *Appendix 2*), while it was absent in the controls, confirming incorporation of IA into the active layer and by extension indicating that 2-AI was also incorporated in the active layers of 2-AI membranes.

#### *3.3.3.2. Impact of procedural variables on concentration of 4-iodoaniline in active layers*

We evaluated the potential effect of compound concentration in the monomer/soak solutions on the concentration of compound incorporated into the membranes. To do this, the IA concentration in each of three solutions used for casting (MPD, TMC, and soak) was varied according to the “low”, “medium” and “high” IA concentrations in monomer/soak solutions listed in **Table 3.3.** For each polyamide active layer casting, one of the three IA solutions was used in place of the regular (IA-lacking) monomer/soak solution. Results for the volume-averaged concentration of IA in active layers measured by RBS are presented in **Figure 3.2.** The results show that the concentration of IA incorporated into the polyamide active layers was independent of the concentration of IA present in the monomer/soak solutions. Therefore, in



subsequent experiments, the “low” concentrations were used to incorporate IA into IA-membranes and 2-AI-para into 2-AI-membranes. The IA concentrations measured in the polyamide made with the “low” concentration IA solutions were used as estimates of the concentration of 2-AI-para incorporated in 2-AI membranes and are indicated as such in **Table 3.4.**

**Table 3.3.** Contents of iodoaniline (IA) in solutions used to fabricate IA membranes.

	IA solution concentrations		
	Low (mM)	Medium (mM)	High (mM)
<b>IA-soak</b>	1.5	3.3	13
<b>IA-MPD</b>	7.5	13	74
<b>IA-TMC</b>	0.85	1.7	3.1

The results in **Figure 3.2.** also show that the IA concentration incorporated into the polyamide active layer was statistically dependent on the method of incorporation. Adding IA to a post-PA-formation soak produced membranes with the highest concentration of IA incorporated. Less IA was observed in the polyamide of membranes produced by adding IA to the MPD solution, and the least IA was observed in polyamide of membranes produced by adding IA to the TMC solution. However, despite the incorporation approach, the IA concentrations in the active layer (0.16-0.95 M) were orders of magnitude higher than the concentration of 2-AI-para required for biofilm inhibition ( $IC_{50}=162\ \mu\text{M}$  as shown in *Chapter 2*). This suggests that all the 2-AI-membranes in this study would inhibit biofilm (as demonstrated experimentally in *Section 3.3.4.1*).

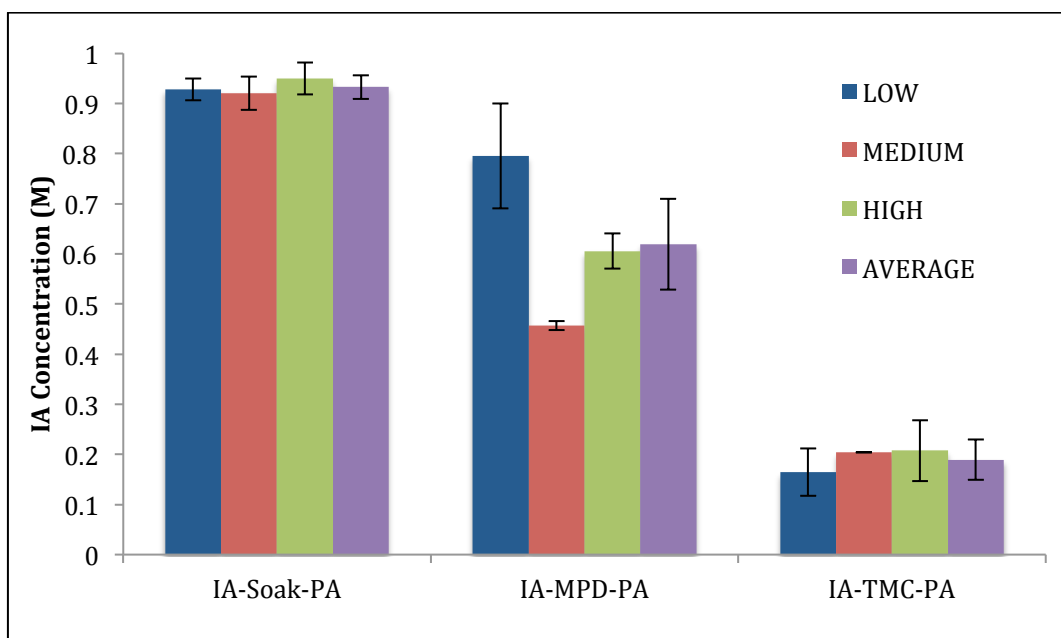


**Figure 3.2.** Concentration of iodoaniline (IA) incorporated into the polyamide active layer of membranes, as measured by RBS, using IA incorporation solutions with varying concentrations as defined in **Table 3.3**. Each bar corresponds to the average of 2-4 replicate samples, and error bars represent standard error.

The near-surface concentration of IA in the membranes was also analyzed using XPS, and the corresponding results are compared in **Figure 3.3** to volume-averaged results measured by RBS. The results show that just as for volume-averaged concentrations, the near-surface IA concentrations were greater when IA was added to the IA-soak solution, than when it was added to the MPD solution or TMC solution. While the near-surface concentration of IA in the IA-Soak-PA membrane was twice as high as the volume-averaged concentration, the near-surface concentration in the IA-MPD-PA and IA-TMC-PA membranes was not significantly different from the volume-averaged concentration. This is consistent with the fact that when IA is added to the IA-soak solution, the IA is contacting mostly the surface of the membrane, needing to diffuse inside it to reach the bulk region. However, when IA is added to the MPD or TMC solutions, it is present throughout the entire reaction zone during the polyamide formation and is therefore more likely to be present throughout the bulk of the active layer rather than concentrated at the surface.

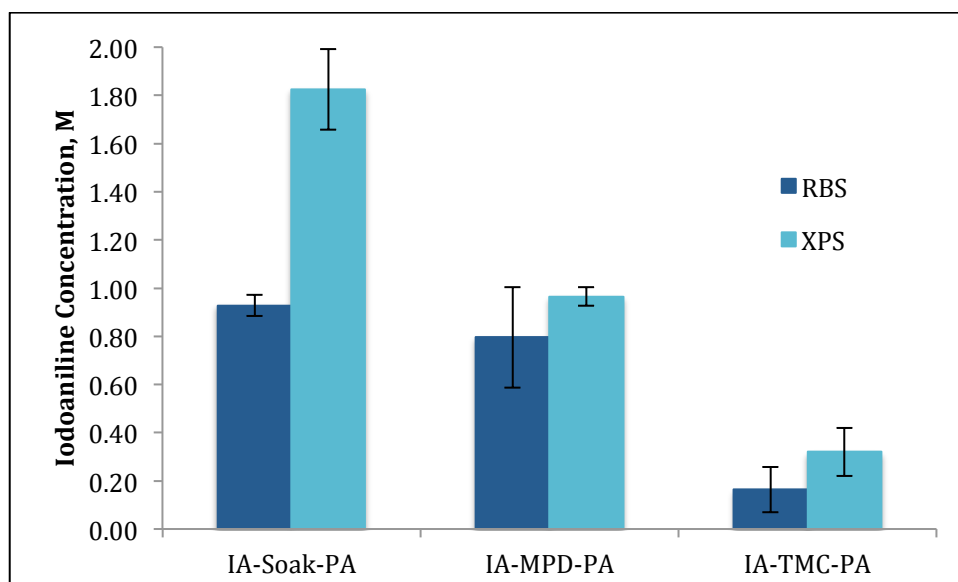


**Figure 3.3.** Concentration of iodoaniline (IA) incorporated into the polyamide active layer of four commercial membranes. RBS and XPS indicate volume-averaged and near-surface concentrations, respectively. Each bar corresponds to the average of 2-4 replicate samples, and error bars represent standard error.

RBS results also indicated that the IA concentration in the polyamide active layer (0.16-0.95 M) was 6 to 37 times higher than in the polysulfone support layer ( $0.026 \pm 0.002$  M). This indicates that 2-AI will mainly incorporate into the polyamide active layer. Also, the method of IA incorporation did not significantly affect the concentration of IA in the polysulfone layer.

### 3.3.3.3. Stability of incorporated iodoaniline

**Figure 3.4.** shows the concentration of IA as measured by RBS for each membrane after water filtration, various membrane cleaning procedures, and storage in pure water. The IA-Soak-PA membrane did not lose any IA after filtration, cleaning, or storage. This indicates that the incorporation approach, a post-PA-formation soak, produces a stable incorporation with the compound strongly bonded to the polyamide. Significant loss of IA occurred from the IA-MPD-PA membrane after being subjected to cleanings, storage, and use to purify water. Using the IA-MPD-PA membrane to purify water yielded the greatest IA loss, 62%, after which the IA

concentration was 0.30 M. There was no significant loss of IA during use of the IA-TMC-PA membrane to purify water for 6 hours, but 43-52% of IA was lost during cleaning and 2 months of storage. Although, there was loss of compound in the IA-MPD-PA and IA-TMC-PA membranes, the concentrations of compound remaining ( $>0.1$  M) remained orders of magnitude above those required for biofilm inhibition ( $162\ \mu\text{M}$ , as shown in *Chapter 2*). The IA lost likely consisted of IA that was sorbed to the membrane matrix rather than chemically bonded.

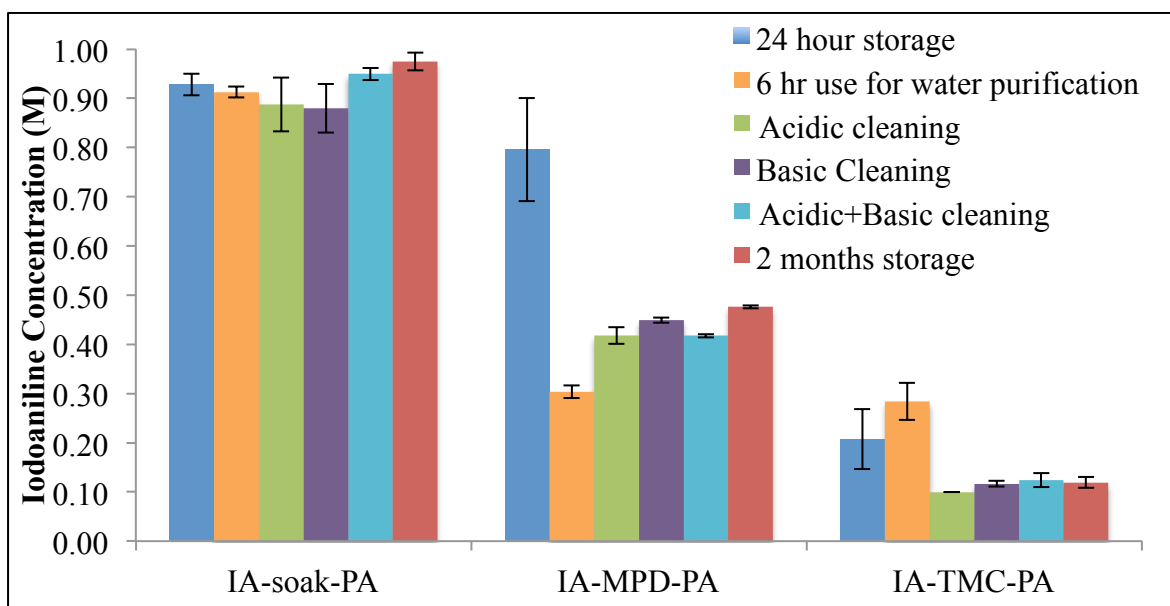


**Figure 3.4.** Concentration of iodoaniline (IA) in IA-membranes after membrane storage, membrane cleaning, and water filtration tests. Each bar corresponds to the average of 2-3 replicate samples, and error bars represent standard deviation.

### 3.3.4. Performance of 2-AI membranes

#### 3.3.4.1. Biofilm inhibition by 2-AI membranes

The main performance parameters that are used to select and compare water purification membranes include their selectivity (i.e. contaminant rejection) and water productivity (i.e. water permeability). In order for 2-AI membranes to be commercially viable, they would need to have

equal or better performance than the control membrane, while having a lower biofouling potential (i.e. they would need to inhibit biofouling). To evaluate whether the 2-AI membranes inhibit biofouling, the surface of the control and 2-AI membranes were exposed to *Pseudomonas aureginosa* (PA14) in nutrient broth solutions under static conditions, and the biomass of the biofilm that formed on the membranes was measured. Under normal operation, hydrodynamic forces from water flowing across the surface of the membrane and turbulence, limits the growth of biofilms.<sup>53,54</sup> In these tests biofilms are allowed to grow essentially uninhibited due to an ample nutrient supply and lack of turbulence and hydrodynamic forces. These test conditions represent what could be considered a worst-case scenario.

**Table 3.4.** and **Figure 3.5.** summarize biofouling results. All the 2-AI membranes significantly inhibited PA14 biofilm ( $p=0.002-0.04$ ) with 39%-92% less biomass growth on the 2-AI membranes than on the control membrane. The percent inhibitions obtained with the 2-AI-Soak polyamide membranes were much higher than those for other anti-biofouling membranes in the literature.<sup>15-17,19,21,22,24</sup> The percent inhibitions observed in **Table 3.4.** and **Figure 3.5.**, even those on the lower end, could potentially translate to a large reduction in the frequency of membrane cleaning needed and better membrane performance over time.

**Table 3.4.** Characteristics of control and 2-AI membranes. Uncertainty indicates standard error. The statistical significance of the difference in means between 2-AI and control membranes are indicated in the key.

Membrane	PA14 Biofilm inhibition <sup>a,f</sup>	[2-AI] in active layer <sup>c</sup> (M)	Water permeability <sup>e</sup> ( $\times 10^{-6} \text{ m.s}^{-1}.\text{bar}^{-1}$ )	Salt Rejection <sup>e</sup>	[Ag <sup>+</sup> ] <sup>d</sup> (M)	Contact Angle (degrees)	RMS Roughness (nm)
<b>Control (2-AI lacking)</b>	–	–	0.594±0.012	98.6±0.2%	0.20±0.002	20±1	48±3
<b>2-AI-Soak-PA</b>	92% <sup>g</sup> , 88% <sup>h</sup>	0.93±0.04	0.333±0.015 <sup>a</sup>	94.3±0.3% <sup>a</sup>	1.58±0.33 <sup>a</sup>	18±1 <sup>a</sup>	100±14 <sup>b</sup>
<b>2-AI-MPD-PA</b>	58% <sup>g</sup> , 39% <sup>h</sup>	0.80±0.21	0.436±0.021 <sup>a</sup>	97.4±0.4% <sup>a</sup>	0.62±0.02 <sup>a</sup>	17±1 <sup>a</sup>	42±4 <sup>b</sup>
<b>2-AI-TMC-PA</b>	62% <sup>g</sup> , 57% <sup>h</sup>	0.16±0.09	0.396±0.016 <sup>a</sup>	96.2±0.4% <sup>a</sup>	0.66±0.32 <sup>a</sup>	17±1 <sup>a</sup>	52±3 <sup>b</sup>

<sup>a</sup>p-value<0.05. <sup>b</sup>p-value≥0.15. <sup>c</sup>Estimated via RBS measurements of iodoaniline in iodoaniline-membranes. <sup>d</sup>Measured as [Ag<sup>+</sup>] in Ag<sup>+</sup>-probed membranes using RBS. <sup>e</sup>Obtained using 500 ppm sodium chloride as feed solution. <sup>f</sup>Samples tested during Day 1 were different from those tested during Day 2. <sup>g</sup>Average of results during testing Day 1. <sup>h</sup>Average of results during testing Day 2.

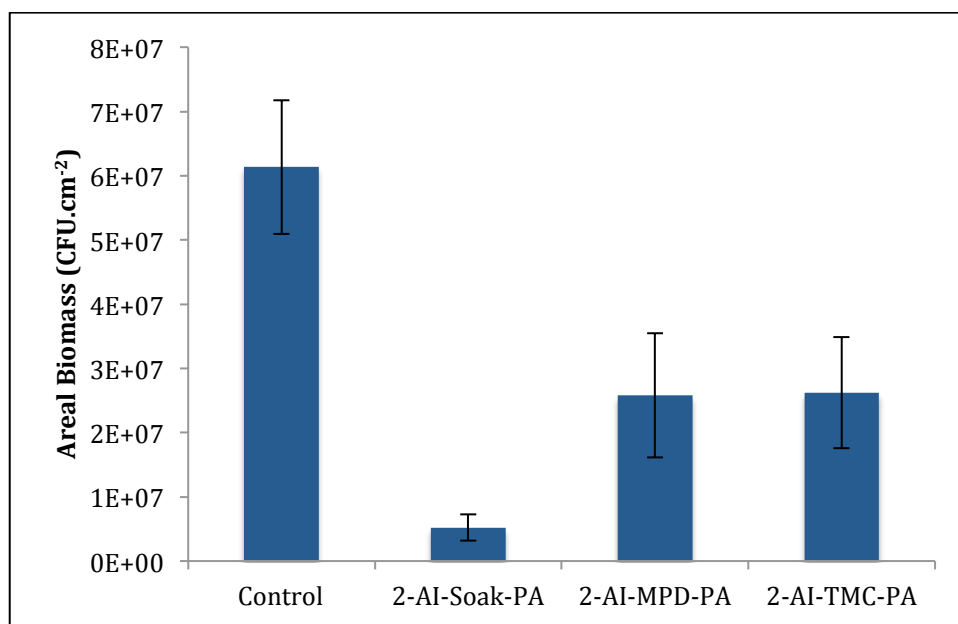


**Figure 3.5.** Areal Biomass of PA14 biofilm (as biomass per membrane area) on the surface of the control and 2-AI membranes. Each bar corresponds to the average of 6-12 replicates, and error bars represent standard error. The data shown corresponds to 92%, 58%, and 57% inhibition for the 2-AI-Soak-PA, 2-AI-MPD-PA, and 2-AI-TMC-PA membranes, respectively. All 2-AI membranes had biomass values statistically significantly lower ( $p$ -values  $\leq 0.01$ ) than control membranes.

As mentioned above, 2-AI-Soak-PA membranes inhibited biofilm the best, with an average of 90% inhibition, which is consistent with them having the highest concentration of 2-AI-para incorporated both in the near-surface and bulk active layer regions. The 2-AI-MPD-PA and 2-AI-TMC-PA membranes inhibited biofilm formation at 49% and 60% on average, respectively. The lower inhibition by the 2-AI-MPD-PA and 2-AI-TMC-PA membranes may be due to either having less 2-AI-para incorporated than the 2-AI-Soak-PA membrane or having 2-AI-para incorporated in the ‘wrong’ orientation. In *Chapter 2* we found that if 2-AI-para is coupled through the amino group of the phenyl linker, it will inhibit biofilm formation, but if it is coupled at the endocyclic imidazole nitrogen (whether or not it is bonded at the other site), it will not. Only a small fraction of 2-AI-para needs to couple through the amino group of the phenyl linker for biofilm to be significantly inhibited, as discussed in *Chapter 2*. Given that the concentration needed to inhibit biofilm ( $IC_{50}$ =162  $\mu$ M) is orders of magnitude lower than the

estimated 2-AI-para concentration in the 2-AI-MPD-PA and 2-AI-TMC-PA membranes, we conclude that the concentration of 2-AI-para in the active layer was not in itself the factor leading to lower biofouling inhibition in these two membranes, as compared to in the 2-AI-Soak-PA membrane. Rather, we speculate that the cause for lower biofouling inhibition in the 2-AI-MPD-PA and 2-AI-TMC-PA membranes is limited 2-AI-para coupling through the amino group of the phenyl linker.

### 3.3.4.2. Water permeability and salt rejection

**Table 3.4.** summarizes water permeability and salt rejection results for the 2-AI and control membranes. Results show that water permeability and salt rejection were 26-46% and 1-4 percentage points lower respectively for 2-AI membranes than for the control membrane ( $0.594 \times 10^{-6} \text{ m.s}^{-1}.\text{bar}^{-1}$  and 98.6%). The 2-AI-Soak-PA membrane had the lowest water permeability ( $0.333 \times 10^{-6} \text{ m.s}^{-1}.\text{bar}^{-1}$ ) and salt rejection (94.3%), followed by the 2-AI-TMC-PA membrane with a better performance ( $0.396 \times 10^{-6} \text{ m.s}^{-1}.\text{bar}^{-1}$  and 96.2%), and the 2-AI-MPD-PA membrane with the best performance ( $0.436 \times 10^{-6} \text{ m.s}^{-1}.\text{bar}^{-1}$  and 97.4%) of the 2-AI membranes. Even though the 2-AI membranes had statistically lower salt rejections than the control membrane, it is important to note that this study constitutes a proof-of-concept study where no systematic attempt was made to maximize water permeability and salt rejection in 2-AI membranes. The 2-AI incorporation process and polyamide casting could potentially be optimized in order to minimize or eliminate differences in permeability between the 2-AI and control membranes. Further, while the water permeability of the 2-AI membranes was lower, the 2-AI membranes biofouled substantially less than the control membranes and therefore could potentially exhibit higher water permeability over the long-term and with real waters. Thus, on the basis of the substantial biofouling inhibition exhibited by the 2-AI membranes, the limited



decrease observed in water permeability and salt rejection, and the compatibility of the 2-AI incorporation method with current membrane casting practices, the results presented in this study support 2-AI incorporation into polyamide active layers as a promising avenue to enhance current RO/NF membranes.

### **3.3.5. Membrane charge, hydrophobicity, and roughness in 2-AI membranes and their potential contribution to biofilm inhibition**

#### *3.3.5.1. Charge*

We compared the active layer charge, hydrophobicity (Section 3.5.2) and roughness (Section 3.5.3) of control and 2-AI membranes to understand the cause of biofilm inhibition by the 2-AI membranes. These physico-chemical properties are known to affect membrane fouling potential, including biofouling.<sup>55,53</sup> **Figure 3.6** shows zeta potential results in the pH=3-10 range for the control and 2-AI membranes. The results for the control, 2-AI-MPD-PA, and 2-AI-TMC-PA membranes are not statistically different. The results for the 2-AI-Soak-PA membrane is significantly different from the results for the control membrane. The zeta potentials are less negative for the 2-AI-Soak-PA membrane than for the control membrane and the isoelectric point is also at a higher pH (pH=3.7 and 3.4) for the 2-AI-Soak-PA and control membranes, respectively). The less negative surface charge of the 2-AI-Soak-PA membrane would indicate higher biofouling potential;<sup>55,53</sup> however, as discussed in 3.3.4.1., the 2-AI-Soak-PA membrane inhibited biofouling by 90% on average. Thus, the significant biofilm inhibition by this membrane is not attributable to changes in surface charge.

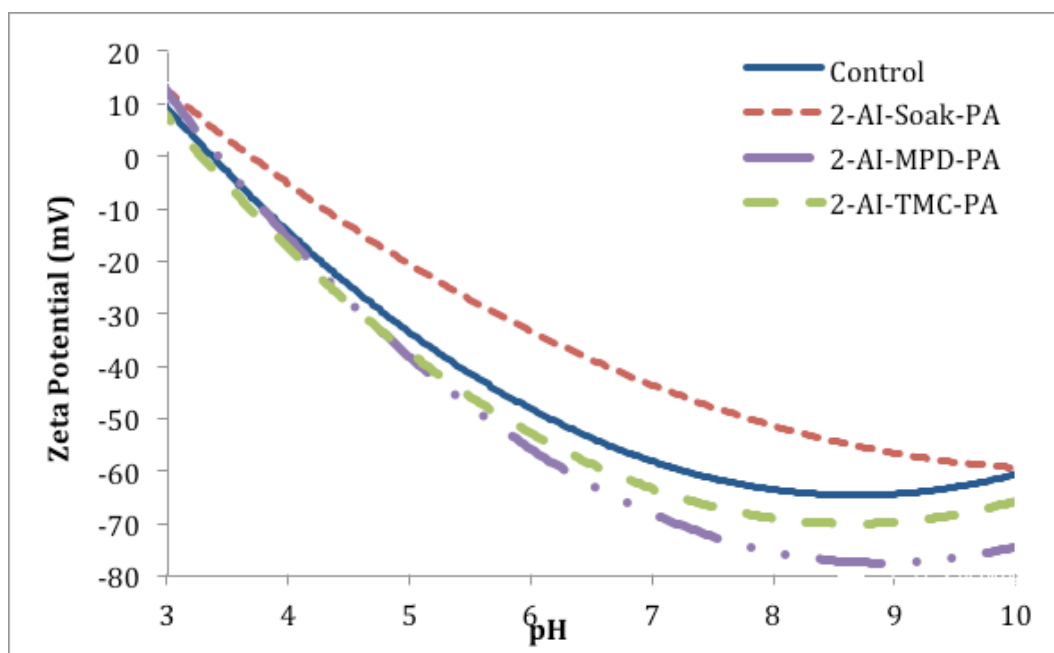


**Figure 3.6.** Comparison of regressed zeta potential in the pH range of 3-10 for the control and 2-AI membranes. Zeta potentials were calculated using the Helmholtz-Smoluchowski equation. The regressions were made using a minimum of 185 streaming current measurements and at maximum 285 streaming current measurements for each membrane type. Measurements were collected for two samples of each membrane type on two separate days and at least four measurements were performed at each pH.

### 3.3.5.2. Hydrophobicity

**Table 3.4.** and **Figure 3.7.** summarize contact angle measurements for the control and 2-AI membranes. The results show that the contact angles of 2-AI membranes (17-18°) were statistically significantly lower ( $p < 0.05$ ) than the contact angle of the control membrane (20°). This indicates that 2-AI membranes were more hydrophilic than control membranes. Although higher hydrophilicity is generally correlated with lower biofouling potential,<sup>53,55</sup> the differences between the contact angles of 2-AI and control membranes were relatively small (2-3°), and therefore unlikely to contribute significantly to the substantial biofouling inhibition (49-90%) exhibited by the 2-AI membranes.

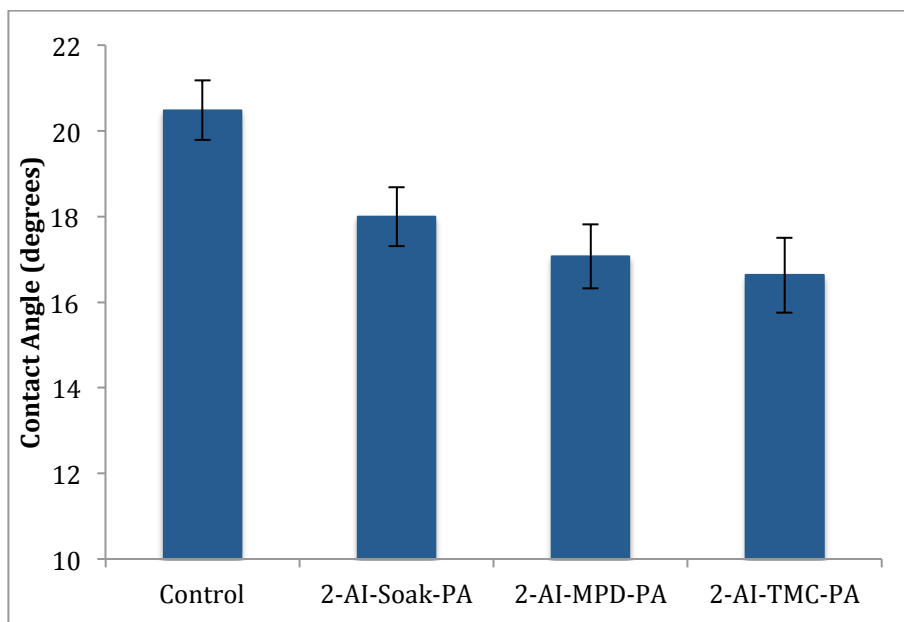


**Figure 3.7.** Contact angle for the control and 2-AI membranes as measured by the captive bubble method. Each bar corresponds to the average of 19 replicate measurements, and error bars represent standard error.

### 3.3.5.3. Roughness

**Table 3.4.** and **Figure 3.8.** present the roughness results for the control and 2-AI membranes. The results show that there were no statistically significant differences in roughness between the control and 2-AI membranes. However, we note that even though with a two-tailed t-test and at the chosen confidence level (95%), there is no statistical difference, the 2-AI-Soak-PA membrane was notably rougher than the other membranes, and when compared to the control membrane gives a p-value of 0.06. Even though a rougher surface would generally indicate higher biofouling potential,<sup>53,55,56</sup> as discussed in *Section 3.3.4.1.* the 2-AI-Soak-PA membrane inhibited biofouling by 90% on average. Thus, the significant biofilm inhibition by this membrane is not attributable to changes in surface roughness.

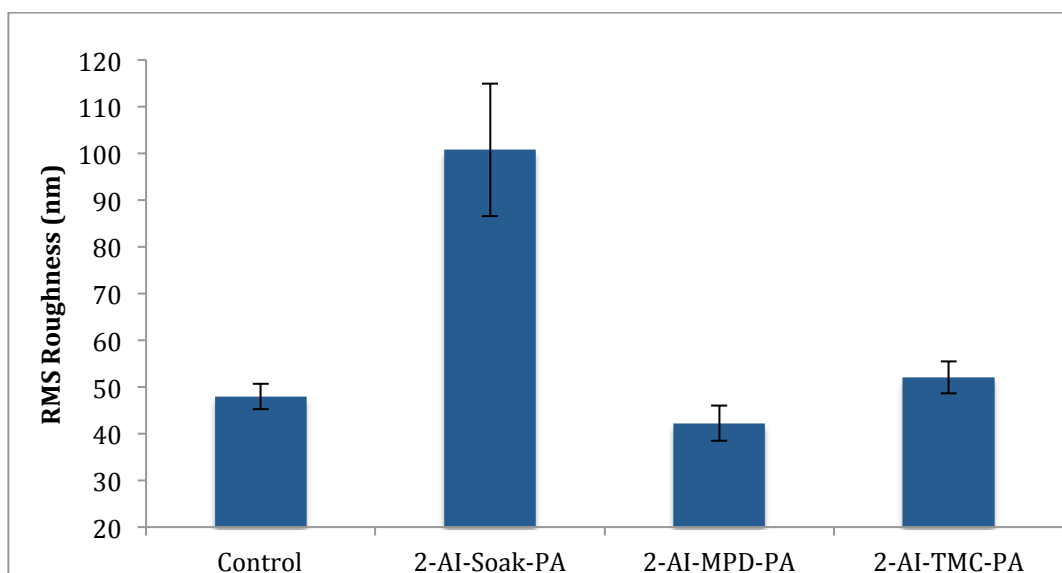


**Figure 3.8.** Root-mean-squared (RMS) roughness of control membranes and 2-AI membranes. Each bar corresponds to the average of measurements on triplicate samples, and error bars represent standard error.

On the basis of the above results for membrane charge, hydrophobicity, and roughness, the observed reduction in biofouling potential of 2-AI membranes compared to the control membrane is not attributable to differences in the physico-chemical properties of polyamide active layers. Thus, we conclude that the observed biofouling inhibition is a direct result of the presence and action of 2-AI-para in the polyamide membranes.

### 3.4. Conclusions

We assessed novel anti-biofouling 2-AI membranes that were prepared through the incorporation of 2-AI-para during the polyamide active layer casting process. The 2-AI incorporation approach, the stability of 2-AI incorporation, the physico-chemical changes due to 2-AI incorporation, and the performance of 2-AI membranes were evaluated. Our experimental results support the following main conclusions:

- PA14 biofilm was significantly ( $p=0.002-0.04$ ) inhibited by 2-AI membranes, 39-92%. 2-AI-Soak-PA membranes inhibited biofilm the best at 90% on average.

- 2-AI incorporation in membrane active layers (0.16-0.95 M) was orders of magnitude higher than required for biofilm inhibition.
- The extent of loss of 2-AI surrogate compound was dependent upon the incorporation approach used and was in the -5-62% range. However, in all cases, the concentration of the compound remained orders of magnitude higher than what was required for significant biofilm inhibition to occur.
- Physico-chemical changes (i.e. charge, hydrophobicity, and roughness) in 2-AI membranes likely did not contribute significantly to biofilm inhibition. Thus, the observed biofouling inhibition in 2-AI membranes is attributed to the presence and action of 2-AI-para.
- Water productivity was 26-44% lower and salt rejection was 1.2-4.3 percentage points lower for 2-AI membranes than for the control membrane; however, the casting procedure of 2-AI membranes was not optimized to maximize water productivity and salt rejection.

These findings serve as a proof-of-concept of (i) the biofouling inhibition properties of 2-AI membranes, and (ii) the feasibility of readily incorporating 2-AI into polyamide active layers during the common commercial membrane manufacturing process. These 2-AI membranes represent a promising, novel enhancement for biofouling prevention and control. Further 2-AI membrane optimization and performance testing, as well as a techno-economic analysis, are needed to evaluate the overall potential benefits of 2-AI incorporation into active layers.

### **3.5. Acknowledgments**

This work was supported by the National Science Foundation (NSF) Grant Opportunities for Academic Liaison with Industry (GOALI) and Chemical, Bioengineering, Environmental,

and Transport Systems (CBET) program under Award#1264690, NSF Environmental Engineering program under Award#1336532, a Sigma Xi Grant-in-Aid of Research (GIAR) award, the National Water Research Institute (NWRI) and American Membrane Technology Association (AMTA) Fellowship for Membrane Technology, and The UNC Graduate School Dissertation Completion Fellowship. The authors would like to thank Dr. Thomas Clegg for his help with RBS analyses, Dr. Carrie Donley for assistance with XPS and AFM analyses, and the Miller research group for use of contact angle equipment. LC-MS analyses were performed at RBS analyses were performed at the Triangle Universities Nuclear Laboratories (TUNL), Durham, NC, which is partially supported by the US Department of Energy Office of Nuclear Physics (Grant Numbers 97ER41041 and 97ER41033). XPS and AFM were performed at the Chapel Hill Analytical and Nanofabrication Laboratory (CHANL) at UNC, a member of the North Carolina Research Triangle Nanotechnology Network (RTNN), which is supported by the National Science Foundation (Grant ECCS-1542015) as part of the National Nanotechnology Coordinated Infrastructure (NNCI).

## REFERENCES

- (1) Flemming, H.-C. Reverse Osmosis Membrane Biofouling. *Exp. Therm. Fluid Sci.* **1997**, *14* (4), 382–391.
- (2) Nguyen, T.; Roddick, F.; Fan, L. Biofouling of Water Treatment Membranes: A Review of the Underlying Causes, Monitoring Techniques and Control Measures. *Membranes (Basel)*. **2012**, *2* (4), 804–840.
- (3) Huertas, E.; Herzberg, M.; Oron, G.; Elimelech, M. Influence of Biofouling on Boron Removal by Nanofiltration and Reverse Osmosis Membranes. *J. Memb. Sci.* **2008**, *318* (1–2), 264–270.
- (4) Xu, P.; Drewes, J. E.; Kim, T.-U.; Bellona, C.; Amy, G. Effect of Membrane Fouling on Transport of Organic Contaminants in NF/RO Membrane Applications. *J. Memb. Sci.* **2006**, *279* (1–2), 165–175.
- (5) Vogel, D.; Simon, A.; Alturki, A. A.; Bilitewski, B.; Price, W. E.; Nghiem, L. D. Effects of Fouling and Scaling on the Retention of Trace Organic Contaminants by a Nanofiltration Membrane: The Role of Cake-Enhanced Concentration Polarisation. *Sep. Purif. Technol.* **2010**, *73* (2), 256–263.
- (6) Sweity, A.; Oren, Y.; Ronen, Z.; Herzberg, M. The Influence of Antiscalants on Biofouling of RO Membranes in Seawater Desalination. *Water Res.* **2013**, *47* (10), 3389–3398.
- (7) Matin, A.; Khan, Z.; Zaidi, S. M. J.; Boyce, M. C. Biofouling in Reverse Osmosis Membranes for Seawater Desalination: Phenomena and Prevention. *Desalination* **2011**, *281*, 1–16.
- (8) Yu, C.; Wu, J.; Contreras, A. E.; Li, Q. Control of Nanofiltration Membrane Biofouling by *Pseudomonas Aeruginosa* Using D-Tyrosine. *J. Memb. Sci.* **2012**, *423–424*, 487–494.
- (9) Ying, W.; Siebdrath, N.; Uhl, W.; Gitis, V.; Herzeberg, M. New Insights on Early Stages of RO Membranes Fouling during Tertiary Wastewater Desalination. *J. Memb. Sci.* **2014**, *466*, 26–35.
- (10) Al-Ahmad, M.; Aleem, F. A.; Mutiri, A.; Ubaisy, A. Biofouling in RO Membrane Systems. Part 1: Fundamentals and Control. *Desalination* **2000**, *132* (October), 173–179.
- (11) Herzberg, M.; Elimelech, M. Physiology and Genetic Traits of Reverse Osmosis Membrane Biofilms: A Case Study with *Pseudomonas Aeruginosa*. *ISME J.* **2008**, *2* (2), 180–194.
- (12) Lee, W.; Ahn, C. H.; Hong, S.; Kim, S.; Lee, S.; Baek, Y.; Yoon, J. Evaluation of Surface Properties of Reverse Osmosis Membranes on the Initial Biofouling Stages under No Filtration Condition. *J. Memb. Sci.* **2010**, *351* (1–2), 112–122.

- (13) Habimana, O.; Semião, a. J. C.; Casey, E. The Role of Cell-Surface Interactions in Bacterial Initial Adhesion and Consequent Biofilm Formation on Nanofiltration/reverse Osmosis Membranes. *J. Memb. Sci.* **2014**, *454*, 82–96.
- (14) Altman, S. J.; Cappelle, M.; Clem, P. G.; Cook, A. W.; Christopher, H.; Hart, W. E.; Hibbs, M. R.; Ho, C. K.; Jones, H. D. T.; Khalsa, S.; Noek, R.; Sun, A. C.; Webb, S. W.; Mcgrath, L. K.; James, D. L.; Adout, A.; Elimelech, M.; Kang, S. *Analysis of Micromixers and Biocidal Coatings on Water Treatment Membranes to Minimize Biofouling*; SAND2009-8316; Albuquerque, NM, 2009.
- (15) Varin, K. J.; Lin, N. H.; Cohen, Y. Biofouling and Cleaning Effectiveness of Surface Nanostructured Reverse Osmosis Membranes. *J. Memb. Sci.* **2013**, *446*, 472–481.
- (16) Malaisamy, R.; Berry, D.; Holder, D.; Raskin, L.; Lepak, L.; Jones, K. L. Development of Reactive Thin Film Polymer Brush Membranes to Prevent Biofouling. *J. Memb. Sci.* **2010**, *350*, 361–370.
- (17) Xu, J.; Wang, Z.; Yu, L.; Wang, J.; Wang, S. A Novel Reverse Osmosis Membrane with Regenerable Anti-Biofouling and Chlorine Resistant Properties. *J. Memb. Sci.* **2013**, *435*, 80–91.
- (18) Kappachery, S.; Paul, D.; Kweon, J. H. Effect of N-Acetylcysteine against Biofouling of Reverse Osmosis Membrane. *Desalination* **2012**, *285*, 184–187.
- (19) Nikkola, J.; Liu, X.; Li, Y.; Raulio, M.; Alakomi, H. L.; Wei, J.; Tang, C. Y. Surface Modification of Thin Film Composite RO Membrane for Enhanced Anti-Biofouling Performance. *J. Memb. Sci.* **2013**, *444*, 192–200.
- (20) Bera, A.; Gol, R. M.; Chatterjee, S.; Jewrajka, S. K. PEGylation and Incorporation of Triazine Ring into Thin Film Composite Reverse Osmosis Membranes for Enhancement of Anti-Organic and Anti-Biofouling Properties. *Desalination* **2015**, *360*, 108–117.
- (21) Zhu, X.; Bai, R.; Wee, K. H.; Liu, C.; Tang, S. L. Membrane Surfaces Immobilized with Ionic or Reduced Silver and Their Anti-Biofouling Performances. *J. Memb. Sci.* **2010**, *363* (1–2), 278–286.
- (22) Karkhanechi, H.; Takagi, R.; Matsuyama, H. Biofouling Resistance of Reverse Osmosis Membrane Modified with Polydopamine. *Desalination* **2014**, *336*, 87–96.
- (23) Blok, A. J.; Chhasatia, R.; Dilag, J.; Ellis, A. V. Surface Initiated Polydopamine Grafted Poly ([2-( Methacryoyloxy) Ethyl] Trimethylammonium Chloride ) Coatings to Produce Reverse Osmosis Desalination Membranes with Anti-Biofouling Properties. *J. Memb. Sci.* **2014**, *468*, 216–223.
- (24) Wei, X.; Wang, Z.; Zhang, Z.; Wang, J.; Wang, S. Surface Modification of Commercial Aromatic Polyamide Reverse Osmosis Membranes by Graft Polymerization of 3-Allyl-5,5-Dimethylhydantoin. *J. Memb. Sci.* **2010**, *351* (1–2), 222–233.



- (25) Vercellino, T.; Morse, A.; Tran, P.; Song, L.; Hamood, A.; Reid, T.; Moseley, T. Attachment of Organo-Selenium to Polyamide Composite Reverse Osmosis Membranes to Inhibit Biofilm Formation of *S. Aureus* and *E. Coli*. *Desalination* **2013**, *309*, 291–295.
- (26) Hoffman, L. R.; D'Argenio, D. a; MacCoss, M. J.; Zhang, Z.; Jones, R. a; Miller, S. I. Aminoglycoside Antibiotics Induce Bacterial Biofilm Formation. *Nature* **2005**, *436*, 1171–1175.
- (27) Worthington, R.; Richards, J.; Melander, C. Small Molecule Control of Bacterial Biofilms. *Org. Biomol. Chem.* **2012**, *10* (37), 7457–7474.
- (28) Rogers, S.; Melander, C. Construction and Screening of a 2-Aminoimidazole Library Identifies a Small Molecule Capable of Inhibiting and Dispersing Bacterial Biofilms across Order, Class, and Phylum. *Angew. Chemie Int. Ed* **2008**, *47* (28), 5229–5231.
- (29) Peng, L.; DeSousa, J.; Su, Z.; Novak, B. M.; Nevzorov, A. a; Garland, E. R.; Melander, C. Inhibition of *Acinetobacter Baumannii* Biofilm Formation on a Methacrylate Polymer Containing a 2-Aminoimidazole Subunit. *Chem. Commun.* **2011**, *47* (17), 4896–4898.
- (30) Thompson, R. J.; Bobay, B. G.; Stowe, S. D.; Olson, A. L.; Peng, L.; Su, Z.; Actis, L. a; Melander, C.; Cavanagh, J. Identification of BfmR , a Response Regulator Involved in Biofilm Development, as a Target for a 2-Aminoimidazole-Based Antibiofilm Agent. *Biochemistry* **2012**, No. 51, 9776–9778.
- (31) Hentzer, M.; Riedel, K.; Rasmussen, T. B.; Heydorn, A.; Andersen, J. B.; Parsek, M. R.; Rice, S. a.; Eberl, L.; Molin, S.; Høiby, N.; Kjelleberg, S.; Givskov, M. Inhibition of Quorum Sensing in *Pseudomonas Aeruginosa* Biofilm Bacteria by a Halogenated Furanone Compound. *Microbiology* **2002**, *148*, 87–102.
- (32) Hentzer, M.; Wu, H.; Andersen, J. B.; Riedel, K.; Rasmussen, T. B.; Bagge, N.; Kumar, N.; Schembri, M. a.; Song, Z.; Kristoffersen, P.; Manefield, M.; Costerton, J. W.; Molin, S.; Eberl, L.; Steinberg, P.; Kjelleberg, S.; Høiby, N.; Givskov, M. Attenuation of *Pseudomonas Aeruginosa* Virulence by Quorum Sensing Inhibitors. *EMBO J.* **2003**, *22* (15), 3803–3815.
- (33) Gotoh, Y.; Eguchi, Y.; Watanabe, T.; Okamoto, S.; Doi, A.; Utsumi, R. Two-Component Signal Transduction as Potential Drug Targets in Pathogenic Bacteria. *Curr. Opin. Microbiol.* **2010**, *13* (2), 232–239.
- (34) Bourret, R. B.; Silversmith, R. E. Two-Component Signal Transduction. *Curr. Opin. Microbiol.* **2010**, *13*, 113–115.
- (35) Rogers, S. A.; Huigens, R. W.; Cavanagh, J.; Melander, C. Synergistic Effects between Conventional Antibiotics and 2-Aminoimidazole-Derived Antibiofilm Agents. *Antimicrob. Agents Chemother.* **2010**, *54* (5), 2112–2118.

- (36) Worthington, R. J.; Bunders, C. A.; Reed, C. S.; Melander, C. Small Molecule Suppression of Carbapenem Resistance in NDM-1 Producing *Klebsiella Pneumonia*. *ACS Med. Chem. Lett.* **2012**, *3*, 357–361.
- (37) Melander, C.; Cavanagh, J.; Ritchie, D.; Huigens III, R.; Ballard, T. E.; Richards, J. J.; Lindsey, T. W.; Lindsey, J. S. Inhibition of Biofilms in Plants with Imidazole Derivatives. US 8,278,340 B2, 2012.
- (38) Coronell, O.; González, M. I.; Mariñas, B. J.; Cahill, D. G. Ionization Behavior, Stoichiometry of Association, and Accessibility of Functional Groups in the Active Layers of Reverse Osmosis and Nanofiltration Membranes. *Environ. Sci. Technol.* **2010**, *44* (17), 6808–6814.
- (39) Coronell, O.; Marinas, B. J.; Cahill, D. G. Depth Heterogeneity of Fully Aromatic Polyamide Active Layers in Reverse Osmosis and Nanofiltration Membranes. *Environ. Sci. Technol.* **2011**, *45* (10), 4513–4520.
- (40) Mi, B.; Coronell, O.; Mariñas, B. J.; Watanabe, F.; Cahill, D. G.; Petrov, I. Physico-Chemical Characterization of NF/RO Membrane Active Layers by Rutherford Backscattering Spectrometry. *J. Memb. Sci.* **2006**, *282*, 71–81.
- (41) Attayek, P. J.; Meyer, E. S.; Lin, L.; Rich, G. C.; Clegg, T. B.; Coronell, O. A Remotely Controlled, Semi-Automatic Target System for Rutherford Backscattering Spectrometry and Elastic Recoil Detection Analyses of Polymeric Membrane Samples. *Nucl. Instruments Methods Phys. Res. Sect. A Accel. Spectrometers, Detect. Assoc. Equip.* **2012**, *676*, 21–25.
- (42) Mi, B.; Cahill, D. G.; Mariñas, B. J. Physico-Chemical Integrity of Nanofiltration/reverse Osmosis Membranes during Characterization by Rutherford Backscattering Spectrometry. *J. Memb. Sci.* **2007**, *291* (1), 77–85.
- (43) Mayer, M. *SIMNRA User's Guide*; Garching, Germany, 2002.
- (44) Baek, Y.; Kang, J.; Theato, P.; Yoon, J. Measuring Hydrophilicity of RO Membranes by Contact Angles via Sessile Drop and Captive Bubble Method: A Comparative Study. *Desalination* **2012**, *303*, 23–28.
- (45) Rasband, W. ImageJ. National Institutes of Health, USA 2013, p 2013.
- (46) Brugnara, M. Contact Angle Plugin. National Institutes of Health, USA 2006.
- (47) Buksek, H.; Luxbacher, T.; Petrinic, I. Zeta Potential Determination of Polymeric Materials Using Two Differently Designed Measuring Cells of an Electrokinetic Analyzer. *Acta Chim Slov* **2010**, *57*, 700–706.
- (48) Al Ashhab, A.; Herzberg, M.; Gillor, O. Biofouling of Reverse-Osmosis Membranes during Tertiary Wastewater Desalination: Microbial Community Composition. *Water Res.* **2014**, *50*, 341–349.

- (49) Tang, C. Y.; Kwon, Y.-N.; Leckie, J. O. Effect of Membrane Chemistry and Coating Layer on Physiochemical Properties of Thin Film Composite Polyamide RO and NF Membranes. *Desalination* **2009**, *242* (1–3), 149–167.
- (50) Coronell, O.; Mariñas, B. J.; Cahill, D. G. Accessibility and Ion Exchange Stoichiometry of Ionized Carboxylic Groups in the Active Layer of FT30 Reverse Osmosis Membrane. *Environ. Sci. Technol.* **2009**, *43* (13), 5042–5048.
- (51) IUPAC. Stability Constants Database. Academic Software: Yorks, UK 2001.
- (52) Ghosh, A. K.; Jeong, B. H.; Huang, X.; Hoek, E. M. V. Impacts of Reaction and Curing Conditions on Polyamide Composite Reverse Osmosis Membrane Properties. *J. Memb. Sci.* **2008**, *311*, 34–45.
- (53) Subramani, A.; Hoek, E. M. V. Direct Observation of Initial Microbial Deposition onto Reverse Osmosis and Nanofiltration Membranes. *J. Memb. Sci.* **2008**, *319*, 111–125.
- (54) van Loosdrecht, M.; Eikelboom, D.; Gjaltema, A.; Mulder, A.; Tijhuis, L.; Heijnen, J. Biofilm Structures. *Water Res.* **1995**, *32* (8), 35–43.
- (55) Kang, S.; Hoek, E. M. V.; Choi, H.; Shin, H. Effect of Membrane Surface Properties During the Fast Evaluation of Cell Attachment. *Sep. Sci. Technol.* **2006**, *41* (7), 1475–1487.
- (56) Li, Q.; Xu, Z.; Pinnau, I. Fouling of Reverse Osmosis Membranes by Biopolymers in Wastewater Secondary Effluent: Role of Membrane Surface Properties and Initial Permeate Flux. *J. Memb. Sci.* **2007**, *290* (1–2), 173–181.

## **CHAPTER 4: CHARACTERIZATION OF PERFORMANCE OF NOVEL 2-AMINOIMIDAZOLE ANTI-BIOFOULING MEMBRANES UNDER OPERATIONALLY REALISTIC CONDITIONS**

### **4.1. Introduction**

Nanofiltration (NF) and reverse osmosis (RO) membranes are commonly used to purify a variety of waters that are difficult to treat (e.g., brackish water, seawater, wastewater effluent, industrial wastewaters). One of the biggest, most widespread challenges in the application of high-pressure water purification membranes is the accumulation or growth of substances on their surfaces, otherwise known as fouling. Fouling increases operational costs and negatively impacts membrane performance. For example, fouling increases the frequency of membrane cleaning and membrane replacement, including the need for chemicals and down time associated with these procedures, and decreases membrane water productivity and the quality of purified water.<sup>1-5</sup>

A variety of substances from the feed water can foul membranes, including precipitated inorganics (scaling), organic matter (organic fouling), colloids (colloidal fouling), and bacterial biofilms (biofouling). Among these four types of fouling, biofouling is the most difficult one to prevent and control.<sup>2,6-9</sup>

Biofouling occurs initially when planktonic microbes in the feed solution, sensing a suitable surface in their environment, attach to the membrane.<sup>1,7,10,11</sup> These sessile bacteria grow, reproduce, and excrete extracellular polymeric substances (EPS) to form a biofilm. Most biofouling control strategies aim to kill, inactivate, or remove bacteria prior to attachment with technologies such as micro-/ultrafiltration and feed water disinfection (e.g., chlorination, chloramination).<sup>12-24</sup> Other unconventional approaches seek to prevent the attachment of bacteria,

or to kill/inactivate bacteria upon attachment through modifying the membrane surface with nanopatterns, incorporating biocides, or by making the surface more hydrophilic.<sup>13–15,25–27</sup> In many cases, these various control methods are unsuccessful, have limited impact on fouling, or even promote biofouling. A major limitation of these methods is that they do not target the EPS (which constitute up to 90% of biofilms by volume<sup>1,7,9</sup>) or the process of biofilm formation and growth by the bacteria. An ideal biofouling control strategy would actively prevent both bacterial attachment and biofilm formation and growth, including bacterial excretion of EPS.

In *Chapters 2 and 3*, we describe such a control technology, where a 2-aminoimidazole (2-AI) is incorporated into the polyamide active layer of polyamide RO/NF membranes. These “2-AI membranes” inhibited biofilms significantly ( $p=0.001-0.12$ ) and substantially (by up to 96% compared to corresponding control 2-AI lacking membranes). The 2-AI is a bioactive, but non-biocidal compound, that blocks a wide range of bacteria from sensing and responding to their environment by disrupting the bacteria’s two-component regulatory system.<sup>28–30</sup> By disrupting this system, the bacteria stay in a planktonic state, do not attach to surfaces, do not excrete EPS, and thus do not form biofilms.<sup>29,31–35</sup> 2-AIs are the only known non-biocidal class of compounds that are effective at preventing and dispersing biofilms of bacteria across different phyla, classes, and orders.<sup>29,31–35</sup>

The results in *Chapters 2 and 3* show that 2-AI membranes performed the best when 2-AI was incorporated after polyamide casting as opposed to during polyamide casting. This conclusion was reached on the basis of the observation that 2-AI membranes with 2-AI incorporated after polyamide casting achieved the highest levels of biofilm inhibition while maintaining salt rejection and sacrificing the least water permeability. More specifically, commercial polyamide RO/NF membranes to which 2-AI was incorporated in our laboratory

significantly ( $p=0.01-0.12$ ) inhibited *Pseudomonas aeruginosa* biofilms by 61-96%, when tested with pure bacterial solutions (i.e., no other types of foulants present) with ample nutrient supply under static conditions (i.e., uninhibited by hydrodynamic forces). These levels of biofilm inhibition are higher than those for anti-biofilm membranes reported in the literature.<sup>14-16,18,20,21,23</sup> Also, in half of the membranes tested (2 out of 4), pure water permeability did not significantly change upon 2-AI incorporation; in the other half, pure water permeability decreased (13-25%) due to 2-AI incorporation. Given that the potential decrease in water permeability in full-scale operation is greater for the control (2-AI lacking) membrane than for the 2-AI membrane, because the 2-AI membranes inhibit biofouling, lower pure water permeabilities for some of the 2-AI membranes would not necessarily translate into lower water permeabilities in full-scale operations. Further, it is important to note that no efforts have been made to optimize 2-AI membranes for maximum water permeability, and therefore it is possible that the 2-AI incorporation method could be tailored to minimize or eliminate observed water permeability reductions.

In order to evaluate anti-biofouling membranes for further development and whether they can be feasibly used commercially, they should be tested under operationally realistic conditions, including using cross-flow filtration configuration and real waters that contain multiple foulants, or multiple waters containing different foulants. Not only is it important to test these membranes under realistic conditions for proof-of-concept, but it is also important to understand the fouling mechanisms on the anti-biofouling membranes, including whether 2-AI incorporation alters organic matter accumulation, bacterial deposition, and biofilm formation. A more complex, systematic understanding of fouling will enable the anti-biofouling technology to be optimized, as well as appropriately and widely applied.

Accordingly, the overall goal of this chapter was to evaluate the differences in overall performance (i.e., fouling, water permeability, salt rejection), and the mechanisms at play in those differences, between 2-AI membranes and corresponding (2-AI lacking) control membranes. In order to achieve this overall research goal we sought to meet the following specific objectives: (1) to evaluate water permeability and salt rejection changes in 2-AI and control membranes due to biofilm formation, bacterial cell deposition, and organic matter accumulation; (2) to quantify and characterize the foulants on 2-AI and control membranes; and (3) to relate the differences in fouling to differences in performance between 2-AI and control membranes.

## **4.2. Materials and Methods**

### ***4.2.1. Reagents, control membranes, and 2-AI membranes***

Unless otherwise noted, all reagents were purchased from commercial sources, were of ACS reagent grade or better, and were used without further purification. The chemical structure of the 2-AI molecule (i.e., 5-(4-aminophenyl)-1*H*-imidazol-2-amine, or 2-AI-para for short) that was incorporated into commercial membranes to produce 2-AI membranes is shown in **Figure 4.1**. 2-AI-para was synthesized in-house and purity confirmed as described in *Chapter 1* and *Appendix 1*. ESPA3 commercial membranes (Hydramautics, Oceanside, CA) were used as the membranes into which 2-AI-para was incorporated. ESPA3 membranes were selected for modification because the ESPA3 with 2-AI incorporated was shown in *Chapter 2* to inhibit biofilm to a high degree (71%,92%) while having a moderate difference in water permeability and no difference in salt rejection compared to the corresponding control (2-AI lacking) membranes. The 2-AI membranes were prepared as described in *Chapter 2*. Briefly, ESPA3 membranes were exposed to a basic (pH=9) aqueous solution of 2-AI-para (1.6 mmol), 1-ethyl-

3-(3-dimethylaminopropyl)carbodiimide (1.0 mmol), N-methylmorpholine (1.5 mmol), and hydroxybenzotriazole (1.0 mmol) overnight ( $\approx 18$  hours), and then rinsed with ultrapure water.

The membranes were prepared immediately prior to use for each experiment.

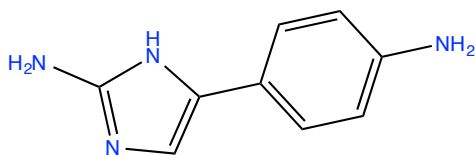


**Figure 4.1.** The 2-AI molecule (5-(4-aminophenyl)-1H-imidazol-2-amine, or 2-AI-para for short) incorporated into commercial membranes to produce 2-AI membranes.

#### 4.2.2. Cross-flow Apparatus

A custom-built laboratory-scale flat sheet membrane cross-flow system, shown in **Figure 4.2**, with four membrane cells (7.65 cm x 4.65 cm effective membrane area each) in series was used for fouling experiments. The equipment, manufacturers, and 2016 costs for the system are given in the *Appendix 3*. The pH, temperature, and dissolved oxygen (DO) of the feed water were monitored throughout experiments. The pH was monitored with a pH electrode connected to a pH meter, the original pH of feed waters was 6.97-7.86, there was no adjustment to the feed pH during the fouling experiments but the pH was steady with less than 0.3 units of pH change over the full 75 hour experiments (typically increasing). The temperature was kept constant at 22.0° C using a recirculating chiller. The DO was measured using a handheld water quality meter with DO probe (YSI, Yellow Springs, OH), and DO concentration was between 6.2 and 7.0 mg.L<sup>-1</sup> in the feed during all runs. The pressures before each cell, at the pump, and at the flow meter on the concentrate line were measured using pressure transducers. The pressure (13.8 $\pm$ 0.3 bar) and cross-flow velocity (14 cm.s<sup>-1</sup>) were regulated by pump speed and adjusting the metering valve on the concentrate line. Permeate samples were collected at the permeate sampling ports and feed samples were taken directly from the feed reservoir. The permeate flow



rate was calculated at least once per day by measuring the weight of permeate collected per unit of time.

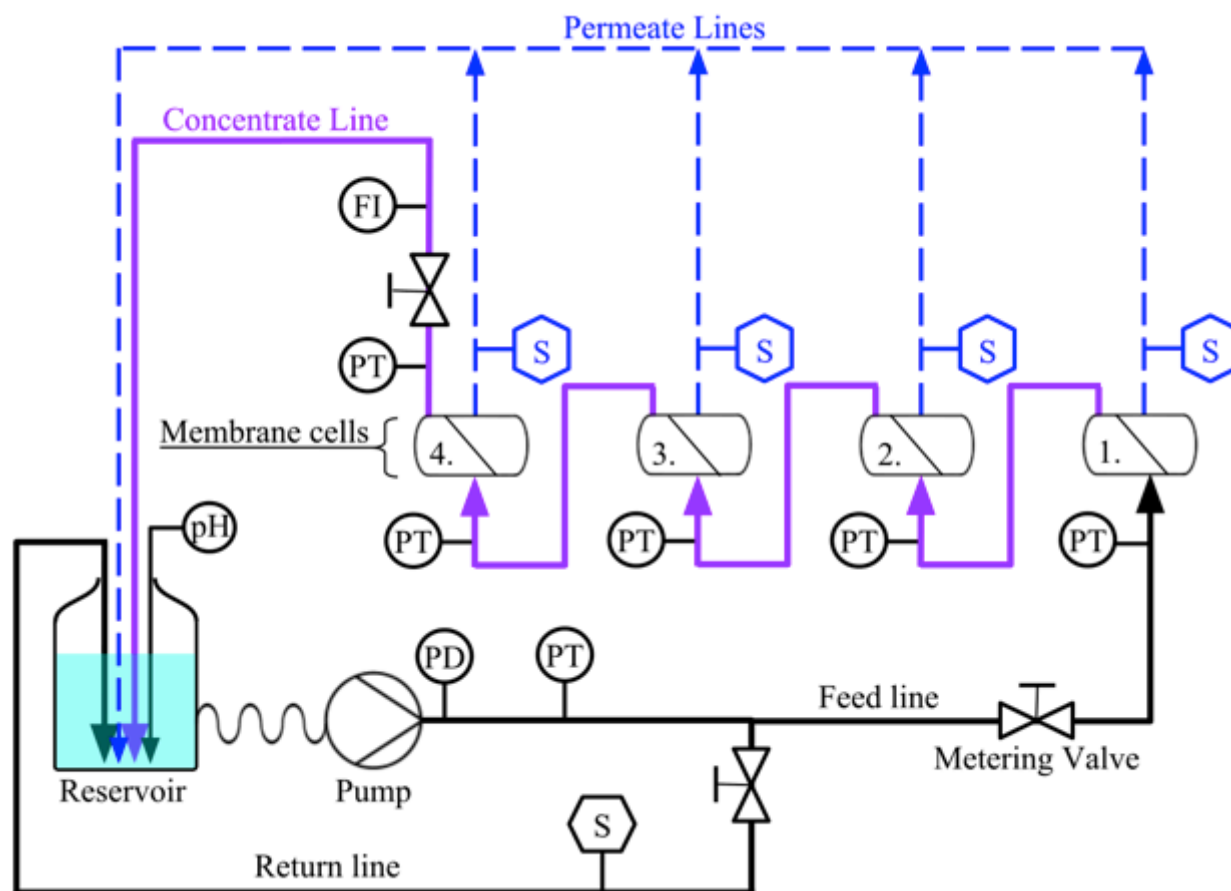


**Figure 4.2.** A custom-built laboratory-scale cross-flow system, equipped with four flat-sheet membrane cells (7.65 cm x 4.65 cm effective membrane area each) in series, electronic pressure transducers, a flow indicator, sampling ports, a recirculating chiller for temperature control, pH electrode and meter, and metering valves to control flow and pressure. The membrane cells are numbered 1 through 4. PD = pulsation dampener, PT = pressure transducer, FI = flow indicator, S = sampling port. Figure prepared and provided by Mikayla D. Armstrong.

#### 4.2.3. Feed solutions

**Table 4.1.** describes the different feed solutions that were used in the cross-flow fouling experiments. The contents of solutions were modeled after a Herzberg and Elimelech biofouling study.<sup>36</sup> The natural water used was a raw drinking water source, University Lake, collected at the OWASA Jones Ferry Drinking Water Treatment Plant in Carrboro, NC (USA) in

September 2016 and stored at 4° C for a maximum of one month prior to use. The non-purgeable dissolved organic carbon concentration (DOC) of the natural water was 7.2 mg.L<sup>-1</sup> and the UV 254 absorbance was 0.23 cm<sup>-1</sup>. The water was filtered using a 1.2 µm G4 glass fiber filter (Fisher Scientific, Hampton, NH, USA), followed by a 0.45 µm hydrophilic mixed cellulose ester filter (EMD Millipore, Billerica, MA). Ultrapure water (≥17.9 MΩ.cm) was prepared in house and had no detectable DOC. In all solutions, Lennox LB broth (1.0 mL.L<sup>-1</sup>) and potassium phosphate (0.45 mM) were added to provide nutrients and stabilize the pH, respectively. Sodium azide (2 mM) was added to some of the feed solutions to inhibit bacterial growth. In the biofouling-only and cell-deposition-only feeds, there was relatively low background conductivity (<10 µS), so the following combination of monovalent and divalent salts<sup>36</sup> were added to achieve conductivity similar to the natural water (≈330 µS): 2.6 mM NaCl, 0.55 mM NaHCO<sub>3</sub>, 0.4 mM MgSO<sub>4</sub>, and 0.6 mM NH<sub>4</sub>Cl.

**Table 4.1.** Description of feed solutions used in cross-flow fouling experiments.

Feed solution <sup>a</sup>	Fouling mechanisms expected	Feed Solution contents
Organic-only	Organic matter deposition	Natural water, nutrients (LB broth), buffer (potassium phosphate)-autoclaved Growth inhibitor (sodium azide)
Biofouling-only	Biofilm formation+ cell deposition	Ultrapure water, nutrients (LB broth), PA14 <sup>b</sup> (10 <sup>7</sup> cells.ml <sup>-1</sup> ), salts, buffer (potassium phosphate)
Cell-deposition-only	Cell deposition	Ultrapure water, nutrients (LB broth), PA14 <sup>b</sup> (10 <sup>9</sup> cells.ml <sup>-1</sup> ), salts, buffer (potassium phosphate)-autoclaved Growth inhibitor (sodium azide)
Organic&biofouling	Organic matter deposition + cell deposition + biofilm formation	Natural water, nutrients (LB broth), buffer (potassium phosphate)--autoclaved PA14 <sup>b</sup> (10 <sup>7</sup> cells.ml <sup>-1</sup> )

<sup>a</sup> Feed solutions have been labeled for the targeted type of fouling.

<sup>b</sup> PA14= *Pseudomonas aeruginosa* strain 14

Feed solutions were autoclaved at 121° C for 60 minutes on a liquid sterilization cycle to prevent undesired bacterial growth. Feed waters were always autoclaved before adding the sodium azide and when applicable, before adding the bacteria.

The bacteria that was used to biofoul the membranes was *Pseudomonas aeruginosa* strain 14 (PA14) because *P. aeruginosa* are ubiquitous in the environment, have been found in foulant on membranes at treatment plants, and known to aggressively form biofilms.<sup>11,37</sup> PA14 was cultured overnight in LB broth to exponential growth phase. The overnight culture was then washed by centrifuging the cultures at 3670 rpm for 10 minutes, decanting the broth,

and then vortexing the pellet in a small volume (e.g., 15 mL) of the appropriate feed solution. This sequence (centrifugation, decanting and vortexing in new feed solution) was performed twice more before the concentration of PA14 solution was measured as optical density at 600 nm. The PA14 solution was diluted in the feed water to achieve the target concentration as indicated in **Table 4.1.**, assuming  $OD_{600}=0.012-0.013=10^7$  cells.mL<sup>-1</sup> and  $OD_{600}=0.7=10^8$  cells.mL<sup>-1</sup>.

#### ***4.2.4. Fouling experiments and cleaning of membrane system***

The cross-flow system was cleaned before and after every experiment to disinfect and remove trace contaminants as described elsewhere.<sup>36</sup> The following cleaning solutions were circulated through the system in sequence for the indicated times: 0.5% sodium hypochlorite for 2 hours, ultrapure water for 15 minutes twice, 5 mM ethylenediaminetetraacetic acid, 2 mM sodium dodecylbenzenesulfonate, ultrapure water for 15 minutes three times, 70% ethanol for 1 hour, and ultrapure water three times.

After cleaning, four fresh membranes were placed in the cells with feed and permeate spacers, with control membranes in cells 1 and 3 and 2-AI membranes in cells 2 and 4. The membranes were compacted with ultrapure water at pH=8 and 13.8 bar for 24 hours, ensuring the pure water permeability was stable (<2% change per hour). The ultrapure water was then replaced with the appropriate feed solution, as listed in **Table 4.1.** Fouling experiments were conducted at constant pressure (13.8 bar) and cross-flow velocity (14 cm.s<sup>-1</sup>) for 75 hours total. Feed and permeate samples were collected at 0, 15, 30, 40, 55, 65, and 75 hours for analyses of water permeability and contaminant rejection, as described in subsequent sections. At 75 hours of filtration, the pressure was slowly decreased to prevent quick changes in pressure that could have altered the foulant layer. The membranes were carefully taken out of the cells,

very lightly rinsed with ultrapure water to remove loose bacteria and residual feed, and analyzed for foulant physico-chemical and biological characteristics as described below.

#### ***4.2.5 Scanning electron microscopy (SEM)***

SEM images of membrane surfaces were obtained to capture visually the foulant layers of 2-AI and control membranes. Both fouled and unfouled membrane samples of each 2-AI and control membranes were imaged. Membrane samples were air dried for >48 hours prior to SEM analysis and the samples were coated with 2–5 nm of a Au/Pd alloy to prevent charging. SEM imaging was performed using a Helios Nanolab 600 dual beam system (FEI, Hillsboro, OR), and accelerating voltage and current of 2.0 kV and 0.34 nA, respectively.

#### ***4.2.6. Attenuated total reflectance-Fourier transform infrared (ATR-FTIR)***

ATR-FTIR analysis was used to characterize the chemical signatures and relative thickness of foulant layers on control and 2-AI-membranes. All samples were gently rinsed with ultrapure water, and then air-dried for > 48 hours prior to analysis. Four replicate samples were analyzed for each sample type and 24 scans were taken per replicate. The spectra reported are the average of the replicates. Analyses were performed on a sample area of 3.1 mm<sup>2</sup> over the 400–3997 cm<sup>-1</sup> wavenumber range with 2 cm<sup>-1</sup> resolution. Analyses were performed using a Bruker Alpha spectrometer (Bruker Optics, Billerica, MA), equipped with an IR source with a 45° incident angle and an Alpha-P ATR accessory.

To compare the relative thickness of foulant layers on different membranes, we used an approach similar to that described by Hausman and Escobar<sup>38</sup>. The IR wave is not able to penetrate fouled membranes as deeply as unfouled membranes due to wave attenuation at the foulant layer. Thus, the relative thicknesses of foulant layers in fouled samples can be assessed based on the attenuation of the intensities of the FTIR peaks associated with the membrane

materials (polyamide and polysulfone). The intensities of the foulant-associated peaks can also be compared among different membrane samples, where higher peak intensities suggest a greater concentration of the associated bond or molecules.

#### ***4.2.7. Dissolved (non-purgeable) organic carbon (DOC)***

Permeate and feed samples for DOC analysis were collected at 75 hours of membrane treatment time during cross-flow experiments. Fouled membrane samples (2 cm<sup>2</sup>) and virgin membrane samples (as blanks) were submerged in ultrapure water (5 mL) immediately after the cross-flow experiment, and the resulting solutions with the membrane still immersed in it were alternately vortexed for 30 seconds and sonicated for 1 minute for a total of three cycles. After the vortexing/sonicating cycles the membrane surface appeared to be free of organic matter. The solution was then analyzed for DOC. Calibration standards were prepared with potassium hydrogen phthalate diluted in ultrapure water. All DOC samples and standards were prepared by filtration through 0.45  $\mu$ m hydrophilic mixed cellulose ester filter, diluting to the appropriate concentration range (1-10 mg.L<sup>-1</sup>), and then adjusting the pH to <2.5 with hydrochloric acid. The samples were analyzed on a Shimadzu TOC-V CPH analyzer equipped with an ASI-V autosampler.

#### ***4.2.8. EPS extraction and characterization of polysaccharide and protein content***

Immediately following cross-flow experiments, fouled membrane samples (4 cm<sup>2</sup>) were added to 20 mL of 0.1 M NaCl and shaken for 45 minutes at 4° C. The EPS was then extracted as described by Liu and Fang,<sup>39</sup> by adding formaldehyde and sodium hydroxide to the solution with the membrane still immersed in it, followed by centrifugation, then the solution was filtered through a 0.22  $\mu$ m nylon filter, and which was then dialyzed against ultrapure water

using a 3.5 kDa membrane (Spectra/Por). EPS extracts for unfouled membranes were used as controls and were prepared in the same manner as the EPS extracts for fouled membranes.

The polysaccharide content in EPS extract samples was quantified as described by Dubois et. al.,<sup>40</sup> using phenol and sulfuric acid, followed by measuring the absorbance at 492 nm against alginic acid standards prepared in ultrapure water. The protein content was quantified as described by Bradford<sup>41</sup> using Coomassie protein assay reagent, standards prepared with bovine serum albumin in ultrapure water, and absorbance measurements at 595 nm.

#### ***4.2.9. PA14 enumeration in feed solutions and membrane samples***

Feed water samples were collected at least twice (at 0 and at 75 hours) for bacterial enumeration during every cross-flow experiment. After the cross-flow run, fouled membrane samples (2 cm<sup>2</sup>) were rinsed with ultrapure water to remove loose bacteria, and the membrane samples were added to 2.0 mL LB broth. These LB solutions with membranes were alternately vortexed for 30 seconds and sonicated for 30 seconds for three cycles. After the vortex-sonication cycles membranes were taken out of membrane bacterial extract solutions.

The bacteria were enumerated in feed water samples and membrane bacterial extract solutions by a colony count method where vortexed solutions were serially diluted (nine 10x dilutions) and spotted (5 µL) onto LB-agar plates, which were incubated at 37° C overnight. The formed colonies were counted and the areal density of biomass (CFU.cm<sup>-2</sup>) was calculated. The areal density of biomass was used as the quantitative descriptor of areal mass of biofilm on fouled membranes. No colonies were detected in the feed, nor on the membranes during the sterile runs (with organic-only and cell-deposition-only feed solutions, see **Table 4.1.**).

#### 4.2.10. Water permeability and solute rejection

Water permeability is the amount of water that is produced by a membrane normalized by unit time, pressure, and membrane area. The water flux ( $J_w$ ,  $\text{m}^3 \cdot \text{s}^{-1}$ ) of each membrane sample tested in fouling experiments was measured at 0, 15, 30, 40, 55, 65, and 75 hours. The measured  $J_w$  was used to obtain the membrane water permeability ( $A$ ,  $\text{m} \cdot \text{s}^{-1} \cdot \text{bar}^{-1}$ ) as

$$A = \frac{J_w}{13.8 \text{ bar} \times 0.00146 \text{ m}^2} \quad . \quad (1)$$

When evaluating decline in performance due to fouling, normalized water permeability ( $A_t/A_0$ ) was reported and was calculated as the water permeability at time  $t$  ( $A_t$ ) divided by the initial water permeability ( $A_0$ ).

The salt rejection ( $\%R_s$ ) of membrane samples (collected at 0, 15, 30, 40, 55, 65, and 75 hours) tested in fouling experiments was also obtained.  $\%R_s$  was calculated as

$$\%R_s = \left[ 1 - \left( \frac{C_p}{C_f} \right) \right] \times 100\% \quad , \quad (2)$$

where  $C_p$  and  $C_f$  correspond to the conductivities of the permeate water and feed water, respectively. Additionally, TOC was measured in permeate and feed water samples collected after 75 hours of fouling. The corresponding TOC concentrations were used in Equation 2 (instead of conductivity values) to calculate the rejection of organics ( $\%R_{org}$ ).

#### 4.2.11. Statistical significance testing

When appropriate, statistical significance testing was used to compare the performance (i.e., water permeability, solute rejection, and fouling) of control and 2-AI-membranes. Unless otherwise stated, a one-tail unpaired two-sample t-test assuming unequal variances was used. The null hypothesis ( $H_0$ ) was that the mean of the control membrane was equal to the mean of



the 2-AI membrane ( $\bar{\mu}_{\text{ctl}} = \bar{\mu}_{2\text{-AI}}$ ), and the alternative hypothesis ( $H_1$ ) was that one of the means was greater than the other ( $\bar{\mu}_{\text{ctl}} > \bar{\mu}_{2\text{-AI}}$  or  $\bar{\mu}_{\text{ctl}} < \bar{\mu}_{2\text{-AI}}$ ). The calculated p-values are reported throughout the results and discussion section and  $p < 0.05$  is considered significant. When p-values were close to being significant (e.g.,  $0.05 < p \leq 0.15$ ), results are discussed further in the results and discussion.

### 4.3. Results and Discussion

#### 4.3.1. Characterization of membrane foulant layers in control and 2-AI membranes

##### 4.3.1.1. Visual Appearance

**Figure 4.3.** shows representative SEM images of control and 2-AI membranes after being fouled with the various feed solutions, listed in **Table 4.1.**, for 75 hours. Fouling the membranes with the organic-only feed solution produced a dense, but smooth fouling layer on both control and 2-AI membranes, with no distinctive differences between the two membrane types. The fouling mechanism that appeared to occur was organic matter accumulation. The cracking in the organic fouling layers was due to the sample drying process.

When the biofouling-only feed solution was used to foul the membranes, both control and 2-AI membranes were covered in what appeared to be a biofilm (the expected fouling mechanism), with distinctive rod shapes associated with the bacteria (PA14). The only visual difference between control and 2-AI membranes was a slightly higher areal density of bacteria on the control membrane.

When the membranes were fouled with the cell-deposition-only feed solution, there was not a clear cohesive fouling layer as with the biofouling-only feed solution, but rather patchy accumulations of dark rod shapes from bacteria on top of the membrane. The images clearly show (particularly at 1000x magnification) that the membrane fouling mechanism was cell deposition, with more cell deposition on the control membrane than on the 2-AI membrane.

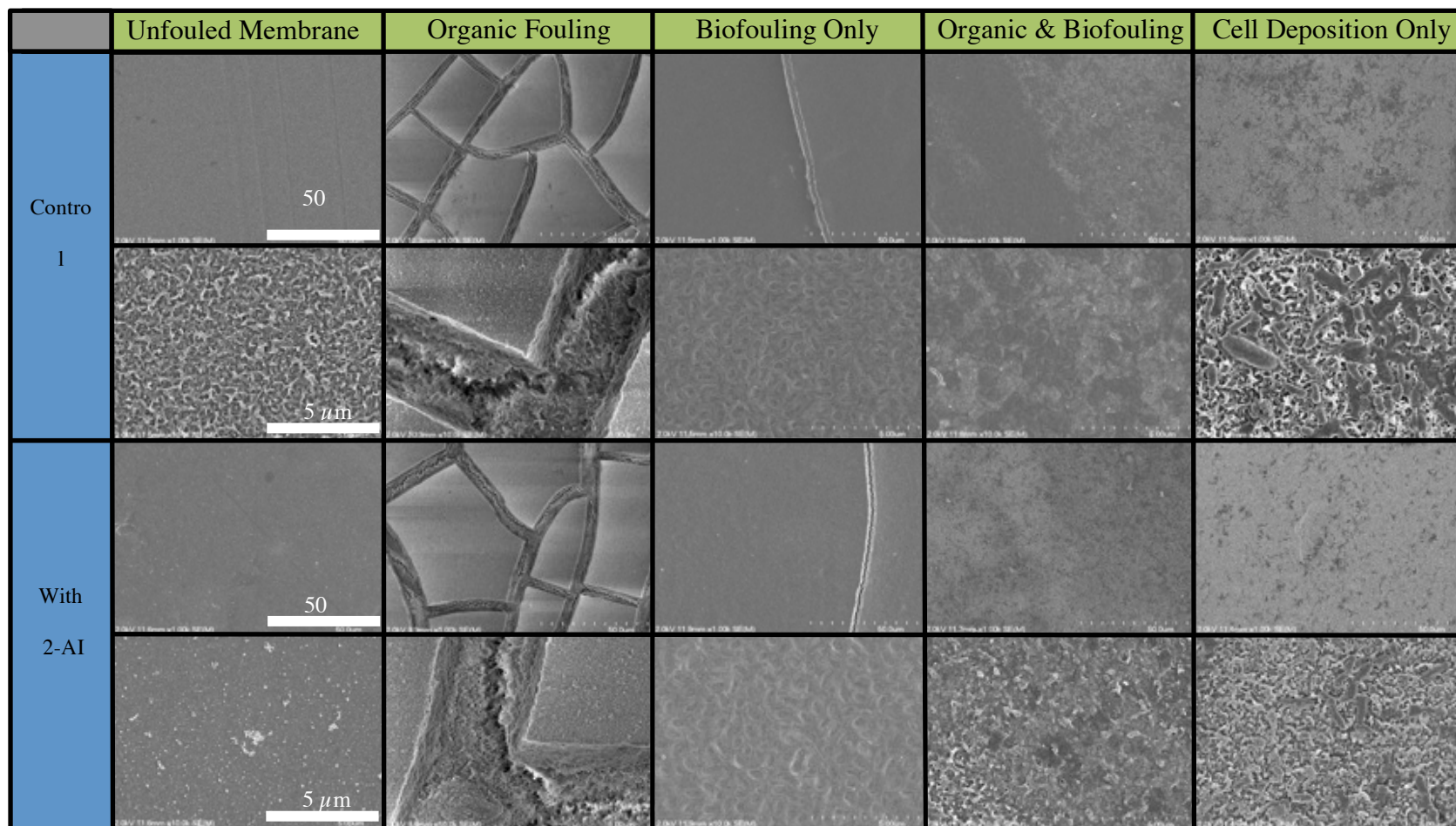


**Figure 4.3.** Representative surface SEM images of fouled control and fouled 2-AI membranes at 1000x (rows 1 and 3) and 10000x (rows 2 and 4) magnifications. The scale bars on the 1000x and 10000x images are 50  $\mu\text{m}$  and 5  $\mu\text{m}$ , respectively.

Finally, when the membranes were fouled using the organic&biofouling feed solution, the fouling layers appeared visually different than when fouled with the other feed solutions. The control membrane was fully covered by the foulant layer, whereas the 2-AI membrane had some areas of clean membrane. On the control membrane, a number of bacteria were embedded in a foulant layer that looked rougher than the foulant layer of membranes fouled with the biofouling-only or organic-only feed solutions. The 2-AI membrane had fewer bacteria overall with the bacteria appearing to be on top of the areas covered by the foulant layer rather than embedded in it. The fouling mechanisms also appeared to be different between control and 2-AI membranes with mature biofilms forming on the control membrane and biofilms dominated by cell deposition forming on the 2-AI membrane.

To summarize, upon visual inspection, the 2-AI membrane appeared to foul less under all experimental conditions that involved biofilm formation and/or cell deposition.

#### *4.3.1.2. Chemical Signature*

ATR-FTIR was used to evaluate differences in chemical signatures of fouled membranes. **Figure 4.4.** presents the spectra of unfouled control, fouled control, and fouled 2-AI membranes, and **Table 4.2.** summarizes specific molecule types (e.g., polysaccharides, proteins, polysulfone) associated with the absorbance peaks observed in the FTIR spectra. For each of the absorbance peaks, *Table 4.2* also indicates the fouling conditions (i.e., feed solutions) at which we observed significantly higher or lower absorbance for the spectra of the 2-AI membrane as compared to for the spectra of the fouled control membrane.

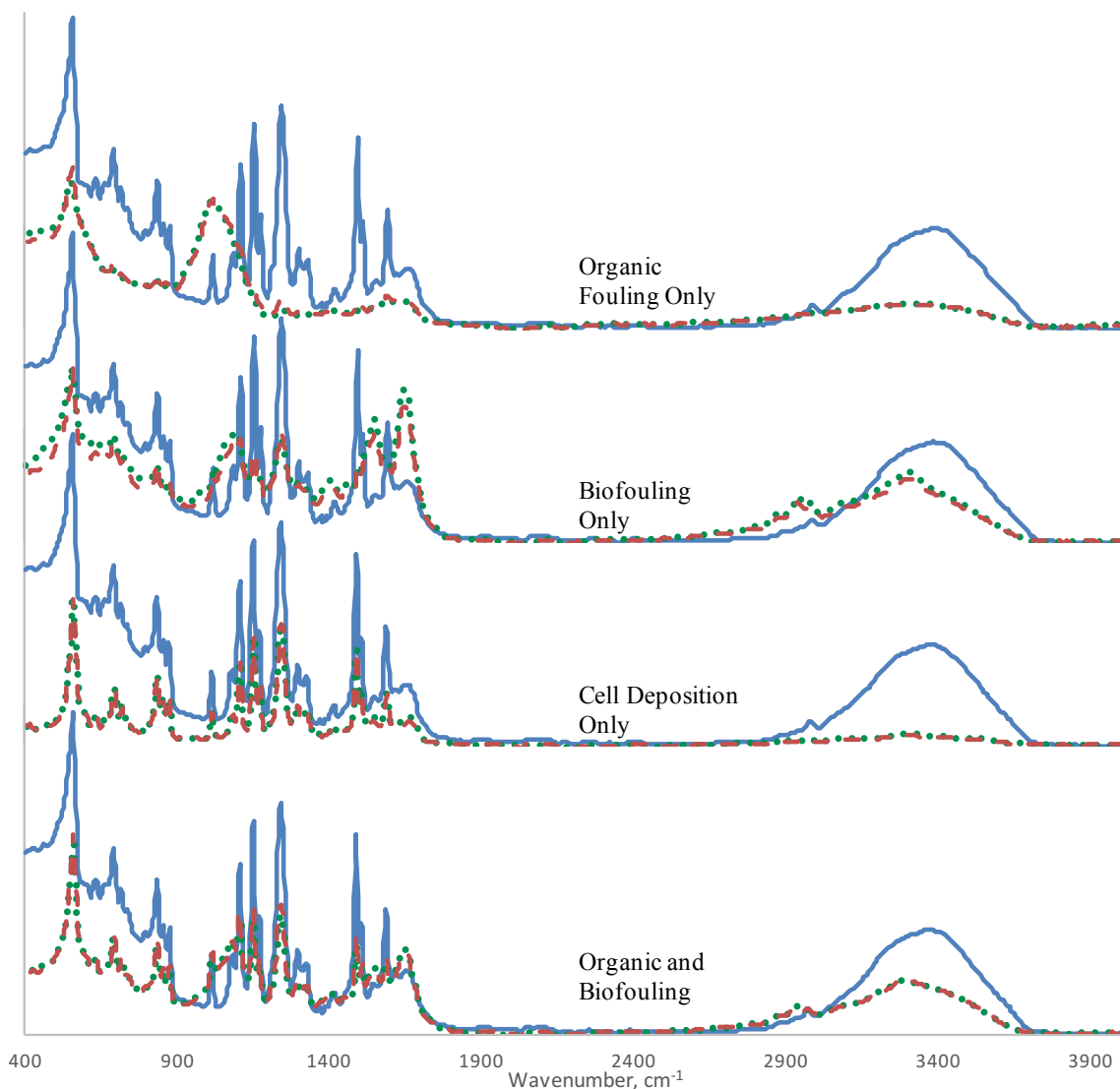


**Figure 4.4.** ATR-FTIR spectra of unfouled control membranes (blue solid line), fouled control membranes (green dotted line), and fouled 2-AI membranes (red dashed line) fouled by using organic-only, biofouling-only, cell-deposition-only, and organic&biofouling feed solutions. Each spectrum corresponds to the average of eight replicate measurements obtained on different locations of the surface of duplicate membrane samples. Peak assignments are listed in **Table 4.2**.

**Figure 4.4** shows that there were no statistical differences between the fouled control and fouled 2-AI membranes in the absorbance associated with polysulfone for all feed solutions. This indicates that there was no significant difference in the thickness of the foulant layers on the control and 2-AI membranes.

**Table 4.2.** Distinctive FTIR peaks of fouled membranes (Column 1). The table specifies the molecules (Column 2) and the bonds (Column 3) associated with each FTIR peak. The table also specifies the fouling conditions under which the absorbance of each distinctive FTIR peak on the 2-AI membranes was significantly ( $p < 0.05$ ) higher (Column 4) or lower (Column 5) than that in the control membranes.

Wavenumber ( $\text{cm}^{-1}$ )	Associated molecule(s)	Specific Bond Assignments	2-AI membrane absorbance is significantly higher with	2-AI membrane absorbance is significantly lower with
3300	Proteins/ Polysaccharides <sup>42</sup>	O-H stretching		Biofouling-only
3080	Aromatics <sup>42</sup>	Aromatic C-H stretching		Biofouling-only
3000-2900	Aliphatics <sup>42</sup>	Aliphatic C-H stretching		Biofouling-only
1735	Polysaccharides <sup>38</sup>	C=O stretch of esters		Cell-deposition-only
1700-1500	Amide I Proteins <sup>38,43,44</sup>	C=O stretch amide I protein ( $1635 \text{ cm}^{-1}$ ) <sup>38</sup>	Organic&biofouling	Biofouling-only, Cell-deposition-only
1575-1500	Amide II Proteins <sup>38,43,44</sup>	N-H bending/deformation, C-N stretching, symmetric stretching of COO- ( $1563 \text{ cm}^{-1}$ ) <sup>38,44</sup> NOH bend of amide II ( $1535 \text{ cm}^{-1}$ ) <sup>38</sup>	Organic&biofouling	Biofouling-only, Cell-deposition-only
1488	Polysulfone <sup>42,43</sup>	Aromatic in-plane ring stretching <sup>42,43</sup>		
1450	Lipopolysaccharides <sup>38</sup>	C-H bending of $\text{CH}_2$		Biofouling-only, Cell-deposition-only
1400	Polysaccharides <sup>38</sup>	Aliphatic C-H deformation, C-O stretching/O-H deformation of phenol		Biofouling-only, Cell-deposition-only
1200-900	Polysaccharides <sup>38,43,44</sup>	C-O ( $1078 \text{ cm}^{-1}$ ) <sup>38,44</sup> C-O/C-O-C stretch ( $1054 \text{ cm}^{-1}$ ) C-O stretch ( $970 \text{ cm}^{-1}$ ) <sup>43</sup>		Biofouling-only, Organic-only
1180-1145	Polysulfone <sup>42</sup>	Symmetric $\text{SO}_2$ stretching		
800-550	Aromatics <sup>38</sup>		Organic-only, Organic&biofouling	Biofouling-only

When the organic-only feed solution was used to foul the membranes, the control membrane had significantly higher polysaccharide fouling ( $1200\text{-}900\text{ cm}^{-1}$ ) than the 2-AI membrane, but aromatics ( $800\text{-}550\text{ cm}^{-1}$ ) on the 2-AI membrane were statistically higher than on the control membrane. Since there was no evidence that biofouling occurred on the control membrane when the organic-only feed solution was used (i.e. no bacteria detected in the feed water), the polysaccharide associated with  $1200\text{-}900\text{ cm}^{-1}$  wavenumbers must be microbially derived organic matter. These differences indicate that when the only mechanism of fouling is organic matter accumulation, the 2-AI membrane slightly alters the composition of the fouling layers, likely due to increased affinity of the membrane surface for specific types of organics (such as polysaccharides).

The fouled control membranes had significantly higher protein, polysaccharide, aromatic ( $3080\text{ cm}^{-1}$ ), and aliphatic fouling than the 2-AI membranes when they were fouled using the biofouling-only or cell-deposition-only feed solutions. Proteins and polysaccharides are associated with biofilm formation and bacterial cell deposition fouling mechanisms.<sup>43,45-47</sup> Therefore, the results indicate that biofilm formation and cell deposition were lower in the 2-AI membranes compared to in control membranes.

When the organic&biofouling feed solution was used to foul the membranes, there was no significant difference between fouled control and fouled 2-AI membranes in the absorbance peaks associated with polysaccharides, but there was significantly more protein on the 2-AI membranes. Proteins (PN) and polysaccharides (PS) are the main components of EPS, and the ratio of polysaccharide to protein (PS/PN) is related to biofilm strength, where the higher the PS/PN ratio the more adherent and cohesive the biofilm is.<sup>43,46</sup> Our FTIR results show that

when the organic&biofouling feed solution was used to foul the membranes, the PS/PN ratio was lower for 2-AI membranes than for the control membranes. Thus, when all fouling mechanisms occurred, the biofilm on the 2-AI membrane was weaker than the biofilm on the control membranes.

EPS was extracted from biofouled membranes (i.e., membranes fouled with the biofouling-only feed solution) and the areal mass density of proteins and polysaccharides was obtained and reported in **Figure 4.5.** The average polysaccharide areal mass density was higher on the fouled control membranes ( $50 \pm 5 \mu\text{g} \cdot \text{cm}^{-2}$ ) than on the fouled 2-AI membranes ( $34 \pm 10 \mu\text{g} \cdot \text{cm}^{-2}$ ), whereas the protein areal mass densities were not significantly different ( $24 \pm 7 \mu\text{g} \cdot \text{cm}^{-2}$  vs  $21 \pm 4 \mu\text{g} \cdot \text{cm}^{-2}$ ). Therefore, the PS/PN ratio was higher for fouled control membranes ( $2.2 \pm 0.4$ ) than for fouled 2-AI membranes ( $1.6 \pm 0.1$ ), indicating that the biofilm was weaker on the 2-AI membranes.

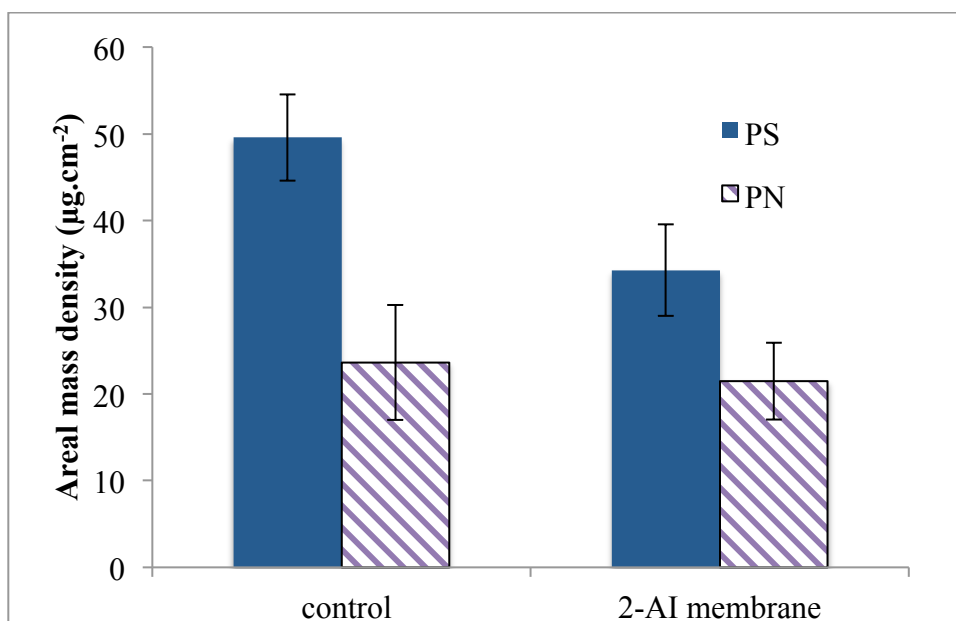


**Figure 4.5.** Areal mass density of polysaccharide (PS, dark blue bars) and protein (PN, purple striped bars) on the surface of fouled control and fouled 2-AI membranes that were fouled using biofouling-only feed solution. The bars represent the average of duplicate membrane samples from different cells. Error bars indicate the difference between the duplicate samples.

Overall, the FTIR and EPS results suggest that there was less severe biofouling on 2-AI membranes than on control membranes, and that the biofilms on 2-AI membranes were less adherent and cohesive than on the 2-AI membranes.

#### 4.3.1.3. Areal Mass of Foulant Layers and Biofilms

Bulk measurements of foulant layers, as opposed to measurement of specific chemical species, include the total areal mass (as carbon) of foulant layer and areal mass of biofilm. **Figure 4.6** shows the total areal density of organic content in foulant layer (mg-C.cm<sup>-2</sup>) on control and 2-AI membranes after fouling with the four feed solutions. When organic-only and cell-deposition-only feed solutions were used to foul the membranes, there were no significant differences between the areal density of organic content in foulant layer on the control and 2-AI membranes. By contrast, areal density of organic content in foulant layer on the 2-AI



membranes was significantly lower than on the control membranes when the biofouling-only ( $p=0.02$ , 35% decrease) and organic&biofouling ( $p=0.01$ , 54% decrease) feed solutions were used to foul the membranes. These results indicate that when biofilm formation is a mechanism of fouling, the 2-AI membranes significantly decreased the areal density of organic content of foulant layer.

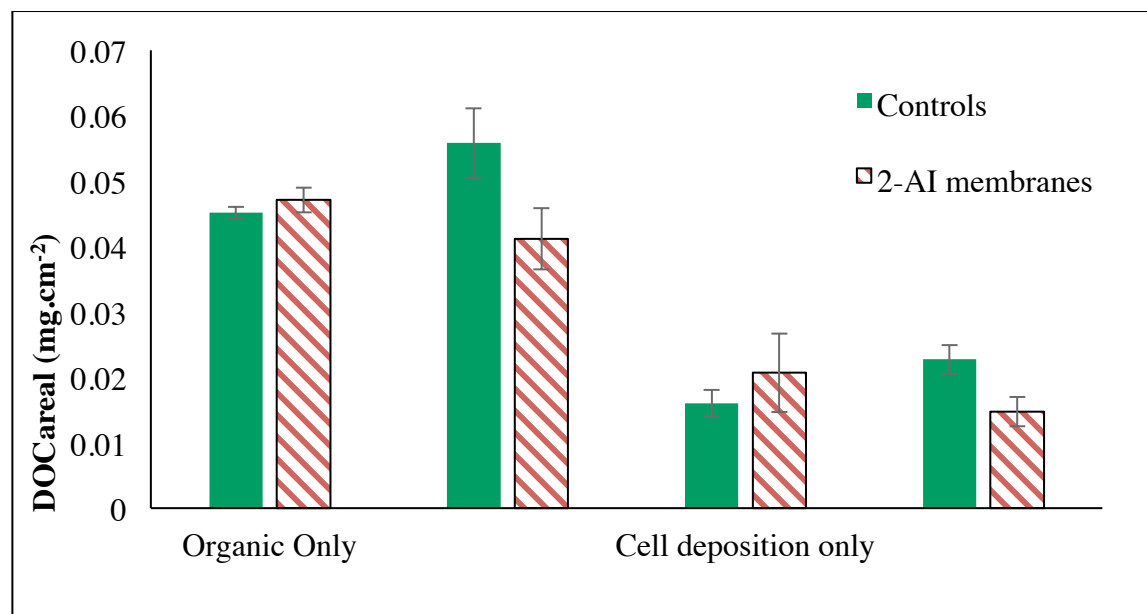


**Figure 4.6.** Areal density of organic content on the surface of fouled control and fouled 2-AI membranes. Labels on the  $x$ -axis correspond to the feed solutions listed in Table 4.1. There were insignificant differences in  $DOC_{areal}$  of foulant between control and 2-AI membranes when fouled with organic-only and cell-deposition-only feed solutions. The areal density of organic content was statistically significantly higher in control membranes than in 2-AI membranes when fouled with biofouling-only ( $p=0.02$ ) and organic&biofouling ( $p=0.01$ ) feed solutions, with areal density of organic content 35% and 54% lower, respectively, in 2-AI membranes. The bars represent the average of 4-6 replicate measurements from duplicate membrane samples (2-3 replicate measurements per sample). Error bars indicate standard error.

**Figure 4.7** shows the areal mass of biofilm (CFU.cm<sup>-2</sup>) on control and 2-AI membranes after fouling with the four feed solutions. Compared to the control membranes, the 2-AI membranes inhibited biofilms by 95% ( $p=0.10$ ) when biofouling-only was the feed solution

used to foul the membranes. Additionally, the 2-AI membranes inhibited biofilms by 98% ( $p < 0.001$ ) when the organic&biofouling feed solution was used to foul the membrane.

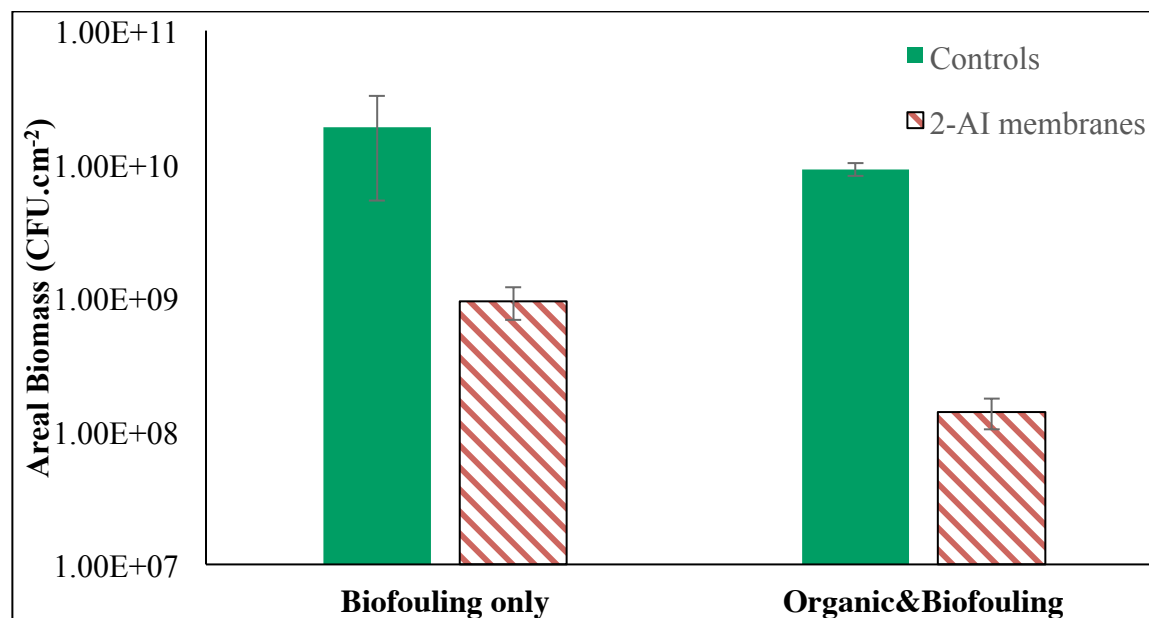


**Figure 4.7.** Areal mass of biofilm (log-scale) on fouled control and fouled 2-AI membranes. No colony counts were observed for membrane samples fouled with the organic-only and cell-deposition-only feed solutions. Compared to the control membranes, the 2-AI membranes inhibited biofilms by 95% and 98% when the biofouling-only feed solution and organic+biofouling feed solution, respectively, were used to foul the membranes. The bars represent the average areal mass of biofilm for 6-11 replicate measurements from duplicate membrane samples (3-6 measurements per sample). Error bars indicate standard error.

Overall, the results for total areal mass of foulant layer and areal mass of biofilm indicate that there substantially less severe biofilm formation on 2-AI membranes than on control membranes, and that 2-AI membranes decreased total fouling by inhibiting biofilm formation.

#### 4.3.2. Membrane performance under fouling conditions

**Figure 4.8.** shows the change in water permeability of the control and 2-AI membranes over 75 hours of filtration under each fouling condition. The water permeability of all membranes dropped over time as fouling took place. Under all fouling conditions the water permeability of the control membranes decreased by 30-40% within 75 hours. The decrease in water permeability of the 2-AI membranes after 75 hours of operation differed by fouling type.

When the organic-only feed solution was used to foul the membranes, the water permeability of the 2-AI membranes dropped the most (29% on average) out of the four fouling conditions, and this drop was insignificantly different from that for the control membrane (34% on average). When the other feed solutions (i.e., biofouling-only, cell-deposition-only, and organic&biofouling) were used to foul the membranes, the water permeability for the 2-AI membranes decreased significantly ( $p<0.05$ ) less over 75 hours than for the control membranes. More specifically, for tests with the biofouling-only, cell-deposition-only, and organic&biofouling feed solutions, water permeability in 2-AI membranes and control membranes decreased by 18 v 34%, 22 v 31 and 21 v 35%, respectively, after 75 hours of filtration.

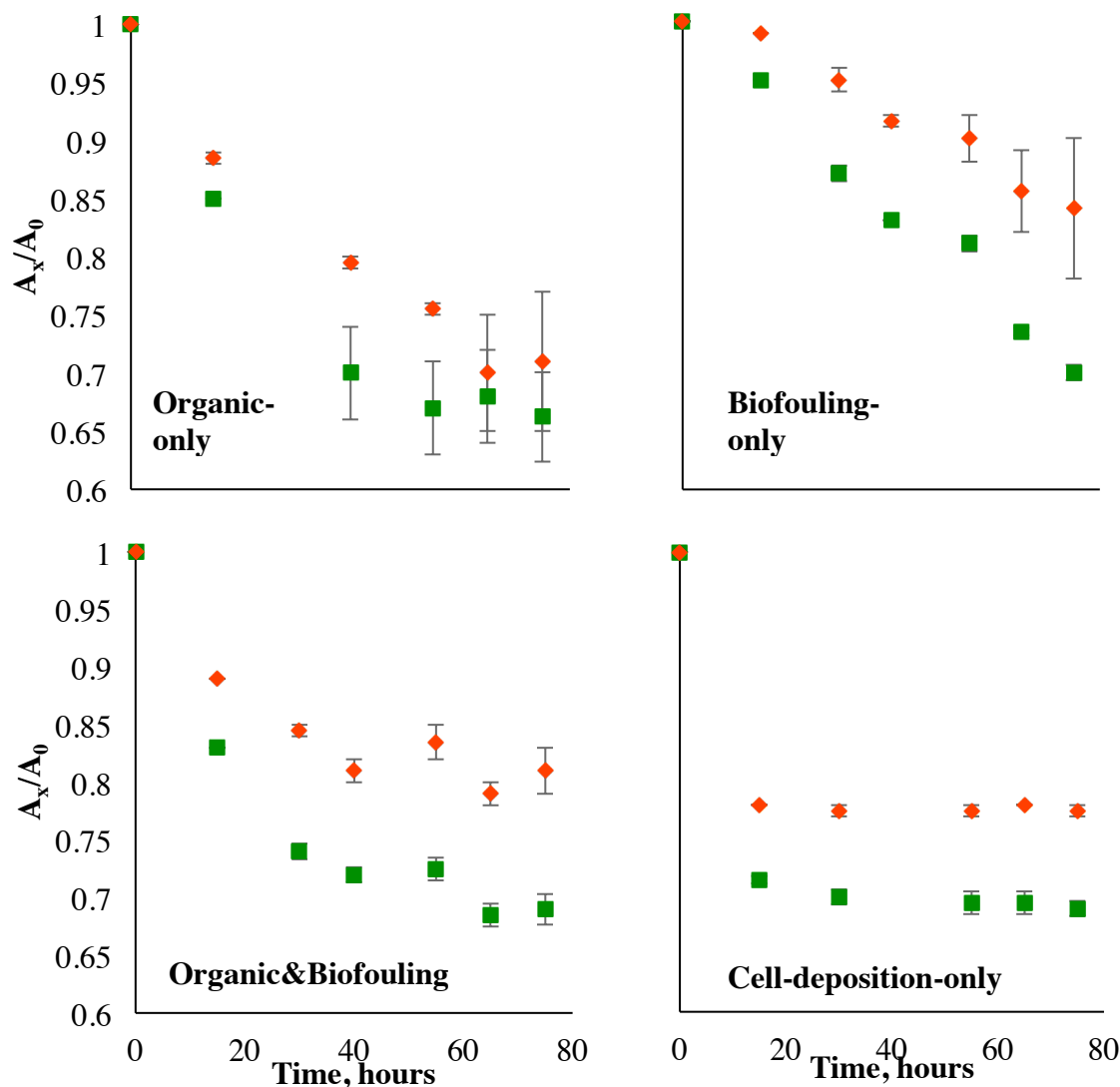


**Figure 4.8.** Normalized water permeabilities ( $A_t/A_0$ ) over 75 hours of filtration under each fouling condition for control membranes (green squares) and 2-AI membranes (red diamonds). Each data point represents the average normalized water permeability from duplicate membrane samples. Error bars indicate the difference between the normalized water permeabilities for the duplicate membrane samples.

Although the water permeability decreases were significantly less for 2-AI membranes, it is also important to consider the absolute water permeability at each time point as shown in **Figure 4.9.**, not just the change over time. In all cases, the initial (i.e., at time 0) water

permeabilities of 2-AI membranes were moderately lower than those of the controls, 11% lower on average. However, after 75 hours of fouling with the organic-only feed solution, the water permeability of 2-AI membranes and control membranes were not significantly different, with the 2-AI membranes having a 1% higher water permeability on average. Also, after 75 hours of fouling with the biofouling-only and organic&biofouling feed solutions, the water permeabilities of 2-AI membranes were higher, by 11% and 10% on average, respectively. The only case in which the water permeabilities of the 2-AI membranes were lower than that of the control membranes after 75 hours, was when the membranes were fouled with the cell-deposition-only feed solution, where the 2-AI membranes had a 6% lower water permeability than the control membranes. We note that even though the initial water permeability of 2-AI membranes was moderately lower than that of control membranes, no effort was made to optimize water permeability in 2-AI membranes, and therefore the 2-AI membrane fabrication procedure could be potentially optimize to minimize or eliminate water permeability differences between 2-AI and control membranes.

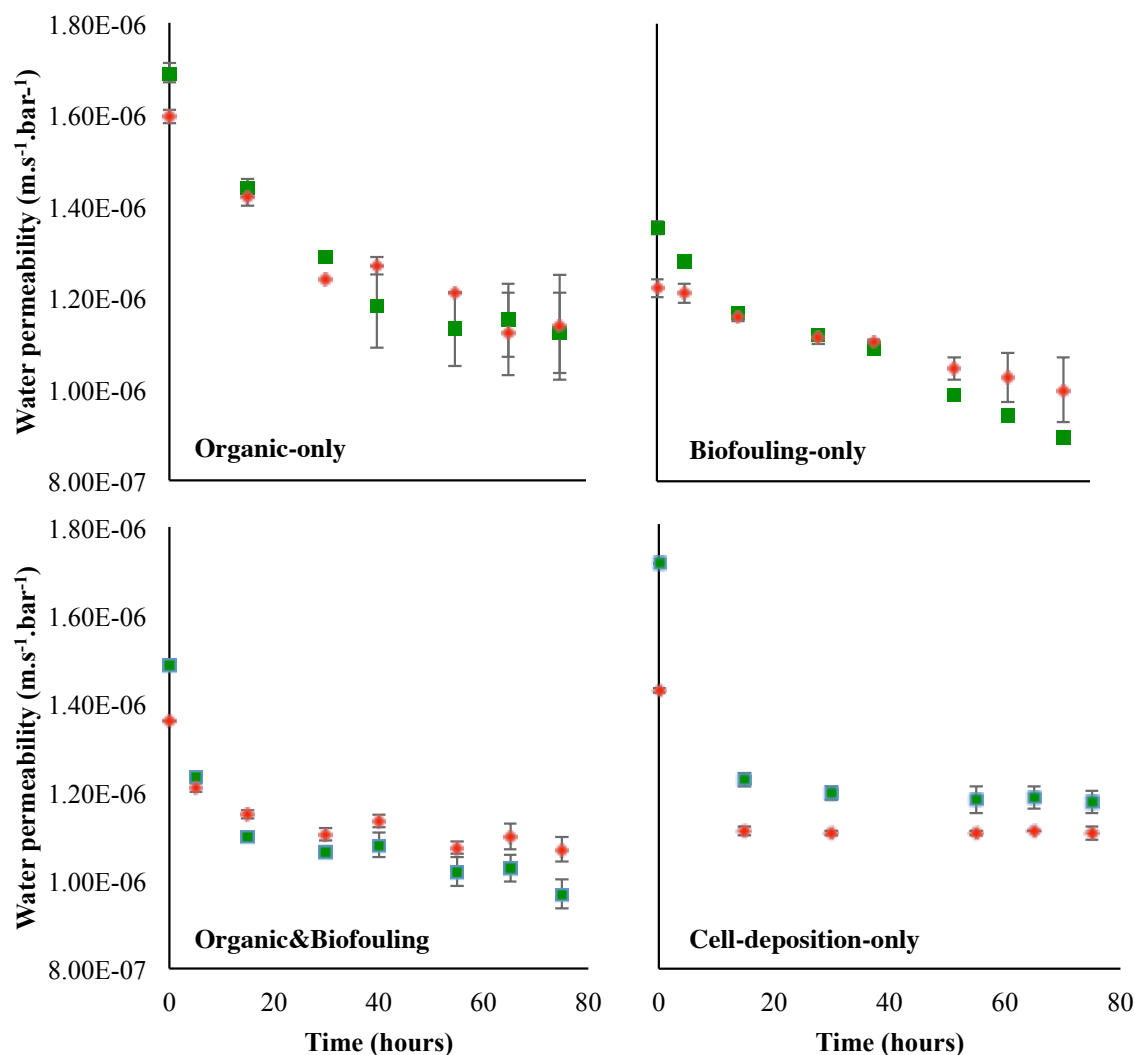


**Figure 4.9.** Water permeabilities over 75 hours of filtration under each fouling condition for control membranes (green squares) and 2-AI membranes (red diamonds). Each data point represents the average water permeability from duplicate membrane samples. Error bars indicate the difference between the water permeabilities for the duplicate membrane samples.

During all fouling experiments, the salt rejection, as shown in *Appendix 3*, by the membranes increased slightly throughout the 75 hours of operation, and was in the 80-99% range, depending on the experiment. Furthermore, the salt rejection was not significantly different ( $p > 0.05$ ) between the control and 2-AI membranes in any of the fouling experiments

**Figure 4.10.** shows the rejection of dissolved organic carbon (DOC) by the control and 2-AI membranes under each fouling condition after 75 hours of operation. When the

organic-only feed solution was used to foul the membranes, there was no substantial difference in DOC rejection (1%) between the control and 2-AI membranes. By contrast, when the membranes were fouled using the biofouling-only, cell-deposition-only and organic&biofouling feed solutions, the DOC rejection by the 2-AI membranes was substantially higher (11% and  $p=0.07$ , 10% and  $p=0.01$ , and 12% and  $p=0.003$ , respectively) than by the control membranes. Therefore, overall, the fouled 2-AI membranes rejected DOC better than the fouled control membranes.

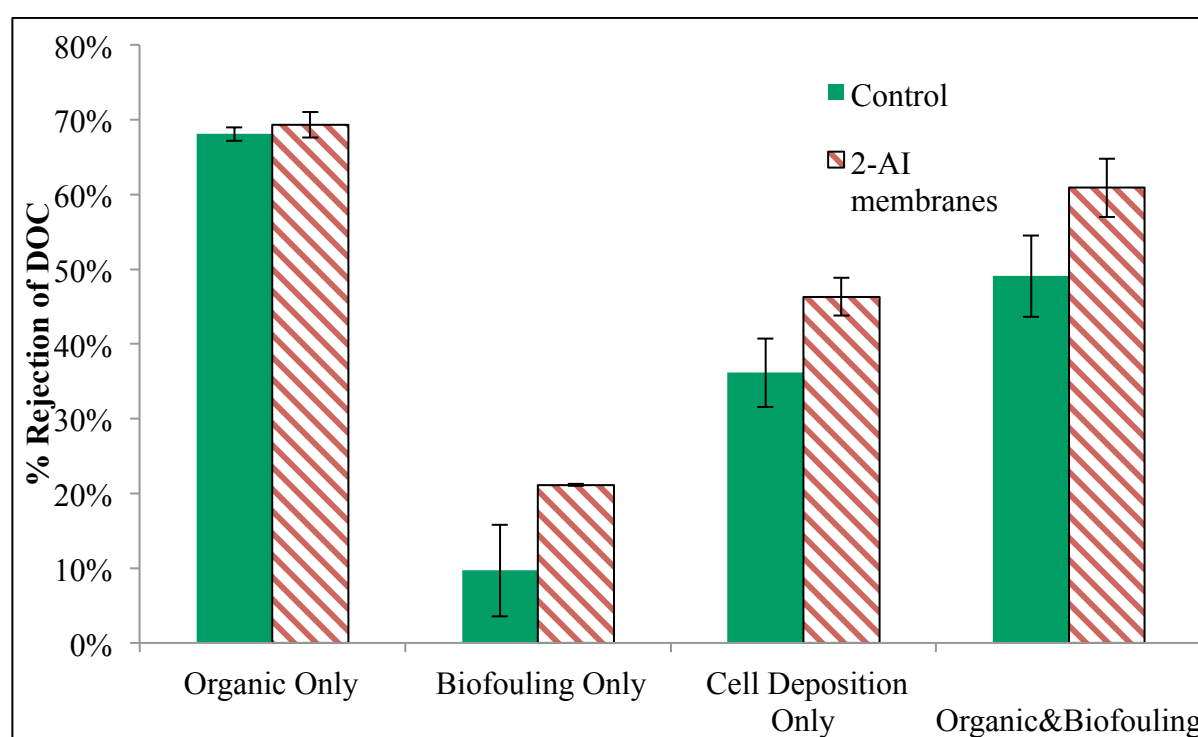


**Figure 4.10.** Rejection of dissolved organic carbon in feed solutions by control membranes (solid green) and 2-AI membranes (red striped) after 75 hours of filtration. Labels on the x-axis correspond to the feed solutions listed in Table 4.1. The bars are the average rejections calculated for duplicate membrane samples, where duplicate and single measurements were obtained for permeate and feed solutions, respectively, for each membrane sample (duplicates per membrane sample). Error bars indicate the difference between the averages for the duplicate membrane samples.

Overall, results indicate that under fouling conditions, 2-AI membranes exhibited a substantially lower water permeability reduction compared to control membranes, there was no

substantial difference in salt rejection between 2-AI and control membranes, and 2-AI membranes exhibited substantially higher DOC rejection compared to control membranes.

#### ***4.3.3. Connections between fouling mechanisms and performance***

On the basis of the results obtained for all fouling runs and analyses of all fouled membranes, there did not appear to be substantial differences in fouling between the 2-AI membranes and (2-AI-lacking) control membranes when the fouling mechanisms were organic matter accumulation or cell deposition; however, biofilm formation was significantly inhibited by 2-AI membranes, whether or not fouling was also occurring by other mechanisms. The ability of 2-AI membranes to inhibit biofilms under multiple fouling conditions is an important finding, as other membrane modification approaches used to provide membranes with anti-biofouling properties have not been effective when other fouling mechanisms occur.

Decreased biofilm formation on 2-AI membranes translated into significantly lower changes in water permeability over time under fouling conditions where biofilm formation was a fouling mechanism. The 2-AI membranes outperformed the control (2-AI-lacking) membranes, as fouled 2-AI membranes had significantly higher water permeability and rejection of organics when the biofouling-only and organic&biofouling feed solutions were used to foul the membranes. Salt rejection was not significantly different between the control and 2-AI membranes and was unaffected by fouling.

#### **4.4. Conclusions**

We evaluated the performance of 2-AI membranes in comparison to 2-AI lacking control membranes under operationally realistic conditions. Our experimental results support the following main conclusions:



- (i) Biofilm formation was significantly inhibited (98%,  $p < 0.001$ ) by 2-AI membranes under operationally realistic conditions
- (ii) 2-AI membranes had highest impact on performance when biofilm formation was a fouling mechanism, with water permeability (10-11%) and organics rejection (11-12 percentage points) being higher than (2-AI-lacking) control membranes.
- (iii) 2-AI incorporation did not affect fouling by organic matter or bacterial cell deposition.

Thus, the results presented constitute the proof-of-concept for 2-AI membranes as RO membranes with comparable water permeability and solute rejection to commercial RO membranes, but significantly lower susceptibility to biofouling. Further performance testing and optimization of polyamide casting or 2-AI incorporation into polyamide to maximize water permeability and solute rejection is warranted.

#### **4.5. Acknowledgements**

This work was supported by the National Science Foundation (NSF) Grant Opportunities for Academic Liaison with Industry (GOALI) and Chemical, Bioengineering, Environmental, and Transport Systems (CBET) program under Award#1264690, NSF Environmental Engineering program under Award#1336532, a Sigma Xi Grant-in-Aid of Research (GIAR) award, the National Water Research Institute (NWRI) and American Membrane Technology Association (AMTA) Fellowship for Membrane Technology, and The UNC Graduate School Dissertation Completion Fellowship. Dr. Amar Kumbhar for assistance with SEM analyses. The authors also thank Hydranautics for donation of membranes. LC-MS analyses were performed at SEM was performed at the Chapel Hill Analytical and Nanofabrication Laboratory (CHANL) at

UNC, a member of the North Carolina Research Triangle Nanotechnology Network (RTNN), which is supported by the National Science Foundation (Grant ECCS-1542015) as part of the National Nanotechnology Coordinated Infrastructure (NNCI).

## REFERENCES

- (1) Flemming, H.-C. Reverse Osmosis Membrane Biofouling. *Exp. Therm. Fluid Sci.* **1997**, *14* (4), 382–391.
- (2) Nguyen, T.; Roddick, F.; Fan, L. Biofouling of Water Treatment Membranes: A Review of the Underlying Causes, Monitoring Techniques and Control Measures. *Membranes (Basel)*. **2012**, *2* (4), 804–840.
- (3) Huertas, E.; Herzberg, M.; Oron, G.; Elimelech, M. Influence of Biofouling on Boron Removal by Nanofiltration and Reverse Osmosis Membranes. *J. Memb. Sci.* **2008**, *318* (1–2), 264–270.
- (4) Xu, P.; Drewes, J. E.; Kim, T.-U.; Bellona, C.; Amy, G. Effect of Membrane Fouling on Transport of Organic Contaminants in NF/RO Membrane Applications. *J. Memb. Sci.* **2006**, *279* (1–2), 165–175.
- (5) Vogel, D.; Simon, A.; Alturki, A. A.; Bilitewski, B.; Price, W. E.; Nghiem, L. D. Effects of Fouling and Scaling on the Retention of Trace Organic Contaminants by a Nanofiltration Membrane: The Role of Cake-Enhanced Concentration Polarisation. *Sep. Purif. Technol.* **2010**, *73* (2), 256–263.
- (6) Sweity, A.; Oren, Y.; Ronen, Z.; Herzberg, M. The Influence of Antiscalants on Biofouling of RO Membranes in Seawater Desalination. *Water Res.* **2013**, *47* (10), 3389–3398.
- (7) Matin, A.; Khan, Z.; Zaidi, S. M. J.; Boyce, M. C. Biofouling in Reverse Osmosis Membranes for Seawater Desalination: Phenomena and Prevention. *Desalination* **2011**, *281*, 1–16.
- (8) Yu, C.; Wu, J.; Contreras, A. E.; Li, Q. Control of Nanofiltration Membrane Biofouling by *Pseudomonas Aeruginosa* Using D-Tyrosine. *J. Memb. Sci.* **2012**, *423–424*, 487–494.
- (9) Ying, W.; Siebdrath, N.; Uhl, W.; Gitis, V.; Herzeberg, M. New Insights on Early Stages of RO Membranes Fouling during Tertiary Wastewater Desalination. *J. Memb. Sci.* **2014**, *466*, 26–35.
- (10) Al-Ahmad, M.; Aleem, F. A.; Mutiri, A.; Ubaisy, A. Biofuoling in RO Membrane Systems. Part 1: Fundamentals and Control. *Desalination* **2000**, *132* (October), 173–179.
- (11) Herzberg, M.; Elimelech, M. Physiology and Genetic Traits of Reverse Osmosis Membrane Biofilms: A Case Study with *Pseudomonas Aeruginosa*. *ISME J.* **2008**, *2* (2), 180–194.
- (12) Habimana, O.; Semião, a. J. C.; Casey, E. The Role of Cell-Surface Interactions in Bacterial Initial Adhesion and Consequent Biofilm Formation on Nanofiltration/reverse Osmosis Membranes. *J. Memb. Sci.* **2014**, *454*, 82–96.

- (13) Altman, S. J.; Cappelle, M.; Clem, P. G.; Cook, A. W.; Christopher, H.; Hart, W. E.; Hibbs, M. R.; Ho, C. K.; Jones, H. D. T.; Khalsa, S.; Noek, R.; Sun, A. C.; Webb, S. W.; McGrath, L. K.; James, D. L.; Adout, A.; Elimelech, M.; Kang, S. *Analysis of Micromixers and Biocidal Coatings on Water Treatment Membranes to Minimize Biofouling*; SAND2009-8316; Albuquerque, NM, 2009.
- (14) Varin, K. J.; Lin, N. H.; Cohen, Y. Biofouling and Cleaning Effectiveness of Surface Nanostructured Reverse Osmosis Membranes. *J. Memb. Sci.* **2013**, *446*, 472–481.
- (15) Malaisamy, R.; Berry, D.; Holder, D.; Raskin, L.; Lepak, L.; Jones, K. L. Development of Reactive Thin Film Polymer Brush Membranes to Prevent Biofouling. *J. Memb. Sci.* **2010**, *350*, 361–370.
- (16) Xu, J.; Wang, Z.; Yu, L.; Wang, J.; Wang, S. A Novel Reverse Osmosis Membrane with Regenerable Anti-Biofouling and Chlorine Resistant Properties. *J. Memb. Sci.* **2013**, *435*, 80–91.
- (17) Kappachery, S.; Paul, D.; Kweon, J. H. Effect of N-Acetylcysteine against Biofouling of Reverse Osmosis Membrane. *Desalination* **2012**, *285*, 184–187.
- (18) Nikkola, J.; Liu, X.; Li, Y.; Raulio, M.; Alakomi, H. L.; Wei, J.; Tang, C. Y. Surface Modification of Thin Film Composite RO Membrane for Enhanced Anti-Biofouling Performance. *J. Memb. Sci.* **2013**, *444*, 192–200.
- (19) Bera, A.; Gol, R. M.; Chatterjee, S.; Jewrajka, S. K. PEGylation and Incorporation of Triazine Ring into Thin Film Composite Reverse Osmosis Membranes for Enhancement of Anti-Organic and Anti-Biofouling Properties. *Desalination* **2015**, *360*, 108–117.
- (20) Zhu, X.; Bai, R.; Wee, K. H.; Liu, C.; Tang, S. L. Membrane Surfaces Immobilized with Ionic or Reduced Silver and Their Anti-Biofouling Performances. *J. Memb. Sci.* **2010**, *363* (1–2), 278–286.
- (21) Karkhanechi, H.; Takagi, R.; Matsuyama, H. Biofouling Resistance of Reverse Osmosis Membrane Modified with Polydopamine. *Desalination* **2014**, *336*, 87–96.
- (22) Blok, A. J.; Chhasatia, R.; Dilag, J.; Ellis, A. V. Surface Initiated Polydopamine Grafted Poly ([2-( Methacryoyloxy) Ethyl] Trimethylammonium Chloride ) Coatings to Produce Reverse Osmosis Desalination Membranes with Anti-Biofouling Properties. *J. Memb. Sci.* **2014**, *468*, 216–223.
- (23) Wei, X.; Wang, Z.; Zhang, Z.; Wang, J.; Wang, S. Surface Modification of Commercial Aromatic Polyamide Reverse Osmosis Membranes by Graft Polymerization of 3-Allyl-5,5-Dimethylhydantoin. *J. Memb. Sci.* **2010**, *351* (1–2), 222–233.
- (24) Vercellino, T.; Morse, A.; Tran, P.; Song, L.; Hamood, A.; Reid, T.; Moseley, T. Attachment of Organo-Selenium to Polyamide Composite Reverse Osmosis Membranes to Inhibit Biofilm Formation of *S. Aureus* and *E. Coli*. *Desalination* **2013**, *309*, 291–295.
- (25) Subramani, A.; Hoek, E. M. V. Direct Observation of Initial Microbial Deposition onto Reverse Osmosis and Nanofiltration Membranes. *J. Memb. Sci.* **2008**, *319*, 111–125.

- (26) Kang, S.; Hoek, E. M. V.; Choi, H.; Shin, H. Effect of Membrane Surface Properties During the Fast Evaluation of Cell Attachment. *Sep. Sci. Technol.* **2006**, *41* (7), 1475–1487.
- (27) Li, Q.; Xu, Z.; Pinnau, I. Fouling of Reverse Osmosis Membranes by Biopolymers in Wastewater Secondary Effluent: Role of Membrane Surface Properties and Initial Permeate Flux. *J. Memb. Sci.* **2007**, *290* (1–2), 173–181.
- (28) Worthington, R.; Richards, J.; Melander, C. Small Molecule Control of Bacterial Biofilms. *Org. Biomol. Chem.* **2012**, *10* (37), 7457–7474.
- (29) Rogers, S.; Melander, C. Construction and Screening of a 2-Aminoimidazole Library Identifies a Small Molecule Capable of Inhibiting and Dispersing Bacterial Biofilms across Order, Class, and Phylum. *Angew. Chemie Int. Ed* **2008**, *47* (28), 5229–5231.
- (30) Peng, L.; DeSousa, J.; Su, Z.; Novak, B. M.; Nevzorov, A. a; Garland, E. R.; Melander, C. Inhibition of *Acinetobacter Baumannii* Biofilm Formation on a Methacrylate Polymer Containing a 2-Aminoimidazole Subunit. *Chem. Commun.* **2011**, *47* (17), 4896–4898.
- (31) Thompson, R. J.; Bobay, B. G.; Stowe, S. D.; Olson, A. L.; Peng, L.; Su, Z.; Actis, L. a; Melander, C.; Cavanagh, J. Identification of BfmR , a Response Regulator Involved in Biofilm Development, as a Target for a 2 - Aminoimidazole-Based Antibiofilm Agent. *Biochemistry* **2012**, No. 51, 9776–9778.
- (32) Hentzer, M.; Riedel, K.; Rasmussen, T. B.; Heydorn, A.; Andersen, J. B.; Parsek, M. R.; Rice, S. a.; Eberl, L.; Molin, S.; Høiby, N.; Kjelleberg, S.; Givskov, M. Inhibition of Quorum Sensing in *Pseudomonas Aeruginosa* Biofilm Bacteria by a Halogenated Furanone Compound. *Microbiology* **2002**, *148*, 87–102.
- (33) Hentzer, M.; Wu, H.; Andersen, J. B.; Riedel, K.; Rasmussen, T. B.; Bagge, N.; Kumar, N.; Schembri, M. a.; Song, Z.; Kristoffersen, P.; Manefield, M.; Costerton, J. W.; Molin, S.; Eberl, L.; Steinberg, P.; Kjelleberg, S.; Høiby, N.; Givskov, M. Attenuation of *Pseudomonas Aeruginosa* Virulence by Quorum Sensing Inhibitors. *EMBO J.* **2003**, *22* (15), 3803–3815.
- (34) Gotoh, Y.; Eguchi, Y.; Watanabe, T.; Okamoto, S.; Doi, A.; Utsumi, R. Two-Component Signal Transduction as Potential Drug Targets in Pathogenic Bacteria. *Curr. Opin. Microbiol.* **2010**, *13* (2), 232–239.
- (35) Bourret, R. B.; Silversmith, R. E. Two-Component Signal Transduction. *Curr. Opin. Microbiol.* **2010**, *13*, 113–115.
- (36) Herzberg, M.; Elimelech, M. Biofouling of Reverse Osmosis Membranes: Role of Biofilm-Enhanced Osmotic Pressure. *J. Memb. Sci.* **2007**, *295* (1–2), 11–20.
- (37) Al Ashhab, A.; Herzberg, M.; Gillor, O. Biofouling of Reverse-Osmosis Membranes during Tertiary Wastewater Desalination: Microbial Community Composition. *Water Res.* **2014**, *50*, 341–349.

- (38) Hausman, R.; Escobar, I. C. A Comparison of Silver- and Copper-Charged Polypropylene Feed Spacers for Biofouling Control. *J. Appl. Polym. Sci.* **2013**, *128*, 1706–1714.
- (39) Liu, H.; Fang, H. H. P. Extraction of Extracellular Polymeric Substances (EPS) of Sludges. *J. Biotechnol.* **2002**, *95*, 249–256.
- (40) DuBois, M.; Gilles, K. a.; Hamilton, J. K.; Rebers, P. a.; Smith, F. Colorimetric Method for Determination of Sugars and Related Substances. *Anal. Chem.* **1956**, *28*, 350–356.
- (41) Bradford, M. M. A Rapid and Sensitive Method for the Quantitation of Microgram Quantities of Protein Utilizing the Principle of Protein-Dye Binding. *Anal. Biochem.* **1976**, *72*, 248–254.
- (42) Tang, C. Y.; Kwon, Y.-N.; Leckie, J. O. Effect of Membrane Chemistry and Coating Layer on Physiochemical Properties of Thin Film Composite Polyamide RO and NF Membranes. *Desalination* **2009**, *242* (1–3), 149–167.
- (43) Ying, W.; Gitis, V.; Lee, J.; Herzberg, M. Effects of Shear Rate on Biofouling of Reverse Osmosis Membrane during Tertiary Wastewater Desalination. *J. Memb. Sci.* **2013**, *427*, 390–398.
- (44) Sweity, A.; Rezene, T.; David, I.; Bason, S.; Oren, Y.; Ronen, Z.; Herzberg, M. Side Effects of Antiscalants on Biofouling of Reverse Osmosis Membranes in Brackish Water Desalination. *J. Memb. Sci.* **2015**, *481*, 172–187.
- (45) Yao, M.; Zhang, K.; Cui, L. Characterization of Protein-Polysaccharide Ratios on Membrane Fouling. *Desalination* **2010**, *259* (1–3), 11–16.
- (46) Ying, W.; Yang, F.; Bick, A.; Oron, G.; Herzberg, M. Extracellular Polymeric Substances (EPS) in a Hybrid Growth Membrane Bioreactor (HG-MBR): Viscoelastic and Adherence Characteristics. *Environ. Sci. Technol.* **2010**, *44* (22), 8636–8643.
- (47) Herzberg, M.; Kang, S.; Elimelech, M. Role of Extracellular Polymeric Substances (EPS) in Biofouling of Reverse Osmosis Membranes. *Environ. Sci. Technol.* **2009**, *43* (12), 4393–4398.

## CHAPTER 5: CONCLUSIONS

The goal of this dissertation was to develop and evaluate the performance of a novel anti-biofouling reverse osmosis (RO) and nanofiltration (NF) membrane(s) with 2-AI(s) incorporated as the active compound. To achieve this goal, the research specifically aimed to:

- (i) synthesize and evaluate 2-AI molecules in terms of their capacity to be incorporated into polyamide active layers and their capability to inhibit biofilm,
- (ii) develop an anti-biofouling water purification membrane(s) through 2-AI incorporation into active layers of commercially available RO membranes,
- (iii) develop an anti-biofouling water purification membrane(s) through 2-AI incorporation into active layers of in-house RO membranes during polyamide casting,
- (iv) characterize 2-AI membrane(s) performance in terms of biofouling inhibition, water productivity, and contaminant removal.

Three 2-AIs were synthesized, and their capacity to be incorporated into polyamide was assessed using model reactions. The ability of the 2-AI conjugates, produced from the model reactions, to inhibit biofilms was quantified. The 2-AI most effective at inhibiting biofilm was then incorporated into four commercially available reverse osmosis (RO) and nanofiltration (NF) membranes using carbodiimide induced grafting. The 2-AI was also incorporated during active layer casting into membranes fabricated in-house using three different approaches. The extent and stability of the 2-AI incorporated into the membranes, and the physico-chemical changes due

to 2-AI incorporation were characterized. The water permeabilities and salt rejections of the 2-AI membranes and corresponding (2-AI lacking) controls were measured in a flat-sheet cross-flow membrane system using salt solutions made with ultrapure water. The biofilm inhibition by 2-AI membranes was quantified using a static bioassay that used nutrient solutions with *Pseudomonas aeruginosa* (PA14). The performance and fouling of one set of 2-AI membranes (prepared using the carbodiimide grafting) and the corresponding (2-AI lacking) control membranes were then tested under operationally realistic conditions. The membranes were systematically fouled with various feed waters to elicit fouling due to a combination of mechanisms. The foulants on the membranes were quantified and characterized using several techniques. The performance of the membranes during operation was also evaluated. The differences in fouling on the 2-AI and control membranes was then related to differences in performance. The major outcomes of this dissertation research are:

- *On 2-AI compound capacity to be incorporated in polyamide and inhibit biofilm:*
  1. The three 2-AIs tested had the capacity to be incorporated into the polyamide active layers of membranes and the capability to inhibit *Pseudomonas aeruginosa* biofilms at relevant concentrations ( $IC_{50}$ s=162-420  $\mu$ M).
- *For 2-AI membranes with 2-AI incorporated using carbodiimide grafting:*
  2. 2-AI membranes significantly inhibited *Pseudomonas aeruginosa* biofilms by 61-96%, due to the presence of 2-AI, not membrane physico-chemical changes.
  3. Partial loss of the 2-AI surrogate compound was observed when the membranes were used to filter water, but concentrations of the compound remained orders of magnitude higher than required for biofilm inhibition.



4. In general, salt rejection of 2-AI membranes was equivalent to that of control (2-AI lacking) membranes.
  5. 2-AI incorporation did not substantially change the water permeability of two (XLE, NF270) of the four membranes. Compared to (2-AI lacking) controls the other two (ESPA3, SWC4+) 2-AI membranes had a slightly lower water permeability (13% and 25%, respectively). Note that no attempt was made to optimize 2-AI membranes to maximize water permeability and salt rejection. Long-term benefits in water permeability due to reduced biofouling could also potentially compensate for lower initial water permeabilities.
- *For membranes with 2-AI incorporated during active layer casting:*
    6. 2-AI membranes significantly inhibited *Pseudomonas aeruginosa* biofilms by 39-92%, due to presence of 2-AI, not membrane physico-chemical changes. 2-AI membranes, prepared using a soak after polyamide casting, inhibited biofilm the best, at 90% on average.
    7. Partial loss of the 2-AI surrogate compound was observed in select membranes and was dependent upon the incorporation approach used; however, in all cases, the concentration of the compound remained orders of magnitude higher than what was required for significant biofilm inhibition to occur.
    8. Compared to (2-AI lacking) control membranes, 2-AI membranes had decreased water permeability by 26-44% and salt rejection by 1.2-4.3 percentage points. Note that no attempt was made to optimize 2-AI membranes to maximize water permeability and salt rejection. Long-term benefits in water permeability due to

reduced biofouling could also potentially compensate for lower initial water permeabilities.

- *Under operationally realistic conditions:*

9. 2-AI membranes significantly inhibited biofilm formation (98%).

10. 2-AI membranes had higher water permeability (10-11%) and higher organics rejection (11-12 percentage points) than (2-AI-lacking) control membranes when biofilm formation was a fouling mechanism.

11. 2-AI incorporation did not affect fouling by organic matter or bacterial cell deposition.

Overall, this dissertation demonstrated proof-of-concept for 2-AI membranes and shows that 2-AI membranes are superior to other anti-biofouling membranes in the literature, 2-AI membranes can be a powerful tool to facilitate more efficient use and widespread implementation of water reuse and desalination. Based on these results, further 2-AI membrane optimization and performance testing is warranted.

## CHAPTER 6: FUTURE WORK

2-aminoimidazole (2-AI) anti-biofouling membranes for water purification applications were developed and evaluated to the proof-of-concept stage. Questions were generated through this research, and questions remain to be answered before this technology can be implemented for industry purposes, including:

1. What technique(s) can be used or developed to directly measure the concentration of 2-AIs in the membrane? Throughout the dissertation, a surrogate compound was used to estimate the 2-AI concentration in the membranes. The chemical properties of the 2-AIs are similar to those of the polyamide active layer, thus the 2-AI and membrane matrix could not be distinguished using the available analytical techniques.
2. Are 2-AI membranes effective at inhibiting biofouling in spiral wound configuration? Are 2-AI membranes effective over long-term use? Are 2-AI membranes effective at inhibiting biofilms of other bacteria and mixed cultures? Are 2-AI membranes effective with many different types of waters? Are 2-AI membranes effective in combination with other treatments (e.g. disinfection)? Though membrane performance was evaluated under some operationally realistic conditions, many conditions that are common or that vary in treatment plants were not assessed. There are numerous factors that could be present in full-scale use that may exacerbate or enhance biofouling, but were not investigated in this dissertation.
3. Are there factors or conditions that could lead to the loss of anti-biofouling properties over time? Various factors could potentially contribute to the loss of some anti-

biofouling properties over time (e.g. loss of 2-AI with use/cleaning, transformation of 2-AI from reactions with constituents in feed waters).

4. How can the 2-AI membranes be optimized for maximum biofilm inhibition, water permeability, contaminant rejection, and stability? There were only three 2-AIs that were considered for incorporation, but there are countless other 2-AIs that could potentially be used that may result in higher and consistent biofilm inhibition. The procedures for incorporating 2-AIs and casting the membranes could also be altered for further optimization. In addition, there are other potential methods for 2-AI incorporation (e.g. embedding 2-AI-nanomaterials in active layer), or additional places (e.g. feed spacers) in which to incorporate 2-AIs, that may prove successful at improving efficacy.
5. Are 2-AI membranes safe to use for drinking water production or other purposes?  
Although the concentration of 2-AIs in the purified water (permeate) will likely be very low (i.e. undetectable), further testing to ensure the safety of 2-AI membranes should be performed. Toxicity tests with select 2-AIs have been performed using cellular and model organism systems, and results have shown that the specific compounds that were tested were non-toxic.<sup>1</sup> However, the specific 2-AI(s) that are incorporated into the anti-biofouling membranes should be evaluated with toxicity tests that are relevant to drinking water.

## REFERENCES

- (1) Stowe, S. D.; Tucker, A. T.; Thompson, R.; Piper, A.; Richards, J. J.; Rogers, S. A.; Mathies, L. D.; Melander, C.; Cavanagh, J. Evaluation of the Toxicity of 2-Aminoimidazole Antibiofilm Agents Using Both Cellular and Model Organism Systems. *Drug Chem. Toxicol.* **2012**, 35 (3), 310–315.

## APPENDIX 1: SUPPORTING INFORMATION FOR CHAPTER 2

### A1.1. Methods

#### A1.1.1. $^1\text{H}$ NMR

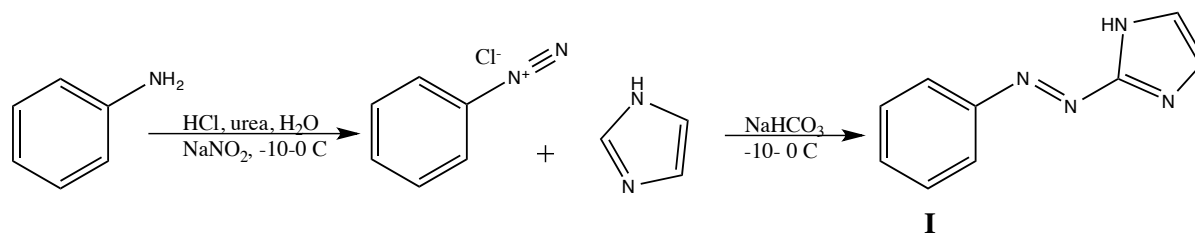
$^1\text{H}$  NMR spectra were acquired on a Varian 400 or Varian Gem2300 spectrometer.

#### A1.1.2. LC/ESI-MS

LC/ESI-MS data were acquired at the UNC Biomarker Mass Spectrometry facility using an Agilent Technologies series 1200 HPLC and 6520 Accurate-Mass Quadrupole Time-of-Flight mass spectrometer in the positive ionization mode. Operating parameters were: capillary voltage of 4000 V, nebulizing gas pressure 35 psi, drying gas temperature 300 °C, drying gas flow 11 L/min, and fragmentor voltage 175 V. The mass spectrometer was operated in high-resolution, low-mass mode and was set to scan from 100 m/z to 1700 m/z at a rate of 1 scan/s. Reference masses used for real-time mass axis adjustment were purine (121.050873 m/z) and HP-0921 (922.009798 m/z).

### A1.2. Syntheses

#### A1.2.1. Synthesis of 2-AI-para



**Scheme A1.1.**

The procedure was adapted from Verma, et. al.<sup>1</sup> Aniline (50 mmol) was dissolved in 50% HCl (30 mL), chilled to  $-10^\circ\text{C}$ . A solution of cold sodium nitrite (64 mmol) in water (23 mL) was dropped into the aniline solution over 30 min while stirring at  $-10^\circ\text{C}$ . Water (10 mL), urea (0.12 g), and ice (10 g) were added to produce a clear brown solution of diazonium chloride.

The diazonium chloride solution at  $-10^{\circ}\text{C}$  was slowly added to a solution of imidazole (51 mmol) in 10%  $\text{NaHCO}_3$  (23 mL) chilled to  $-10^{\circ}\text{C}$  in a salt bath. The solution was stirred for 30 min at  $<-5^{\circ}\text{C}$ , then allowed to stand for 90 min. The resulting orange-brown powder was washed with water and dried under vacuum to yield 6.4 mmol **I** (13%).  $^1\text{H}$  NMR (400 MHz,  $\text{CDCl}_3$ ):  $\delta$  7.9 (m, 2H, Ar-H), 7.5 (m, 3H, Ar-H), 7.2 (s, 1H, imidazole CH); LC/ESI-MS  $m/z$ : 345  $[\text{2M}+\text{H}^+]$ .

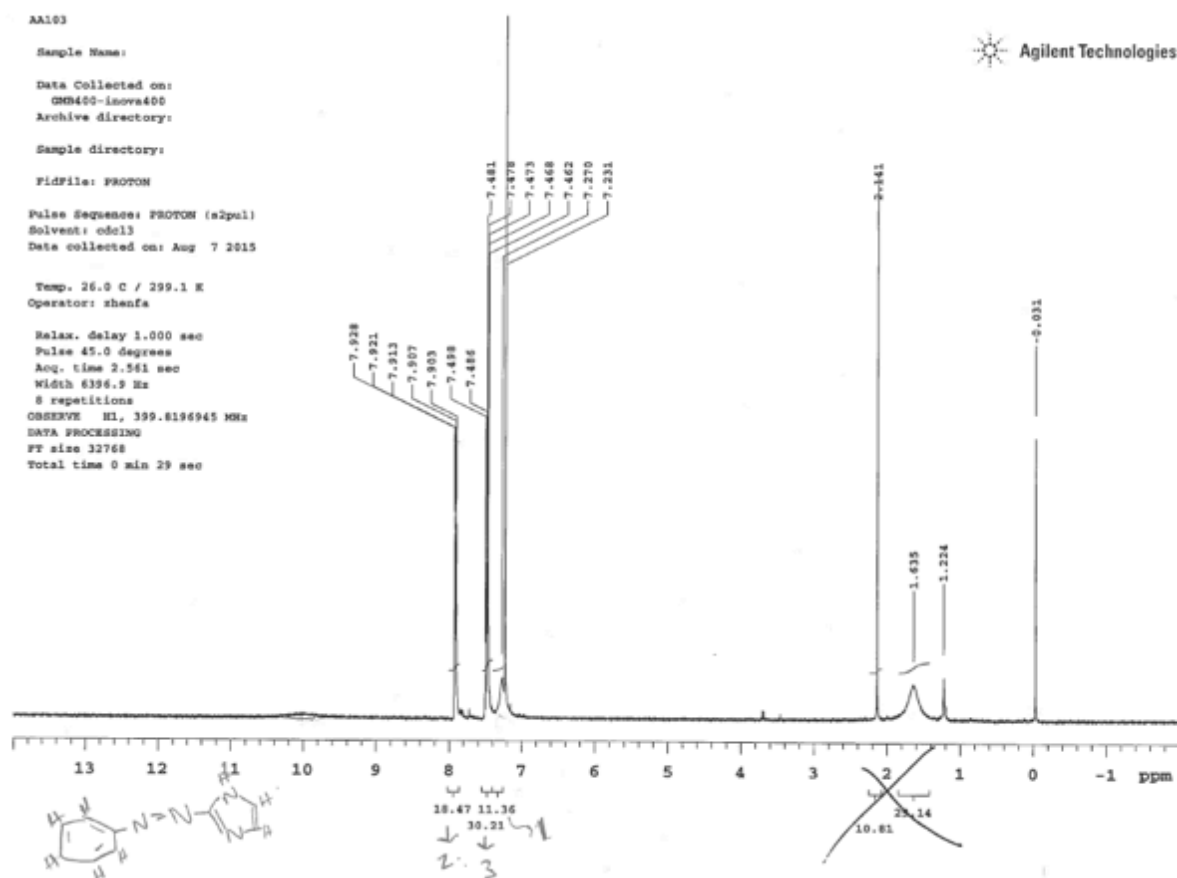
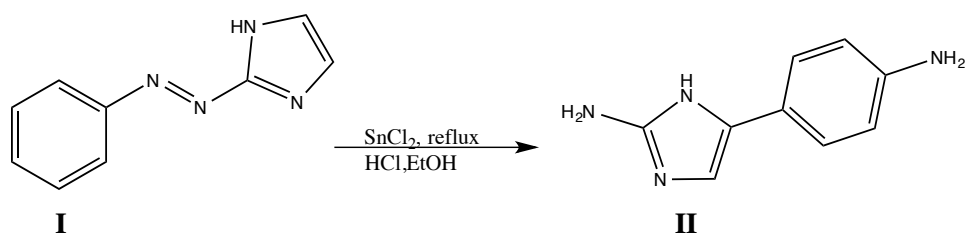


**Figure A1.1.** Raw  $^1\text{H}$  NMR spectrum of compound **I**.



**Scheme A1.2.**

Solid **I** was dissolved in EtOH (11 mL) and brought to a boil. A warm solution of tin(II) chloride (13 mmol) in concentrated HCl (6 mL) was added and the solution was refluxed for 1.5 h at 110° C, and filtered to obtain a white powder, which was recrystallized from 20:80 EtOH/H<sub>2</sub>O to yield 2.8 mmol 2-AI-para (**II**) (44%). <sup>1</sup>H NMR (400 MHz, D<sub>2</sub>O): δ 7.6 (d, 2H, Ar-H), 7.5 (d, 2H, Ar-H), 7.1 (s, 1H, imidazole CH); LC/ESI-MS *m/z*: 175 [M+H<sup>+</sup>].



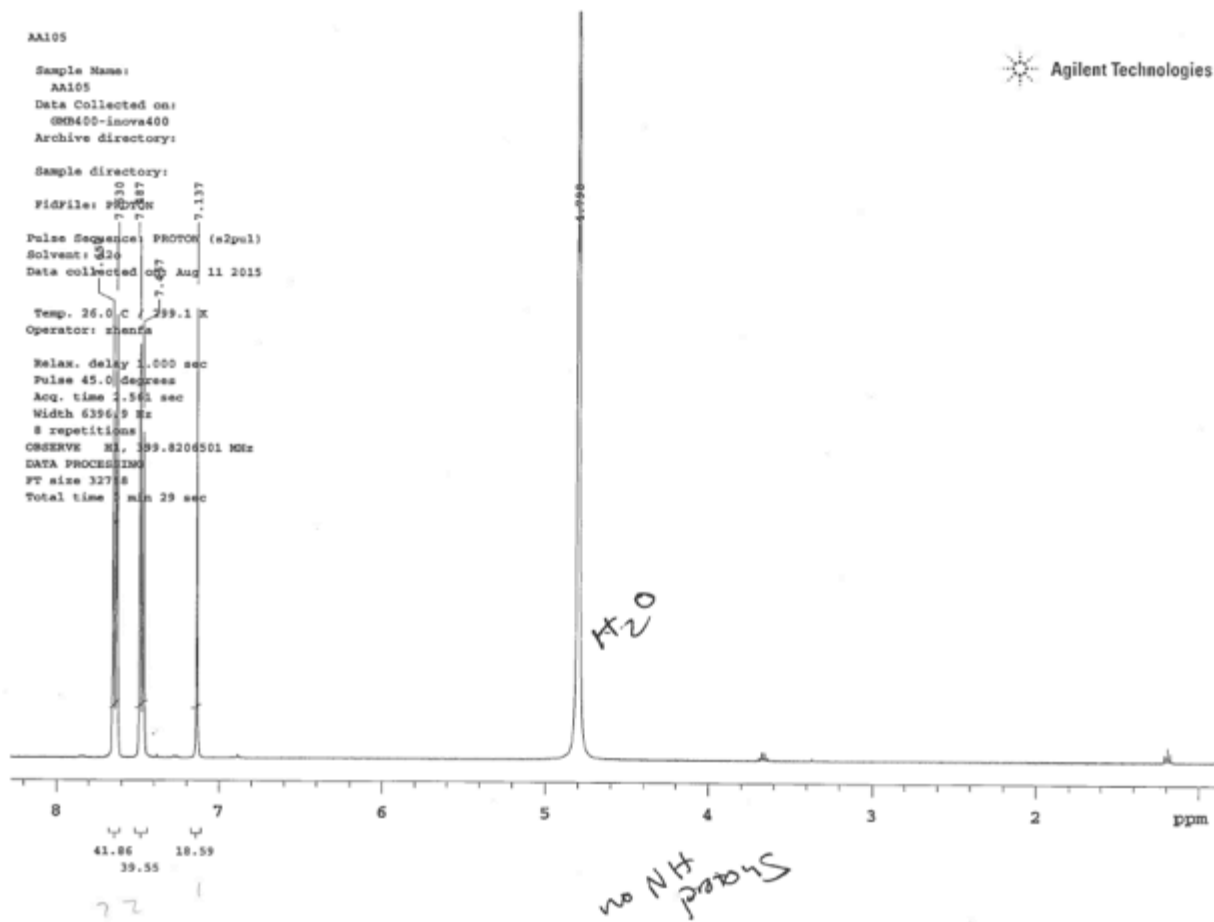


**Figure A1.2.** Raw  $^1\text{H}$  NMR spectrum of 2-AI-para (compound II).

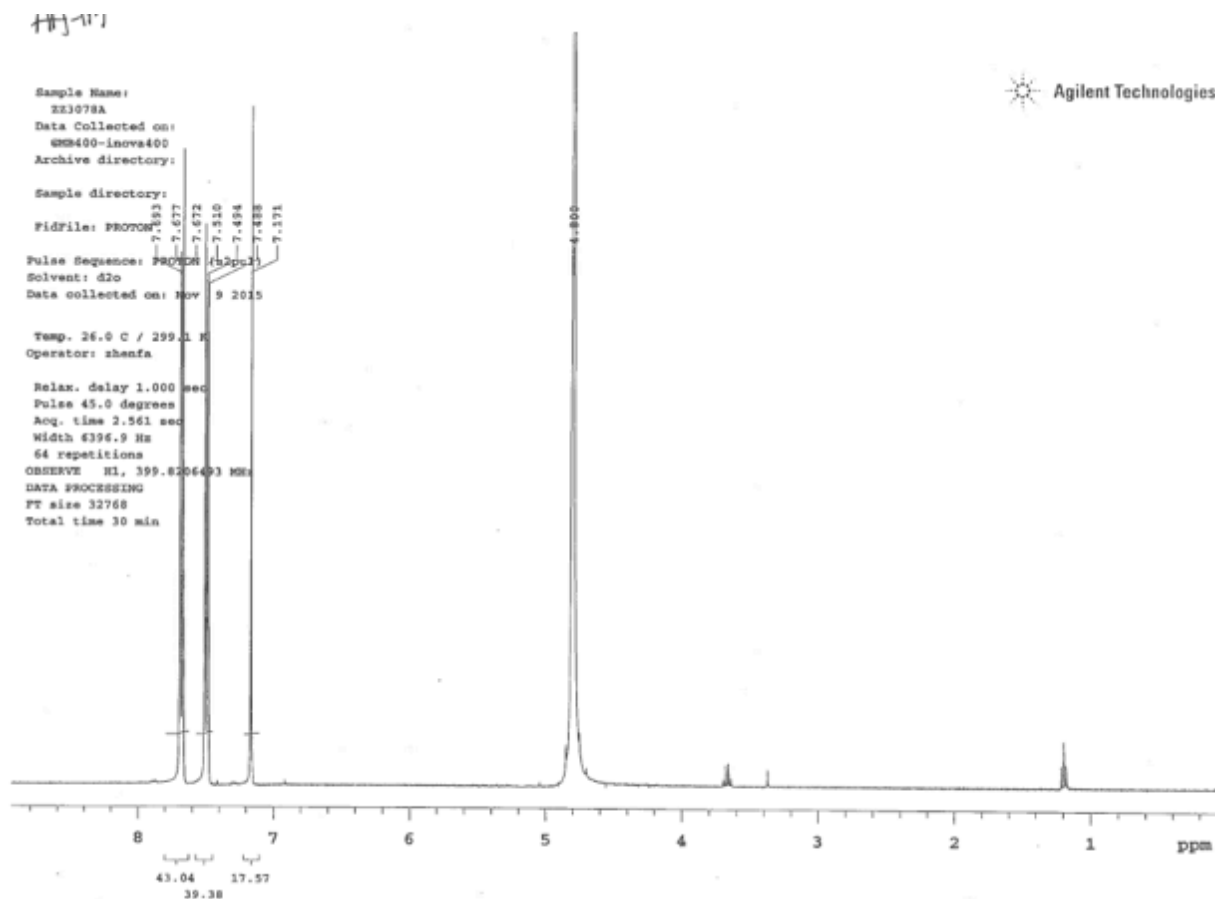
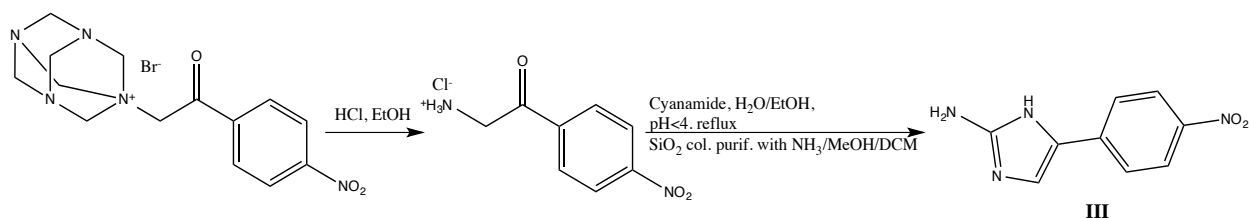


**Figure A1.3.** Raw  $^1\text{H}$  NMR spectrum of 2-AI-para (compound II).

### A1.2.2. 5-(4-nitrophenyl) 2-AI



**Scheme A1.3.**

1-Hexamethylenetetramine-4'-nitroacetophenone bromide (10 mmol) was suspended in EtOH, excess concentrated HCl (5 mL) added and the solution was stirred overnight. The white precipitate was collected, washed with EtOH and dried under vacuum. The solid (7.4 mmol) was suspended in water (adjusted with acetic acid to  $\text{pH} < 4$ ) and cyanamide (53 mmol) was added.

The solution was refluxed at 120° C for 1 h, then stirred at room temperature overnight. On adjusting to pH>8 with NaOH, a dark red solid precipitated and was collected by filtration and dried under vacuum. The solid was recrystallized in 40:60 EtOH/H<sub>2</sub>O, dissolved in MeOH and purified on a silica column eluted with 1:9 7N methanolic ammonia/DCM, yielding 3.4 mmol 5-(4-nitrophenyl) 2-AI (**III**) as a dark red solid (34%). <sup>1</sup>H NMR (400 MHz, MeOH-*d*<sub>4</sub>): δ 8.4 (d, 2H Ar-H-3/5), 7.9 (d, 2H, Ar-H-2/6), 7.6 (s, 2H, NH<sub>2</sub>), 7.3 (s, 1H, imidazole CH).

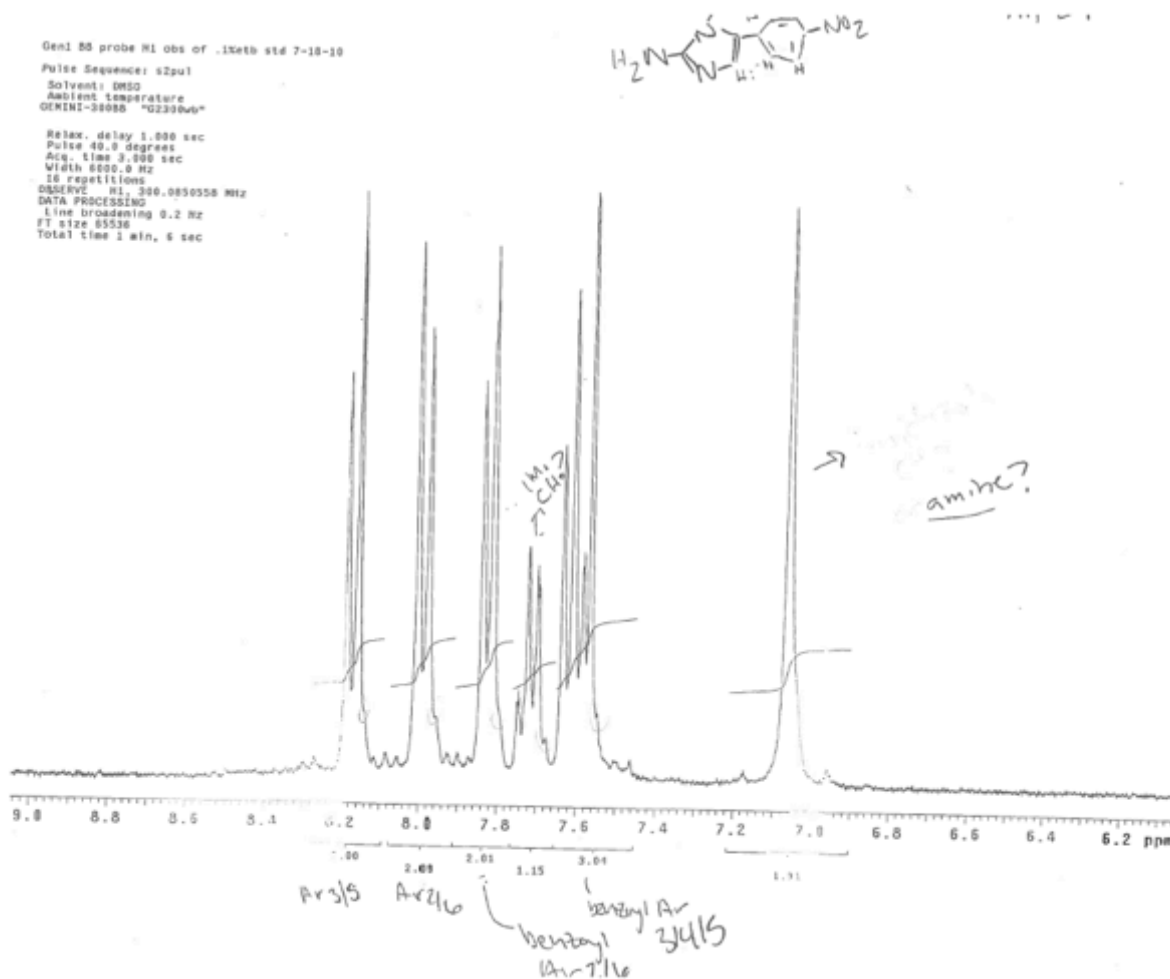


**Figure A1.4.** Raw <sup>1</sup>H NMR spectrum of 5-(4-nitrophenyl) 2-AI (compound III).

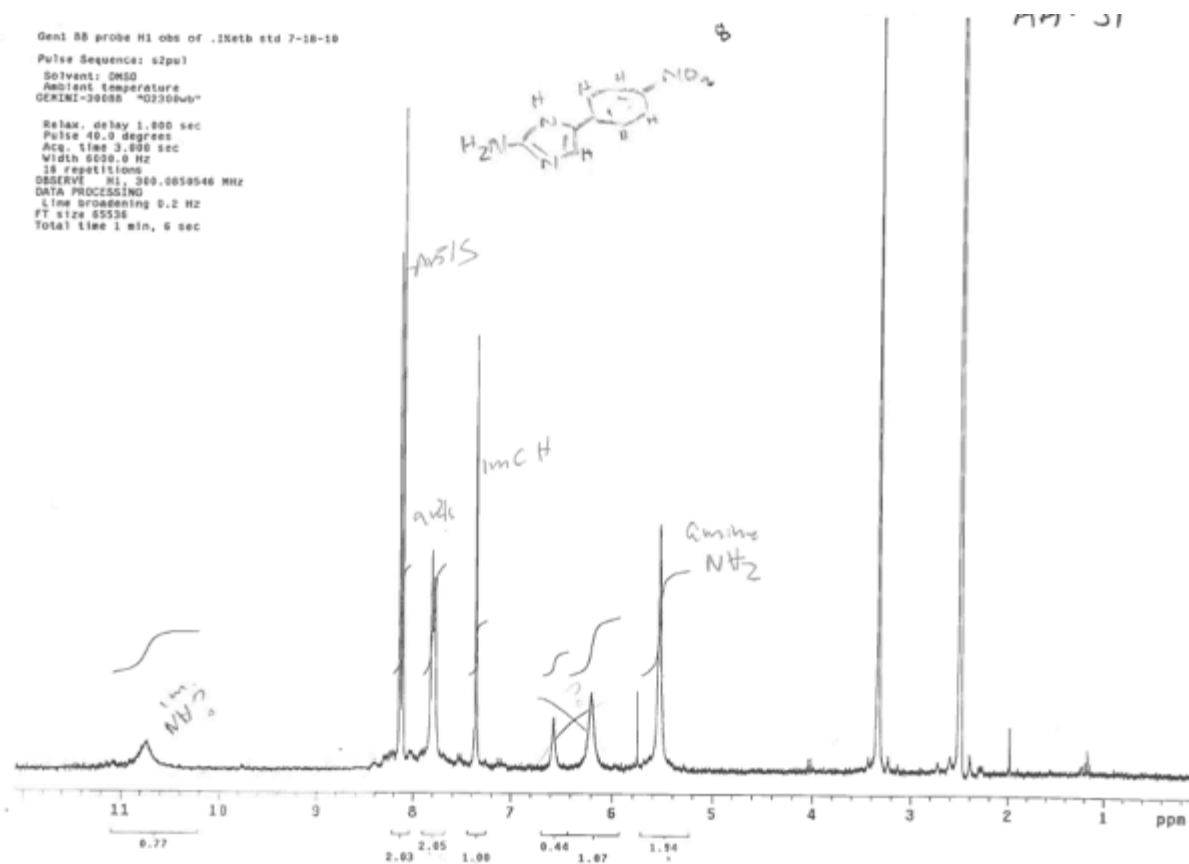


**Figure A1.5.** Raw  $^1\text{H}$  NMR spectrum of 5-(4-nitrophenyl) 2-AI (compound III).

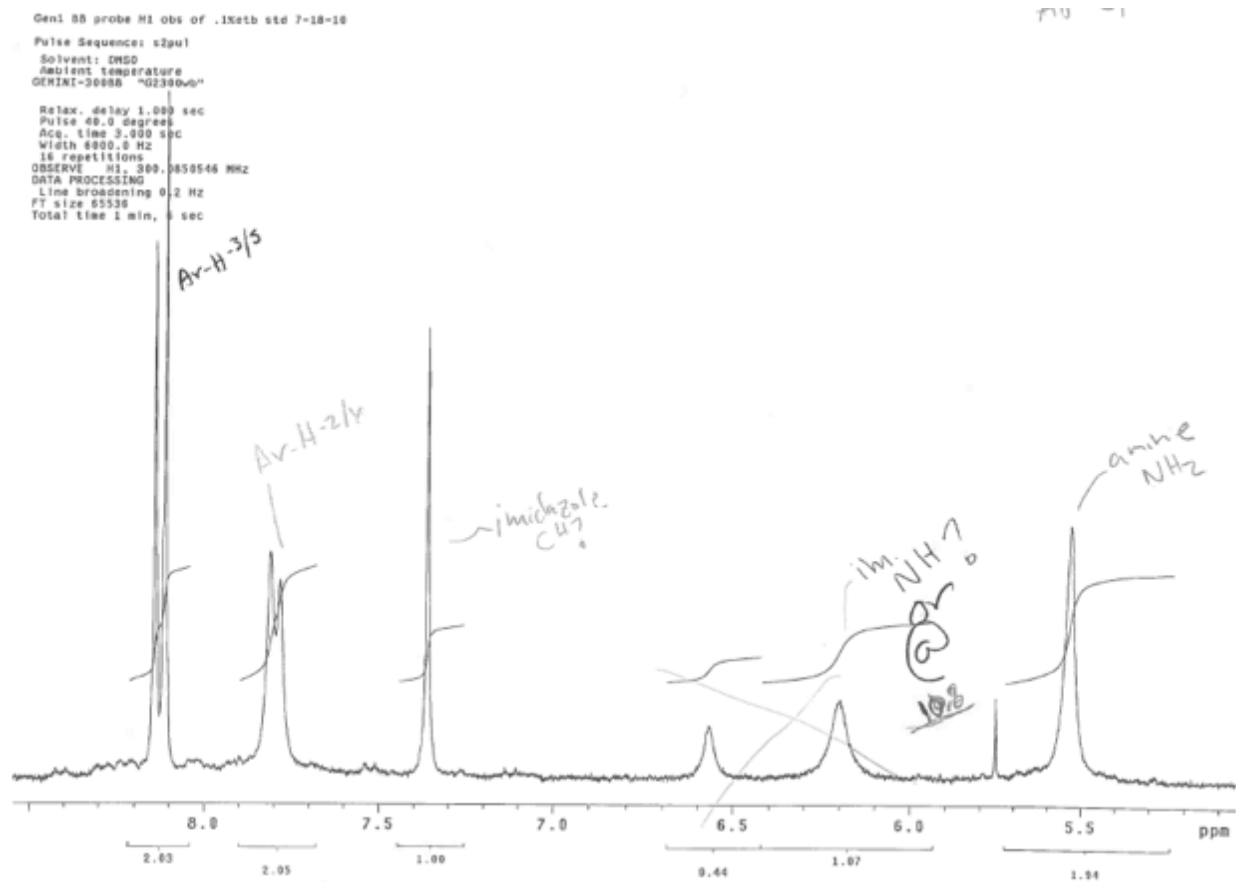


**Figure A1.6.** Raw  $^1\text{H}$  NMR spectrum of 5-(4-nitrophenyl) 2-AI (compound III).

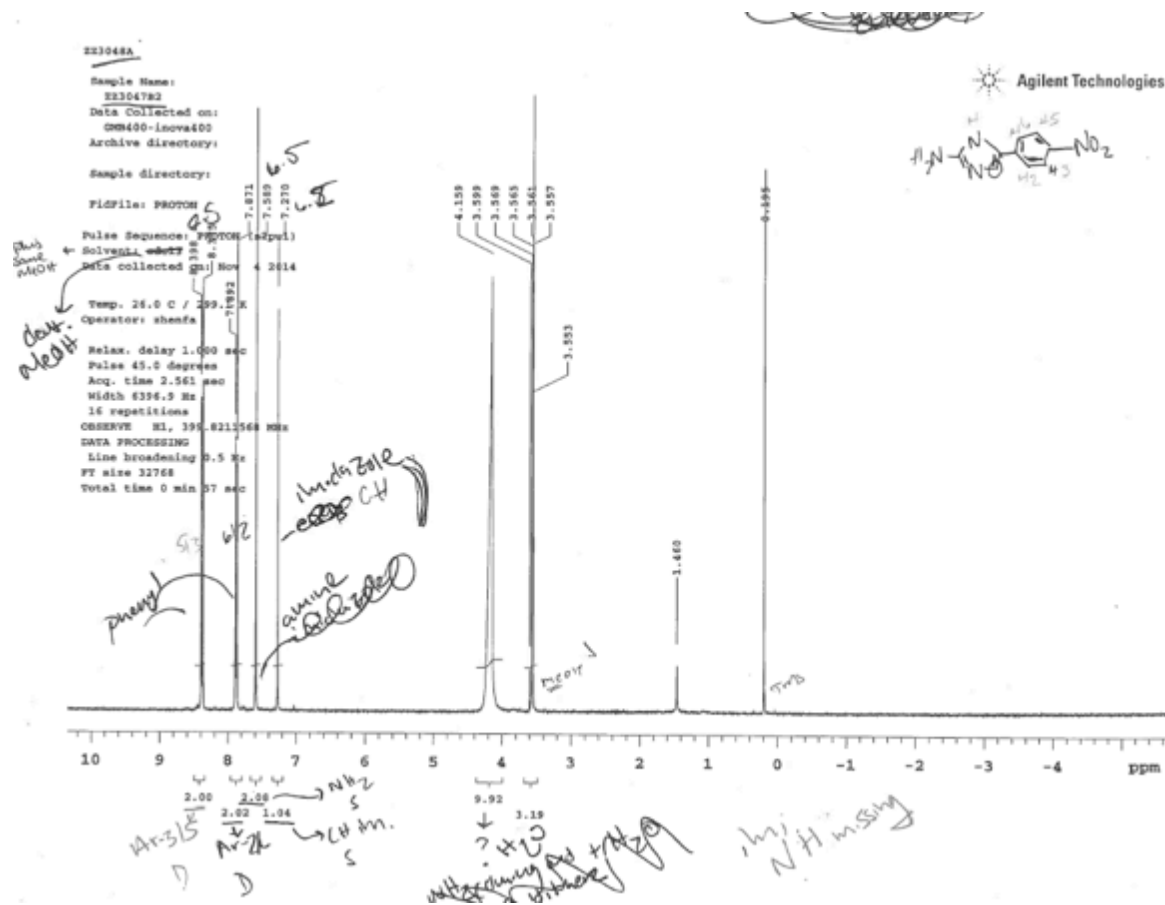
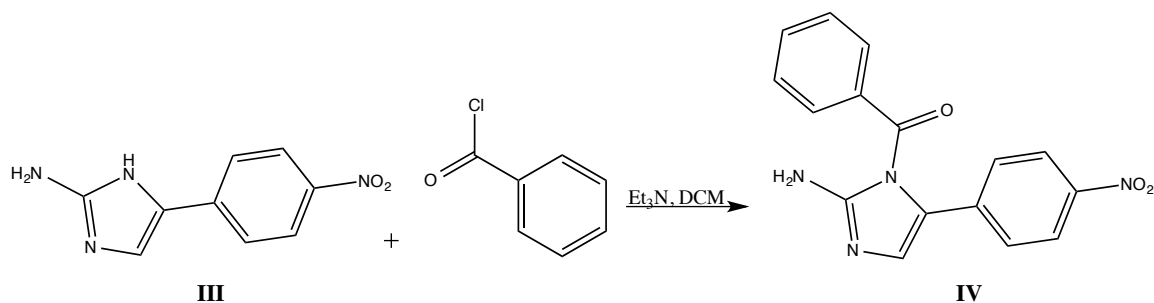


**Figure A1.7.** Raw  $^1\text{H}$  NMR spectrum of 5-(4-nitrophenyl) 2-AI (compound III).

### A1.2.3. 5-(4-nitrophenyl)-1-benzoyl 2-AI conjugate



**Scheme A1.4.**

**III** (0.64 mmol) was dissolved in DCM, and triethylamine (2.5 mmol), benzoyl chloride (1.3 mmol) added and the solution stirred overnight. The reaction was quenched with sodium bicarbonate, separated and the organic extract dried over  $\text{Na}_2\text{SO}_4$ . Following evaporation of the

solvent, the product was purified on a silica column eluted with 50:50 EtOAc/hexane. Material collected as an orange solid was triturated with DCM and MeOH, then dried under vacuum to give 0.17 mmol 5-(4-nitrophenyl)-1-benzoyl 2-AI conjugate (**IV**) (27%).  $^1\text{H}$  NMR (400 MHz,  $\text{DMSO}-d_6$ ):  $\delta$  8.2 (d, 2H, Ar-H-3/5), 8.0 (d, 2H, Ar-H-2/6), 7.8 (d, 2H, benzoyl Ar-H-2/6); 7.7 (t, 1H, imidazole CH); 7.6 (q, 3H, benzoyl Ar-H-2/6); 7.1 (s, 2H,  $\text{NH}_2$ ).

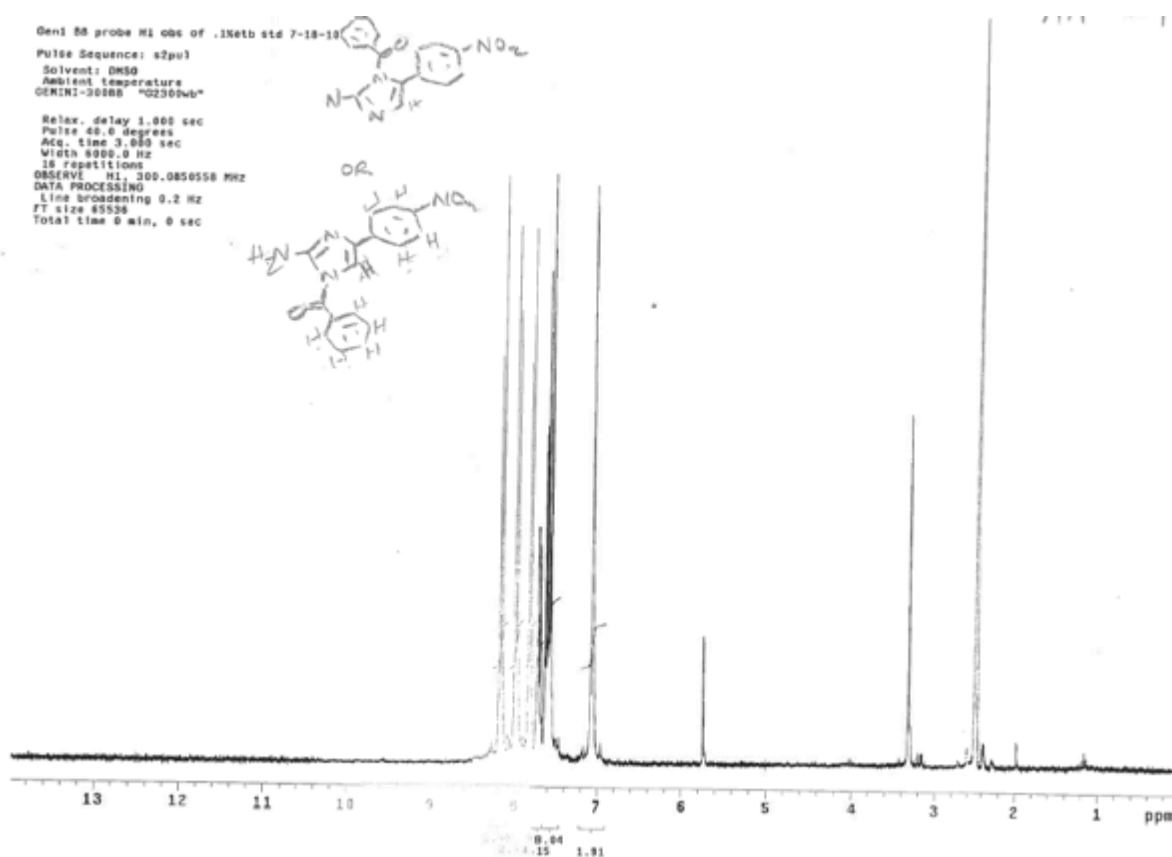
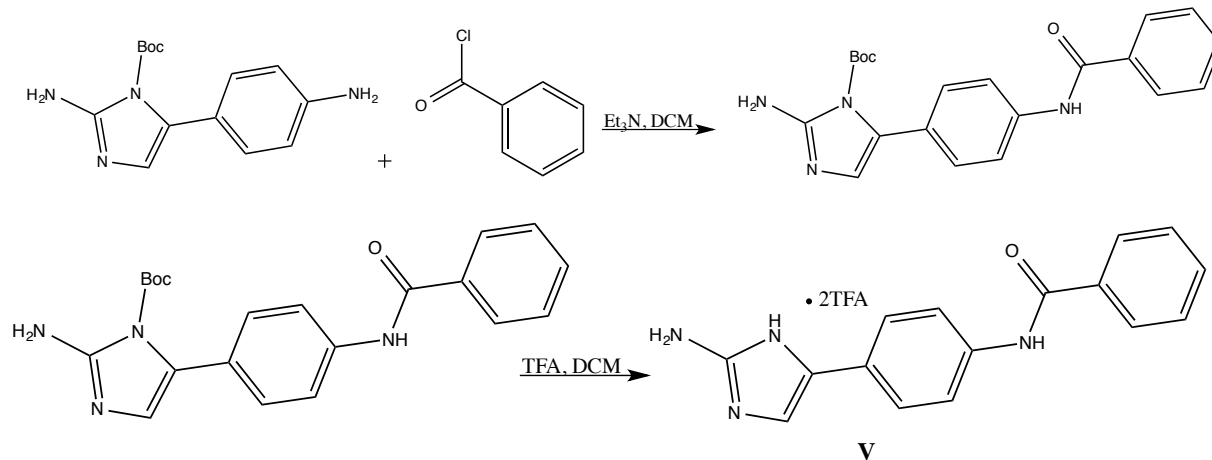


**Figure A1.8.** Raw  $^1\text{H}$  NMR spectrum of 5-(4-nitrophenyl)-1-benzoyl 2-AI conjugate (compound **IV**).

#### A1.2.4. 2-AI-para-mono-benzoyl conjugate for bioassay



**Scheme A1.5.**

The *t*-butyl-2-amino-4-(4-aminophenyl)-1*H*-imidazole-1-carboxylate (0.2 mmol) was dissolved in DCM. Then 4 equivalents of triethylamine and 1.5 equivalents of benzoyl chloride were added and the solution was stirred vigorously overnight. The reaction was quenched with sodium bicarbonate, then the organics were extracted, collected, and dried over Na<sub>2</sub>SO<sub>4</sub>. Excess TFA was then added and the solution stirred for 30 minutes until the reaction came to completion. The solvent was evaporated with rotary evaporator, diethyl ether was added and evaporated 4 times to give light pink solids, which were triturated with DCM and dried over vacuum to give 0.15 mmol 2-AI-para-mono-benzoyl conjugate (V) (75%). <sup>1</sup>H NMR (300 MHz, DMSO-*d*<sub>6</sub>): δ 12.9 (s, 1H, imidazole NH), 12.2 (s, 1H, imidazole NH), 10.4 (s, 1H, benzoyl NH), 8.0 (d, 2H, Ar-H-3/5), 7.9 (d, 2H, Ar-H-2/6), 7.6 (m, 6H, imidazole CH, benzoyl Ar-H); 7.3 (s, 2H, NH<sub>2</sub>).



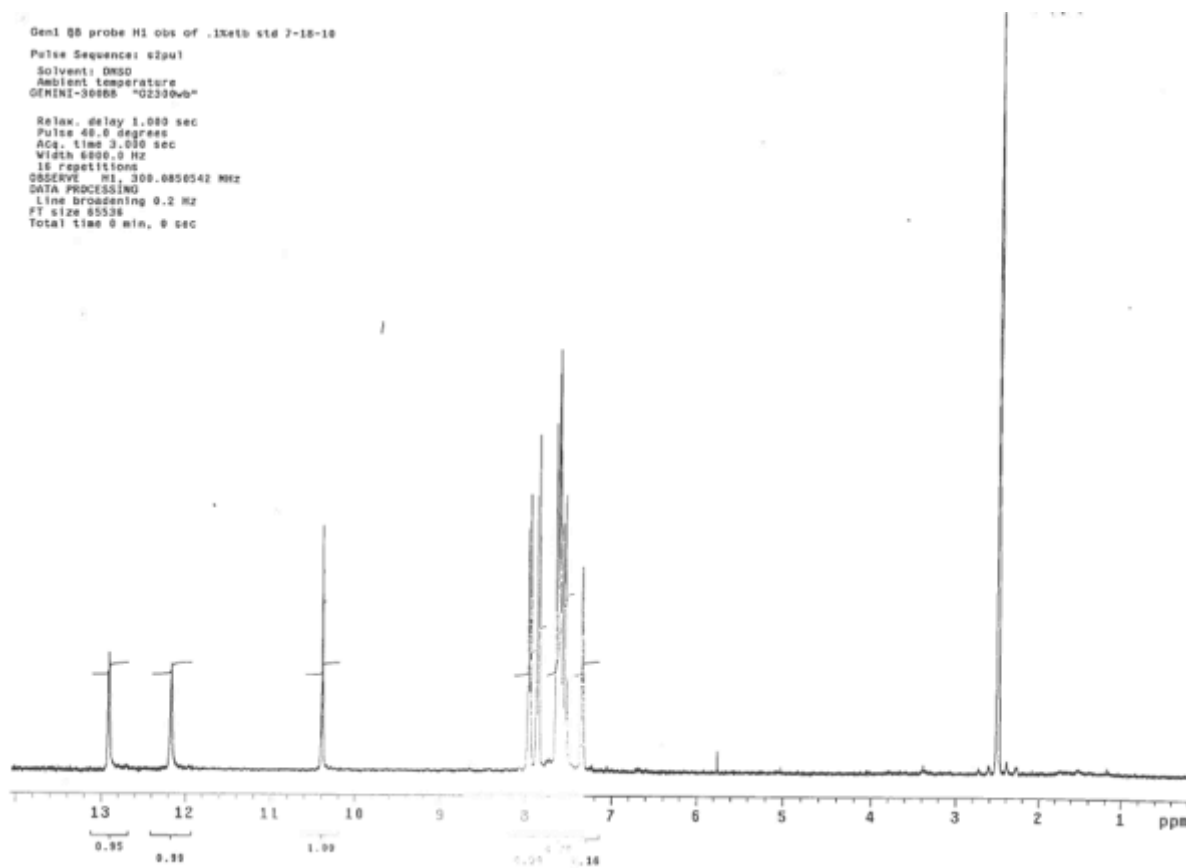


**Figure A1.9.** Raw  $^1\text{H}$  NMR spectrum of 2-AI-para-mono-benzoyl conjugate (compound V).

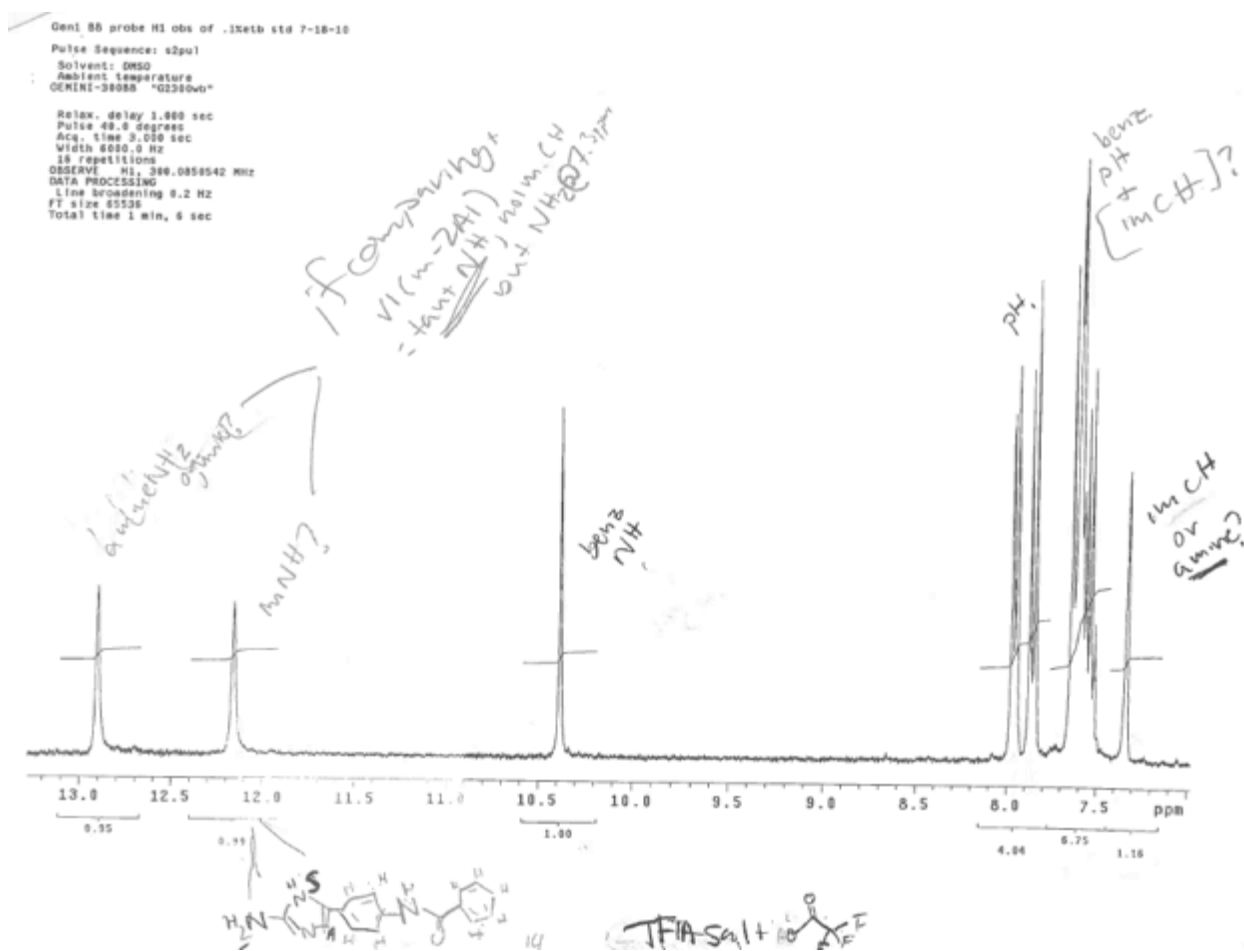
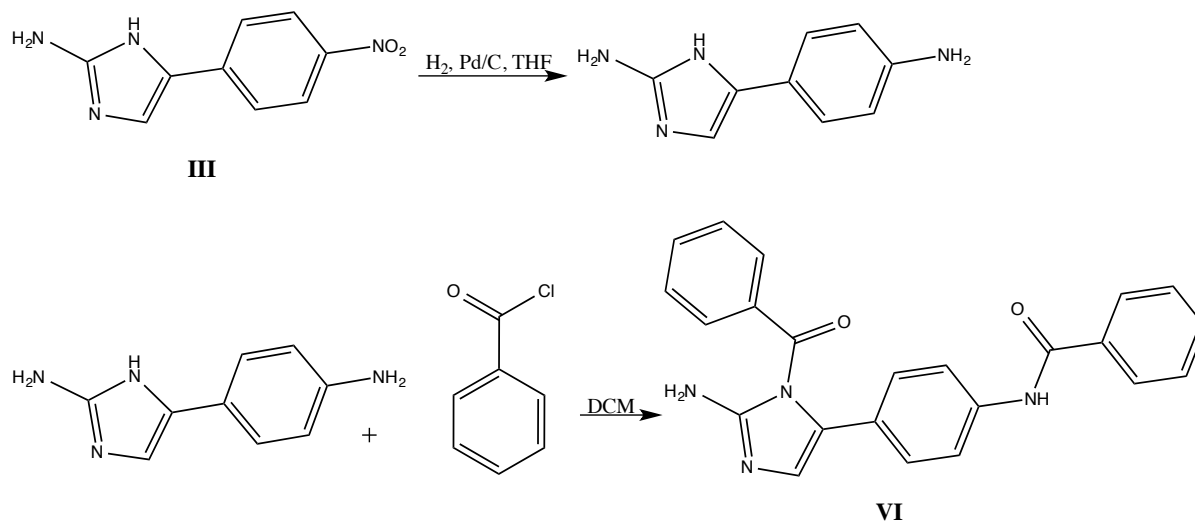


**Figure A1.10.** Raw  $^1\text{H}$  NMR spectrum of 2-Al-para-mono-benzoyl conjugate (compound V).

### A1.2.5. Dibenzoyl 2-AI-para conjugate for bioassay



**Scheme A1.6.**

**III** was dissolved in THF under an  $\text{H}_2$  atmosphere,  $\sim 20$  mg Pd/C was added to the solution stirred overnight under  $\text{H}_2$ . The Pd/C catalyst was filtered off and solvent evaporated on a rotary evaporator. The residue was dissolved in DCM, 1 equivalent of benzoyl chloride added and the solution stirred overnight. The reaction was quenched with sodium bicarbonate, and the organic layer collected and dried over  $\text{Na}_2\text{SO}_4$ . Following evaporation of solvent, the solid was triturated with DCM and dried under vacuum to give 2-AI-para-di-benzoyl conjugate (**VI**).

$^1\text{H}$  NMR (300 MHz,  $\text{DMSO}-d_6$ ):  $\delta$  10.2 (s, 1H, benzoyl NH), 8.0 (d, 2H, Ar-H-3/5), 7.8 (d, 2H, Ar-H-2/6), 7.7 (m, 5H, benzoyl Ar-H), 7.6 (m, 5H, benzoyl Ar-H), 7.2 (s, 1H, imidazole CH), 7.0 (s, 2H,  $\text{NH}_2$ ).

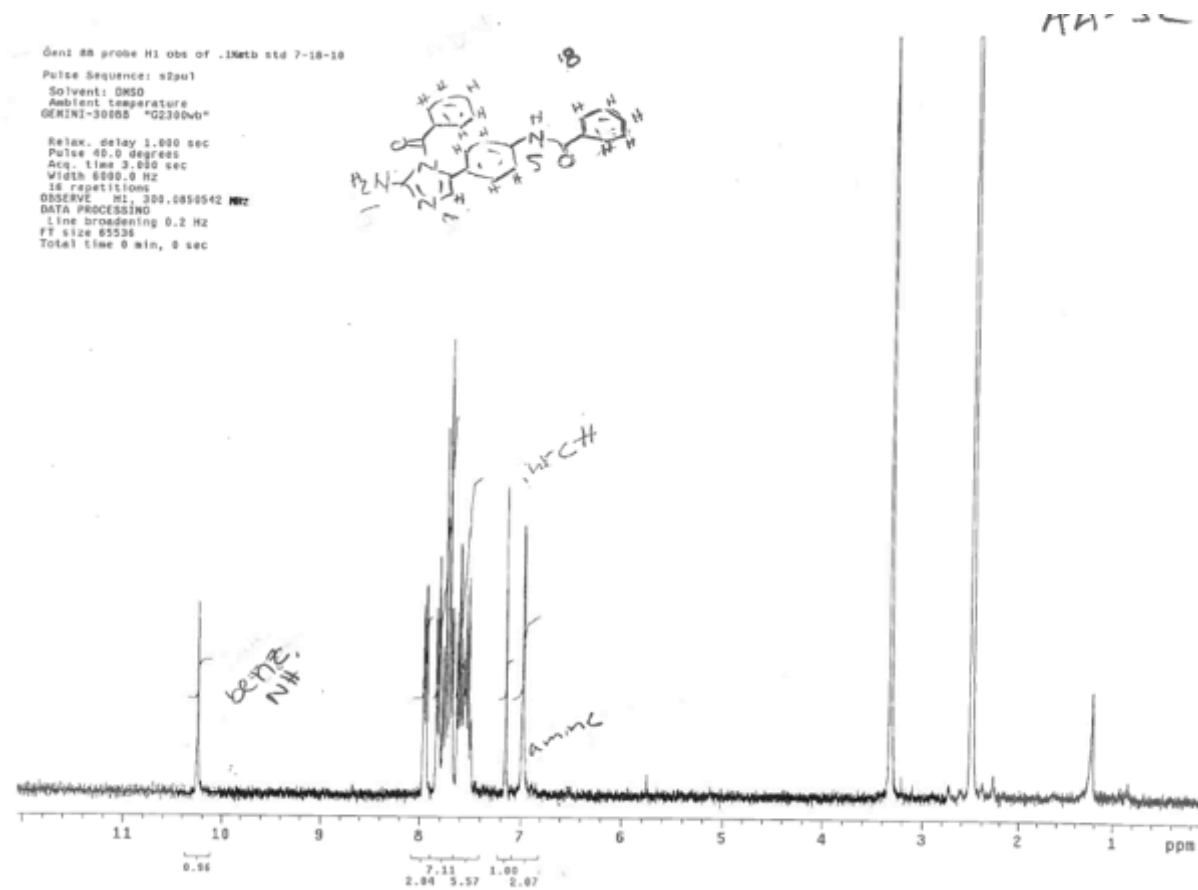


**Figure A1.11.** Raw  $^1\text{H}$  NMR spectrum of dibenzoyl 2-AI-para conjugate (compound VI).

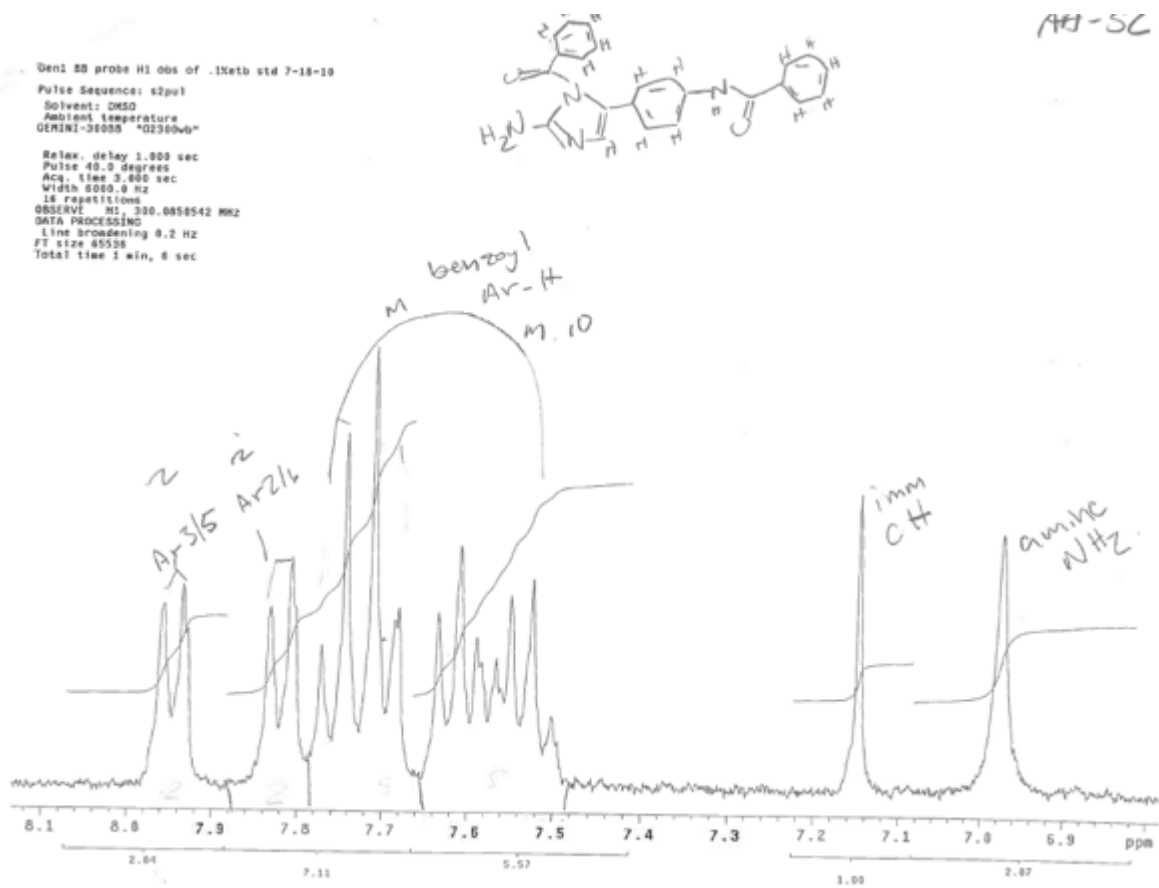


**Figure A1.12.** Raw  $^1\text{H}$  NMR spectrum of dibenzoyl 2-AI-para conjugate (compound VI).

Chemical reaction scheme showing the synthesis of compound VII. The reaction involves the coupling of a benzimidazole derivative (1-(4-aminophenyl)-3-(aminomethyl)-1H-imidazole-4-carboxylic acid tert-butyl ester) with benzoyl chloride (a benzene ring with a -COCl group) in the presence of triethylamine ( $\text{Et}_3\text{N}$ ) and dichloromethane (DCM). The product is compound VII, which is 1-(4-(benzoylamino)phenyl)-3-(aminomethyl)-1H-imidazole-4-carboxylic acid tert-butyl ester.

The starting material (1.0 mmol) was dissolved in DCM, benzoyl chloride (1.1 mmol) and triethylamine (10.2 mmol) added, and the solution stirred for 3 h. Following removal of solvent on a rotary evaporator, the residue was dissolved in EtOAc and saturated aqueous sodium bicarbonate solution added. The solution was stirred for 15 min, the organic layer separated and dried over Na<sub>2</sub>SO<sub>4</sub>. Evaporation of solvent gave a quantitative yield of **VII** as a light yellow powder. <sup>1</sup>H NMR (400 MHz, DMSO-*d*<sub>6</sub>): δ 10.2 (s, 1H, benzoyl NH), 8.1 (s, 1H, Ar-H-2), 8.0 (m, 2H, Ar-H-4/6), 7.6 (m, 4H, benzoyl Ar-H); 7.5 (m, 1H, Ar-H-5), 7.3 (m, 1H, imidazole CH); 6.6 (s, 2H, NH<sub>2</sub>); 1.6 (s, 9H, *t*-Bu).

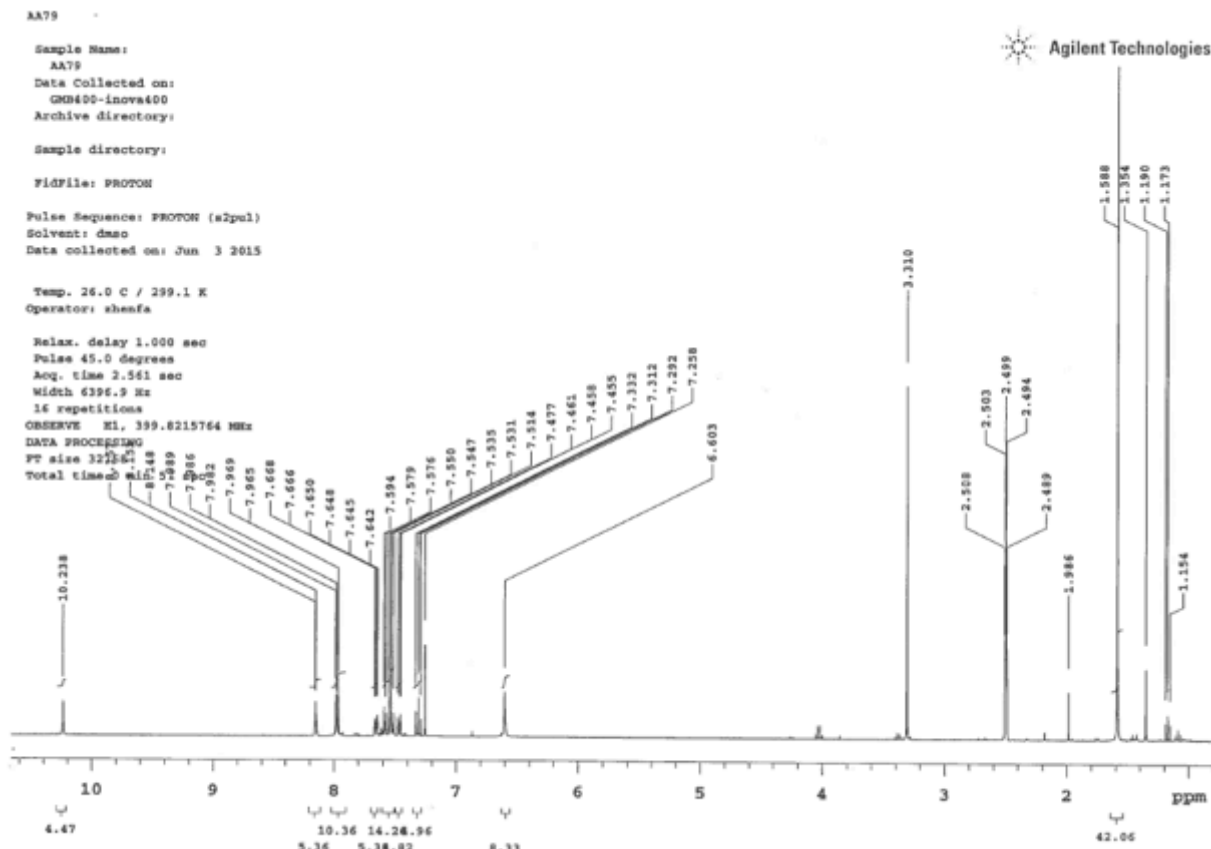
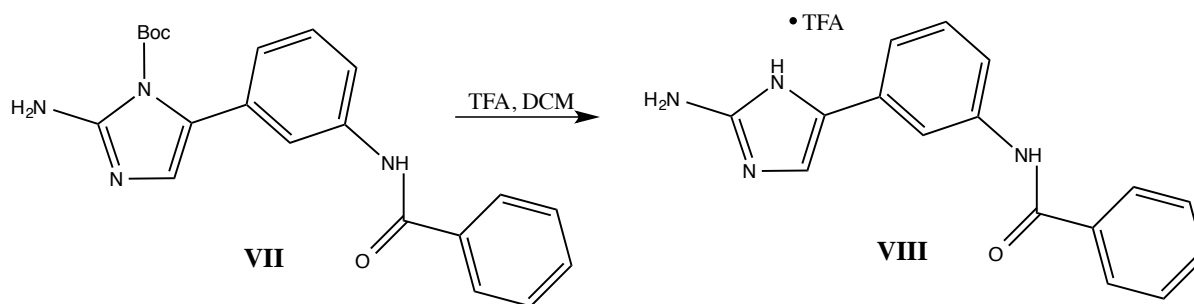


**Figure A1.13.** Raw  $^1\text{H}$  NMR spectrum of compound VII.



**Scheme A1.8.**

**VII** (1.0 mmol) was dissolved in DCM, excess TFA was added and the solution stirred overnight. The solvent was removed under reduced pressure. The residue was dissolved in DCM and evaporated to dryness, repeating 3 times. The resulting solid triturated with DCM and dried under vacuum to give 0.70 mmol 2-AI-meta-benzoyl conjugate (**VIII**) as a fine off-white powder (70%).  $^1\text{H}$  NMR (400 MHz,  $\text{DMSO}-d_6$ ):  $\delta$  12.8 (br s, 1H, imidazole NH), 12.2 (br, s, 1H,

imidazole NH), 10.4 (s, 1H, benzoyl NH), 8.1 (s, 1H, Ar-H-2), 8.0 (m, 2H, Ar-H-4/6), 7.5 (m, 6H, benzoyl Ar-H); 7.4 (m, 1H, Ar-H-5), 7.3 (s, 1H, imidazole CH).

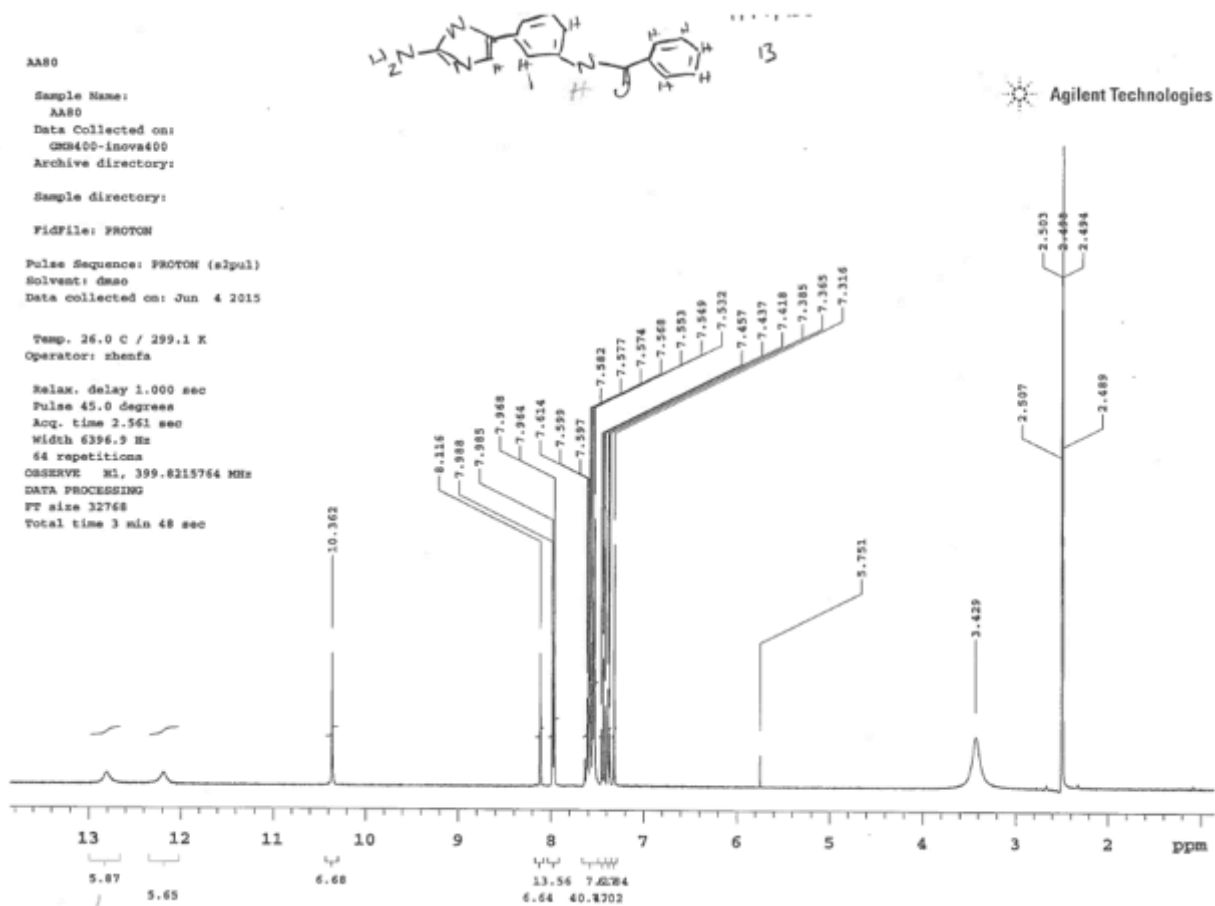
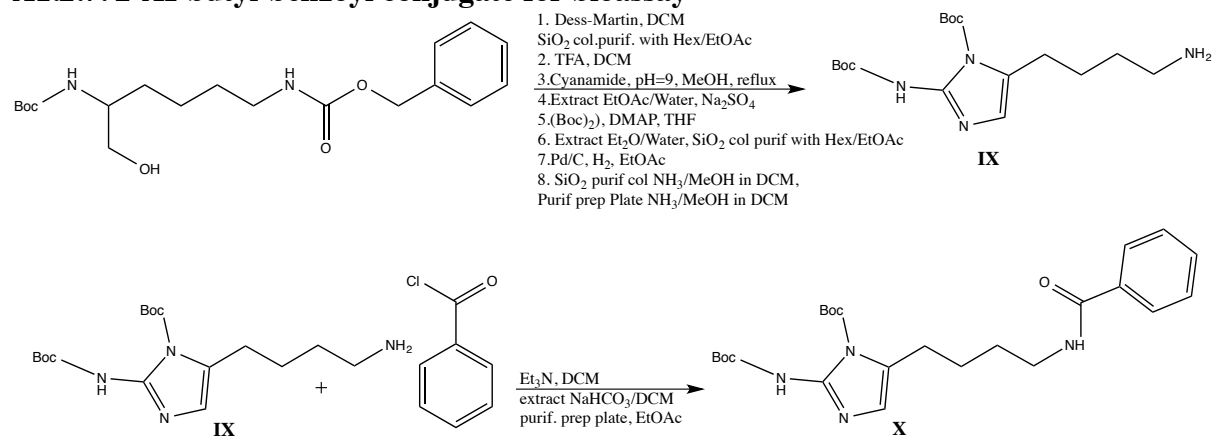


**Figure A1.14.** Raw  $^1\text{H}$  NMR spectrum of 2-AI-meta-benzoyl conjugate (compound VIII).



### A1.2.7. 2-AI-butyl-benzoyl conjugate for bioassay



### Scheme A1.9.

The starting alcohol (2.7 mmol) was dissolved in DCM, then 1.1 equivalent of Dess-Martin reagent was added and solution stirred for 10 min. The solution was loaded onto a silica column prepared in hexanes, and eluted with 40:60 EtOAc/hexane. Fractions containing the product were combined, concentrated and diluted with DCM. Excess TFA was added and the solution was stirred 20 min until Boc removal was completed as verified by TLC. The solvent was removed under reduced pressure and the residue dissolved in MeOH. Cyanamide was added (23.8 mmol), pH adjusted to 9 with NaOH, and the solution refluxed for 2 h. Following evaporation of solvent, the residue was partitioned between EtOAc and water. The organic layer was separated, dried over Na<sub>2</sub>SO<sub>4</sub>, and evaporated to dryness. The residue was dissolved in THF, (Boc)<sub>2</sub>O (27.6 mmol) and 4-dimethylaminopyridine (7.3 mmol) added, and the solution stirred for 4 da. Et<sub>2</sub>O and water were added and organic layer separated and evaporated to dryness. The residue was loaded onto a silica column prepared in hexane and eluted with 35:65 EtOAc/hexane. The fractions containing product were combined, evaporated to dryness, then the residue was dissolved in EtOAc. Pd/C (~20 mg) was added under an H<sub>2</sub> atmosphere and the solution stirred overnight. The Pd/C was filtered off and the solvent evaporated. The residue was dissolved in

DCM loaded onto a silica column prepared in DCM and eluted with 1:4 7 N methanolic ammonia/DCM. Fractions containing product were combined, and evaporation of solvent yielded a solid. The solid was dissolved in DCM and purified by preparative TLC developed with a mobile phase of 1:9 7 N methanolic ammonia/DCM. The product-containing bands were collected and extracted with 1:3 7 N methanolic ammonia/DCM, and the extract evaporated to dryness yielding 0.02 mmol **IX**. The residue was dissolved in DCM, benzoyl chloride (0.03 mmol) and triethylamine (0.2 mmol) added and the solution stirred overnight. The reaction was quenched with saturated aqueous sodium bicarbonate solution and extracted with DCM. The organic layer was separated, dried over Na<sub>2</sub>SO<sub>4</sub> and evaporated to dryness. The residue was dissolved in DCM and purified by preparative TLC developed with EtOAc. The band containing product was collected and extracted with EtOAc and the extract evaporated to dryness to give **X**. <sup>1</sup>H NMR (300 MHz, DMSO-*d*<sub>6</sub>): δ 7.8 (d, 2H, Ar-H-2/6), 7.4 (m, 3H, Ar-H-3/4/5), 7.1 (s, 1H, imidazole CH), 6.5 (br s, 1H, benzoyl NH), 3.5 (m, 2H, CH<sub>2</sub>), 2.6 (t, 2H, CH<sub>2</sub>), 1.7 (m, 13H, 2x CH<sub>2</sub>), 1.4 (s, 18H, 2x *t*-Bu).

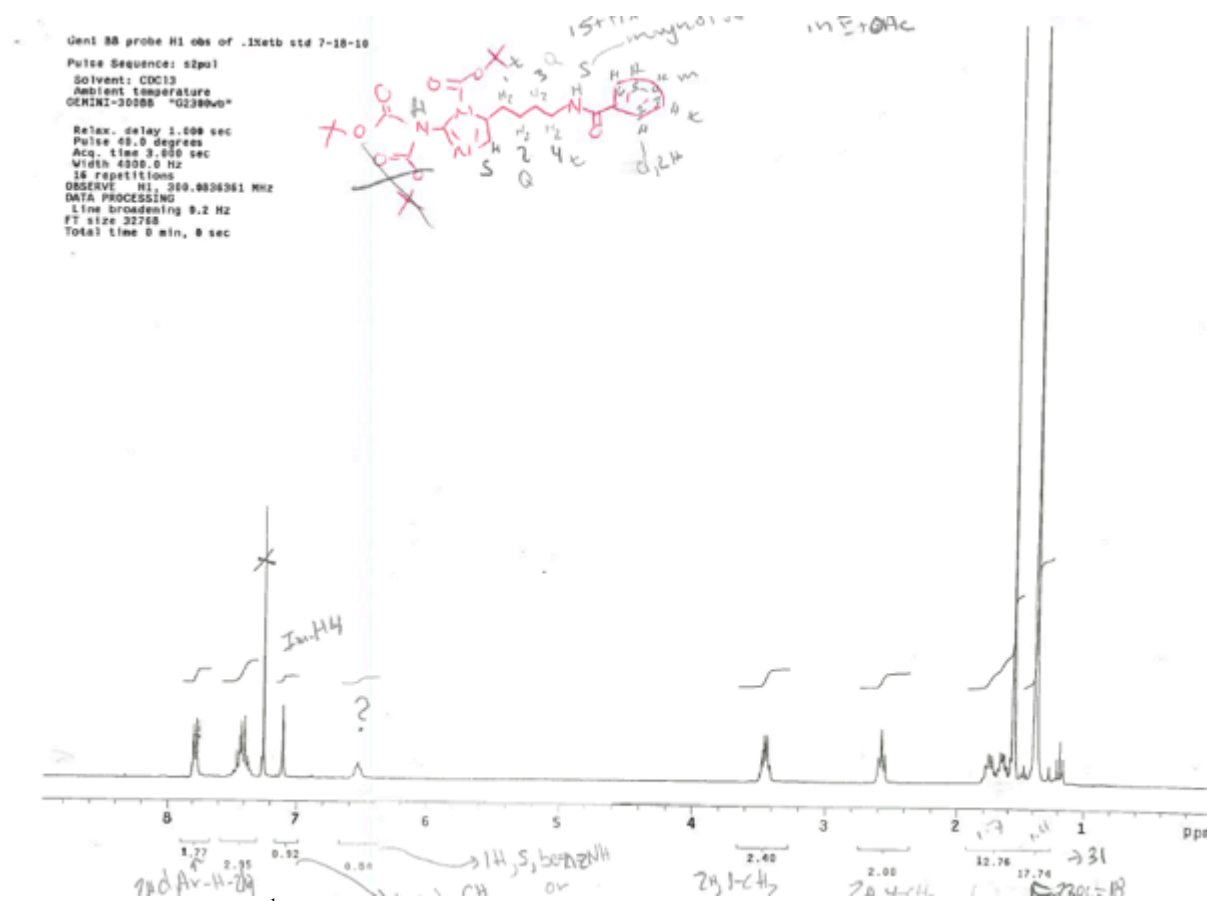
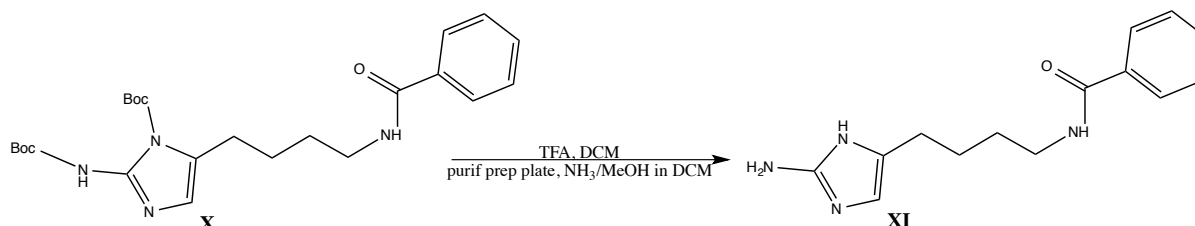


**Figure A1.15.** Raw  $^1\text{H}$  NMR spectrum of compound X.



**Scheme A1.10.**

**X** was dissolved in DCM, an excess of TFA was added, the solution stirred for 30 min and the solvent evaporated. The residue was dissolved in DCM and concentrated to dryness, then redissolved in DCM and concentrated to dryness once more. The residue was dissolved in  $\text{Et}_2\text{O}$  and concentrated to dryness, then redissolved in  $\text{Et}_2\text{O}$  and concentrated to dryness once more. The residue was dissolved 1:9 7 N methanolic ammonia/DCM and loaded onto preparative TLC plate developed with a mobile phase of 1:3 7 N methanolic ammonia/DCM. The product was

extracted with 1:4 7 N methanolic ammonia/DCM, the solvent evaporated and the residue dissolved in Et<sub>2</sub>O/THF and evaporated to dryness once more. The residue was dissolved in Et<sub>2</sub>O, filtered, and the filtrate was concentrated to give 0.02 mmol 2-AI-butyl-benzoyl conjugate (**XI**) (0.1%). <sup>1</sup>H NMR (300 MHz, DMSO-*d*<sub>6</sub>): δ 8.5(s, 1H, benzoyl NH), 7.8 (d, 2H, Ar-H-2/6), 7.4 (m, 3H, Ar-H-3/4/5), 6.2 (s, 1H, imidazole CH), 5.2 (br s, 1H, imidazole NH), 3.3 (m, 4H, 2xCH<sub>2</sub>), 1.5 (m, 4H, 2xCH<sub>2</sub>).

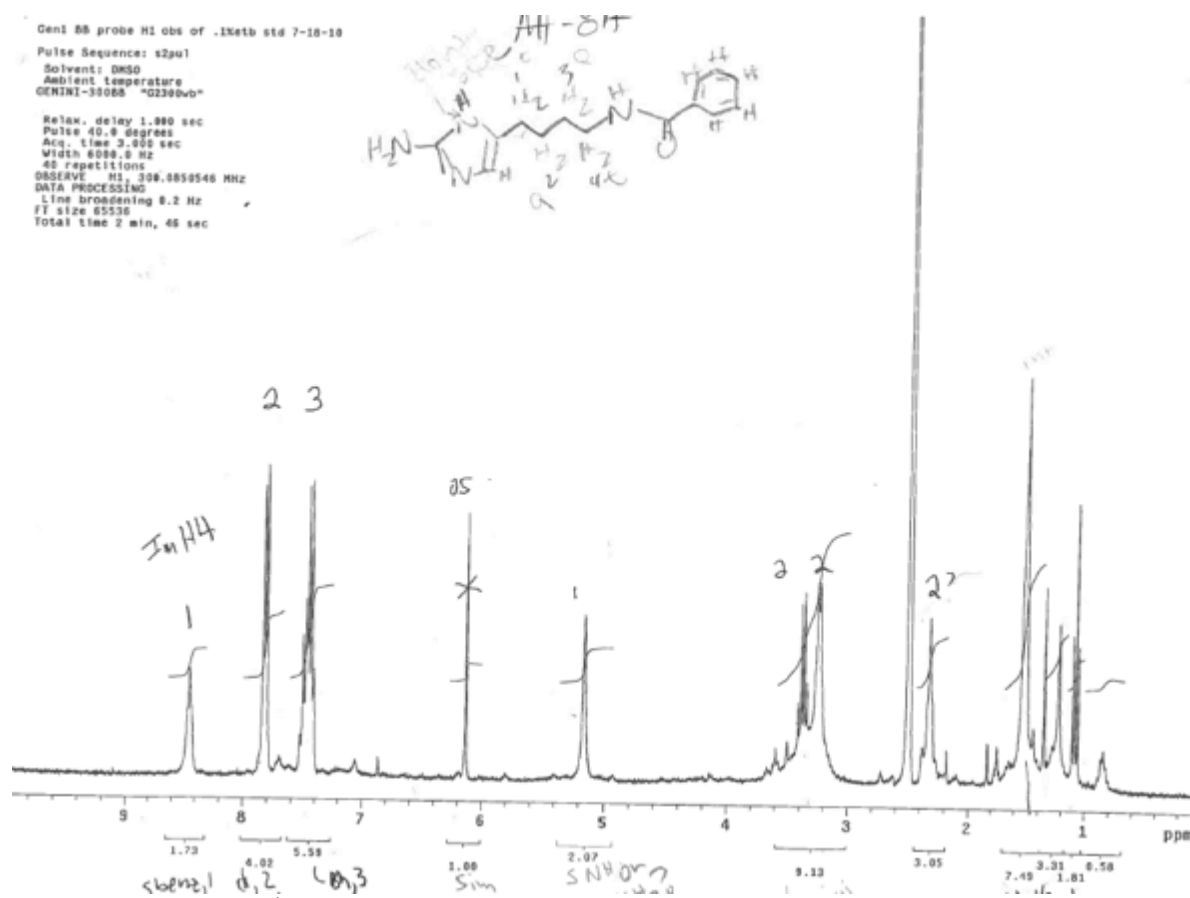


**Figure A1.16.** Raw <sup>1</sup>H NMR spectrum of 2-AI-butyl-benzoyl conjugate (compound **XI**).

### A1.3. Supporting Figures

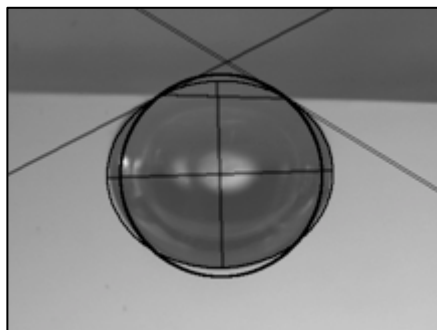


**Figure A1.17.** A representative captive bubble image and corresponding circular, ellipse, and 2-sided manual angle best-fits for contact angle measurement.

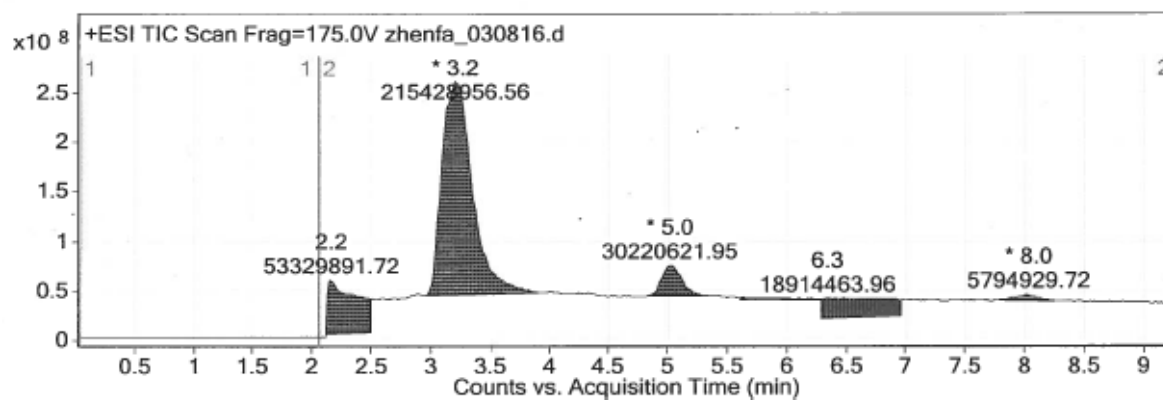


**Figure A1.18.** Raw LC/ESI-MS chromatogram of model reaction from *Section 2.2.3 and 2.3.1.1*.

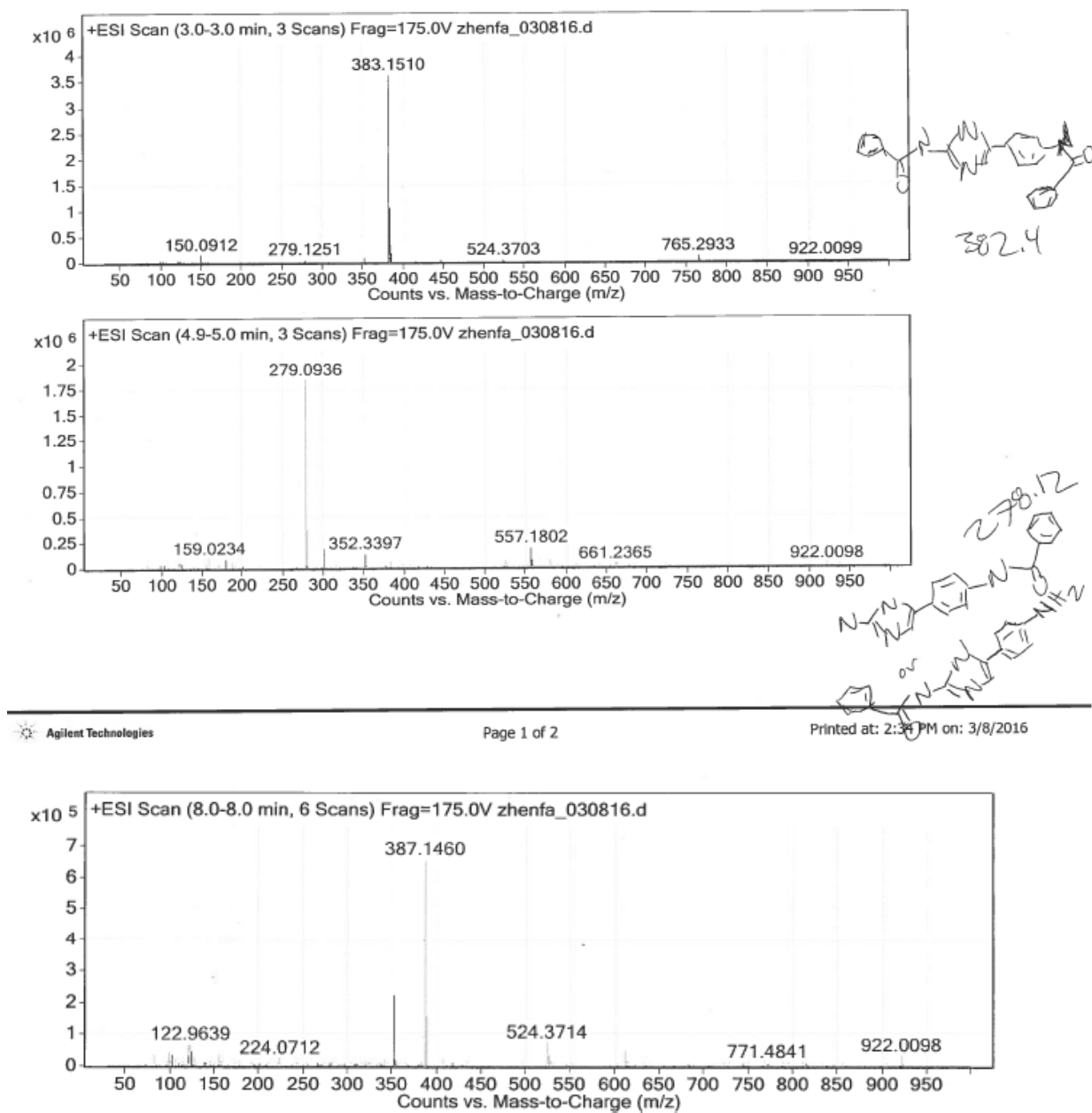


**Figure A1.19.** Raw LC/ESI-MS mass spectra of model reaction from 2.2.3 and 2.3.1.1.

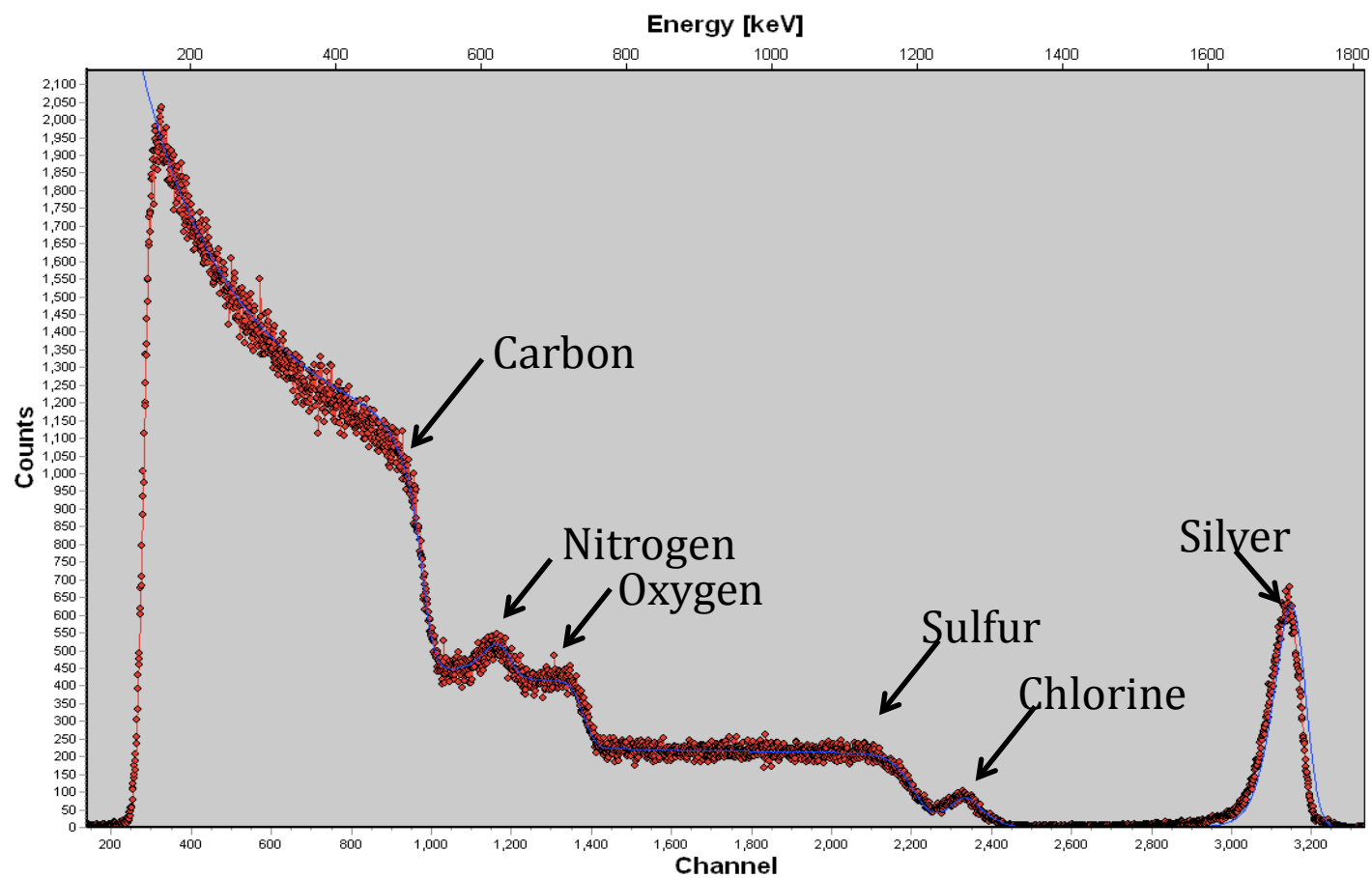


**Figure A1.20.** Example RBS spectrum silver probed membrane. RBS spectrum of an ESPA3 membrane that's been probed with silver. The red diamonds are the raw data and the blue line is the fitted simulated data.

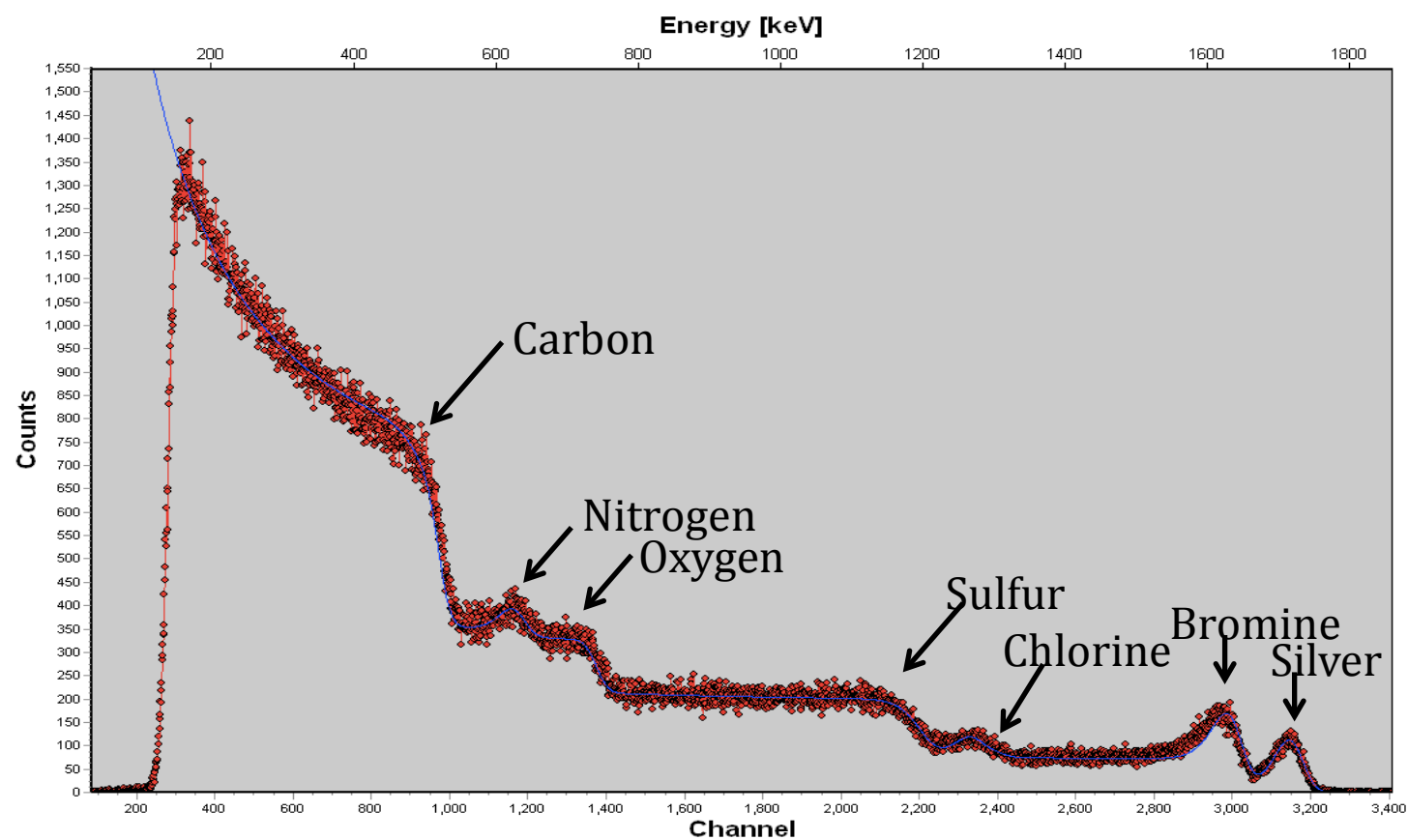


**Figure A1.21.** Example RBS spectrum of bromoaniline membrane. RBS spectrum of an ESPA3+BA membrane that's been probed with silver. The red diamonds are the raw data and the blue line is the fitted simulated data.



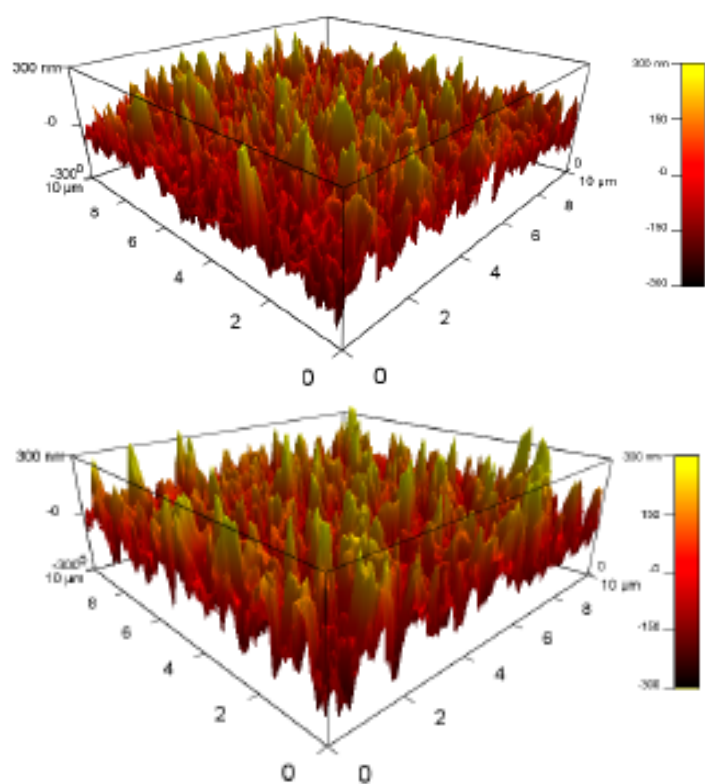


**Figure A1.22.** Example 3-D contour surface roughness plots collected with AFM, ESPA3 (top) and ESPA3+2-AI (bottom).

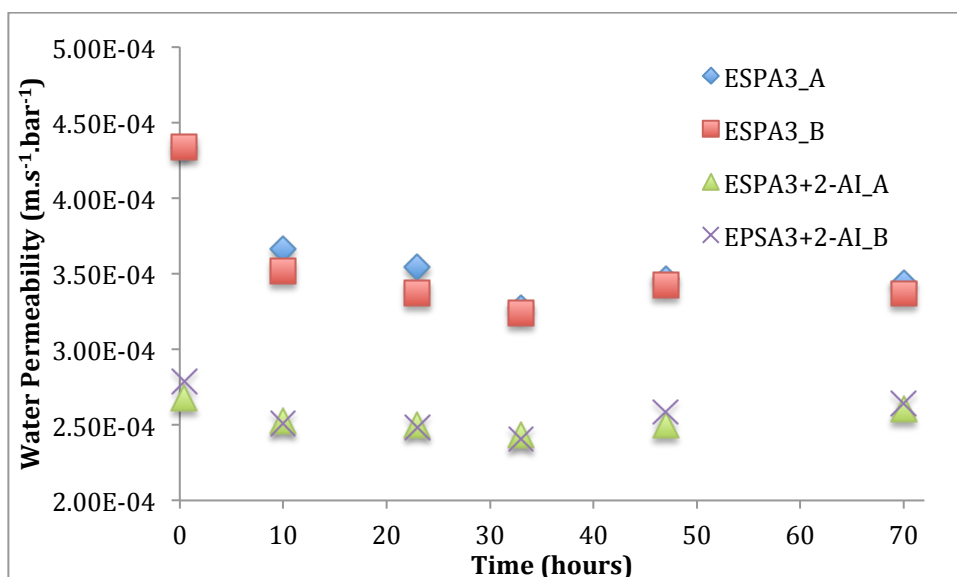


**Figure A1.23.** Water permeability of ESPA3 and ESPA3+2-AI membranes operated in cross-flow with 500 ppm sodium chloride feed solution as described in *Section 2.2.15.2*. A and B denote experimental duplicates.

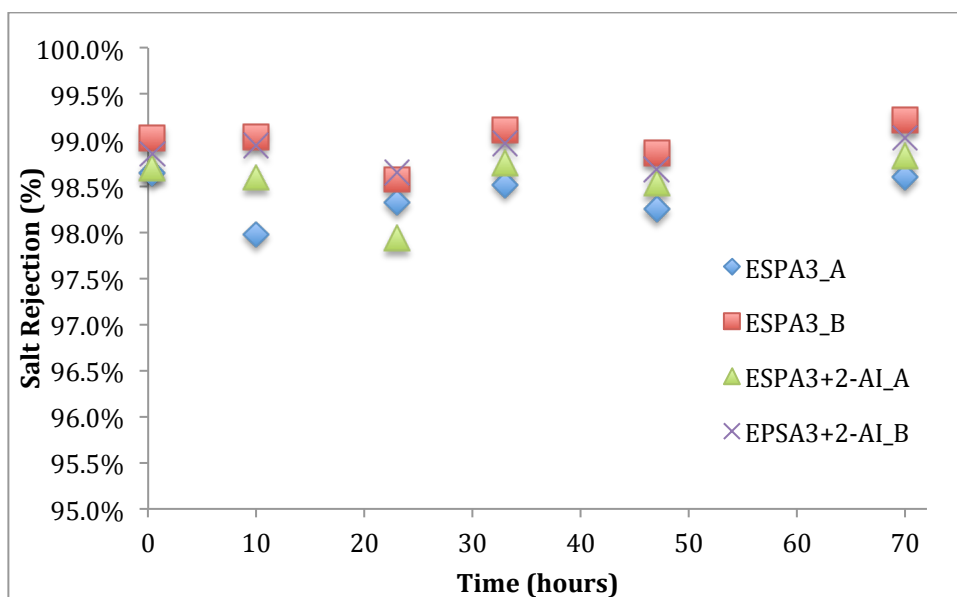


**Figure A1.24.** Salt rejection by ESPA3 and ESPA3+2-AI membranes operated in cross-flow with 500 ppm sodium chloride feed solution as described in *Section 2.2.15.2*. A and B denote experimental duplicates.

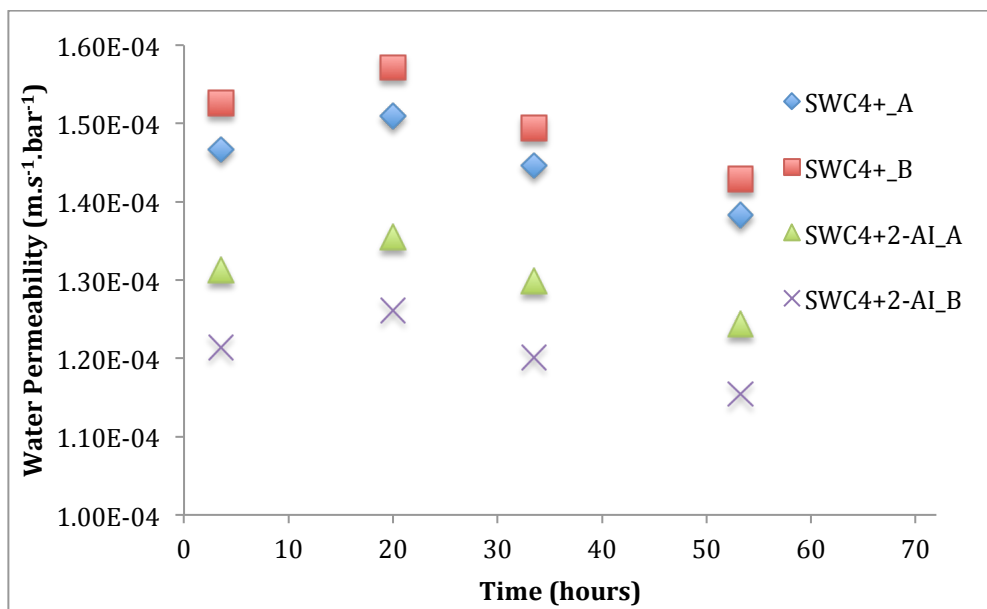


**Figure A1.25.** Water permeability of SWC4+ and SWC4+2-AI membranes operated in cross-flow with 500 ppm sodium chloride feed solution as described in *Section 2.2.15.2*. A and B denote experimental duplicates.

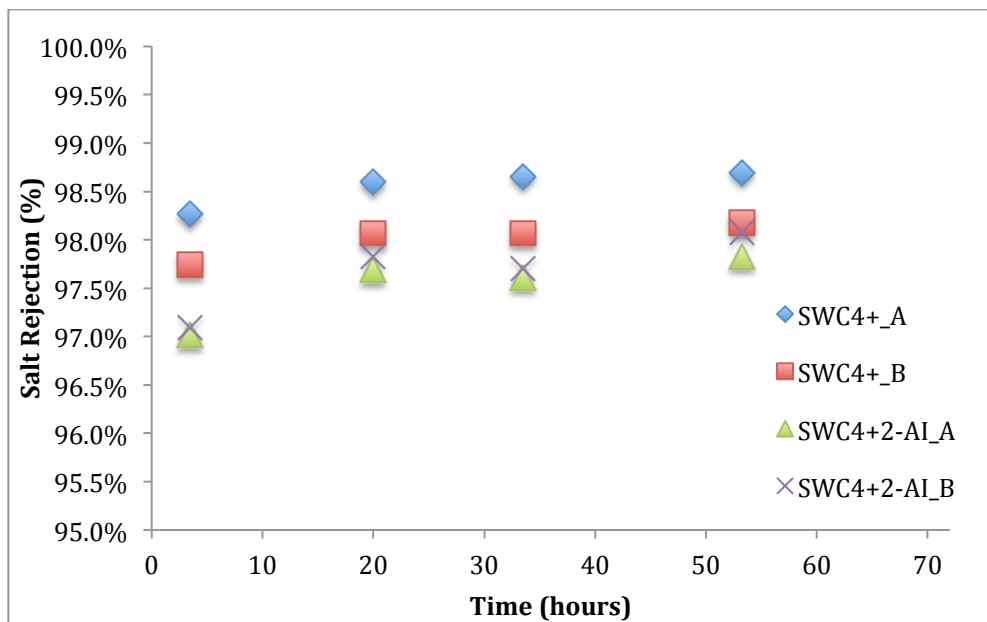


**Figure A1.26.** Salt rejection by SWC4+ and SWC4+ 2-AI membranes operated in cross-flow with 500 ppm sodium chloride feed solution as described in *Section 2.2.15.2*. A and B denote experimental duplicates.

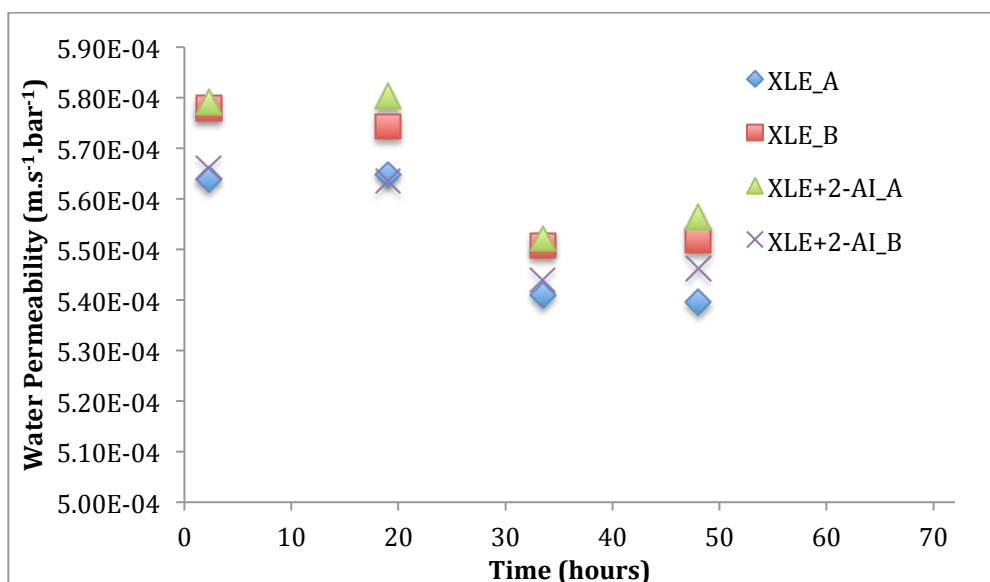


**Figure A1.27.** Water permeability of XLE and XLE +2-AI membranes operated in cross-flow with 500 ppm sodium chloride feed solution as described in *Section 2.2.15.2*. A and B denote experimental duplicates.

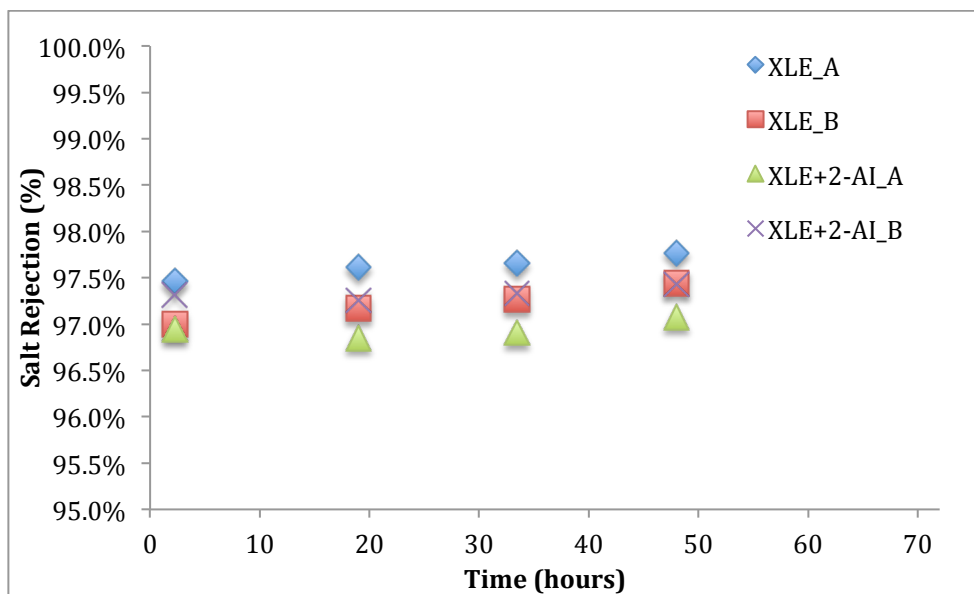


**Figure A1.28.** Salt rejection by XLE and XLE+2-AI membranes operated in cross-flow with 500 ppm sodium chloride feed solution as described in *Section 2.2.15.2*. A and B denote experimental duplicates.

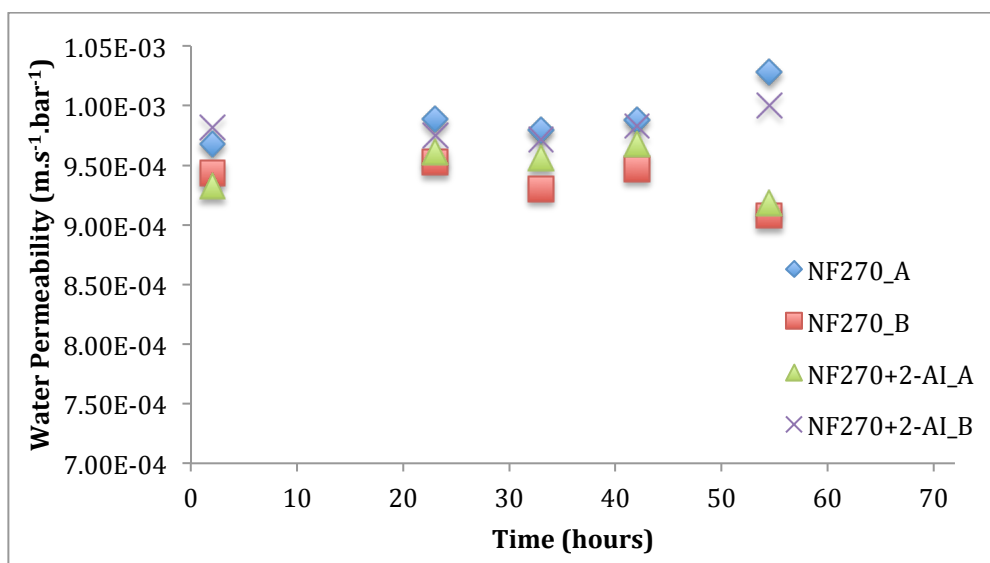


**Figure A1.29.** Water permeability of NF270 NF270+2-AI membranes operated in cross-flow with 500 ppm magnesium sulfate feed solution as described in *Section 2.2.15.2*. A and B denote experimental duplicates.

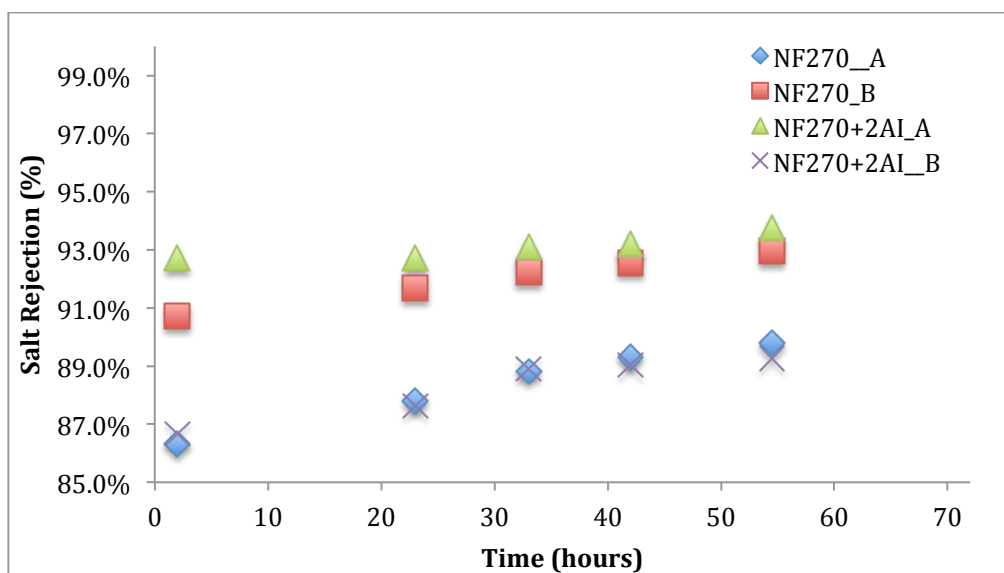


**Figure A1.30.** Salt rejection by NF270 and NF270+2-AI membranes operated in cross-flow with 500 ppm magnesium sulfate feed solution as described in *Section 2.2.15.2*. A and B denote experimental duplicates.

**Table A1.1.** Comparison of submersion versus subjecting only the top of the membranes to incorporation solutions. The concentrations of bromoaniline and iodoaniline that was incorporated into XLE membranes that were exposed to either bromoaniline incorporation solution or iodoaniline incorporation solution. Duplicate samples of each sample type were analyzed using RBS.

	<i>Bromoaniline incorporation</i>		<i>Iodoaniline incorporation</i>	
	Average Concentration of Bromoaniline (M)	Difference in Duplicates (M)	Average Concentration of Iodoaniline (M)	Difference in Duplicates (M)
Submerged	0.59	<0.01	0.39	<0.01
Top Only	0.65	<0.01	0.38	0.02
%Difference	10%		2%	

## REFERENCES

- (1) Verma, R. K.; Aggarwal, M.; Bansal, M.; Preet, I. A Facile and New Approach to Synthesize 2-Amino-4-(4-Alkylaminophenyl)-1H-1,3-Diazol-1-Yl-Alkylaminomethanethiones. *Med. Chem. Res.* **2007**, *15* (9), 483–491.

## APPENDIX 2: SUPPORTING INFORMATION FOR CHAPTER 3

172

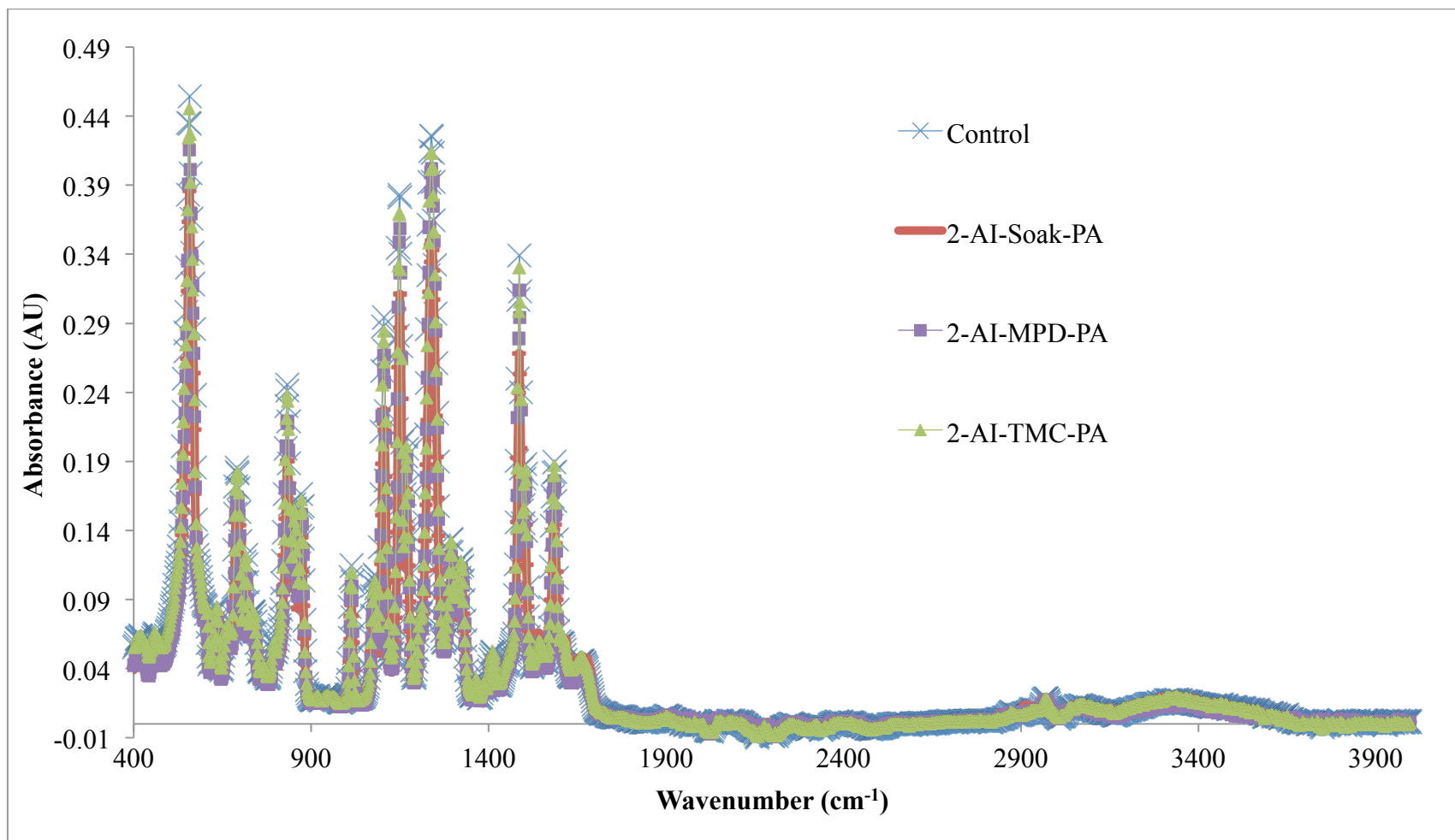


**Figure A2.1.** FTIR spectra of the control and 2-AI membranes. For each membrane, the spectrum shown corresponds to the average of three replicates, each of which was obtained through 24 scans of the sample analysis area.



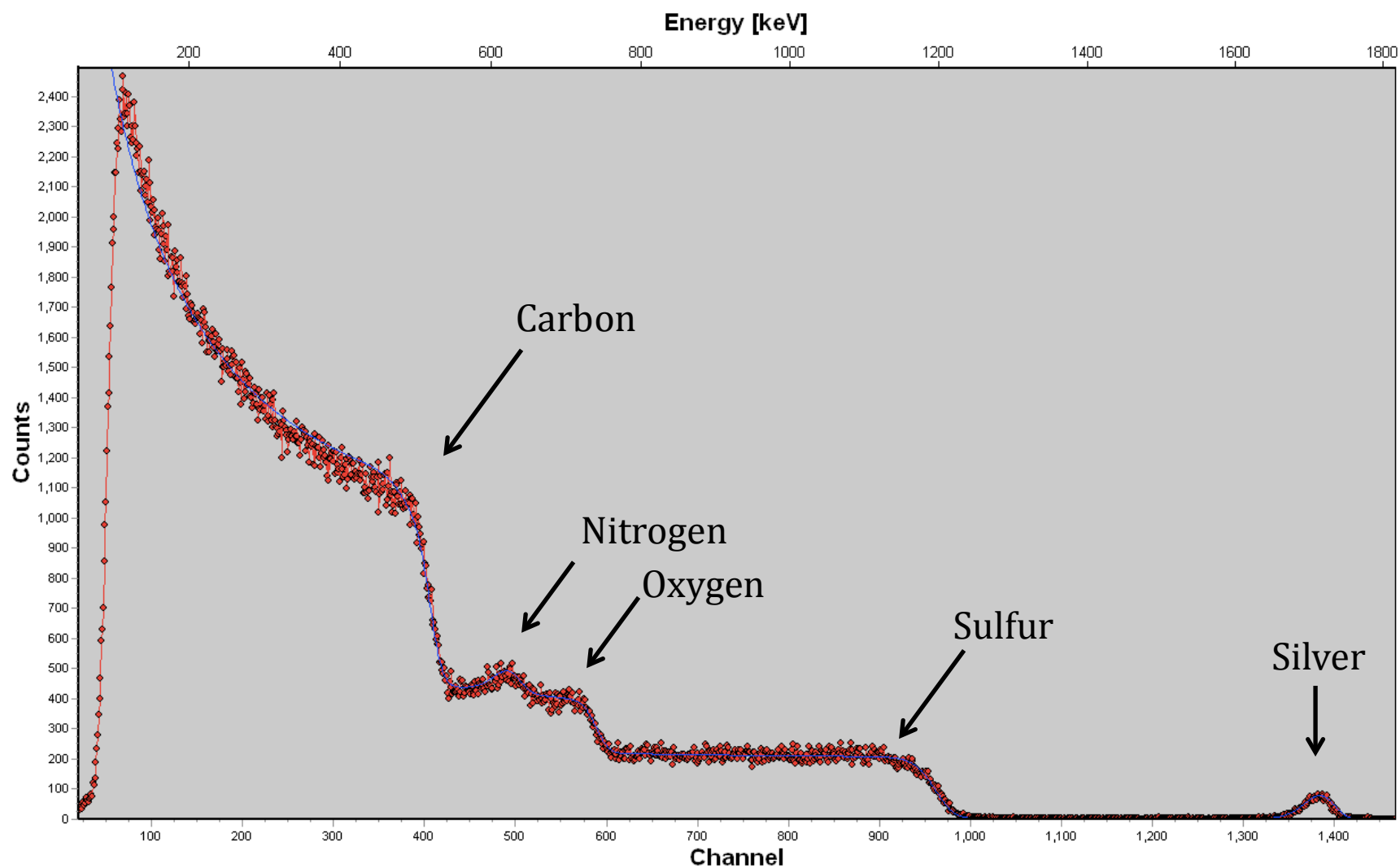


**Figure A2.2.** Example spectrum of silver probed membrane. RBS spectrum of a control membrane that's been probed with silver. The red diamonds are the raw data and the blue line is the fitted simulated data.

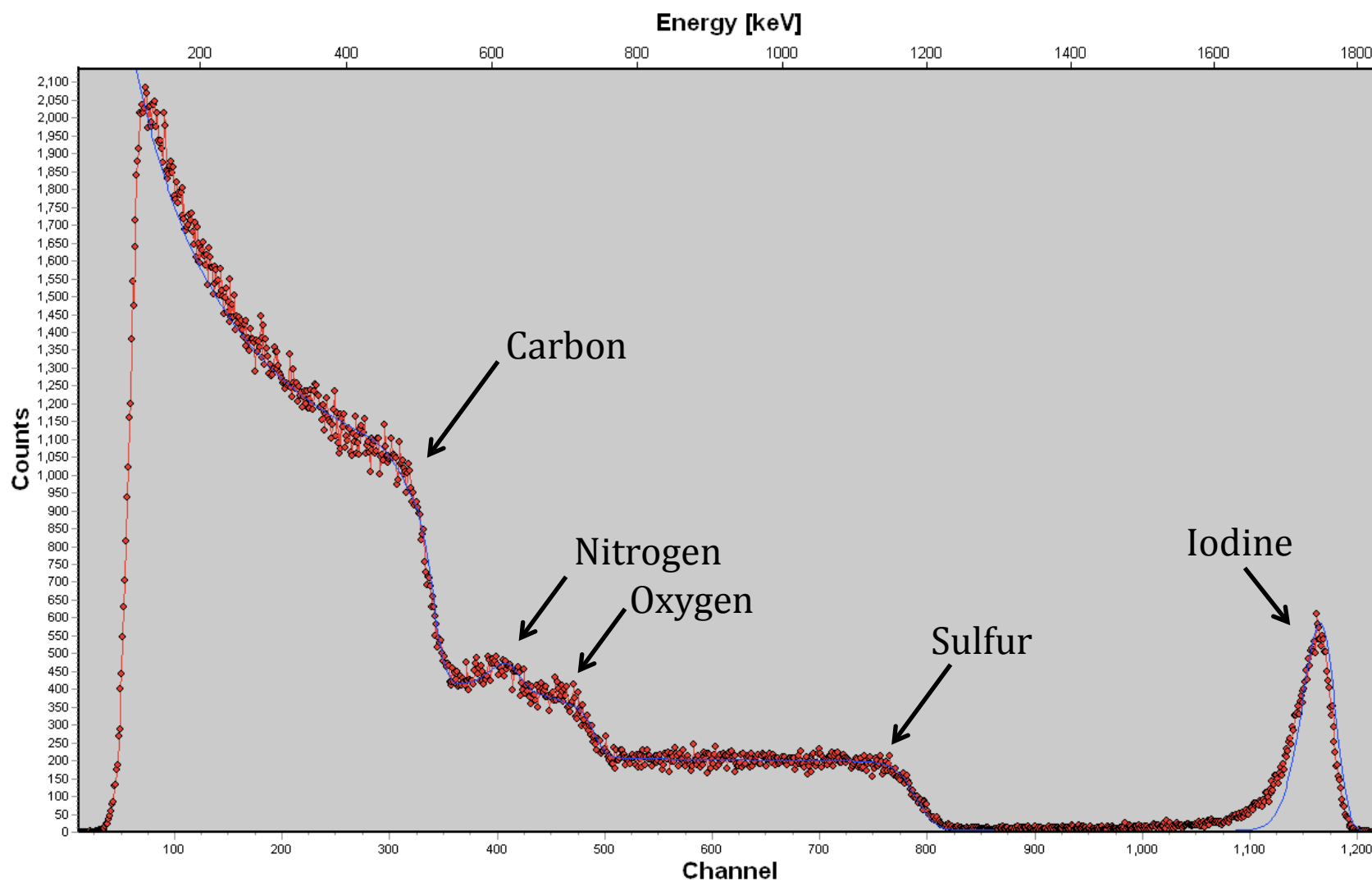


**Figure A2.3** Example spectrum of iodoaniline membrane. RBS spectrum of an IA-soak membrane. The red diamonds are the raw data and the blue line is the fitted simulated data

Quantification Report  
 /Coronell/Ariel/16098\_PolyamideMembranes\_withIodoaniline.dset Tue Oct 4 11:20:54 2016

State : Angle Name : REGa

Peak	Type	Position BE (eV)	FWHM (eV)	Raw Area (cps eV)	RSF	Atomic Mass	Atomic Conc %	Mass Conc %
O 1s	Reg	531.141	1.534	16137.5	0.780	15.999	11.47	13.97
C 1s	Reg	284.541	1.896	34722.2	0.278	12.011	74.97	68.57
N 1s	Reg	399.741	1.480	10818.7	0.477	14.007	13.14	14.01
Ag 3d	Reg	368.241	1.303	4291.6	5.987	107.878	0.42	3.44
I 3d	Reg	634.441	0.000	8.0	10.343	126.904	0.00	0.00

State : Angle Name : REGb

Peak	Type	Position BE (eV)	FWHM (eV)	Raw Area (cps eV)	RSF	Atomic Mass	Atomic Conc %	Mass Conc %
O 1s	Reg	531.050	1.511	17050.4	0.780	15.999	12.76	15.54
C 1s	Reg	284.650	1.790	32593.3	0.278	12.011	74.12	67.77
N 1s	Reg	399.850	1.401	9964.3	0.477	14.007	12.74	13.59
Ag 3d	Reg	368.250	1.278	3666.3	5.987	107.878	0.38	3.10
I 3d	Reg	634.450	0.000	0.0	10.343	126.904	0.00	0.00

State : Angle Name : REGc

Peak	Type	Position BE (eV)	FWHM (eV)	Raw Area (cps eV)	RSF	Atomic Mass	Atomic Conc %	Mass Conc %
O 1s	Reg	531.121	1.592	18461.3	0.780	15.999	12.68	15.46
C 1s	Reg	284.621	1.924	35053.6	0.278	12.011	73.14	66.96
N 1s	Reg	399.921	1.430	11792.1	0.477	14.007	13.84	14.77
Ag 3d	Reg	368.221	1.346	3622.4	5.987	107.878	0.34	2.81
I 3d	Reg	634.321	16.600	0.0	10.343	126.904	0.00	0.00

State : Angle Name : 2A1a

Peak	Type	Position BE (eV)	FWHM (eV)	Raw Area (cps eV)	RSF	Atomic Mass	Atomic Conc %	Mass Conc %
O 1s	Reg	531.292	1.447	1894.5	0.780	15.999	8.61	8.72
C 1s	Reg	284.592	1.550	5590.8	0.278	12.011	77.21	58.72
N 1s	Reg	399.792	1.659	1454.7	0.477	14.007	11.30	10.02
Ag 3d	Reg	368.192	1.284	752.0	5.987	107.878	0.47	3.21
I 3d	Reg	620.492	1.180	7237.2	10.343	126.904	2.41	19.33

State : Angle Name : 2A1b

Peak	Type	Position BE (eV)	FWHM (eV)	Raw Area (cps eV)	RSF	Atomic Mass	Atomic Conc %	Mass Conc %
O 1s	Reg	531.537	2.038	10880.1	0.780	15.999	8.26	8.80
C 1s	Reg	284.537	1.521	34045.9	0.278	12.011	78.57	62.81
N 1s	Reg	399.937	1.860	8447.4	0.477	14.007	10.96	10.22
Ag 3d	Reg	368.237	1.333	3564.9	5.987	107.878	0.37	2.67
I 3d	Reg	620.737	1.302	33031.0	10.343	126.904	1.83	15.50

State : Angle Name : 2A1c

Peak	Type	Position BE (eV)	FWHM (eV)	Raw Area (cps eV)	RSF	Atomic Mass	Atomic Conc %	Mass Conc %
O 1s	Reg	530.988	1.770	12163.2	0.780	15.999	9.05	9.15
C 1s	Reg	284.688	1.722	33806.4	0.278	12.011	76.44	57.98
N 1s	Reg	399.688	1.732	9133.6	0.477	14.007	11.62	10.27
Ag 3d	Reg	368.288	1.377	4379.9	5.987	107.878	0.45	3.05
I 3d	Reg	620.288	1.288	44789.2	10.343	126.904	2.44	19.54

State : Angle Name : MPDa

Peak	Type	Position BE (eV)	FWHM (eV)	Raw Area (cps eV)	RSF	Atomic Mass	Atomic Conc %	Mass Conc %
O 1s	Reg	531.115	1.630	11870.2	0.780	15.999	9.21	10.29
C 1s	Reg	284.515	2.130	31052.4	0.278	12.011	73.23	61.42
N 1s	Reg	399.715	1.845	12121.9	0.477	14.007	16.08	15.73
Ag 3d	Reg	368.315	1.244	3850.1	5.987	107.878	0.41	3.09
I 3d	Reg	620.615	1.253	18812.4	10.343	126.904	1.07	9.46

State : Angle Name : MPDb

Peak	Type	Position BE (eV)	FWHM (eV)	Raw Area (cps eV)	RSF	Atomic Mass	Atomic Conc %	Mass Conc %
O 1s	Reg	530.939	1.553	12733.2	0.780	15.999	9.10	10.23
C 1s	Reg	284.539	2.071	34114.6	0.278	12.011	74.06	62.49
N 1s	Reg	399.539	1.755	12639.5	0.477	14.007	15.43	15.19
Ag 3d	Reg	368.239	1.309	4005.9	5.987	107.878	0.39	2.98
I 3d	Reg	620.539	1.275	19563.9	10.343	126.904	1.02	9.12

State : Angle Name : MPDc

Peak	Type	Position BE (eV)	FWHM (eV)	Raw Area (cps eV)	RSF	Atomic Mass	Atomic Conc %	Mass Conc %
O 1s	Reg	531.192	1.604	12994.9	0.780	15.999	9.37	10.12
C 1s	Reg	284.592	2.076	33366.4	0.278	12.011	73.08	59.25
N 1s	Reg	399.592	1.826	12639.8	0.477	14.007	15.57	14.72
Ag 3d	Reg	368.292	1.261	8442.9	5.987	107.878	0.84	6.09
I 3d	Reg	620.592	1.273	21746.9	10.343	126.904	1.15	9.82

State : Angle Name : TMCa

Peak	Type	Position BE (eV)	FWHM (eV)	Raw Area (cps eV)	RSF	Atomic Mass	Atomic Conc %	Mass Conc %
O 1s	Reg	530.928	1.592	16571.8	0.780	15.999	12.42	14.39
C 1s	Reg	284.628	1.998	31752.5	0.278	12.011	72.32	62.88
N 1s	Reg	399.828	1.676	11162.9	0.477	14.007	14.30	14.50
Ag 3d	Reg	368.328	1.509	4254.8	5.987	107.878	0.44	3.42
I 3d	Reg	620.628	1.506	9539.1	10.343	126.904	0.52	4.81

State : Angle Name : TMCb

Peak	Type	Position BE (eV)	FWHM (eV)	Raw Area (cps eV)	RSF	Atomic Mass	Atomic Conc %	Mass Conc %
O 1s	Reg	531.270	1.467	17130.1	0.780	15.999	12.10	14.35
C 1s	Reg	284.670	1.802	34371.2	0.278	12.011	73.77	65.66
N 1s	Reg	399.970	1.471	11119.2	0.477	14.007	13.42	13.93
Ag 3d	Reg	368.170	1.313	4777.4	5.987	107.878	0.46	3.71
I 3d	Reg	620.670	1.303	4849.7	10.343	126.904	0.25	2.36

State : Angle Name : TMCc

Peak	Type	Position BE (eV)	FWHM (eV)	Raw Area (cps eV)	RSF	Atomic Mass	Atomic Conc %	Mass Conc %
O 1s	Reg	531.148	1.520	16969.8	0.780	15.999	11.91	14.11
C 1s	Reg	284.648	1.852	34743.0	0.278	12.011	74.08	65.91
N 1s	Reg	399.848	1.466	11075.9	0.477	14.007	13.28	13.78
Ag 3d	Reg	368.148	1.340	4967.5	5.987	107.878	0.48	3.83
I 3d	Reg	620.448	1.391	4891.3	10.343	126.904	0.25	2.36

**Figure A2.4.** Raw XPS data of IA-membranes that have been probed with silver. Triplicate sample analyses are presented. REG=control membranes, 2-AI=IA-soak membranes, MPD= IA-MPD membranes, TMC=IA-TMC membranes.

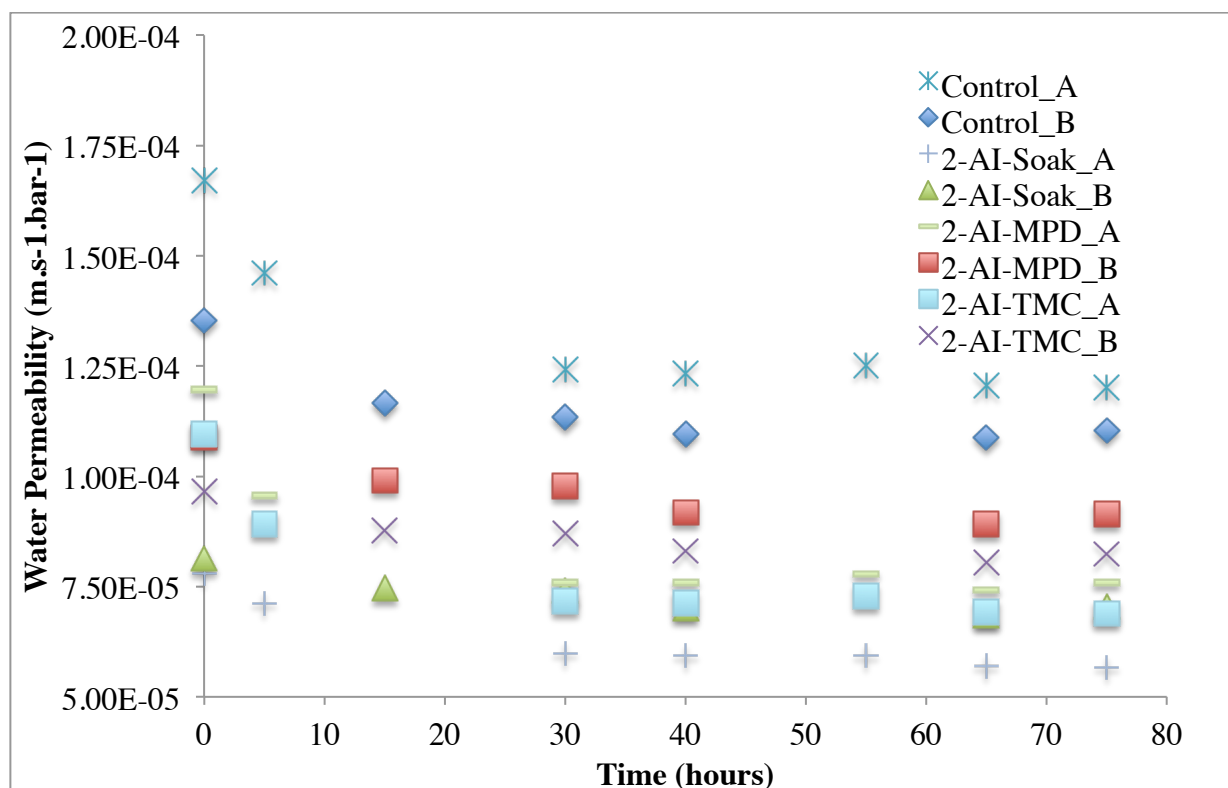


**Figure A2.5.** Water permeability of control and 2-AI membranes over 75 hours of operation in cross-flow with 500 ppm sodium chloride feed solution as described in *Section 3.2.7.2*. A and B denote duplicates, different coupons operated in separate runs.

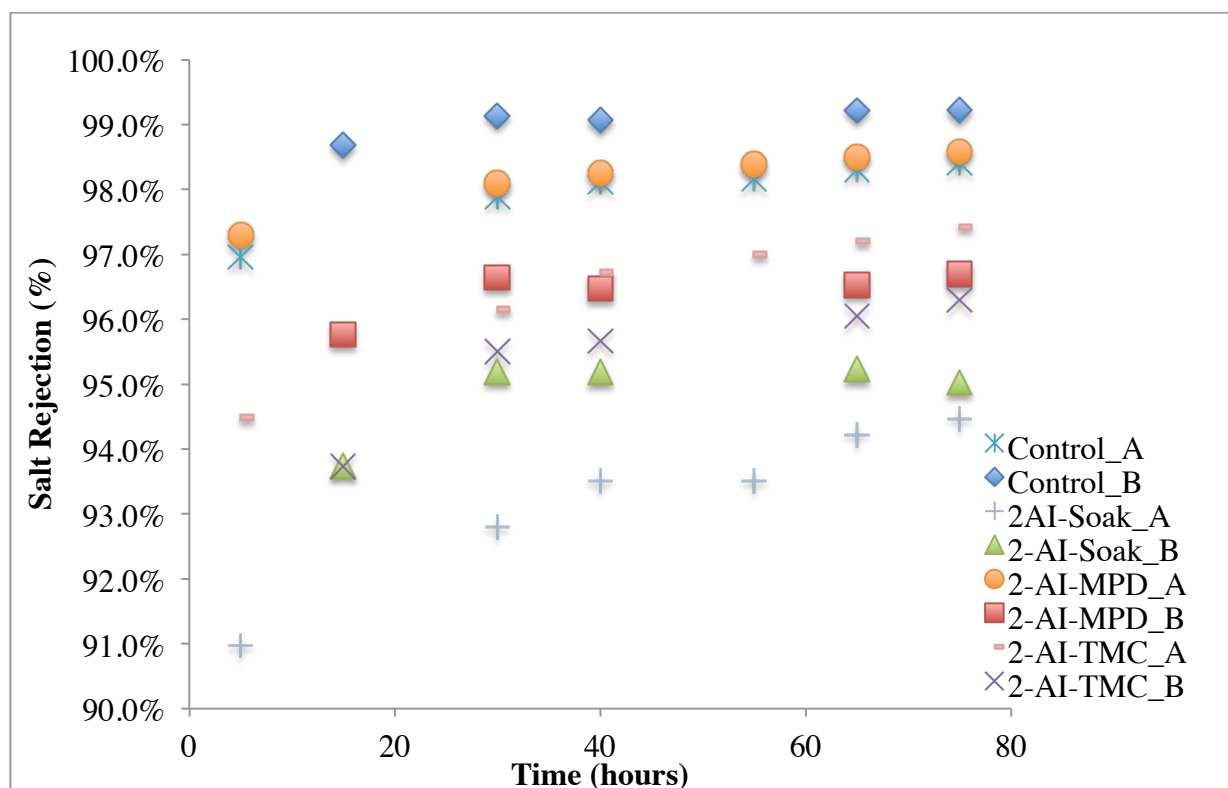


**Figure A2.6.** Salt rejection of control and 2-AI membranes over 75 hours of operation in cross-flow with 500 ppm sodium chloride feed solution as described in *Section 3.2.7.2*. A and B denote duplicates, different coupons operated in separate runs.

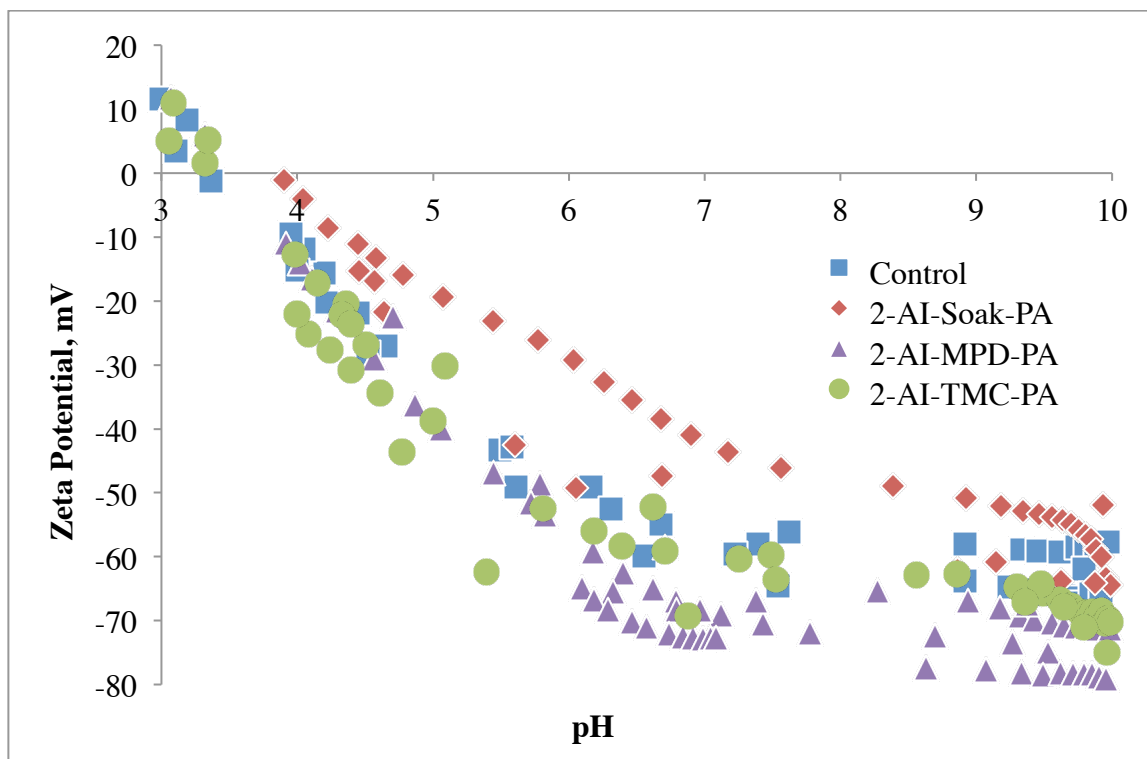


**Figure A2.7.** Raw data of zeta potential as a function of pH for control and 2-AI membranes, the data that was used to produce regressions shown in *Figure 3.6*.



### APPENDIX 3: SUPPORTING INFORMATION FOR CHAPTER 4

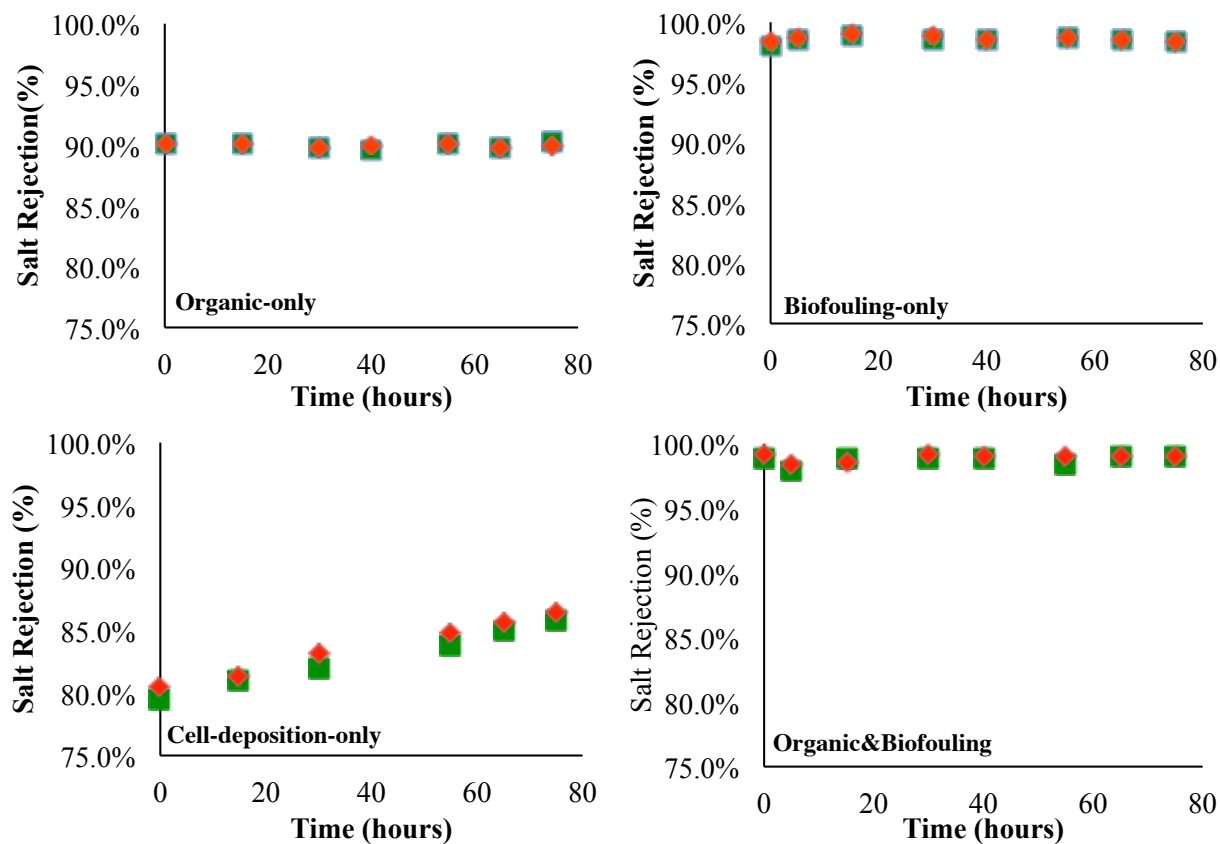


**Figure A3.1.** Salt rejection of control and 2-AI membranes over 75 hours of operation in cross-flow with

**Table A3.1.** Materials used to build the custom laboratory-scale reverse osmosis cross-flow system, prices from 2015. Provided by Mikayla D. Armstrong.

<b>Material</b>	<b>Manufacturer</b>	<b>Price</b>
Diaphragm pump	Hydra-Cell	\$5400
Pulsation dampener	Cat pumps	\$770
Motor	Baldor	\$440
Motor adapter kit	Baldor	\$200
Gear reducer	Baldor	\$300
Motor Controller	Dart	\$250
Glass carboy with spigot	Greatglas	\$500
Carboy modification	Prism Research Glass	\$240
Compression fitting, straight adapter for 3/4 in. tube OD x 3/4 in. female pipe	McMaster Carr	\$80
Thermoflex recirculating chiller	Fisher-Scientific	\$4420
alpha-190 pH controller	Eutech Instruments	\$370
pH electrode	Accumet	\$240
pH electrode extension cable	Cole-Parmer	\$50
Stainless steel corrugated hose – 316SS	Swagelok	\$450
316/316L SS seamless tubing 3/8 in. OD 0.035 wall	Swagelok	\$120
Tee 3/8 in. compression x 3/8 in. compression x 1/2 in. FNPT	Swagelok	\$70
Reducing adapter 3/4 “ FNPT x 1/2 in. MNPT	Swagelok	\$30
Pressure transducers	Omega	\$3420
90° elbows 3/8 in. x 3/8 in. compression	Swagelok	\$60
Union tee 3/8 in. x 3/8 in. x 3/8 in. compression	Swagelok	\$30
Metering valves 3/8 in. x 3/8 in. compression	Swagelok	\$420
3-way ball valve 3/8 in. x 3/8 in. x 3/8 in. compression	Swagelok	\$50
Union tees 3/8 in. x 3/8 in. x 1/4 in. FNPT	Swagelok	\$180
Connectors 3/8 in. compression x 1/4 in. MNPT	Swagelok	\$60
Pressurized membrane cells	UNC Design Center	\$5600
Pipe plug 1/8 in. MNPT	Swagelok	\$30
Pipe plug 1/4 in. MNPT	Swagelok	\$60
Connectors 1/8 in. MNPT x 1/8 in. compression	Swagelok	\$30
316/316L SS seamless tubing 1/8 in. OD 0.028 wall	Swagelok	\$120
3-way ball valves 1/8 in. x 1/8 in. x 1/8 in. compression	Swagelok	\$360
Connector 3/8 in. compression x 1/2 in. MNPT	Swagelok	\$10
Flow indicator	King	\$710
Shelving unit	Safco	\$160
<b>Total</b>		<b>\$25520</b>